Māris Tamanis

Dr.fiz.

Divatomu molekulu radiācijas, magnētisko un elektrisko īpašību eksperimentālie pētījumi

(Habilitācijas darba rakstu kopa)

Latvijas Universitāte

Fizikas un matemātikas fakultāte

Atomfizikas un spektroskopijas institūts

1996

ANOTĀCIJA

Habilitācijai piedāvātais darbs "Divatomu molekulu radiācijas, magnētisko un elektrisko īpašību eksperimentālie pētījumi" ir autora darbu kopa, kas sastāv no 21 publicēta raksta fizikas žurnālos un rakstu krājumos ar kopapjomu 166 lpp. un 27 zinātnisko konferenču tēzēm. Pievienotas publikācijas, kurās atspoguļoti visi iegūtie galvenie rezultāti.

ZINĀTNISKO PUBLIKĀCIJU KOPAS SATURS

1. R.S.Ferber, M.Ya.Tamanis Lifetimes in the $A0^+_u$ state of $^{130}Te_2$, *Chem. Phys. Lett.* 1983, **98**, p.577-578.

2. М.П.Аузиньш, М.Я.Таманис, Р.С.Фербер, Определение знака фактора Ланде двухатомных молекул в основном и возбужденном состояниях по эффекту Ханле, *Оптика и спектр.*,1987, **63**, с.989-997.

3.М.П.Аузиньш, М.Я.Таманис, Я.А.Харья, Времена жизни колебательно-вращательных уровней электронно-возбужденных состояний $^{130}Te_2$, *XX Всес.съезд по спектроскопии, Тез.докл.*, ч.1,"Наукова думка", Киев,1988,с.263.

4. I.P.Klintsare, M.Ya.Tamanis, R.S.Ferber, Quantum beats in the fluorescence kinetics of $Te_2(A0^+_u)$ molecules, *Opt.Spectrosc. (USSR)*, 1989, **66**, p.484-485.

5. I.P.Klintsare, A.V.Stolyarov, M.Ya.Tamanis, R.S.Ferber, Ya.A.Kharya, Anomalous behaviour of Lande factors of the $Te_2(B0^+_u)$ molecule of the intensities of the $B0^+_u$--$X1^+_g$ transition, *Opt.Spectrosc. (USSR)*, 1989, **66**, p.595-597.

6. I.P.Klintsare, M.Ya.Tamanis, R.S.Ferber, Determination of the lifetime and relaxation cross section of the $Te_2(A1^-_u)$ molecule by the Hanle method, *Opt.Spectrosc. (USSR)*, 1989, **67**, p.720-721.

7. I.P.Klincare, M.Ya.Tamanis, Lifetime and Lande factor measurements of $A1_u$ and $A0^-_u$ state of Te_2 by laser-induced fluorescence, *Chem.Phys. Lett.*, 1991, **180**, p.63-67.

8. A.V.Stolyarov, I.P.Klincare, M.P.Auzinsh, M.Ya.Tamanis, R.S.Ferber, Rotational magnetic moment of the Na_2 molecule in $A^1\Sigma^+_u$ state: Perturbation effects, *J.Chem. Phys.*,1992, **96**, p.3510-3522.

9. A.V.Stolyarov, I.P.Klincare, M.Tamanis, R.S.Ferber, Observation of $A^1\Sigma^+_u$~$b^3\Pi_u$ interaction in g factors of weakly coupled Na_2 $A^1\Sigma^-_u$ state levels, *J.Chem. Phys.*, 1993, **98**, p.826-835.

10. I.P.Klincare, A.V.Stolyarov, M.P.Auzinsh, M.Ya.Tamanis, R.S.Ferber, Alignment-orientation conversion by quadratic Zeeman effect: Analysis and observation for Te_2, *J.Chem. Phys.*, 1993, **99**, p.5748-5753.

11. E.A.Pazyuk, A.V.Stolyarov, M.Ya.Tamanis, R.S.Ferber, Global deperturbation analysis from energetic, magnetic and radiative measurements: Application to Te_2, *J.Chem. Phys.*, 1993, **99**, p.7873-7887.

12. M.Auzinsh, A.V.Stolyarov, M.Tamanis, R.S.Ferber, Magnetic field induced alignement-orientation conversion: Non-linear energy shift and predoissociation in Te_2 $B1_u$ state, *J.Chem.Phys.*, 1996, **105**, p.37-49.

13. M.Tamanis, M.Auzinsh, I.Klincare, O.Nikloayeva, A.V.Stolyarov, R.Ferber, NaK $D^1\Pi$ electric dipole moment measurement by Stark level crossing and *e-f* mixing spectroscopy, *J.Chem.Phys.*, 1996, accepted.

14. M.Tamanis, A.V.Stolyarov, M.Auzinsh, I.Klincare, O.Nikolayeva, R.Ferber, Electric dipole moment and Λ-doubling measurements in ($D^1\Pi$) NaK, *Abstr.15-th International Conference on Atomic Physics*, Amsterdam, Netherlands, 1996, p.ThH1.

Volume 98, number 6 CHEMICAL PHYSICS LETTERS 15 July 1983

LIFETIMES IN THE A 0_u^+ STATE OF $^{130}Te_2$

R.S. FERBER and M.Ya. TAMANIS
P. Stuchka Latvian State University, 226098 Riga, USSR

Received 17 February 1983; in final form 3 May 1983

Lifetime measurements have been performed for two vibrotational levels of the A 0_u^+ states of the $^{130}Te_2$ molecule, excited by the 496.5 nm Ar^+-laser line. Deactivation cross sections for Te_2-Te_2 collisions have been determined.

In our previous paper [1] lifetime measurement results have been reported for four vibrotational levels in the B 0_u^+ state of the $^{130}Te_2$ molecule, excited by 488.0 and 496.5 nm Ar^+-laser lines, as well as of one level in the A 0_u^+ state excited at 514.5 nm *. The main result obtained was the fact that the lifetime for the ($v' = 11, J' = 53$) A 0_u^+ state, equalling 670 ns, exceeds by about an order of magnitude those of B 0_u^+ levels with $v' = 0, 1, 3$, lying between 54 and 73 ns (levels were identified according to refs. [2,3]).

However, quite recently results have been published [4] containing data on lifetime measurements for four v', J' levels of the A 0_u^+ state with $v' = 16$ and 17, yielding τ values between 62 and 71 ns, the levels being non-perturbed, according to the authors of ref. [4]. We consider it of interest, in this connection, to report on additional τ measurements for $^{130}Te_2$ in A 0_u^+ state. The assembly employed was that used for measuring kinetics of laser-induced fluorescence (LIF), described in ref. [1].

The LIF spectrum of $^{130}Te_2$ excited by the 496.5 nm line showed that at TEM_{00} operation and at a current of ≈25 A through the laser tube (amplification contour ≈10 GHz) in addition to the progression from (0, 107) B 0_u^+, mentioned in ref. [2], other doublet progressions could be observed, as shown in

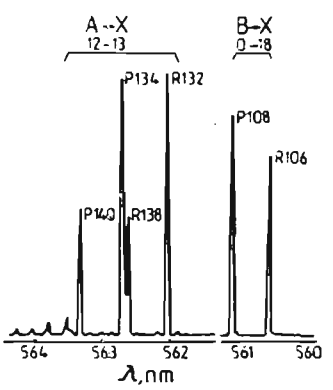

Fig. 1. Part of the LIF spectrum of $^{130}Te_2$, excited by the 496.5 nm Ar^+-laser line.

fig. 1. For two of them lifetimes were recorded exceeding that of the (0, 107) B 0_u^+ level by an order of magnitude. Passing over to single-mode operation of the laser made it possible, through frequency-tuning, to excite these two progressions only, the rest practically remaining suppressed. It was inferred from the number of anti-Stokes lines in LIF, that we have $v'' = 3$ for both progressions, since intensity varied smoothly up to the third anti-Stokes, then abruptly falling to zero (sensitivity of registration permitted identification of the signal 10^4 times weaker than the last anti-Stokes line observed). Measurement of doublet splitting, as dependent on v'', yielded an estimated value for J' equalling 133 ± 2 for one transition (P absorption), and 139 ± 2 for the other one (R absorption). It may be easily seen that the photon energy of the laser beam is insufficient for excitation

* There has been a flaw in the setting of table 1 in our previous paper [1]. As clearly follows from the text of that article, the $v' = 0, J' = 107$ level excited by $\lambda = 496.5$ nm wavelength has been attributed by us to the B 0_u^+ state, and not to the A 0_u^+ state, as might have been erroneously inferred from table 1 in ref. [1].

0009-2614/83/0000–0000/$03.00 © 1983 North-Holland

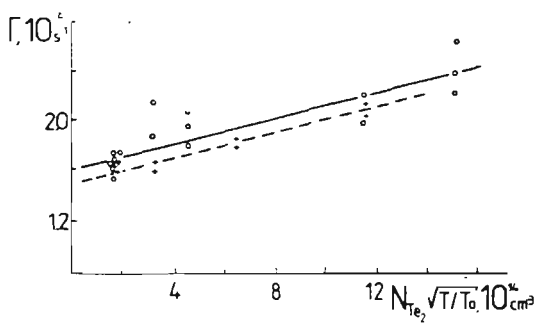

Fig. 2. Dependence of the decay rate Γ on concentration N_{Te_2} with temperature change from $T = T_0 = 650$ K to $T = 700$ K; + for (12,133), o for (12,139) A 0_u^+.

of B 0_u^+ from the ($v'' = 3$) X 0_g^+ state. The term structure and the spectroscopic constants given in refs. [2,3,5] show that the A 0_u^+ term can be excited, and in this case $v' = 12$. The obtained v', J' values do not contradict coincidence calculations of energy differences between the combining states and the laser frequency. The same considerations exclude X 1_g – A 1_u excitation.

Fig. 2 shows decay rates of the levels under consideration, as dependent on Te_2 concentration. Extrapolation to zero concentration permitted determination of the spontaneous lifetimes presented in table 1. These values are in good agreement with the τ value for (11, 53) A 0_u^+, as reported previously in ref. [1].

Table 1
Lifetimes and effective cross sections for the A 0_u^+ state of $^{130}Te_2$

v'	J'	τ (ns)	$\sigma(Te_2-Te_2)$ (10^{-14} cm^2)	Ref.
12	133 ± 2	670 ± 40	1.6 ± 0.4	this work
12	139 ± 2	620 ± 50	1.6 ± 0.5	this work
11	53	670 ± 30	1.6 ± 0.3	[1]

The slope of the straight lines in fig. 2 yields equal values for effective cross sections of level deactivation also presented in table 1. The error corresponding to two standard deviations is given in each case.

We consider that the lifetime values contained in table 1 are characteristic for the A 0_u^+ state.

It is difficult to give a convincing explanation of the discrepancy between this conclusion and results of measurements [4]. The following suggestions might be proposed. The authors of ref. [4] measured τ values for different (v', J') levels – thus, they had $v' = 16, 17$, whereas we had $v' = 11$ and 12. Further, it may be pointed out that the Stern–Volmer plots in ref. [4] start at Te_2 concentrations exceeding the last point in our Stern–Volmer plots. This may lead to extrapolation errors towards lower τ values, owing to possible bending of the curves at high concentrations. Finally, one must not exclude the possibility of the levels studied in ref. [4] belonging to the B-state, which is not impossible from energy considerations.

It is worth noting that τ measurements for the adjoining group VI A molecule $^{80}Se_2$ yielded a value of 780 ns for the A 0_u^+ state, and 85 ± 10 ns for the B 0_u^+ state [6].

References

[1] R.S. Ferber, O.A. Shmit and M.Ya. Tamanis, Chem. Phys. Letters 92 (1982) 393.
[3] T.J. Stone and R.F. Barrow, Can. J. Phys. 53 (1975) 1976.
[3] J. Verges, J. d'Incan, C. Effantin, D.J. Greenwood and R.F. Barrow, J. Phys. B12 (1979) L301.
[4] J. Cariou, Y. Guern, J. Lotrian and P. Luc, J. Phys. B15 (1982) L841.
[5] J. Verges, C. Effantin, O. Babaky, J. d'Incan, S.J. Prosser and R.F. Barrow, Physica Scripta 25 (1982) 338.
[6] M. Heaven, T.A. Miller, J.H. English and V.E. Bondybey, Chem. Phys. Letters 91 (1982) 251.

ТОМ 63, ВЫП. 5 • ОПТИКА И СПЕКТРОСКОПИЯ • 1987 год

УДК 539.194.01

ОПРЕДЕЛЕНИЕ ЗНАКА ФАКТОРА ЛАНДЕ ДВУХАТОМНЫХ МОЛЕКУЛ В ОСНОВНОМ И ВОЗБУЖДЕННОМ СОСТОЯНИЯХ ПО ЭФФЕКТУ ХАНЛЕ

Аузиньш М. П., Таманис М. Я., Фербер Р. С.

Приводятся и анализируются аналитические выражения, описывающие в аппарате поляризационных моментов сигналы пересечения магнитных подуровней в нулевом магнитном поле (эффект Ханле) дисперсионной формы при линейно поляризованном возбуждении для случая предельно слабой накачки («линейный» отклик системы) при переходах Q- и P, R-типа в двухатомных молекулах с большими значениями углового момента $J \gg 1$. Рассмотрен случай эффективной оптической накачки «опустошением», при которой проявляется суперпозиционный сигнал Ханле «дисперсионной» формы основного и возбужденного состояний, связанных оптическим переходом. Представлены результаты экспериментов, проведенных на молекулах $^{39}K_2$ при $X^1\Sigma_g^+ \rightarrow B^1\Pi_u$ возбуждении линией 632.8 нм He—Ne-лазера и $^{130}Te_2$ при $XO_g^+ - AO_u^+$ возбуждении линиями 488.0 и 514.5 нм Ar^+-лазера. Из полученных сигналов дисперсионной формы определены знаки факторов Ланде комбинирующих состояний.

Магнитные моменты двухатомных молекул обусловлены не только орбитальными и собственными моментами электронов и ядер, но и вращением молекулы (см., например, [1, 2]). Строгий расчет магнитного момента для конкретного электронно-колебательно-вращательного (ЭКВ) уровня может быть произведен лишь в случае чистого типа связи по Гунду [1, 3]. Так, для связи a-типа величина μ_z проекции магнитного момента на направление внешнего магнитного поля B равна [1]

$$\mu_z = -\frac{(\Lambda + 2\Sigma)(\Lambda + \Sigma) M'}{J'(J'+1)} \mu_0 = g_{J'} M' \mu_0 \qquad (1)$$

где Λ, Σ — проекции орбитального и спинового моментов электронов на молекулярную ось, M' — магнитное квантовое число углового момента J', $g_{J'}$ — фактор Ланде, μ_0 — магнетон Бора; при этом изменение энергии в поле B есть $\Delta W_B = -\mu_z B$. Следуя (1), авторами [4] рассчитывался фактор Ланде для ЭКВ уровня Na_2 ($B^1\Pi_u$, $v'=10$, $J'=12$) с $\Lambda=1$, $\Sigma=0$, что приводит к $g_{J'} = -1/J'(J'+1)$. На этом состоянии в [4] реализован первый эксперимент по эффекту Ханле для двухатомных молекул с применением лазерно-индуцированной флуоресценции, из которого определено время жизни. Выражения для типов связи b и c по Гунду приведены в [5]. Однако для состояний, в которых $\Lambda = \Sigma = 0$ либо проекция полного момента $\Omega=0$, выражения типа (1) дают ноль, и магнитный момент определяется вращательным движением молекулы [6]. При этом в большинстве случаев сложно заранее предсказать не только величину, но и знак фактора Ланде, поэтому основным источником информации здесь служат эксперименты, число которых невелико. В [7, 8] исследовались BO_u^+-состояния $^{80}Se_2$ с $\Omega=0$. В [6] методом радиочастотного резонанса в молекулярных пучках определены магнитные моменты $X^1\Sigma_g^+$-состояний для щелочных димеров Li_2, Na_2, K_2, Rb_2, Cs_2 без селекции по КВ уровням v'', J''. При этом для Li_2 ($X^1\Sigma_g^+$) определено также, что направление магнитного момента совпадает с угловым моментом J (в этом случае будем считать фактор Ланде положительным). Авторы [6] сделали вывод об определяющем вкладе вращения

ядер. Недавно нами [9-11] для определения величины магнитного момента от дельного ЭКВ уровня (α'', v'', J'') основного электронного состояния α'' был использованы нелинейные варианты методов интерференции магнитных под уровней при лазерной оптической накачке: резонанс биений для $^{130}Te_2$ (XO_g^+

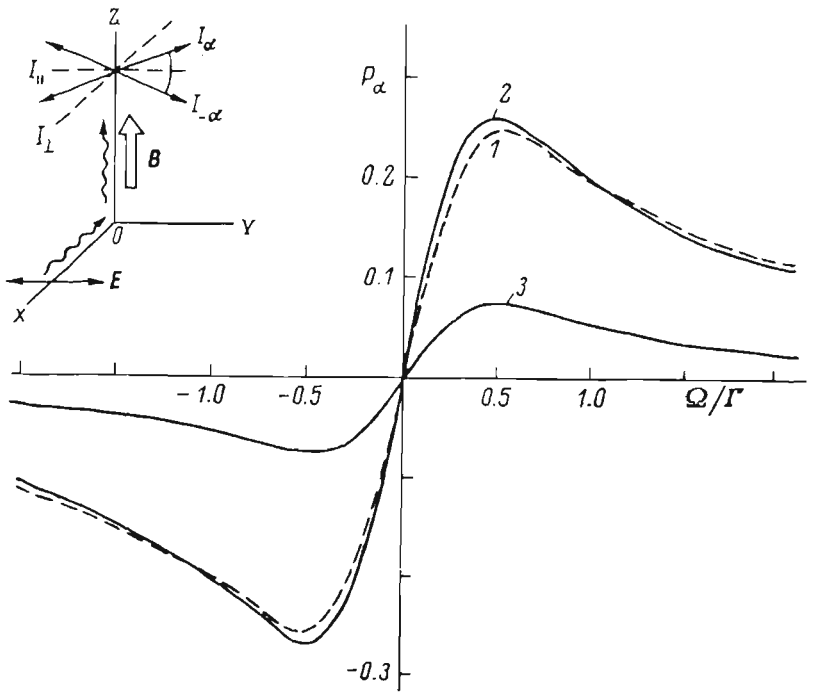

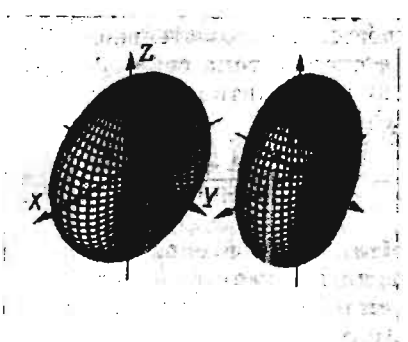

Рис. 1. Расчетные сигналы Ханле дисперсионной формы в двухатомных молекулах для линейного отклика.

6, 53) [9], эффект Ханле [10] и квантовые биения в переходном процессе [11] для $^{39}K_2$ ($X^1\Sigma_g^+$, 1, 73). Однако знак фактора Ланде в этих экспериментах не определялся.

Одну из возможностей определения знака g дает эффект Ханле, заключающийся в деполяризации флуоресценции внешним магнитным полем [12]. Но в традиционной геометрии эксперимента (рис. 1), когда измеряется степень линейной поляризации $P=(I_\parallel-I_\perp)/(I_\parallel+I_\perp)$, где $I_{\parallel,\perp}$ — интенсивность флуоресценции, поляризованной параллельно либо перпендикулярно вектору E возбуждающего света, зависимость от магнитного поля B имеет лоренцовский вид

$$P_L(B) = \frac{P_L(0)\,\Gamma_2^2}{\Gamma_2^2 + 4g^2B^2\mu_0^2/\hbar^2}, \qquad (2)$$

и поэтому информация о знаке магнитного момента теряется. Здесь Γ_2 — скорость релаксации выстраивания [13]. Как хорошо известно [3], знак фактора Ланде принято измерять в сигнале Ханле дисперсионной формы, регистрируя интенсивности, поляризованные под углом $\pm 45°$ к вектору E (т. е. $\alpha = \pm 45°$ на схеме рис. 1). Тогда

$$P_{45°}(B) = \frac{I_\alpha - I_{-\alpha}}{I_\alpha + I_{-\alpha}} = \frac{2\mu_0 g B P_L(0)/\hbar}{\Gamma_2^2 + 4\mu_0^2 g^2 B^2/\hbar^2}. \qquad (3)$$

Сигналы такой формы регистрировались, например, в [7] для полосы $^{80}Se_2$ $B-X$.

В настоящей работе с использованием аппарата поляризационных моментов анализируется вид сигналов дисперсионной формы $P_\alpha(B)$ для произвольного угла α и переходов Q- и P, R-типа в двухатомных молекулах с большими угловыми моментами $J \gg 1$. С целью определения знака фактора Ланде основного состояния анализируется дисперсионная форма нелинейного сигнала Ханле в случае, когда сигнал от основного состояния накладывается на контур Ханле возбужденного уровня (впервые такой эффект зарегистрирован в [14] для сигналов лорентцовской формы). Приводятся результаты эксперимента по определению знака фактора Ланде основного электронного состояния димеров калия $^{39}K_2$ ($X^1\Sigma_g^+$) и теллура $^{130}Te_2$ (XO_g^+).

Дисперсионная форма сигнала Ханле двухатомных молекул при слабом возбуждении

Пусть возбуждающее оптический переход $(\alpha'', v_a'', J_a'') \to (\alpha', v_b', J_b')$ (или сокращенно $a \to b$) излучение направлено вдоль OX (рис. 1) и линейно поляризовано вдоль OY. Будем следить за интенсивностью флуоресценции I_α на переходе $(\alpha', v_b', J_b') \to (\alpha'', v_a'', J_c'')$, или $b \to c$, линейно поляризованной под углом α к вектору E $\parallel OY$. Рассмотрение будем проводить в аппарате поляризационных моментов (ПМ) [13, 15] с использованием асимптотических выражений для случая $J \to \infty$ [16]. Выражение для интенсивности

$$I_\alpha = (-1)^\Delta \sum_K \sqrt{2K+1}\, C^{K0}_{1-\Delta 1\Delta} \sum_Q (-1)^Q f_Q^K \Phi^K_{-Q}(\alpha), \qquad (4)$$

где $\Phi_Q^K(\alpha)$ — функция, введенная в [15]; f_Q^K — ПМ возбужденного состояния ранга K и проекции Q; $C^{\alpha\alpha}_{b\beta c\gamma}$ — коэффициенты Клебша—Гордона; $\Delta = J_b'' - J_c''$. В нашем случае $K = 0$ и 2, а отличные от нуля $\Phi_0^0 = -1\sqrt{3}$, $\Phi_0^2 = -1\sqrt{30}$, $\Phi_{\pm 2}^2 = (1/2\sqrt{5})\,e^{\pm i(\pi+2\alpha)}$.

Q-переход ($J_b' = J_{a,c}''$). Значения f_Q^K определяются функцией Дьяконова при поглощении и для случая, когда световое поле не меняет заселенности основного ЭКВ уровня (α'', v_a'', J_a''), с которого идет поглощение, могут быть записаны как $f_0^0 = \frac{1}{3}\frac{\Gamma_p}{\Gamma_0}\varphi_0^0$, $f_0^2 = -\frac{1}{15}\frac{\Gamma_p}{\Gamma_2}\varphi_0^0$, $f_{\pm 2}^2 = -\frac{1}{5\sqrt{6}}\frac{\Gamma_p}{\Gamma_2 \mp 2i\Omega}\varphi_0^0$.

Эти выражения прямо следуют из формулы (2) [11]. Здесь φ_0^0 — ПМ основного состояния нулевого ранга, соответствующий концентрации частиц на уровне a, Γ_p — скорость поглощения, Γ_0 — скорость релаксации заселенности. Подстановка f_Q^K в (4) приводит к

$$\left.\begin{aligned} I_{\pm\alpha}^{(Q)} &= \frac{\Gamma_p \varphi_0^0}{3}\left[\frac{1}{3\Gamma_0} + \frac{1}{15\Gamma_2} + \frac{1}{5}\left(\frac{\Gamma_2\cos\alpha \pm 2\Omega\sin 2\alpha}{\Gamma_2^2 + 4\Omega^2}\right)\right], \\ P_\alpha^{(Q)} &= \frac{0.4\Omega\sin 2\alpha}{(\Gamma_2^2 + 4\Omega^2)\left(\frac{1}{3\Gamma_0} + \frac{1}{15\Gamma_2}\right) + 0.2\Gamma_2\cos 2\alpha}. \end{aligned}\right\} \qquad (5)$$

Здесь частота $\Omega = g_b B\mu_0/\hbar$. Для двухатомных молекул с $J \gg 1$, по-видимому, допустимо приближение $\Gamma_0 = \Gamma_2 = \Gamma$; для Te_2 (AO_u^+) это показано в [17]. Тогда (5) упрощается

$$P_\alpha^{(Q)} = \frac{2\frac{\Omega}{\Gamma}\sin 2\alpha}{2\left(1+4\frac{\Omega^2}{\Gamma^2}\right)+\cos 2\alpha}. \qquad (6)$$

Видно, что зависимость степени поляризации от Ω/Γ имеет дисперсионную форму. Для обычно выбираемого угла $\alpha = 45°$ получаем

$$P_{45°}^{(Q)} = \frac{\Omega/\Gamma}{1+4\Omega^2/\Gamma^2} \qquad (7)$$

Зависимость (7) приведена на рис. 1, кривая *1*; экстремумы расположены на $\Omega/\Gamma = \pm 0.5$, соответствующие значения степени поляризации равны ± 0.25. Однако эти значения степени не являются наибольшими. Определение абсолютных экстремумов $P_\alpha^{(Q)}$ по двум переменным α и Ω/Γ из (6) дает значение угла $\alpha_m = (1/2)\arccos\left[-1/(2+\sqrt{3})\right] \approx 52.8°$ и $\Omega/\Gamma = \pm\sqrt[4]{12}/4 \approx \pm 0.465$, при этом $P_{\alpha_m}^{Q} \approx \pm 0.2588$. Итак, с точки зрения получения наибольших значений степени поляризации для переходов Q-типа оптимальным является не угол $\alpha = 45°$, а угол $\alpha_m = \pm 52.77°$. Правда, выигрыш в амплитуде сигнала получается небольшой — порядка 3.5 % от максимума; вид контура Ханле приведен на рис. 1, кривая *2*.

P, R-переходы ($J_b' = J_c'' \pm 1$). Рассмотрим флуоресценцию при переходах *P, R*-типа в цикле $J_a'' \to J_b' \to J_c''$. В этом случае в выражении (4) $\Delta = \pm 1$. Связь отличных от нуля ПМ верхнего состояния f_Q^k и нижнего φ_0^0 выражается [11] как $f_0^0 = (\Gamma_p/3\Gamma_0)\,\varphi_0^0$, $f_0^2 = (\Gamma_p/30\Gamma_2)\,\varphi_0^0$ и $f_{\pm 2}^2 = \Gamma_p\varphi_0^0/(\Gamma_2 \mp 2i\Omega)\,10\sqrt{6}$. Интенсивность

$$I_{\pm\alpha}^{(P,R)} = (f_0^0/3) + (f_0^2/6) - (1/\sqrt{6})\,\mathrm{Re}\,(f_{\pm 2}^2 e^{-i(\pi\pm 2\alpha)}) =$$

$$= (\Gamma_p\varphi_0^0/3)\,[1/3\Gamma_0 + 1/60\Gamma_2 + (\Gamma_2\cos 2\alpha \pm 2\Omega\sin 2\alpha)/20\,(\Gamma_2^2 + 4\Omega^2)]. \qquad (8)$$

Выражение для степени линейной поляризации $P_\alpha^{(P,R)}$ в случае $\Gamma_2 = \Gamma_0 \equiv \Gamma$ имеет вид

$$P_\alpha^{(P,R)} = \frac{2\frac{\Omega}{\Gamma}\sin 2\alpha}{7\left(1+4\frac{\Omega^2}{\Gamma^2}\right)+\cos 2\alpha}. \qquad (9)$$

Оптимальная величина угла α может быть найдена аналогично случаю Q-переходов как $\alpha_m = (1/2)\arccos\left[-1/(7+4\sqrt{3})\right] \approx 47.1°$, чему соответствует $\Omega/\Gamma = \pm\sqrt[4]{147}/7 \approx 0.497$. Отсюда для перехода *P, R*-типа контур Ханле при оптимальном угле α_m практически неотличим от контура при $\alpha = 45°$ (рис. 1, кривая *3*).

Для $J \gg 1$ с помощью классического представления можно построить картину пространственного распределения моментов $\mathbf{J}_b$ возбужденного состояния (подробнее см. далее), наглядно иллюстрирующую суть эффекта Ханле. Изображения для *P, R*-переходов приведены на рис. 1 (внизу справа); они соответствуют значениям $\Omega/\Gamma = 0$ и $1/3$. Такой вид пространственного распределения угловых моментов обусловлен тем, что для переходов *P, R*-типа в классической модели осциллирующий диполь жестко связан с межъядерной осью молекулы и вращается вместе с ней вокруг $\mathbf{J}$ [18]. Видно, что распределение моментов $\mathbf{J}_b$ поворачивается вокруг $\mathbf{B}$ в направлении, зависящем от знака фактора Ланде.

Проявление дисперсионного сигнала Ханле основного состояния

Перейдем к случаю, когда нельзя пренебречь когерентностью основного состояния, возникающей при его опустошении в процессе поглощения $a \to b$, если скорость поглощения Γ_p сравнима со скоростью заселения безызлучатель-

ными процессами γ. Эффект достигается при лазерной оптической накачке [19] и дает возможность наблюдать эффект Ханле основного состояния [14] для Q-переходов в Na_2 ($X^1\Sigma_g^+$), K_2 ($X^1\Sigma_g^+$) и [20] для P, R-переходов Te_2 (XO_g^+). В этих работах регистрировались сигналы Ханле лорентцовской формы. Проследим, как проявляется суперпозиционный сигнал Ханле дисперсионной формы от основного и возбужденного состояний (анализ ситуации для циркулярно поляризованного возбуждения содержится в [21]). Теперь в основном состоянии имеются не только ПМ φ_0^0 (заселенность), но и моменты $\varphi_q^\varkappa$ более высоких рангов $\varkappa$ ($\varkappa$ — четное число для схемы возбуждения на рис. 1). Для нахождения ПМ возбужденного состояния f_Q^K, определяющих, следуя (4), интенсивность флуоресценции, необходимо решать систему уравнений движения

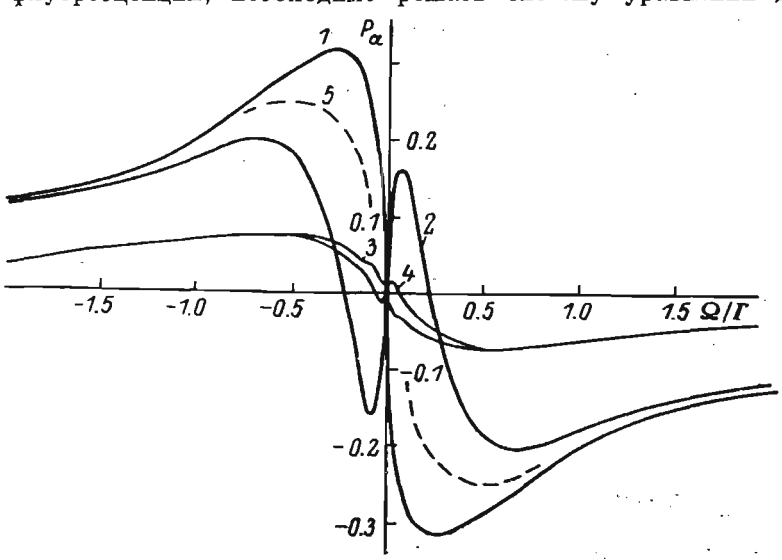

Рис. 2. Суперпозиционные сигналы Ханле дисперсионной формы (α=45°), рассчитанные по (9), (10).

Кривые *1* и *2* — для Q-перехода при равных и одинаковых знаках g_a и g_b; $\gamma_\varkappa = 3 \cdot 10^6$ с$^{-1}$, $\Gamma_p = 3 \cdot 10^6$ с$^{-1}$, $\Gamma_K = 86.2 \cdot 10^6$ с$^{-1}$. Кривые *3* и *4* — для P, R-переходов при равных и одинаковых знаках g_a и g_b; $\gamma_\varkappa = 2 \cdot 10^5$ с$^{-1}$, $\Gamma_K = 15.4 \cdot 10^5$ с$^{-1}$, $\Gamma_p = 3 \cdot 10^6$ с$^{-1}$. Кривая *5* соответствует графику *1* на рис. 1.

для f_Q^K и $\varphi_q^\varkappa$. Во многих случаях для незамкнутого (по [18]) цикла оптической накачки двухатомных молекул можно пользоваться моделью так называемой полностью открытой системы, когда в результате безызлучательной релаксации состояния, соседние с исходным уровнем (α'', v_a'', J_a'), поставляют только заселенность, а обратными спонтанными переходами $b \to a$ пренебрегают. Уравнения в такой форме приведены в [9]; здесь они записаны в асимптотическом пределе $J \to \infty$, следуя [16], где также анализируются их структура и алгоритм численного решения. Для стационарных условий возбуждения имеем

$$\left.\begin{aligned}
&\Gamma_p\Big(\sum_{\varkappa q} {}^K_Q D^\varkappa_q \varphi^\varkappa_q - \sum_{K'Q'} {}^K_Q D^{K'}_{Q'} f^{K'}_{Q'}\Big) - (\Gamma_K - iQ\Omega) f^K_Q = 0,\\
&\Gamma_p\Big(\sum_{KQ} {}^\varkappa_q D^K_Q f^K_Q - \sum_{\varkappa' q'} {}^\varkappa_q D^{\varkappa'}_{q'} \varphi^{\varkappa'}_{q'}\Big) - (\gamma_\varkappa - iq\omega_a)\varphi^\varkappa_q + \lambda^\varkappa_q \delta_{\varkappa 0} = 0,\\
&{}^\varkappa_q D^{\varkappa'}_{q'} = (-1)^\Delta \sqrt{\frac{2\varkappa'+1}{2\varkappa+1}} \sum_X \sqrt{2X+1}\, C^{X0}_{1\Delta 1-\Delta} C^{\varkappa' 0}_{X0\,\varkappa 0} C^{\varkappa q}_{Xq-q'\varkappa' q'} \Phi^X_{q-q'}(0).
\end{aligned}\right\} \qquad (10)$$

В уравнениях (10) учтены вынужденные переходы, а $\Delta = J_b' - J_a''$. Ясно, что задача определения зависимости наблюдаемых величин I_a и P_a от поля B содержит большое число параметров. Мы сочли целесообразным привести на рис. 2 результаты расчетов для параметров, имевших место в экспериментах при Q-переходах на K_2 [10, 14] и P, R-переходах на Te_2 [9, 20], и описание экс-

перимента настоящей работы. В обоих случаях ширина контура Ханле возбужденного состояния больше, чем основного, т. е. $g_a/\gamma \ll g_b/\Gamma$. При расчетах учитывались ПМ с $\varkappa \leqslant 10$, $K \leqslant 2$.

Из рис. 2 видно, что форма суперпозиционного сигнала Ханле существенно зависит от того, имеют ли факторы Ланде комбинирующих состояний g_a и g_b одинаковые или разные знаки (их величина $1 \cdot 10^{-5}$ [10] и $1.9 \cdot 10^{-4}$ соответство-

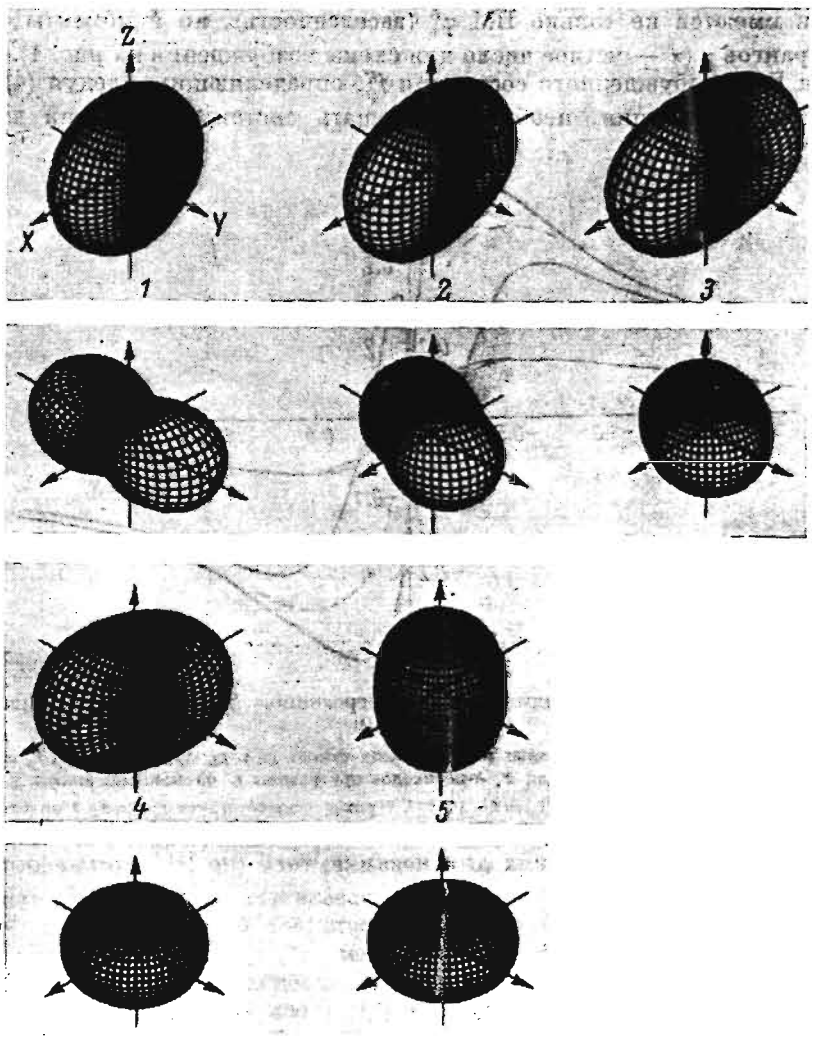

Рис. 3. Графические изображения пространственного распределения угловых моментов основного (внизу) и возбужденного (вверху) состояний в присутствии внешнего магнитного поля $\mathbf{B} \parallel OZ$.

Отношения $\omega/\gamma_\varkappa$ и $2/\Gamma_K$ соответственно равны: *1* — нулю, *2* — $\frac{1}{2}$ и 0.05, *3* — 2.6 и 0.11, *4* — 10 и 0.46, *5* — бесконечности. Плотность вероятности вверху содержит множитель $\Gamma_k/\gamma_\varkappa$.

вала ($X^1\Sigma_g^+$, 1, 73) и ($B^1\Pi_u$, 8, 73) для K_2). В случае разных знаков суперпозиционный сигнал по форме не слишком отличается от линейного сигнала Ханле возбужденного состояния (рис. 2, кривые *1* и *3*). Если знаки g_a и g_b одинаковы, то экстремумы в дисперсионной структуре от основного и возбужденного состояний имеют противоположные знаки (рис. 2, кривая *2*). Для переходов P, R-типа наблюдается похожая ситуация. Меньшая относительная амплитуда дополнительной структуры, возникающей от основного состояния (рис. 2, кривая *4*) связана в основном с меньшим значением параметра оптической накачки Γ_p/γ, принятым при расчетах. Небольшое нарушение монотонности

возрастания сигнала при разных знаках g_a и g_b (их величина $1.68\cdot10^{-4}$ [9] и $0.54\cdot10^{-4}$ [17]) на кривой *3* объясняется тем, что отношение g_a/γ к g_b/Γ имеет бо́льшую величину, чем для кривой *1*. Понятно, что если величина g_b/Γ пренебрежимо мала по сравнению с g_a/γ, то структура, связанная с основным состоянием, будет выделяться также и при разных знаках g_a и g_b.

Так как решение (10) достаточно сложно, здесь представляет интерес графическое изображение пространственного распределения угловых моментов ансамбля в присутствии внешнего магнитного поля (рис. 3). Распределение получено при помощи ЭВМ с использованием графопостроителя по методике, описанной в [22]. При этом осуществляется переход от представления распределения угловых моментов при помощи ПМ к представлению классической плотности вероятности [23-26]. На рис. 3 приведен случай переходов P, R-типа, который был реализован в эксперименте в настоящей работе: знаки g_a и g_b состояний одинаковы. Видно, что угловые моменты нижнего состояния оптически выстроены преимущественно вдоль вектора **E** возбуждающего света. С наложением поля **B** вдоль OZ распределение поворачивается и уменьшается анизотропия в плоскости XOY. При этом анизотропия в возбужденном состоянии увеличивается («вытягивание» тороида вдоль OX), что соответствует проявлению сигнала Ханле основного состояния. Это связано с тем [20, 25], что, когда эффект Ханле от основного состояния уже проявился, а от возбужденного еще не заметен (рис. 3, положение *3*), поляризация P_L превышает достижимую в пределе слабого возбуждения величину $P=1/7$, т. е. анизотропия распределения больше, чем на рис. 2 для $B=0$. При еще больших полях разворачивается распределение возбужденного состояния (рис. 3, положение *4*) вплоть до полной изотропии в плоскости XOY внизу и наверху (рис. 3, положение *5*).

Эксперимент

Приведенное рассмотрение показывает, что суперпозиционный сигнал Ханле основного и возбужденного состояний дисперсионной формы позволяет определить знаки магнитных моментов комбинирующих состояний. В эксперименте ставилась задача получить такие сигналы для молекул $^{39}K_2$ и $^{130}Te_2$.

Экспериментальная установка подобна использованной ранее в [9, 10, 20]. Луч аргонового (типа ЛГН-402) либо гелий-неонового (типа ЛГ-38) лазера направляется в ячейку с насыщенными парами теллура либо калия. Ячейка помещается между полюсами электромагнита и соединяется с вакуумным постом. Флуоресценция наблюдается вдоль магнитного поля по схеме, приведенной на рис. 1, что обеспечивается установленным между полюсами магнита поворотным зеркалом. Удобная для регистрации линия резонансной серии выделяется монохроматором ДФС-12 (0,5 нм/мм). Входная щель ДФС-12 разделяется по высоте на две части, перед которыми устанавливаются поляроиды под углом 45° и −45° к **E** (рис. 1). Соответствующие участки выходной щели с помощью световодов соединяются с двумя ФЭУ-79, работающими в режиме счета фотонов. Таким образом, одновременно по двум каналам накапливаются одноэлектронные импульсы с ФЭУ, число которых определяет интенсивность $I_{\pm\alpha}$.

В молекуле $^{39}K_2$ лазерная линия 632.8 нм эффективно возбуждает ЭКВ переход Q-типа ($X^1\Sigma_g^+$, 1, 73) → ($B^1\Pi_u$, 8, 73); идентификация КВ чисел по [27]. Сигнал Ханле дисперсионной формы на линии Q_{11} резонансной серии представлен на рис. 4 для двух случаев накачки: слабой ($\Gamma_p \ll \gamma$) и сильной ($\Gamma_p \gg \gamma$). В первом случае данные эксперимента хорошо аппроксимируются зависимостью (7); сплошная кривая *1* соответствует $\tau_{sp}=11.6$ нс [14] и величине фактора Ланде $1/J_b'(J_b'+1)=1.9\cdot10^{-5}$.

Во втором случае отношение Γ_p/γ увеличено за счет повышения мощности лазера и понижения T от 503 до 453 К, что уменьшает скорость релаксации γ из-за соударений K_2 с атомами калия. Из зависимости *2* на рис. 4 хорошо видно обусловленное суперпозицией эффекта Ханле верхнего и нижнего состояний значительное сужение сигнала, но без дополнительной структуры (здесь и далее пунктирные линии лишь соединяют экспериментальные точки). Сравнение с кривыми *1* и *5* на рис. 2 позволяет утверждать, что знаки факто-

ров Ланде g_a и g_b основного и возбужденного состояний противоположны. А так как g_b обусловлен орбитальным моментом электрона в $^1\Pi$-состоянии (см. (1)), т. е. отрицателен, то g_a положителен и обусловлен вращением ядер. Этот вывод согласуется с результатом измерения знака g_a для $Li_2(X^1\Sigma_g^+)$ в [6], см. также [28].

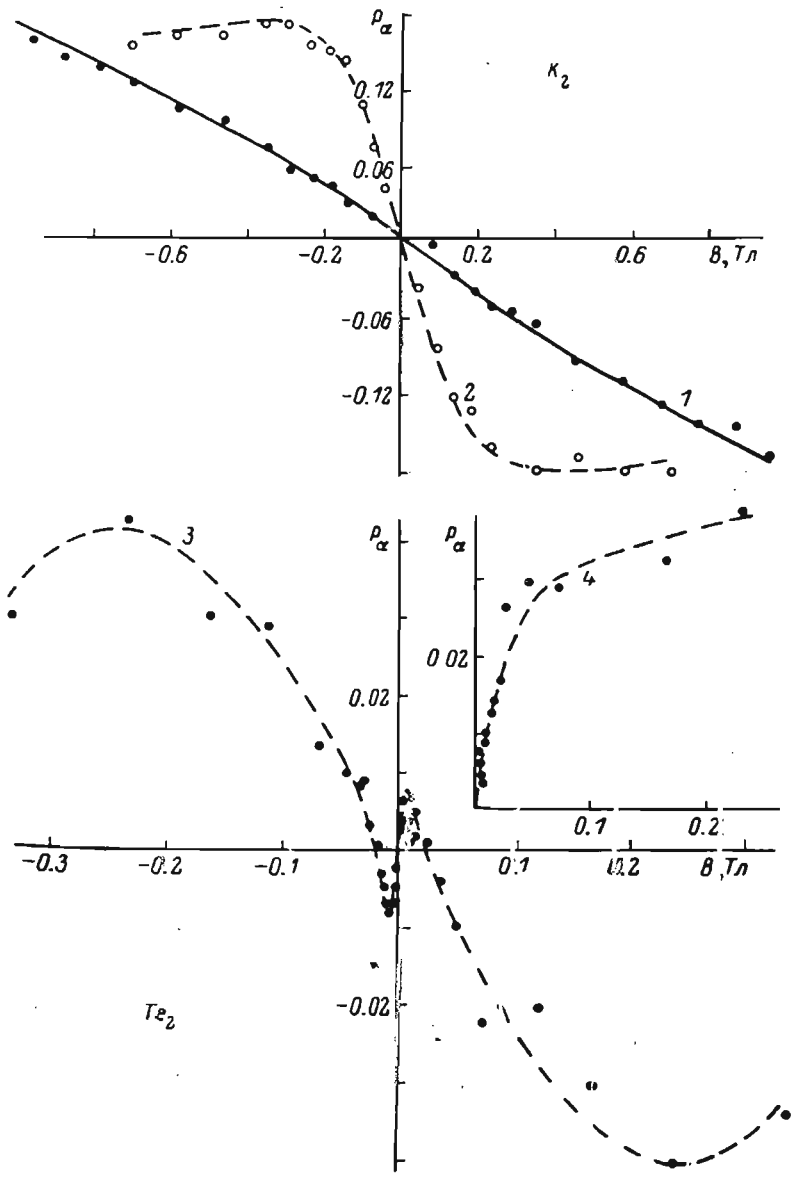

Рис. 4. Экспериментально зарегистрированные сигналы Ханле дисперсионной формы для $^{39}K_2$ и $^{130}Te_2$.

В молекуле $^{130}Te_2$ исследовались два ЭКВ перехода в полосе $AO_u^+ - XO_u^+$: а именно переход $(XO_g^+, 6, 52) \rightarrow (AO_u^+, 11, 53)$ при возбуждении лазерной линией 514.5 нм и $(XO_g^+, 1, 132) \rightarrow (AO_u^+, 11, 131)$, возбуждаемый линией 488.0 нм. Идентификация переходов здесь приведена согласно данным [29]. Условия эксперимента (T=600 K, $[Te_2]=2\cdot10^{13}$ см$^{-3}$) выбирались такими, при которых, согласно [20], $\Gamma_p/\gamma \geqslant 1$ и заметно проявление нелинейного сигнала Ханле нижнего ЭКВ уровня. Результаты эксперимента демонстрируют кривые *3* и *4* на рис. 4. Из крупномасштабной структуры графиков, отражающей главным образом вид контуров Ханле возбужденных уровней, видно, что магнитные

моменты для (AO_u^+, 11, 53) и (AO_u^+, 11, 131) имеют разные знаки, что по аналогии с [8] для Se_2 свидетельствует о наличии возмущений в AO_u^+-состоянии $^{130}Te_2$. При этом знак фактора Ланде для (11, 131) такой же, как и для K_2 ($B^1\Pi_u$), т. е. отрицателен, а для (11, 53) — положителен. Представляет интерес установление знака магнитного момента основного состояния Te_2 (XO_g^+), для которого абсолютная величина фактора Ланде определена в [9] как $g_a=(1.68\pm\pm0.05)\cdot10^{-4}$. Так как в зависимости *3* на рис. 4 отчетливо проявляется узкая (полуширина порядка 0.005 Тл) структура дисперсионной формы, то знаки магнитных моментов для (XO_g^+, 1, 131) и (AO_u^+ 11, 131) одинаковы. Это следует из сравнения с расчетной кривой *4* на рис. 2. Следовательно, фактор Ланде XO_g^+-состояния Te_2 отрицателен. Такой вывод согласуется со знаком, который дает приблизительное выражение [3, 5] $g_a=-4B''/\lambda''$, где B'' — вращательная константа, $2\lambda''=1975$ см$^{-1}$ — расщепление между термом XO_g^+ и лежащим выше термом $X1^+$ для димера теллура.

Литература

[1] Герцберг Г. Спектры и строение двухатомных молекул. М., 1949.
[2] Таунс Ч., Шавлов А. Радиоспектроскопия. М., 1959.
[3] Büchler A., Meschi D. J. — J. Chem. Phys., 1975, v. 61, p. 3586.
[4] Mc Clintock M., Demtröder W., Zare R. N. — J. Chem. Phys., 1969, v. 51, p. 5509.
[5] Gouedard G., Lehmann J. C. — J. de Phys. Lett., 1977, v. 38, p. L85.
[6] Brooks R. A., Anderson C. N., Ramsey N. F. — Phys. Rev., 1964, v. 136A, p. 62.
[7] Dalby F. W., Vigue J., Lehmann J. C. — Can. J. Phys., 1975, v. 53, p. 140.
[8] Gouedard G., Lehmann J. C. — Faraday Disc. Chem. Soc., 1981, v. 71, p. 143.
[9] Ferber R. S., Okunevich A. I., Schmit O. A., Tamanis M. Ya. — Chem. Phys. Lett., 1982, v. 90, p. 476.
[10] Аузиньш М. П., Таманис М. Я., Фербер Р. С. — Опт. и спектр., 1985, т. 59, в. 6, с. 1328.
[11] Аузиньш М. П., Таманис М. Я., Фербер Р. С. — ЖЭТФ, 1986, т. 90, с. 1182.
[12] Hanle W. — Z. Phys., 1924, v. 30, p. 93.
[13] Чайка М. П. Интерференция вырожденных атомных состояний. Л., 1975.
[14] Ferber R. S., Schmit O. A., Tamanis M. Ya. — Chem. Phys. Lett., 1979, v. 61, p. 441.
[15] Дьяконов М. И. — ЖЭТФ, 1964, т. 47, с. 2219.
[16] Аузиньш М. П. — Изв. АН ЛатвССР. Сер. физ. и техн. наук, 1984, т. 1, с. 9.
[17] Ferber R. S., Schmit O. A., Tamanis M. Ya. — Chem. Phys. Lett., 1982, v. 92, p. 393.
[18] Феофилов П. П. Поляризованная люминесценция атомов, молекул и кристаллов. М., 1959.
[19] Drullinger R. E., Zare R. N. — J. Chem. Phys., 1969, v. 51, p. 5532.
[20] Таманис М. Я., Фербер Р. С., Шмит О. А. — Опт. и спектр., 1982, т. 53, в. 4, с. 755.
[21] Аузиньш М. П., Фербер Р. С. — ЖТФ, 1985, т. 55, с. 1591.
[22] Аузиньш М. П. — Опт. и спектр., 1986, т. 60, в. 3, с. 403.
[23] Ducloy M. — J. Phys. B, 1976, v. 9, p. 357.
[24] Насыров К. А., Шалагин А. М. — ЖЭТФ, 1981, т. 81, с. 1649.
[25] Аузиньш М. П., Фербер Р. С. — Изв. АН ЛатвССР. Сер. физ. и техн. наук, 1984, т. 1, с. 16.
[26] Аузиньш М. П., Фербер Р. С. — Опт. и спектр., 1985, т. 59, в. 1, с. 11.
[27] Engelke F., Hage H., Schüle U. — Chem. Phys. Lett., 1984, v. 106, p. 535.
[28] Flygare W. H., Benson R. C. — Mol. Phys., 1971, v. 20, p. 225.
[29] Verges J., Effantin C., Babaky O., d'Incan J., Prosser S. J., Barrow R. F. — Phys. Scripta, 1982, v. 25, p. 338.

Поступило в Редакцию 14 января 1987 г.

АКАДЕМИЯ НАУК СССР
Научный совет по проблеме "Спектроскопия атомов и молекул"
Институт спектроскопии

АКАДЕМИЯ НАУК УССР
Институт полупроводников
Институт физики

МИНИСТЕРСТВО ВЫСШЕГО И СРЕДНЕГО СПЕЦИАЛЬНОГО ОБРАЗОВАНИЯ УССР
Киевский государственный университет им. Т.Г.Шевченко.

XX ВСЕСОЮЗНЫЙ СЪЕЗД ПО СПЕКТРОСКОПИИ

Тезисы докладов

Часть I
Киев, сентябрь 1988 г.

Киев Наукова думка 1988

УДК 539.196

ВРЕМЕНА ЖИЗНИ КОЛЕБАТЕЛЬНО-ВРАЩАТЕЛЬНЫХ УРОВНЕЙ ЭЛЕКТРОННО-ВОЗБУЖДЕННЫХ СОСТОЯНИЙ $^{130}Te_2$

М.П.Аузиньш, М.Я.Таманис, Я.А.Харья

Работа посвящена определению времени жизни $\tau_{сп}$ колебательно-вращательных (КВ) v',J'-уровней $A0_u^+$ и $B0_u^+$ -состояний двухатомной молекулы теллура. Информация об этой характеристике в настоящее время недостаточно полна и противоречива. В/I/ для $B0_u^+$ уровней с $v'=0,1,3$ измерены значения $\tau_{сп}$ от 50 до 70 нс, а в /2/ для $v'=5$ указано $\tau_{сп}$ равное 4 нс. Аналогично для $A0_u^+$ уровней с $v'=11,12$ $\tau_{сп} \approx 700$ нс/I/, а с $v'=16,17$ по данным /3/ 60-70 нс. Настоящий эксперимент проведен нами с целью уточнить ситуацию.

Терм	v'	J'	$\tau_{сп}$, нс
$B0_u^+$	2	197	75±10
	3	99	68± 5
	5	103	67± 3
	5	137	45± 6
	7	95	55± 5
$A0_u^+$	6	87	800±100
	11	131	620±50
	13	133	160±20
	14	89	40±10

$A0_u^+$ и $B0_u^+$-состояния возбуждались линиями Ar^+ и He-Cd лазеров. КВ уровни идентифицировались при расшифровке фотоэлектрически зарегистрированных спектров молекулярной флуоресценции, содержащих, как правило, несколько дублетных прогрессий. Длительность флуоресценции после импульсного возбуждения измерялась на отдельных спектральных линиях методом задержанных совпадений с применением счета фотонов, время-амплитудного преобразователя и анализатора импульсов АИ-256. Полученные значения $\tau_{сп}$ приведены в таблице. Следует отметить два факта. Во первых, в противоположность /2/, нами получено, что $B0_u^+$ уровень $v'=5$ имеет характерное для этого состояния время жизни равное ~50 нс. Во вторых, в $A0_u^+$-состоянии действительно имеет место резкое уменьшение $\tau_{сп}$, которое по нашим данным наступает с $v'=13$. Причина этого интересного факта выясняется.

/I/ R.S.Ferber, O.A.Shmit, M.Ya.Tamanis – Chem.Phys.Lett., 92, 393, 1982.
/2/ А.С.Редчук. Автореферат кандидатской диссертации. МГУ, М, 1985.
/3/ J.Carion, Y.Guern, J.Lotrian, P.Luc,- J.Phys.B:At.Mol.Phys., 15, L841, 1982.

Quantum beats in the fluorescence kinetics of $Te_2(A0_u^+)$ molecules

I. P. Klintsare, M. Ya. Tamanis, and R. S. Ferber

(Received 3 December 1987, in revised form, 19 August 1988)
Opt. Spektrosk. **66**, 827–829 (April 1989)

The method of quantum beats in the kinetics of laser-induced fluorescence during pulse excitation with the 514.5-nm line of an Ar^+ laser is used to determine the dependence of the splitting frequency of Zeeman sublevels with $\Delta M' = \pm 2$ on the external magnetic field for the $^{130}Te_2$ state ($A\,0_u^+, v' = 6, J' = 87$). A Landé factor value for this level equal to $g_{J'} = -(1.07 \pm 0.08) \times 10^{-4}$ is obtained.

Quantum beats (QB) in the emission following excitation by a pulse of width $\Delta t \ll \Gamma^{-1}$, where Γ^{-1} is the characteristic relaxation time, are a clear manifestation of interference of nondegenerate coherent states,[1] in particular, in a system of Zeeman sublevels M_J, split by an external magnetic field B. The effect was applied quite extensively to atoms (see the surveys of Refs. 1 and 2), and, beginning with Ref. 3, to $^{127}I_2(B\,^3\Pi_{0_u^+})$, and for diatomic molecules in the variant of laser-induced fluorescence (LIF). References 4–8 investigated the magnetism of electronically excited vibrational–rotational (EVR) states; in particular, Landé factors, hyperfine structure, and influence of the interaction between terms were measured. Thus, the rotational Landé factor in the Br_2 molecule was determined in Ref. 4, and it was determined in the free radical OH in Ref. 5. Particular mention should be made of Ref. 6, where a combination of QB spectroscopy and scanning over EVR levels permitted a detailed study of the magnetism and perturbation of states on the $^{80}Se_2(BO_u^+)$ molecule. The QB effect was also studied in Ref. 7 on $NO_2(A\,^2B_2)$ and in Ref. 8 on SO_2. The QB effect in the system of magnetic sublevels M_J'' of the ground electronic state, after its pulsed optical emptying, was recorded in Ref. 9 on $^{39}K_2(X\,^1\Sigma_g^+)$. Thus, magnetic QB have recently begun to be applied to the study of small molecules. Of particular interest here are states in which the projections of the orbital and spin angular momenta are $\Lambda = 0$, $S = 0$ (or $\Omega = 0$ for the Hund c coupling), i.e., with closed electron shells.[10] Moreover, as was found in Ref. 6, the magnetic moment is extremely sensitive to weak perturbations caused by interaction between terms.

In the present work, the QB method in LIF is applied to $^{130}Te_2$ molecules in the $A\,0_u^+$ state. Measurements of the $g_{J'}$ factor carried out in Refs. 11 and 12 by the method of the Hanle effect showed that for $Te_2(A\,0_u^+, v', J')$, the $g_{J'}$ factors are small, lend themselves poorly to interpretation, and change in both magnitude and sign for different v' and J'. In this connection, it is desirable to expand the studies by applying the QB method. An advantage of the QB method in comparison with the Hanle effect[1,13] is the possibility of direct determination of $g_{J'}$ (the Hanle method gives the product $g_{J'}\Gamma^{-1}$).

The experimental apparatus is similar to the one described in Ref. 14. A beam from a LGN-402 continuous Ar^+ laser in multiple-frequency operation was modulated by an ML-102 Pockels-effect electrooptical modulator; the pulse duration was $\Delta t \approx 100$ nsec. A magnetic field up to $B = 1$ T was generated by an electromagnet, between the poles of which was placed a quartz fluorescence cell measuring $10 \times 10 \times 30$ mm, connected to a vacuum station. A small rotatable mirror between the pole and the cell made it possible to achieve an experimental geometry in which the vector E of the linearly polarized laser beam was orthogonal to the field B and to the direction of observation of LIF. The afterglow kinetics were recorded by the delayed coincidence method, the photon counting being done with an FEU-79 photomultiplier in the start–stop mode with storage over time by means of an amplitude converter using an AI-256-6 pulse analyzer.

We chose for the measurements the $^{130}Te_2(A\,0_u^+)$ level with $v' = 6, J' = 87$, excited by the 514.5-nm laser line from

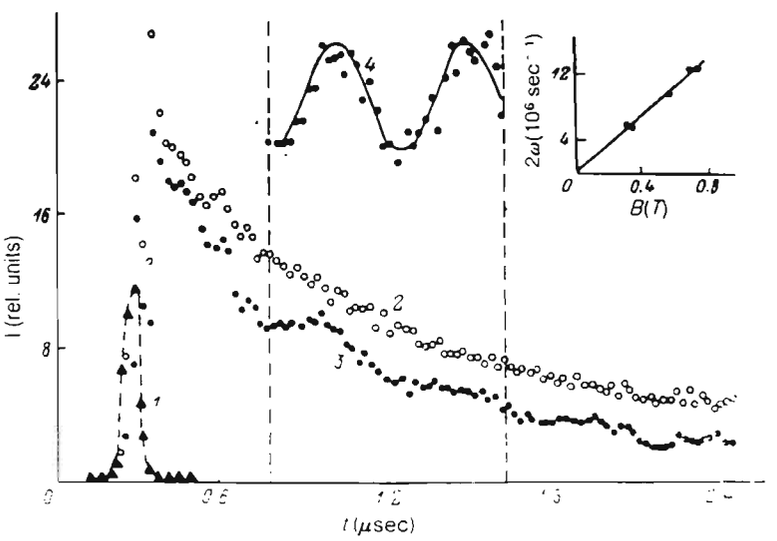

FIG. 1. Signal of quantum beats of $^{130}Te_2(A\,0_u^+, v' = 6, J' = 87)$. 1—exciting pulse, 2—LIF kinetics at $B = 0$, 3—LIF kinetics at $B = 0.702$ T, 4—QB signal corrected for the damping of the beat amplitude. Vapor temperature, 700 K.

 0030-400X/89/040484-02$05.00

the $^{130}Te_2(X\,0_g^+, 3, 88)$ state.[15] The radiation was recorded on the R_5 line, isolated by a DFS-12 monochromator. Figure 1 shows the recorded signals of the exciting pulse (curve *1*) as well as the signals of LIF kinetics without in the absence of a magnetic field (curve *2*) and in the presence of a field $B = 0.702$ T (curve *3*). Radiation linearly polarized parallel to **E** was recorded. It is evident that the presence of a magnetic field gives rise to harmonic modulation with a falling amplitude against a background of exponential decay of LIF. For *P*- and *R*-type transitions in the approximation of $J', J'' \to \infty$ and δ-pulse excitation, such a signal can be described as follows[13,14]:

$$I_{\parallel,\perp} \sim 20 \exp(-\Gamma_0 t) \div (1 \pm 3\cos 2\omega t) \exp(-\Gamma_2 t), \quad (1)$$

where the plus or minus signs correspond to the observation of polarization parallel or orthogonal to **E**, Γ_0 and Γ_2 are the rates of population relaxation or alignment, and $2\omega = 2\mu_0 B g_{J'}/\hbar$ is the frequency of magnetic splitting of coherent sublevels with $\Delta M' = \pm 2$. Assuming $\Gamma_0 = \Gamma_2 \equiv \Gamma$ (which is entirely sound for molecules with large J'), we arrive at the simple expression

$$I_{\parallel,\perp} \sim (21 \pm 3\cos 2\omega t) \exp(-\Gamma t). \quad (2)$$

Under actual experimental conditions, the finite duration of the exciting pulse (see Fig. 1) and other depolarizing factors lead to a decrease of the modulation index and to the appearance of the initial phase φ, and therefore

$$I_{\parallel,\perp} = |A \pm B\cos(2\omega t + \varphi)| \exp(-\Gamma t), \quad (3)$$

where $B/A < 1/7$ (let us recall that 1/7 is the limiting degree of LIF polarization in the case of *P*- and *R*-type transitions).

To determine the frequency of the QB level, we first determined Γ from the kinetic signal at $B = 0$ (curve *2*), then multiplied the values of curve *3* by $\exp(\Gamma t)$. This makes it possible to change to

$$I_1 = C_1 \cos 2\omega t + C_2 \sin 2\omega t + C_3 \quad (4)$$

and determine one nonlinear parameter ω by fitting. The result of the approximation is demonstrated by curve *4*, obtained for $\omega = 0.133 \times 10^8$ Hz, $\Gamma = 1.72 \times 10^6$ sec^{-1}. The analysis involved the use of the middle region of the decay curve, since initially, the form of the excitation has an effect, and the last channels do not contain information because of the small amplitude of QB.

The inset of Fig. 1 shows the dependence of the 2ω values thus determined for different magnetic fields. Linear approximation leads to the value of the Landé factor $g_{J'} = (1.07 \pm 0.08) \times 10^{-4}$ for $^{130}Te(A\,0_u^+, v' = 6, J' = 87)$; the error here is one standard deviation. As in Ref. 12, determination of the sign of the Landé factor from the Hanle signal of dispersion form showed that $g_{J'} < 0$, i.e., the magnetic moment is antiparallel to the mechanical moment. It is interesting to note that according to Refs. 11 and 12 for the state $v' = 11$, $J' = 53$ of the same term $A\,0_u^+$, $g_{J'} = 0.52 \times 10^{-4}$ and has a different sign, and for $v' = 11$, $J' = 131$, $g_{J'} = -0.45 \times 10^{-4}$.

The authors thank M. P. Auzinsh and A. P. Brukhovetskii for helpful consultations and assistance in the analysis of the data.

[1]E. B. Aleksandrov, Usp. Fiz. Nauk **107**, 592 (1972) [Sov. Phys. Usp. **15**, 209 (1972)].
[2]E. B. Alexandrov, *Quantum Beats*, in *Proceedings 6. International Conference on Atomic Physics, Zinatne, Riga* (Plenum P., New York, 1979), p. 521.
[3]R. Wallenstein, J. A. Paisner, and A. L. Schawlow, Phys. Rev. Lett. **32**, 1333 (1974).
[4]R. Luypaert, J. Van Graen, J. Coremans, and G. De Vlieger, J. Phys. **14**, 2575 (1981).
[5]P. Lebow, F. Raab, and M. Metcalf, Phys. Rev. Lett. **42**, 85 (1979).
[6]G. Gouedard and J.-C. Lehmann, Farad. Discus. Chem. Soc. **71**, 143 (1981).
[7]P. J. Brucat and R. N. Zare, J. Chem. Phys. **78**, 100 (1983).
[8]H. Watanabe and S. Tsuchlya, J. Phys. Chem. **87**, 906 (1983).
[9]M. P. Auzinsh, M. Ya. Tamanis, and R. S. Ferber, Pisma Zh. Eksp. Teor. Fiz. **42**, 132 (1985) [JETP Lett.].
[10]T. K. Rebane, *Contemporary Problems in Quantum Chemistry* (Leningrad, 1986), p. 165.
[11]R. S. Ferber, O. A. Shmit, and M. Ya. Tamanis, Chem. Phys. Lett. **92**, 393 (1982).
[12]M. P. Auzinsh, M. Ya. Tamanis, and R. S. Ferber, Opt. Spektrosk. **63**, 989 (1987) [Opt. Spectrosc. (USSR) **63**, 582 (1987)].
[13]M. P. Chaika, *Interference of Degenerate Atomic States* (Leningrad, 1975).
[14]M. P. Auzinsh, M. Ya. Tamanis, and R. S. Ferber, Zh. Eksp. Teor. Fiz. **90**, 1182 (1986) [Sov. Phys. JETP **63**, 688 (1986)].
[15]J. Vergas, C. Effantin, O. Babaky, J. d'Incan, S. J. Prosser, and R. F. Barrow, Phys. Scripta **25**, 338 (1982).

Anomalous behavior of Lande factors of the $Te_2(B0_u^+)$ molecule of the intensities of the $B0_u^+ - X1_g^+$ transition

I.P. Klintsare, A.V. Stolyarov, M.Ya. Tamanis, R.S. Ferber, and Ya.A. Kharya

(Received 21 April 1988)
Opt. Spektrosk. 66, 1018–1021 (May 1989)

From measurements of the fluorescence polarization of tellurium vapor molecules $Te_2(B0_u^+, v', J')$ as a function of the external magnetic field (Hanle effect) and independently of measured times of radiative decay, we have determined the magnitude and sign of Lande factors $g_{v'J'}$ for different vibration–rotation (VR) levels with vibrational numbers v' from 0 to 7, excited by the lines of Ar^+ and He–Cd lasers. Considerable variations of the magnitude and sign of $g_{v'J'}$ were observed for different VR levels of the $Te_2(B0_u^+)$ state. Recorded at the same time were the singularities in the ratios of the P, R, and Q branches of the intensities of the intercombination series of laser-induced fluorescence $(B0_u^-, v', J') \rightarrow (X1_g^+, v'', J'')$. Both effects are interpreted from a unified standpoint as a manifestation of rotation-induced heterogeneous ($\Delta\Omega = 1$) interaction of the electronic terms $(B0_u^+)$ and $A1_u$.

The magnetism of molecular states with closed electron shells, when the projections of orbital and spin angular momenta on the axis $\Lambda = \Sigma = 0$ are zero, is a direct result of the mixing of wave functions with states having a nonzero electronic paramagnetism (concerning the nature of such magnetism, see Ref. 1). Hence, the Lande factors (magnitude and sign) of such diamagnetic states can give a highly sensitive method for studying perturbations and determining the parameters of the perturbing term. Studies dealing with the ground state $X\Sigma_g^+$ of alkali dimers,[2–4] as well as with the $X0_u^+$ state of the tellurium dimer,[5] involved measurement of Lande factors, which characterize the electronic state as a whole. For the electronically excited term of the selenium dimer $^{80}Se(B0_u^+)$, according to Ref. 6, one can also indicate a typical value of the Lande factor with variations only near local perturbations. An entirely different situation was observed in the case $^{130}Te_2(B0_u^+)$ (see Table I), where it is generally difficult to talk about the magnitude and sign of the Lande factor which are characteristic of the term as a whole.

The experimental values of Lande factors $g_{v'J'}$ were obtained from Hanle signals[7] of laser-induced fluorescence (LIF) of tellurium vapor in a quartz cell ($T = 650$ to 720 K) during excitation by laser lines of wavelength λ_{exc} equal to 457.9, 476.5, and 488.0 nm of an argon Ar^+ laser, as well as the 441.6-nm line of helium–cadmium laser. Examples of Hanle profiles are given in Fig. 1(a), and from them, the values of $g_{v'J'}$ τ_{sp} were determined. Then, with the aid of separately measured lifetimes[8] τ_{sp}, the values of $g_{v'J'}$ for the tabulated vibrational–rotational (VR) levels are determined. The error of determination of $g_{v'J'}$ amounts to ~ 15–20%. The sign of the Lande factors was determined from Hanle signals of dispersions shape [see Fig. 1(b) and (c), Refs. 7 and 9].

To interpret the data obtained, we shall assume that the VR length $Te_2(B0_u^+, v', J')$ is perturbed by the neighborhood $A1_u$ state $Te_2(A1_u, v', J')$ (the difference between T_e is 13 cm^{-1}; see the term diagram in Ref. 10), and this interaction is weak and caused by the nondiagonal terms of the rotation operator H_R. Then the effective wave function may be represented in the form

$$|\psi^*\rangle = (1 - c^2)^{-1/2} |B0_u^+\rangle + c\,|A1_u^+\rangle, \tag{1}$$

where c is the mixing coefficient, equal to

$$c = \frac{H_R}{\Delta E} = \frac{2\eta \langle 0v'J' | R^{-2} | 1v^*J'\rangle \sqrt{J'(J'+1)}}{E(0, v', J') - E(1, v^*, J')}. \tag{2}$$

and η is a parameter which for heterogeneous perturbation is of the order of unity.[11] The Lande factor is calculated from the mean value of the Zeeman Hamiltonian of the level studied, and for $Te_2(A1_u, v', J')$ is equal to

$$g_{v'J'} \approx 2c \sqrt{1 - c^2}\, G\Omega \langle 0v'J' | 1v^*J'\rangle \sqrt{2J'(J'+1)}. \tag{3}$$

where $\Omega = 1$ and $G = \langle 0|L_+ + 2S_+ | -1\rangle$ is a parameter to unity, which is difficult to calculate theoretically. Using Eq. (2), we obtain for $g_{v'J'}$, the approximate expression

$$g_{v'J'} \approx 2\sqrt{2}\, G\eta \frac{\langle 0v'J' | R^{-2} | 1v^*J'\rangle \langle 0v'J' | 1v^*J'\rangle}{E(0, v', J') - E(1, v^*, J')}. \tag{4}$$

When $G\eta = 3$, the calculation gives values of $g_{v'J'}$ which have the same sign as the measured values and are close to them in magnitude (see Table I). The VR wave functions necessary for the calculation were determined from the solution of the radial Schrödinger equation with

TABLE I. Measured $g_{v'J'}^{exp}$ and calculated $g_{v'J'}^{theor}$ Lande factors for different VR levels v', J'' of the diatomic molecule $^{130}Te_2(B0_u^+)$.

λ_{exc}	v'	J'	$g_{v'J'}^{exp} \cdot 10^3$	$g_{v'J'}^{theor} \cdot 10^3$
496.5	0	107	−2.00	−2.14
488.0	0	179	−1.15	−1.27
488.0	1	243	0.36	0.36
476.5	2	197	0.10	0.27
457.9	3	99	0.15	0.20
488.0	3	251	−0.30	−0.31
441.6	5	103	−0.23	−0.29
457.9	5	137	−0.36	−0.40
488.6	7	95	0.31	0.28

 0030-400X/89/050595-03$05.00

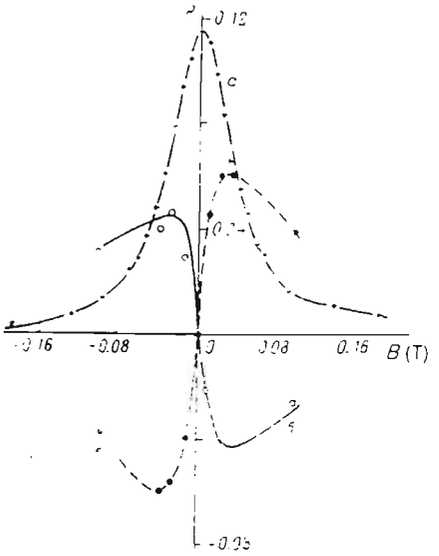

FIG. 1. Degree of polarization of LIF $P = (I_1 - I_2)/(I_1 + I_2)$ as a function of magnetic field B (Hanle effect) of the $^{130}Te_2$ ($B0_u^+$, 13.251) level for signals of Lorentzian shape (a), when the polarization of $I_{1,2}$ is either parallel or orthogonal to the excitation vector E, and signals of dispersion shape (b), when $I_{1,2}$ are polarized at an angle $\pm\pi/4$ to E [dashes denote the dispersion signal of the $(B)_u$, 11.234) level].

effective vibrational potentials[12] on the basis of the RKR procedure with molecular constants taken from Refs. 10 and 13. It was found that the oscillations of sign were related to the sign of ΔE in the denominator of Eq. (4). In Eq. (1), it is understood that the RV level ($B\,0_u^+$,v',J') interacts primarily with one VR level ($A\,1_u$,v^*,J'), and it is also assumed that $c \ll 1$. The above was confirmed by a calculation of c for different v^*; their small contribution is due to the increase in ΔE and decrease in $\langle 0v'J'|1v^*J'\rangle$.

Special measurements were carried out in order to determine how the interaction (1) changes the intensity of the P, R, and Q branches of the intercombination ($\Delta\Omega = 1$) transition $B\,0_u^+ - X\,1_g^+$ in comparison with the expected ones when the charger of the transitions is adiabatic (a qualitative discussion of such an effect is given in Ref. 10). The results are shown in Fig. 2. For their interpretation, we shall also proceed from (1) and (2); the intensity of the transition is

$$I_{v'J'}^{v''J''} = \frac{64\pi^4\nu^3}{3h}\left[(1-c^2)\,|d_{01}|^2 + c^2\,|d_{11}|^2 + 2c(1-c^2)\,d_{01}d_{11}\right], \tag{5}$$

where the dipole moments of the transition are

$$\left.\begin{aligned} d_{01} &= \mu_\perp \langle v'J' | v''J''\rangle\, \alpha(J', J'', \Delta\Omega = -1), \\ d_{11} &= \mu_\parallel \langle v^*J' | v''J''\rangle\, \alpha(J', J'', \Delta\Omega = 0), \end{aligned}\right\} \tag{6}$$

and α are the direction cosines.[11] Finally, for the intensities of the P, R, and Q branches, one can obtain expressions which, allowing for the simplifications used for $J' \gg 1$, $c \ll 1$, are

$$I_Q \approx \frac{64\pi^4\nu_Q^3}{3h}\,\mu_\perp^2\,|\langle v'J' | v''J''\rangle|^2\,(2J'+1), \tag{7}$$

$$I_P \approx \frac{64\pi^4\nu_P^3}{3h}\,\mu_\perp^2\,|\langle v'J' | v''J''\rangle|^2\,(J'+2)\,(1+\chi)^2, \tag{8}$$

$$I_R \approx \frac{64\pi^4\nu_R^3}{3h}\,\mu_\perp^2\,|\langle v'J' | v''J''\rangle|^2\,(J'-1)\,(1-\chi)^2, \tag{9}$$

$$\chi = c\mu_\parallel \langle v^*J' | v''J''\rangle / \mu_\perp \langle v'J' | v''J''\rangle. \tag{10}$$

It is evident that the interference term containing $\mu_\perp\mu_\parallel$ enters only into I_P and I_R [the contribution of μ_- to I_Q is small because of the factor $1/\sqrt{J'(J'+1)}$]. Therefore, the distribution of I_Q in the progression in v'' should be described in the adiabatic approximation by the Franck-Condon factors of the $B\,0_u^+ - X\,1_g^+$ transition, as was indeed recorded. For I_P and I_R from Eqs. (8) and (9), the ratio $I_P/I_R = (1+\chi)^2/(1-\chi)^2$ is calculated from Eq. (10). As a whole, what we have said makes it possible to interpret the observed anomalous ratios of intensities (Fig. 2). On the basis of experimental data on I_P and I_R in the progression with Te_2 ($B0_u^+$,5,103), the value $\mu_\parallel/\mu_\perp = 20.0 \pm 4.0$ was obtained. The large error is explained by both the experimental error ($\lesssim 15\%$) and by an appreciable error in the calculation of the wave functions.

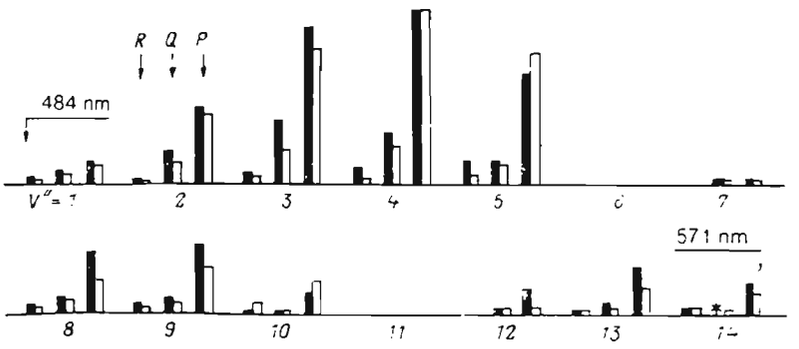

FIG. 2. Measured (dark columns) and calculated (light columns) intensities of the LIF series of $^{130}Te_2$ with ($B0_u^+$,5,103) on ($X\,1_g^+$,$v''J''$); asterisk—overlap with other lines; absent lines with $v'' = 6, 7, 11, 12$ were not recorded because of low intensity (in the calculations $\mu_\parallel/\mu_\perp$ is assumed independent of the internuclear distance).

[1]T. K. Regane, in *Contemporary Problems in Quantum Chemistry* (Leningrad, 1986), p. 165.
[2]R. A. Brooks, C. H. Anderson, and N. F. Ramsay, Phys. Rev. **136**, A62 (1964).
[3]M. P. Auzinsh, M. Ya. Tamanis, and R. S. Ferber, Pisma Zh. Eksp. Teor. Fiz. **42**, 132 (1985) [JETP Lett. **42**, 160 (1985)].
[4]M. P. Auzinsh, K. A. Nasyrov, M. Ya. Tamanis, R. S. Ferber, and A. M. Shalagin, Zh. Eksp. Teor. Fiz., **92**, 1590 (1987) [Sov. Phys. JETP **65**, 891 (1987)].
[5]R. S. Ferber, A. I. Okunevich, O. A. Shmit, and M. Ya. Tamanis, Chem. Phys. Lett. **90**, 476 (1982).
[6]G. Gouedard and I. C. Lehmann, Faraday Disc. Chem. Soc. **71**, 143 (1981).
[7]M. P. Chaika, *Interference of Degenerate Atomic States* (Leningrad, 1975), p. 191.
[8]R. S. Ferber, O. A. Schmit, and M. Ya. Tamanis, Chem. Phys. Lett. **92**, 393 (1982).
[9]M. P. Auzinsh, M. Ya. Tamanis, and R. S. Ferber, Opt. Spectrosk. **63**, 989 (1987) [Opt. Spectrosc. (USSR) **63**, 582 (1987)].
[10]J. Verges, C. Effantin, O. Babaky, K. d'Incan, S. J. Prosser, and R. F. Barrow, Phys. Scripta **25**, 338 (1982).
[11]J. T. Hougen, *The Calculation of Rotational Energy Levels and Rotational Line Intensities in Diatomic Molecules* (NBS Monograph, 115, 1970).
[12]A. V. Stolyarov and N. E. Kuzmenko, Czechosl. J. Phys. **37B**, 529 (1987).
[13]C. Effantin, J. d'Incan, M. T. Macpherson, and R. F. Barrow, Chem. Phys. Lett. **70**, 560 (1980).

Determination of the lifetime and relaxation cross section of the $Te_2(A\,1_u^-)$ molecule by the Hanle method

I. P. Klintsare, M. Ya. Tamanis, and R. S. Ferber

(Received 13 June 1988)
Opt. Spektrosk. **67**, 1222–1224 (November 1989)

The Hanle effect is a very widely used method of obtaining data on the radiative and collisional constants of atoms and molecules.[1] Beginning with Ref. 2 the Hanle effect was successfully applied in the variant of laser induced fluorescence (LIF) for determination of the value $\tau_{v'J'}$, the lifetime of the individual vibrational–rotational (VR) level $v'J'$ of an electronically excited state, and also the relaxation cross section. However, for diatomic molecules the method is convenient only in the case of pure Hund coupling[3] where the Landé factor of the VR state $g_{v'J'}$ is subject to simple calculation, which permits from the product $g_{v'J'}\tau_{v'J'}$ obtained from the Hanle signal going over to the lifetime $\tau_{v'J'}$.

In an investigation of the magnetic properties of the $^3\Sigma$ states of heavy molecules of the 6A group of the periodic table such as Se_2 (Ref. 4) and especially Te_2 (Ref. 5), it was clarified that the Lande factors of the VR states as a rule itself need experimental determination. Theoretical calculation is complicated by the fact that in these cases interaction between the terms must be taken into account. The largest contribution is introduced by the rotation-induced heterogeneous interaction between the terms with $\Omega = 0$ and 1,[6–8] which substantially affects the magnetism of the 0_u^+ and 1_u^+ states. In some sense the inverse problem was solved for the indicated reason in Refs. 5 and 9 for $^{130}Te_2$ in the $A\,0_u^+$ and $B\,0_u^+$ states: From the Hanle effect and the independently measured lifetimes the values of $G_{v'J'}$ were determined. For these diamagnetic states perturbations were the single factor determining the magnetism; estimates show that also for the paramagnetic 1_u^+ states perturbations in many cases must be taken into account, at least for large J'. An interesting exception is the 1_u^- state, for which interaction with the 0_u^+ state is forbidden by the selection rules. This leads to the simple expression[6,7]

$$G_{v'J'} = -\frac{2}{J'(J'+1)} \tag{1}$$

and permits using the Hanle effect to determine the lifetime and relaxation parameters. The purpose of this work is determination of the lifetime $\tau_{v'J'}$ and the cross section for alignment relaxation for the VR level of the $^{130}Te_2(A\,1_u^-)$ molecule. Up to now information on $\tau_{v'J'}$ of the tellurium molecule exists only for the states with $\Omega = 0$, specifically $A\,0_u^+$ and $B\,0_u^+$.[5,9–12]

The experimental setup is similar to that we used earlier in Refs. 5 and 9. The ^{130}Te isotope was placed in a quartz cell, connected with a vacuum post (residual pressure no worse than 10^{-6} Torr). The working temperatures of the branch with tellurium varied from $T_0 = 653$ K to $T = 725$ K, which corresponds to a concentration of vapors from 2×10^{14} to 62×10^{14} cm^{-3}.[13] In this temperature region the vapor consists of approximately 98% dimers. The $^{130}Te_2$ molecules were excited by the 514.5-nm line of an Ar^+ laser operating in the multifrequency regime. The resonance series of LIF was recorded, which fluoresced as a result of the R transition $(X\,1_g^-,\ J'' = 95) \rightarrow (A\,1_u^-,\ v' = 2,\ J' = 96)$; identification of the states was performed by the data of Ref. 14. The LIF spectrum was recorded photoelectrically in the photon count regime using a DFS-12 monochromator (5 Å/mm). The cell was placed between the poles of an electromagnet, to one of which a rotatable mirror was cemented, guaranteeing observation of LIF along the magnetic field **B**. The degree of linear polarization $P = (I_\parallel - I_\perp)/(I_\parallel + I_\perp)$ of the LIF was measured, where the intensity components $I_{\parallel,\perp}$ are polarized either along or transverse to the vector of the exciting light E. The dependence of the degree of polarization P on the magnetic field **B** (Hanle signal) is given in Fig. 1; it was approximated by the expression

$$P(B) = \frac{a}{1+\left(\frac{2g_{v'J'}\mu_0 B}{\Gamma_2\hbar}\right)^2} + b, \tag{2}$$

where Γ_2 is the rate constant of relaxation of alignment,[1] μ_0 is the Bohr magneton, and a and b are adjustment parameters. One nonlinear parameter, the ratio $\Gamma_2/g_{v'J'}$ was determined by the least-squares method. The values of $\Gamma_2/g_{v'J'}$ for various concentrations of $^{130}Te_2$ molecules are given in Fig. 1. The points were approximated by a linear dependence according to

$$\frac{\Gamma_2}{g_{v'J'}} = \frac{1}{g_{v'J'}\tau_{v'J'}^{sp}} + \frac{N\bar{v}_0\sigma_2\sqrt{\frac{T}{T_0}}}{g_{v'J'}}, \tag{3}$$

where N is the concentration of particles, $\bar{v}_0$ is the mean rela-

 0030-400X/89/110720-02$05.00

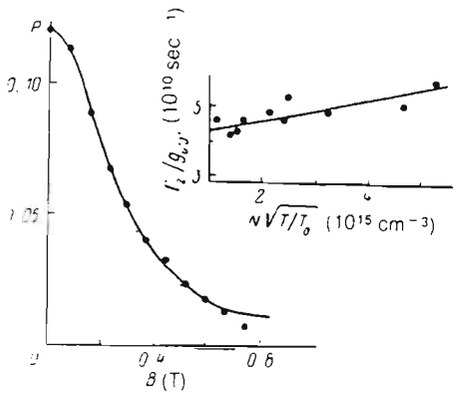

FIG. 1. Hanle signal $P(B) = (1/2)\{P(+B) = P(-B)\}$ of the $A\,1_u^-$ level ($v' = 2$, $J' = 96$) of the $^{130}Te_2$ molecule. Solid line—calculation. On the upper right the concentration dependence of the width of the signal is given.

tive velocity of Te_2 molecules at the temperature T_0, σ_2 is the effective cross section for relaxation of alignment for Te_2–Te_2 collisions.

As a result of the approximation the value $1/g_{v'J'}\tau^{sp}_{v'J'} = 4.32\times10^{10}\ \text{sec}^{-1}$ was obtained. For $J' = 96$ Eq. (1) leads to $g_{v'J'} = -2.15\times10^{-4}$. From this it follows that the value of the spontaneous lifetime is equal to $\tau^{sp}_{v'J'} = (108 \pm 7)$ nsec; the error corresponds to a confidence probability of 0.95. The negative sign of the Landé factor was confirmed by us in a separate experiment by the method of recording the Hanle signal of dispersion form[15] and indicates the antiparallel nature of the corresponding components of the magnetic and mechanical moments. Correspondingly from Eq. (3) values of the cross section were obtained equal to $\sigma_2 = (1.2 \pm 0.5)\times10^{-14}\ \text{cm}^2$.

We note that the value of the lifetime obtained somewhat exceeds the lifetime for the VR levels of the $B\,0_u^-$ state, where $\tau^{sp}_{v'J'}$ is within the limits from 54 to 90 sec.[5,12] In this case it is considerably less than the value of $\tau_{v'J'}$ characteristic for low-lying VR levels with $v' \leqslant 12$ for $Te_2(A\,0_u^+)$ lying within the limits from 620 to 800 nsec.[5,10,12] The value of the alignment relaxation cross section for Te_2–Te_2 collisions is close to the previously measured cross sections for the VR levels of the $A\,0_u^+$ and $B\,0_u^+$ states of the $^{130}Te_2$ molecule.

In conclusion a remark should be made concerning the applicability of Eq. (1). It was obtained under the condition that the 1_u^- term is a component of the $^3\Sigma_u^-$ state. In distinction from earlier works some authors[14] attributed to the state discussed 1_u together with $A\,0_u^+$ orgin from the $^3\Pi$ term. However, in ab initio calculations performed recently[16] in the basis used by the author 1_u the term on such origin has a repulsive character, and proceeding from $^3\Sigma_u^-$ a bound state is obtained. Evidently here it would be useful to study the magnetic properities of the given 1_u^- state.

The authors thank A. P. Bryukhovetskii for cooperation in data processing and Ya. A. Khar for fruitful discussions.

[1]M. P. Chaika, *Interference of Degenerate Atomic States* (Leningrad, 1975).
[2]M. McClintock, W. Demtroder, and R. N. Zare, J. Chem. Phys. **51**, 5509 (1969).
[3]G. Herzberg, *Molecular Spectra and Molecular Structure. Vol. I. Spectra of Diatomic Molecules* (D. Van Nostrand, New York, 1950).
[4]G. Gouedard and J. C. Lehmann, C. R. Acad. Sci. **280**, 81 (1975).
[5]R. S. Ferber, O. A. Shmit and M. Ya. Tamanis, Chem. Phys. Lett. **82**, 393 (1982).
[6]A. Buchler and D. J. Meschi, J. Chem. Phys. **63**, 3586 (1975).
[7]G. Gouedard and J. C. Lehmann, J. Phys. Lett. **38**, L 85 (1977).
[8]G. Gouedard and J. C. Lehmann, Faraday Disc. Chem. Soc. **71**, 143 (1981).
[9]M. Ya. Tamanis, Izv. Akad. Nauk Latvian SSR, Ser. Fiz. i Tekhn. Nauk **1**, 13 (1983).
[10]R. S. Ferber and M. Ya. Tamanis, Chem. Phys. Lett. **98**, 577 (1983).
[11]J. Carion, Y. Guern, J. Lotrian, and P. Luc, J. Phys. B (Paris) **15**, L841 (1982).
[12]W. G. Thorpe, W. R. Carper and S. J. Davis, Chem. Phys. Lett. **123**, 493 (1986).
[13]R. F. Brebrick, J. Phys. Chem. **72**, 1032 (1968).
[14]J. Verges, C. Effantin, O. Babaky, J. d'Incan, S. J. Prosser, and R. F. Barrow, Phys. Scripta **25**, 338 (1982).
[15]M. P. Auzinsh, M. Ya. Tamanis, and R. S. Ferber, Opt. Spektrosk. **63**, 989 (1987) [Opt. Spectrosc. (USSR) **63**, 582 (1987)].
[16]K. Balasubramanian and C. Ravimohan, J. Mol. Spectrosc. **126**, 220 (1987).

Volume 180, number 1,2 CHEMICAL PHYSICS LETTERS 10 May 1991

Lifetime and Landé-factor measurements of $A1_u^{\pm}$ and $A0_u^+$ states of $^{130}Te_2$ by laser-induced fluorescence

I.P. Klincare and M.Ya. Tamanis
Department of Spectroscopy, Latvian University, 226098 Riga, USSR

Received 12 October 1990; in final form 21 February 1991

Spontaneous lifetimes of the $A1_u^{\pm}$ state $v'J'$ levels, excited by an Ar^+ laser in pulse mode, have been measured. Estimated values decrease from 117 to 10 ns when v' levels increase from 2 to 8, respectively. The measured lifetimes have been used to obtain Landé factors by the Hanle-effect method for $A1_u^{\pm}$ and $A0_u^+$ states.

1. Introduction

Accurate spectroscopic information about the Te_2 molecule [1] stimulates investigations of its other characteristics including radiational and magnetic ones. Thus, lifetimes of $B0_u^+$ and $A0_u^+$ states have been measured in refs. [2–7] and Landé factors in refs. [2,8–10]. A new $A1_u$ state has been registered [11] near the $B0_u^+$ state. It is shown that $A1_u$ causes many local perturbations in $B0_u^+$ [1] and gives rise to the rather strong magnetism of this state [8,10]. We used the Hanle effect to measure the lifetime of a vibrotational level ($v'=2$, $J'=96$) $A1_u^-$ and obtained the value $\tau_{sp}=118$ ns [12]. In the present work, direct measurements of τ_{sp} for the group of $v'J'$ levels of $A1_u$ and $A0_u^+$, excited by an Ar^+ laser available to us, have been performed and Landé factors for them have been obtained.

2. Experiment

Our experiment is based on registration of laser-induced fluorescence (LIF) of Te_2 molecules and consists of three stages: (1) The recording of the LIF spectrum and identification and choosing of $v'J'$ levels; (2) measurements of fluorescence decay in real time after pulsed excitation of selected levels; and (3) measurements of degree of linear polarization of LIF dependence on the external magnetic field.

Fig. 1 shows all essential elements of the experimental arrangement. Isotope ^{130}Te was distilled into the fused silica cell which was connected with the vacuum system. For excitation, Ar^+ lasers were used: LGN-503 in multimode or Spectra Physics model-171 in the single-mode regime. LIF was focused onto the entrance slit of a double spectrometer (SP) which had an inverse dispersion of 0.5 nm/mm. As a rule, spectra were registered by a photon-counting technique using a photomultiplier (PM), counter (C), digital–analog converter (DAC) and a recording potentiometer (RP).

The LIF kinetic was recorded by a time-correlated single-photon-counting technique. The excitation

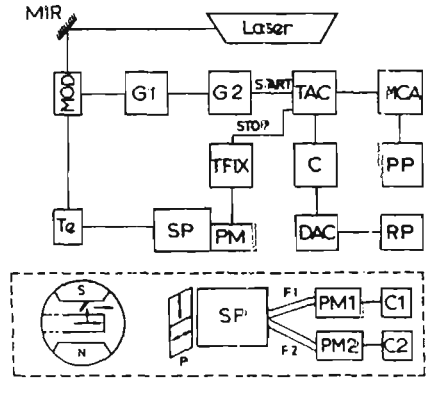

Fig. 1. Experimental setup for kinetic (upper) and magnetic (lower) measurements.

pulses were obtained by an electro-optical modulator (MOD) driven with a pulse generator (G1). The width of the pulses was 80–120 ns, rear front −40 ns. The repetition frequency N_{start} was 10^5 s^{-1} and the nonmodulated background was 3–5% from the pulse peak. The other nanosecond generator (G2) started a time–amplitude convertor (TAC) and synchronized it with G1. Standard stop-pulses were produced by a fast time-fixing scheme (TFIX), when the peak of the one-electron pulse from PM was achieved. The pulses from TAC were stored in a multichannel analyser (MCA). The time width of channels was 1–3 ns/channel. The rate of N_{start}, N_{stop} and N_{cor} was controlled through service output by the counter (C). The ratio $N_{cor}/N_{start} < 10^3/10^5$ was kept in accordance with one-photon statistics conditions. Data from MCA were fixed by a paper punch (PP).

For the Hanle-signal measurements, the registration part was modified as shown in fig. 1 (lower part). The cell, together with a miniature oven, was placed between the poles of the electromagnet. A small mirror was stuck to one of the magnet poles to ensure observation along the magnetic field $\boldsymbol{B}$. The input slit of SP was divided in equal parts and linear polarizers with orthogonal axes were placed before them. The output slit was also divided accordingly. The intensities I_α and $I_{\alpha+\pi/2}$ of LIF polarized along the directions α and $\alpha+\pi/2$, where the α-angles between the axes of the polarizer and the $\boldsymbol{E}$ vector of excitation were registered through fibers F1, F2 by PM1 and PM2 and stored by counters C1, C2. The channels were carefully balanced. An electromagnet, with 70 mm diameter poles and a 40 mm gap between them, provided magnetic fields up to 1.1 T. In the experiments, the current I in the coils of the electromagnet was measured. The graduation curve $B(I)$ was determined by a calibrated Hall detector.

At first, $^{130}Te_2$ LIF spectra were registered and corrected to the relative spectral sensitivity of the registration system. Usually, they contain a few P, R series of $A1_u^{\pm}$–X, $B0_u^+$–X and $A0_u^+$–X systems, see fig. 2. In the most complex parts of the spectrum where lines of different series overlapped, a single-frequency excitation mode was used. Most of these series and excited levels have been previously observed and indicated [1,13]. We used these data and molecular constants [1,14] to construct LIF spectra,

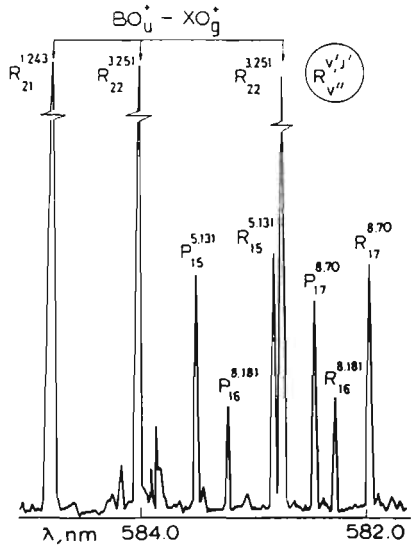

Fig. 2. Fragment of spectrum $^{130}Te_2$, $\lambda_{ex}=488.0$ nm. $B0_u^+-X0_g^+$ and $A1_u^{\pm}-X1_g^{\pm}$ (unsigned) systems.

which were compared with the experimental ones. In all cases, the relative intensity distribution in the extracted series was checked by Franck–Condon factors (FCF), which we calculated taking into account vibrational–rotational interaction [#1]. Satisfactory coincidence was obtained and the quantum numbers v' and v'' were estimated. Then, from the experimental doublet-spacing dependence of v'', values of J' were calculated, which, in turn, agreed well with data from refs. [1,13]. By a similar procedure, the levels $A0_u^+(v'=12)$ in our earlier work [3] and $A1_u^+(v'=4)$ in this work were identified. For further investigations, we chose all estimated $A1_u^{\pm}$ and $A0_u^+$ $v'J'$ levels.

Kinetic measurements were made on well-resolved fluorescence lines from selected $v'J'$ levels. LIF and excitation pulses were registered alternatively and, in every case, absence of time drift was checked. Some pulses are shown in fig. 3. Response signals were fitted by a function $\Phi(t)$, which was represented in the form

$$\Phi(t)=\int_0^t F(\tau')I(t-\tau')\,\mathrm{d}\tau'+b\,, \qquad (1)$$

[#1] FCF calculating program complex has been elaborated in Moscow University [15].

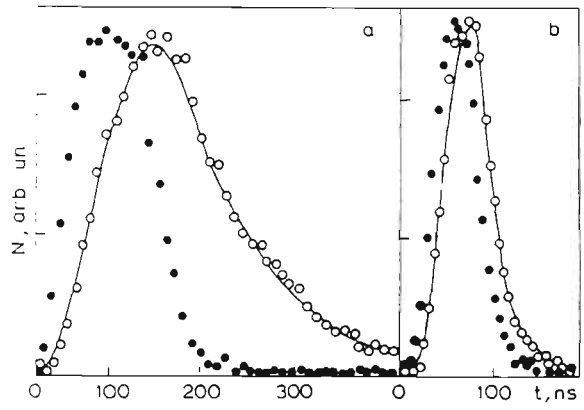

Fig. 3. Time-resolved fluorescence decay: (●) excitation pulse $F(\tau')$; (○) LIF reply; solid line – fitted with (1). (a) Level $A1_u^-$ ($v'=4$, $J'=52$); (b) level $A1_u^+$ ($v'=8$, $J'=181$).

where $F(\tau')$ is the scattered laser pulse and $I(t-\tau')=\exp[(t-\tau')/\tau_{ef}]$ is the true function of decay with time constant τ_{ef} and background b. Solid lines in fig. 3 represent signals for the $A1_u^{\pm}$ state levels $v'=4$ and 8 fitted to (1). Responses for levels $v'=8$ are very similar to excitation pulses. Nevertheless, we believe in the correctness of extracted τ_{ef} values ≈ 10 ns because, for both of these levels, more than ten couples of pulses were recorded and all results lay within 2 ns limits about the values obtained. To determine the spontaneous lifetime τ_{sp}, small corrections were used according to $\tau_{ef}^{-1}=\tau_{sp}^{-1}+\sigma vN$, where N is the concentration of molecules, v the mean relative velocity, and the σ relaxation cross section for collisions $Te_2^*+Te_2$. For the $A1_u$ state, σ equals $(1.2\pm 0.5)\times 10^{-14}$ cm^2 [9]. Due to the various intensity of the lines, measurements were made at different temperatures in the range from 680 to 730 K ($N_{Te_2}=(6.4\text{–}33)\times 10^{14}$ cm^{-3} [16]). It must be mentioned that corrections were essential only for $\tau_{ef}\approx 100$ ns.

When the Hanle signals were registered, the dependence of the degree of linear polarization, $P=(I_\alpha-I_{\alpha+\pi/2})/(I_\alpha+I_{\alpha+\pi/2})$, on $\boldsymbol{B}$ was measured. When $\alpha=0$, the contours $P(B)$ were approximated by

$$P_{0,\pi/2}(B)=P(0)\,\frac{a}{1+4(\mu_B g_{v'J'}B/\hbar\Gamma_2)^2}+b\,, \qquad (2)$$

where $g_{v'J'}$ is the Landé factor of the $v'J'$ level, μ_B is the Bohr magneton, b the background, and Γ_2 the alignment relaxation rate which in our case equals to τ_{sp}^{-1} [2]. $P(0)$ for transitions of the P, R-type is 1/7. The coefficient a accounts for a small depolarization which took place in the experiment. At $\alpha=\pi/4$, signals have the dispersion form,

$$P_{\pm\pi/4}(B)=P(0)\,\frac{2a\mu_B g_{v'J'}B/\hbar\Gamma_2}{1+4(\mu_B g_{v'J'}B/\hbar\Gamma_2)^2}+b\,. \qquad (3)$$

Experimental contours of both types are shown in fig. 4. During the processing, values $P(+B)$ and $P(-B)$ were averaged and approximated by (2) or (3) using the least-squares method with variable parameters $|g_{v'J'}|/\Gamma_2$, a, b. In most cases, the $|g_{v'J'}|$ were obtained from more accurately recorded Lorenzian shape signals, but their signs from dispersion signals. For some especially wide $A0_u^+$ and $A1_u^{\pm}$ contours, the $g_{v'J'}$, were approximately estimated from dispersion signals, because $P_{\pm\pi/4}(B)$ in the range $\mu_B g_{v'J'}B/\Gamma_2 \ll 1$ varies more sharply than $P_{0,\pi/2}(B)$.

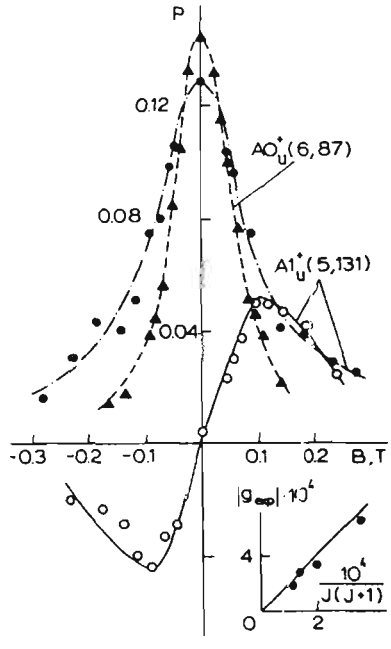

Fig. 4. Lorentz and dispersion-mode Hanle signals. Lines are drawn for illustration. On right, below – g_{exp} dependence on $1/J(J+1)$ for $A1_u^-$. Straight line corresponds to the slope coefficient 2.

Measurements were made at the same temperatures as kinetics.

3. Discussion

3.1. Lifetimes

$A1_u^+$: The values of τ_{sp} $A1_u^+$ are given in table 1. It is seen that for low v' levels, τ_{sp} equals ≈ 100 ns and decreases, when v' increases, for both components approximately to the same extent. However, we must not lose sight of the fact that $A1_u^+$ interacts rotationally with the close-lying $B0_u^+$, which has a lifetime of 50–90 ns [2,5], and slows down the decrease of $\tau_{sp}(A1_u^+)$ compared to $\tau_{sp}(A1_u^-)$. Obviously, weak predissociation with the rate $\Gamma_{pr} \approx 10^8$ s^{-1} takes place in this case. From energy considerations [1], it follows that the predissociating state correlates with ground-state atoms $^3P_2+{}^3P_2$. According to selection rules, from the vast number of such states [17] we must retain 0_u^-, 0_u^-, 1_u, 1_u, 2_u only. The terms 1_u, 1_u, 2_u are bound and located [17,18] so that, most probably, 1_u interacts with $A1_u$ through the left part of the potential. If the role of 2_u is essential we must observe τ_{sp} dependence on J. Data for $v'=2$, at least, give opposite evidence. The unstable states 0_u^- obviously can be neglected because we did not observe a substantial difference between Γ_{pr} for 1_u^+ and 1_u^- components in this region and, at the same time, τ_{sp} for $B0_u^+$ does not diminish even for higher v' levels.

$A0_u^+$: In table 2, our previously obtained results are given. Values of τ_{sp} slowly decrease when v' increases; at $v'=13$, τ_{sp} falls sharply. In general, such behaviour of τ_{sp} is in accordance with the values 1080 ± 60 ns ($v'=5$–10) [6], 730 ± 55 ns ($v'=8$) [5], 60–70 ns ($v'=16$, 17) [4]. More detailed investigations are needed to determine which state causes this τ_{sp} shortening. We only mention here that the energy of the level $v'=13$, $J'=133$ ($E\approx21600$ cm^{-1}) exceeds quite slightly the dissociation energy of the ground $X0_g^+$ state, the latter being 21300 cm^{-1} [1].

3.2. Landé factors

$A1_u^+$: The experimental $g_{v'J'}$ values given in table 1 for the 1_u^- term are all negative and proportional to J^{-2}. For the $A1_u^+$ term, the $g_{v'J'}$ values vary more strongly, where a change of sign even occurs for $v'=5$. Such a difference arises from rotational interaction which mixes $A1_u^+$ and $B0_u^+$ states. The diamagnetic $B0_u^+$ state exhibits a magnetic moment, as has been shown, for example, for Se_2 in ref. [19]. In the case of Te_2, this interaction fully determines the $g_{v'J'}$ behaviour in $B0_u^+$ [8,10]. On the other hand, $g_{v'J'}(A1_u^+)$ is also influenced by the same interaction, according to [10]

$$g_{v'J'}(1_u^+) = \frac{2c_0c_1G_-\langle v_J^{1+}|v_J^{0+}\rangle}{\sqrt{2J(J+1)}} - \frac{c_1^2G_z}{J(J+1)}, \quad (4)$$

where c_0, c_1 are mixing coefficients of the interacting rovibronic levels, and G_-, G_z the corresponding electronic matrix elements. The first term in (4) varies from level to level and causes changes of the $g_{v'J'}(1_u^+)$ which have been actually observed.

For the component of 1_u^- which does not interact with $B0_u^+$, $g_{v'J'} = -G_z/J(J+1)$. If 1_u^- arises from the

Table 1
Lifetimes and Landé factors of $A1_u^\pm(v'J')$ levels of $^{130}Te_2$. Errors for g_{exp} in the interval 2σ are 15–20%, for levels $v'=8$, 40%

	λ_{exc} (nm)	$v''(J'')$–$v'(J')$	τ_{sp} (ns)	$g_{exp}\times10^{-4}$	$g_{calc}\times10^{-4}$ [a]
$X1_g^-$–$A1_u^-$	514.5	4(87)–2(86)	107±7	−2.7	−2.67
		4(95)–2(96)	117±11	−2.0	−2.15
	488.0	1(53)–4(52)	49±4	−6.4	−7.26
		3(71)–8(70)	10±2	−3.3	−4.02
$X1_g^+$–$A1_u^+$	501.7	3(110)–4(111)	66±5	−3.8	
	488.0	1(132)–5(131)	45±6	+15.0	
		2(180)–8(181)	14±2	−2.7	

[a] $g_{calc} = -2J(J+1)$.

Table 2
Lifetimes and Landé factors of $A0_u^+(v'J')$ levels of $^{130}Te_2$. Errors for g_{exp} in interval 2σ are 15–20%

	λ_{exc} (nm)	$v''(J'')$–$v'(J')$	τ_{sp} (ns)	$g_{exp}\times10^{-4}$
$X0_g^+$–$A0_u^+$	514.5	3(88)–6(87)	800 ± 100 [a]	−1.2
		6(52)–11(53)	670 ± 30 [b]	+0.52
	488.0	1(132)–11(131)	620 ± 50 [a]	−0.45
	496.5	3(134)–12(133)	670 ± 40 [c]	+0.03 [a]
		3(138)–12(139)	620 ± 50 [c]	−0.16
	476.5	0(134)–13(133)	160 ± 20 [a]	−0.2
		1(88)–14(89)	40 ± 10 [a]	−0.7

[a] Ref. [7]. [b] Ref. [2]. [c] Ref. [3]. [d] Value estimated tentatively.

$^3\Sigma$ state, $G_z=2$ [19]; in the case of the $^3\Pi$ state, G_z would be two times smaller. As can be seen from table 1 and fig. 4 (quadrant 4), the value of the coefficient $G_z=2$ is satisfactory. Some discrepancy appears here, due to the fact that this term, as well as the well-known $A0_u^+$, arises from the same $^3\Pi_u$ state, as spectroscopic studies have shown [1]. Thus, further investigations are needed.

$A0_u^+$: The values of $g_{v'J'}(A0_u^+)$ given in table 2 are about two orders of magnitude smaller than for the $B0_u^+$ state [8,10]. This fact is easy to understand in the framework of the above-mentioned model, but variations of $g_{v'J'}$ and changes of sign cannot be explained by the influence of a single $A1_u^+$ term. Of course, other 1_u^+ terms must be taken in account. However, the available information about 1_u^+ states is not sufficient to explain the behaviour of $g_{v'J'}$. We hope that further accumulation of data about $g_{v'J'}(A0_u^+)$ would contribute to a more detailed knowledge about 1_u terms.

Acknowledgement

The authors are indebted to R.S. Ferber and A.V. Stolyarov for fruitful discussions, and to the latter for providing us with the Franck–Condon-factor-calculation programs. M.P. Auzin'sh and A.P. Brjuhovetsky are acknowledged for aiding in data processing.

References

[1] J. Verges, C. Effantin, O. Babaky, J. d'Incan, S.J. Prosser and R.F. Barrow, Physica Scripta 25 (1982) 338.
[2] R.S. Ferber, O.A. Shmit and M.Ya. Tamanis, Chem. Phys. Letters 92 (1982) 393.
[3] R.S. Ferber and M.Ya. Tamanis, Chem. Phys. Letters 98 (1983) 577.
[4] J. Cariou, Y. Guern, J. Lotrian and P. Luc, J. Phys. B 15 (1982) 1976.
[5] W.G. Thorpe, W.R. Carper and S.J. Davis, Chem. Phys. Letters 123 (1986) 493.
[6] E. Martinez, P. Puyelo, F.J. Basterrechea and M.T. Martinez, Chem. Phys. Letters 156 (1989) 564.
[7] M.P. Auzin'sh, M.Ya. Tamanis and Ya.A. Harya, in: Abstracts of the 20th All Union Congress on Spectroscopy, Kijev (1988) p. 263.
[8] I.P. Klincare, A.V. Stolyarov, M.Ya. Tamanis, R.S. Ferber and Ya.A. Harya, Optika i Spektroskopiya 66 (1989) 1018.
[9] I.P. Klincare, M.Ya. Tamanis and R.S. Ferber, Optika i Spektroskopiya 66 (1989) 827.
[10] A.V. Stolyarov, E.A. Pazyuk, L.A. Kuznetsova, Ya.A. Harya and R.S. Ferber, Chem. Phys. Letters 166 (1990) 290.
[11] J. Verges, J. d'Incan, C. Effantin, D.J. Greenwood and R.F. Barrow, J. Phys. B 12 (1979) 1301.
[12] I.P. Klincare, M.Ya. Tamanis and R.S. Ferber, Optika i Spektroskopiya 67 (1989) 1222.
[13] A. Topouzkhanian, O. Babaky, J. Verges, R. Willems and B. Wellegehausen, J. Mol. Spectry. 113 (1985) 39.
[14] C. Effantin, J. d'Incan, J. Verges, M.T. Machperson and R.F. Barrow, Chem. Phys. Letters 70 (1980) 560.
[15] A.V. Stolyarov and N.E. Kuz'menko, Spectrosc. Letters 19 (1986) 1113.
[16] R.F. Brebrick, J. Phys. Chem. 72 (1968) 1032.
[17] K. Balasubramanian and Ch. Ravimohan, J. Mol. Spectry. 126 (1987) 220.
[18] V.E. Bondybey and J.H. English, J. Chem. Phys. 72 (1980) 6479.
[19] G. Goudedard and J.C. Lehmann, Faraday Discussions Chem. Soc. 71 (1981) 143.

Rotational magnetic moment of the Na_2 molecule in $A\ ^1\Sigma_u^+$ state: Perturbation effects

A. V. Stolyarov,[a] I. P. Klincare, M. Ya. Tamanis, M. P. Auzin'sh, and R. S. Ferber
Department of Physics and Mathematics, The University of Latvia, Riga, Latvia, 226098

(Received 11 March 1991; accepted 5 November 1991)

Values and signs of Landè factors (g) have been measured for four rovibronic levels of the $A\ ^1\Sigma_u^-$ state of the Na_2 molecule. Because of a very small product $g\tau \sim 10^{-12}$ s, the level crossing signal of a dispersion shape was employed using circular light polarization and mutually orthogonal excitation, observation of laser induced fluorescence, and external magnetic field directions. The effects of the $b\ ^3\Pi_u$, $B\ ^1\Pi_u$, and $a\ ^3\Sigma_u^+$ states on the g factors of the Na_2 ($A\ ^1\Sigma_u^-$), as well as their dependence on vibrational and rotational quantum numbers, have been theoretically analyzed. An analytical connection has been found between the constants of Λ doubling (q) and Landè factors of the interacting singlet states. Simple expressions have been found for estimating the effects of distant electronic states on q and the g factors without summing over bounded and integrating over continuum levels of the perturbing state.

I. INTRODUCTION

The Na_2 molecule has been used for many years as a test molecule for spectroscopic theory and techniques. The first excited singlet state $A\ ^1\Sigma_u^-$ and the second excited triplet state $b\ ^3\Pi_u$ have been known to interact for a long time.[1-3] One of the most obvious manifestations of this interaction is the disturbance in the regular structure of the rotational bands, as observed both in emission and absorption. It is hardly surprising therefore that high-resolution spectroscopy is employed for studying such perturbations, since it makes it possible to determine small divergences in the position of rovibronic levels in the interacting electronic states. In the course of the past ten years, a number of laser spectroscopic methods have evolved which make it possible to obtain highly resolved spectra. These methods have been successfully employed for studying the $A\ ^1\Sigma_u^-$ and $b\ ^3\Pi_u$ states and their interaction.[4-8]

It is rather obvious that any perturbation affects not only the energy of the states, but also their wave functions. This naturally leads to changes in other affiliated molecular characteristics, such as radiational and magnetic properties.[2-9]

The present study deals with some peculiarities in the effects of $A\ ^1\Sigma_u^- - B\ ^1\Pi_u$, $A\ ^1\Sigma_u^- - b\ ^3\Pi_u$, and $A\ ^1\Sigma_u^+ - b\ ^3\Pi_u - a\ ^3\Sigma_u^-$ interactions on the rotational magnetic moment of the A state by means of determining Landè factors for a number of rovibronic levels of A state.

It ought to be noted that the method proposed for studying molecular perturbations[10] does not require such high spectral resolving power, as is necessary in the experiments based solely on the measurements of the positions of rovibronic energy levels. The main advantage, however, of the use of Landè factors for studying perturbations of diamagnetic ($\Omega = 0$) states is their extreme sensitivity to the value and type of not only local, but also of regular interactions. This is easily understood, if one keeps in mind that a nonperturbed diamagnetic state possesses a near zero magnetic moment, which is independent of vibrational and rotational quantum numbers. Accordingly, any, even small, perturbation due to paramagnetic electronic states leads to drastic relative changes of the magnetic moment value. This in turn is easily observed experimentally, since modern methods permit Landè factor measurements of the order of (10^{-4}–10^{-5}).[11,12] It may also be noted that the sign of the Landè factors is an additional source of information on the type of perturbation.[13]

The present work consists of the study of the basic causes of the appearance of a nonzero magnetic moment in the diamagnetic $A\ ^1\Sigma_u^+$ state, as well as the calculation of the dependence of the g factors on vibrational and rotational quantum number values, and finally, performing experimental testing of results on a number of rovibronic levels of Na_2 ($A\ ^1\Sigma_u^+$). Although the viability of the above statements can manifest itself most fully only in systematic g factor measurements over a large group of rovibronic levels of the $A\ ^1\Sigma_u^+$ state, we have undertaken, by way of a first stage, measurements of four well known[14] v, J levels, excited by the 632.8 nm He–Ne laser line. An initial report on the results obtained can be found in Ref. 15. For these levels the product $g\tau$ value is extremely small ($\sim 10^{-13}$–10^{-12} s). To avoid the usage of very large magnetic field, we developed a special kind of method based on Hanle effect in laser induced fluorescence under circulary polarized excitation and mutually orthogonal excitation, observation and magnetic field directions. For $^1\Sigma$–$^1\Sigma$ transitions of P, R type, this leads to Hanle signal of dispersion shape having the greatest steepness when the magnetic field strength is equal to zero.

Expected Landè factors for Na_2 ($A\ ^1\Sigma_u^-$) were located taking into account the "nuclear" contribution caused by the rotation of shielded sodium atom cores as well as the electronic part connected with $A\ ^1\Sigma_u^- - b\ ^3\Pi_u$ and $A\ ^1\Sigma_u^- - B\ ^1\Pi_u$ mixing. It is shown that in this concrete situation one can neglect the influence of the $a\ ^3\Sigma_u^-$ state as well

[a] Present address: Department of Chemistry, Moscow M. Lomonosov State University, Moscow W-234, 119899, USSR.

 0021-9606/92/053510-13$06.00

as the role of the second order perturbation effects according to magnetic field strength. The interaction between the states $A\,^1\Sigma_u^+$ and $B\,^1\Pi_u$ has been used for analyzing the possibility of employing Landè factors for investigating structural and magnetic properties of mutually distant electronic terms, and that between the states $A\,^1\Sigma_u^+$ and $b\,^3\Pi_u$ for investigating local perturbations caused by the crossing terms.

II. EXPERIMENT

A. Method of measurement

The experimental determination of the g-factor values in Na_2 ($A\,^1\Sigma_u^+$) state is connected with certain difficulties. Indeed, application of optomagnetic methods of measurements requires that the product $\omega\tau$, where ω is the frequency of magnetic splitting, should have a value of the order of (or larger than) unity. If we consider that τ in the case of Na_2 ($A\,^1\Sigma_u^+$) has a characteristic value of 12.5 ns (Ref. 16), then the condition $\omega\tau = 1$ corresponds to magnetic fields of the order of $B = \hbar/(\mu_B g_J \tau) = 10$–$20$ T, which by far exceeds the possibilities of the electromagnet at our disposal. However, a certain chance of measuring the Landè factor under conditions when $\omega\tau$ lies considerably below unity value can be obtained by applying the Hanle effect in a variant implying a "dispersion shape" of signal. Such a variant of the method yielding information both on the value and the sign of the g factor, as far as we know, has been used with linearly polarized excitation, see e.g., Refs. 17–19.

Let us consider the fluorescence in the cycle $J''\to J'_e\to J''$ (Fig. 1), excited by directed light with a given polarization $\hat{\mathbf{E}}$. In order to describe the effect of the magnetic field on polarization we shall apply a treatment in terms of polarization moments, e.g., Refs. 20–22. The intensity $I(\hat{\mathbf{E}}')$ of given polarization $\hat{\mathbf{E}}'$ propagating in a definite direction on transition $J'_e\to J''$ may be represented, according to Ref. 21 in the following form:

$$I(\hat{\mathbf{E}}') = (-1)^{J''_e-J''}(2J'_e+1)^{1/2}I_0 \times \sum_{K=0}^{2}(2K+1)\begin{Bmatrix}1 & 1 & K\\ J'_e & J'_e & J''\end{Bmatrix} \times \sum_{Q=-K}^{K}(-1)^Q f_Q^K \Phi^K_{-Q}(\hat{\mathbf{E}}'), \qquad (1)$$

Here $\{\cdots\}$ is a 6j-symbol, f_Q^K-the polarization moment of state J'_e, K-its rank, while its projection Q varies from $-K$ to K. The tensor $\Phi^K_{-Q}(\hat{\mathbf{E}}')$ has been introduced in Ref. 21 and it characterizes the polarization of light. Its components may be calculated through the cyclic components E^q of the polarization vector $\hat{\mathbf{E}}'$ as

$$\Phi_Q^K(\hat{\mathbf{E}}) = (2K+1)^{-1/2} \times \sum_{q',q''=-1}^{1}(-1)^{q''}E^{q'}(E^{q''})^* C^{KQ}_{1-q'1q''} \qquad (2)$$

using Clebsch–Gordan coefficients $C^{\alpha\gamma}_{a\alpha b\beta}$. The necessary values of Φ_Q^K can be found in table form, e.g., in Ref. 23. The polarization moments f_Q^K formed by the light in the act of absorption $J''\to J'_e$, (Fig. 1) proceeding at the rate Γ_p in the presence of an external magnetic field B can be calculated as follows:

$$f_Q^K = (-1)^{J'_e-J''}\Gamma_p(\Gamma_K - iQ\omega)^{-1}(2J'_e-1)^{3/2} \times (2J''-1)^{-1}\begin{Bmatrix}1 & 1 & K\\ J'_e & J'_e & J''\end{Bmatrix}\Phi_Q^K(\hat{\mathbf{E}})n_{J''}, \qquad (3)$$

where $n_{J''}$ is the concentration of absorbing molecules, Γ_K is the relaxation rate of the moment of rank K (under assumption of $\Gamma_p \ll \Gamma_K$), but $\Phi_Q^K(\hat{\mathbf{E}})$ characterizes the polarization of the exciting radiation.

The Hanle effect is traditionally recorded with linearly polarized excitation [Figs. 2, 3(a), and 3(b)] with magnetic field $\mathbf{B}\perp\hat{\mathbf{E}}$, while observation takes place along the Z axis. The signal is observed through the degree of linear polarization $\mathscr{P}$ from the intensities of orthogonally polarized components $I_\perp = I_y, I_\parallel = I_{x-y/2}$, which can easily be expressed through f_0^1, f_0^2, and f_0^0 (e.g., Ref. 24)

$$\mathscr{P}(\gamma) = \frac{I_\perp - I_\parallel}{I_\perp + I_\parallel} = -\mathscr{P}(0)\frac{\cos 2\alpha - 2\gamma\sin 2\alpha}{1+4\gamma^2}, \qquad (4)$$

$\gamma = \omega/\Gamma_{J'_e}$.

Here $\mathscr{P}(0)$ denotes the degree of polarization of fluorescence, as it would be at $\alpha = \pi/2$, $\gamma = 0$, i.e., in the absence of

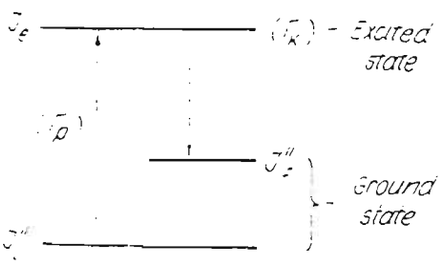

FIG. 1. Optical transition scheme.

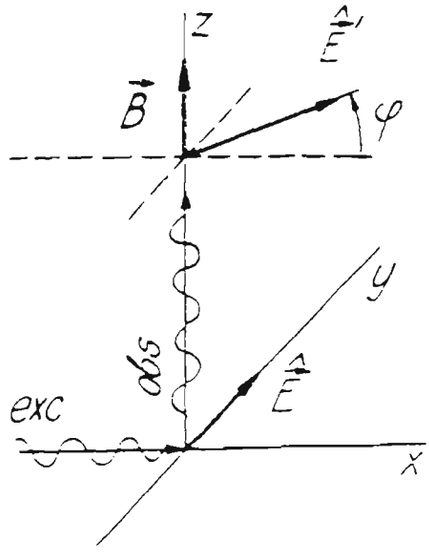

FIG. 2. Experimental geometry for linear polarized excitation ($\hat{\mathbf{E}}'$) and observation ($\hat{\mathbf{E}}$).

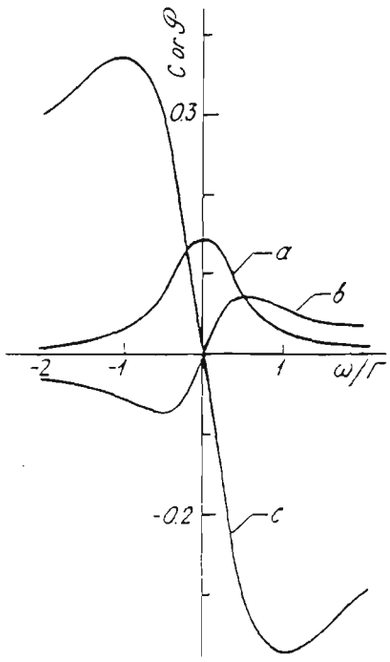

FIG. 3. Calculated Hanle signal curves. (a) linear polarized excitation (Fig. 2), $\varphi = \pi/2$ in Eq. (4); (b) the same conditions, except $\varphi = \pi/4$; (c) circularly polarized excitation (Fig. 4), cf. Eq. (8).

magnetic field. In the $J \to \infty$ limit the known[24] $\mathcal{P}(0)$ values are 1/7 for (P,R) ↑, ↓ and 1/2 for Q ↑, Q↓ transitions (here the arrows ↑ or ↓ denote absorption or emission). In order to ascertain the possibility of observing a Hanle signal at $\gamma \ll 1$, let us examine the behavior of the derivative

$$\frac{d\mathcal{P}}{d\gamma} = -\mathcal{P}(0) \times \frac{2\sin 2\varphi(1+4\gamma^2) - (\cos 2\varphi - 2\gamma \sin 2\varphi)8\gamma}{(1+4\gamma^2)^2}. \tag{5}$$

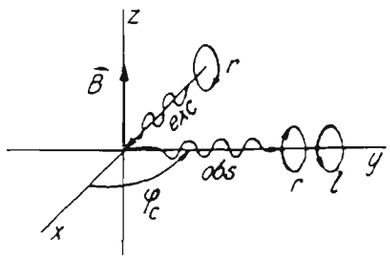

FIG. 4. Experimental geometry for circularly polarized excitation.

If $\varphi = 0$, then the derivative becomes zero at $\gamma \to 0$. Hence the traditionally most frequently observed signal is of Lorentzian shape $\mathcal{P}(\gamma) = \mathcal{P}(0)/(1+4\gamma^2)$, dating back from Hanle's time,[25] Fig. 3(a). On the other hand, we get the largest value of $d\mathcal{P}/d\gamma$ in the vicinity of $\gamma = 0$ for $\varphi = \pi/4$, when the slope of the straight line equals $2\mathcal{P}(0)$, Fig. 3(b).

For Q-type transitions such conditions are, indeed, optimal, since $2\mathcal{P}(0) = 1$ at $J \to \infty$. At the same time, we get $2\mathcal{P}(0) = 2/7$ for P or R transitions, i.e., just the ones that take place in the $^1\Sigma$–$^1\Sigma$ system of Na_2. As it turns out, one can find more advantageous conditions in this case. Let excitation, polarized along a right-hand circle, take place, as shown in Fig. 4. Let us now follow the degree of circularity

$$C = (I_r - I_l)/(I_r + I_l) \tag{6}$$

by measuring, at right angles to the field **B** direction,[20] the intensity I_r, I_l polarized along the right-hand (I_r) or left-hand (I_l) circle. The value of C for arbitrary angles φ_C between the excitation and observation directions, see Fig. 4, can be expressed through $f_1^1, f_2^2, f_0^2, f_0^0$ as

$$C = \frac{\begin{Bmatrix} 1 & 1 & 1 \\ J_i & J_i & J'' \end{Bmatrix} \mathrm{Re}(e^{-i\varphi_C} f_1^1)}{-(1/3)\begin{Bmatrix} 1 & 1 & 0 \\ J_i & J_i & J'' \end{Bmatrix} f_0^0 - \begin{Bmatrix} 1 & 1 & 2 \\ J_i & J_i & J'' \end{Bmatrix} \left[(1/6)\sqrt{5/2} f_0^2 - (1/2)\sqrt{5/3}\,\mathrm{Re}(e^{-2i\varphi_C} f_2^2)\right]}. \tag{7}$$

Substituting f_Q^K from Eq. (3), we obtain

$$C = \frac{36\begin{Bmatrix} 1 & 1 & 1 \\ J_i & J_i & J'' \end{Bmatrix}\begin{Bmatrix} 1 & 1 & 1 \\ J_i & J_i & J'' \end{Bmatrix} (\Gamma_2, \Gamma_1)(\cos\varphi_C - \gamma \sin\varphi_C)/(1+\gamma^2)}{\left[3(-1)^{J_i - J''}(2J_i - 1)\right] - \begin{Bmatrix} 1 & 1 & 2 \\ J_i & J_i & J'' \end{Bmatrix}\begin{Bmatrix} 1 & 1 & 2 \\ J_i & J_i & J'' \end{Bmatrix} (\Gamma_2, \Gamma_2)\left[3 - 9(\cos 2\varphi_C - 2\gamma \sin 2\varphi_C)/(1+4\gamma^2)\right]}. \tag{8}$$

The necessary values of the 6*j*-symbols are

$$\begin{Bmatrix} 1 & 1 \\ J' & J \end{Bmatrix} = \begin{cases} J'-J=-1(P); & \frac{1}{2}\left[\frac{2J'}{(2J'+1)(J'+1)3}\right]^{1/2} \\ J'-J=0(Q); & \frac{1}{2}\left[\frac{2}{J'(2J'+1)(J'+1)3}\right]^{1/2} \\ J'-1=1(R); & (-1)^{2J'+1}\frac{1}{2}\left[\frac{2(J'+1)}{J'(2J'+1)3}\right]^{1/2} \end{cases} \tag{9}$$

the signal we are interested in will be determined by the derivative, which in the $J' \to \infty$ limit for P,R transitions is as follows:

$$\left.\frac{dC}{d\chi}\right|_{\chi=0} = \pm 60\frac{\sin\varphi_C(81+3\cos 2\varphi_C)-6\cos\varphi_C\sin 2\varphi_C}{(81+3\cos 2\varphi_C)^2}. \tag{10}$$

The derivative assumes zero value at $\varphi_C = 0$. Its maximum value is attained in the case $\varphi_C = \pi/2$, as shown in Fig. 4, being equal to $\mp 10/13$, which exceeds the value for linear polarization by a factor of almost 3. Thus maximum slope of the Hanle signal can be achieved in the region of $\chi = 0$, cf. Fig. 3(c). This provides a new possibility to measure the g-factor values in conditions when $\omega\tau \ll 1$. An additional advantage consists in the fact that this situation provides the most favorable geometry for collecting fluorescence from the cell in the gap of the electromagnet, since observation is performed at right angles with respect to the direction of the magnetic field (Fig. 4). Unlike the situation in Fig. 2, here we have no problem of deflecting the fluorescent beam in order to direct it out the gap of the electromagnet.

B. Experimental details

Metallic sodium was placed into a glass cell joined to the vacuum system by means of a dry valve. The optical part of the cell was positioned in the gap of the electromagnet (up to 1 T) of 40 mm width. The saturating sodium vapor was at a temperature of 550–630 K, which corresponds to a content of $[Na] = 1\text{–}16\times10^{14}$ cm^{-3}, $[Na_2] = 7\text{–}240\times10^{11}$ cm^{-3}.[27] The exciting light from a He–Ne laser was cut down to a power of ~ 1 mW in order to avoid nonlinear effects of optical pumping of the lower state,[28] since at a working power of $\sim$49 mW a nonlinear Hanle effect of the lower state had been observed of $\sim$0.2 T half-width that is similar to the results in Ref. 29.

Convenient working lines of the $A\,^1\Sigma_u^+ - X\,^1\Sigma_g^+$ fluorescence spectrum corresponding to the v', J' levels (Table I) were selected out by means of a double diffraction monochromator (5 Å/mm). The degree of linear polarization or circularity was measured in the following way. The entrance slit of the spectrometer was divided in height into two parts, and two orthogonal analyzers were placed in front of them. Light guides conducted the light from two respective parts of the exit slit of the monochromator to the two photomultipliers, which counted simultaneously one-photon pulses from two channels. Circular polarization was provided by inserting two mica quarter-wave plates.

C. Results

Dispersion-shaped initial parts of Hanle signals in the regions $\omega/\Gamma \ll 1$, as obtained within the $B = \pm 1$ T range were of rather insignificant magnitude at linear polarization of light. However, they made it possible to obtain a preliminary estimate of the g factors for Na_2 ($A\,^1\Sigma_u^+$), as well as to determine their sign. More definite results were obtained from signals received in an arrangement according to Fig. 4

TABLE I. Calculated mixing coefficients S_{Π_u}, S_Σ and g factors for rovibronic states of Na_2 ($A\,^1\Sigma_u^+, v', J'$) involved in this work. Here $g_{v'J'}^{A\,^1\Sigma_u^+}(b\,^3\Pi_u)$ and $g_{v'J'}^{A\,^1\Sigma_u^+}(B\,^1\Pi_u)$ denote the corresponding parts due to $A\,^1\Sigma_u^+ - b\,^3\Pi_u$ or $A\,^1\Sigma_u^+ - B\,^1\Pi_u$ interaction, $g_{v'J'}^{in}(\text{tot}) = g_{v'J'}^{A\,^1\Sigma_u^+}(b\,^3\Pi_u) + g_{v'J'}^{A\,^1\Sigma_u^+}(B\,^1\Pi_u) + g_{rot}$, while $g_{v'J'}^{exp}$ are experimentally measured values.

	$v'=14, J'=45$	$v'=22, J'=86$	$v'=25, J'=87$	$v'=16, J'=17$
S_{Π_u}	4.56×10^{-2}	-1.64×10^{-3}	-8.06×10^{-5}	6.17×10^{-3}
S_{Π_g}	-2.42×10^{-2}	-5.07×10^{-3}	4.77×10^{-3}	-7.74×10^{-4}
S_{Π_u}	1.38×10^{-2}	-4.11×10^{-3}	-5.78×10^{-3}	1.23×10^{-4}
S_Σ	9.98×10^{-1}	9.98×10^{-1}	9.97×10^{-1}	1.0000
$g_{v'J'}^{A\,^1\Sigma_u^+}(b\,^3\Pi_u)$	8.88×10^{-5}	-7.21×10^{-5}	8.32×10^{-5}	7.86×10^{-7}
$g_{v'J'}^{A\,^1\Sigma_u^+}(B\,^1\Pi_u)$	-7.32×10^{-5}	-6.88×10^{-5}	-6.84×10^{-5}	-7.44×10^{-5}
$g_{v'J'}^{in}(\text{tot})$	-3.95×10^{-5}	-11.7×10^{-5}	-3.87×10^{-5}	-5.05×10^{-5}
$g_{v'J'}^{exp}$	-3.13×10^{-5}	-13.6×10^{-5}	-2.41×10^{-5}	-5.32×10^{-5}

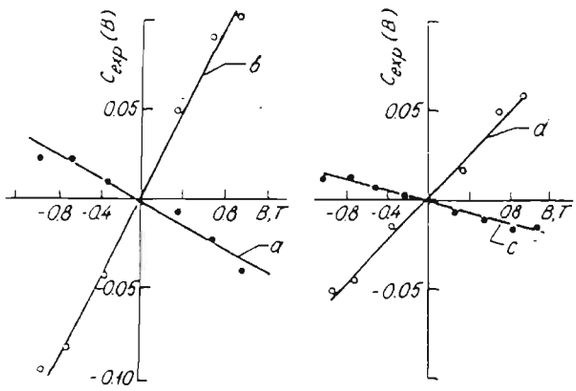

FIG. 5. Magnetic field dependence for the degree of circularity C measured using the geometry shown in Fig. 4. The quantum numbers involved in a transition $(v'',J'') \rightarrow (v',J')$ are as follows: (a) (2,46) → (14,45); (b) (6,35) → (22,86); (c) (8,86) → (25,87); (d) (4,18) → (16,17).

($\varphi_C = \pi/2$). Examples of $C_{exp}(B)$ dependences obtained are presented in Fig. 5. Satisfactory accuracy within the given ω/Γ range can be achieved by approximating the results obtained by straight lines

$$C_{exp}(B) = a\left(\frac{dC}{d\chi}\right)_{\chi=0} g^{exp}_{v'J'}\mu_B B/\hbar\Gamma + \delta. \tag{11}$$

For better fit the term δ is introduced to compensate for the residual errors of calibrating the channels. The data in Fig. 5 are normalized allowing for condition $\delta = 0$ for better clarity. The correcting coefficient a, which is close to unity, accounts for the depolarizing effect of the optical channel. Its value was found from results of testing the setup. For $R\uparrow, P\downarrow$ or $P\uparrow, R\downarrow$ transitions, which took place in the cases represented in Fig. 5, the value $(dC/d\chi)_{\chi=0} = \pm 10/13$ was assumed, as obtained for $J \rightarrow \infty$. This may be done, since it is well known[24] that for this type of transition the values of the degree of circularity do not depend on J. In the case when circularity was measured for the second component of the doublet, which would correspond to $P\uparrow, P\downarrow$ or $R\uparrow, R\downarrow$ transitions, use of expression (10) leads to a certain error, which becomes particularly significant for $J'_e \equiv J' = 17$. Therefore, one must use, in such cases, values of the derivative $dC/d\chi$ for arbitrary J values, as obtained by employing expressions (1)–(3) and (6)–(9). At $\varphi_C = \pm\pi/2$ they are of the form

$$\left.\frac{dC}{d\chi}\right|_{\chi=0} = \begin{cases} \pm\dfrac{6}{8(J'+1)/J' - (1/5)(2J'-1)/(2J'+3)}, & (P\uparrow,P\downarrow) \\ \pm\dfrac{6}{8J'/(J'-1) - (1/5)(2J'+3)/(2J'-1)}, & (R\uparrow,R\downarrow) \end{cases} \tag{12}$$

This yields $(dC/d\chi)_{\chi=0}$ values of 0.7236 ($J' = 17$), and 0.7513 ($J' = 45$), as opposed to the value of $10/13 = 0.7692$ ($J' \rightarrow \infty$). The relaxation constant Γ was found through the time of spontaneous decay. This lies within the range of $\tau_{sp} = 12.45$–12.50 ns[16] for the v', J' levels of Na_2 ($A\,^1\Sigma_u^+$) included in the present discussion. The contribution of collisions at the working concentrations of vapors is expected to be insignificant. It was accounted for, assuming, as a fair estimate, a quenching cross section of 5×10^{-14} cm^2, as given in Ref. 30 for Na_2 ($B\,^1\Pi_u$)–Na collisions, leading to an increase in Γ by 4% with respect to τ_{sp}^{-1}.

The g-factor values obtained from the above procedure, as averaged over a number of experimental trials, are presented in Table I. The relative error of the values obtained was estimated to be 15%.

III. CAUSES FOR THE APPEARANCE OF A NONZERO ROTATIONAL MAGNETIC MOMENT IN THE $A\,^1\Sigma_u^+$ STATE OF Na_2

The Landè factor (g) of a diatomic molecule is well known to consist of a nuclear contribution (g_n) caused by the rotation of the nuclear core of the molecule, and of the electronic contribution ($g^e_{v'J'}$) created by the electronic shell of the rotating molecule.[31] In the case of a diamagnetic electronic state, as we have it in the $A\,^1\Sigma_u^+$ state ($\Omega = 0$) of Na_2, the electronic contribution is exclusively due to interaction of the given state with other electronic states which themselves possess a nonzero magnetic moment.

Obviously, the degree of the effect of different electronic states on the magnetic properties of the $A\,^1\Sigma_u^+$ state is determined by the ratio between the interaction matrix element value and the distance between the interacting states. Considering this circumstance, as well as the necessity of paramagnetism of the perturbing state, as well as the $u \leftrightarrow u$ selection rules, it becomes possible to select the basic electronic states, interaction with which leads to the appearance of a nonzero magnetic moment in the $A\,^1\Sigma_u^+$ state. The relative positions of potential curves employed in the present work are presented in Fig. 6.

A. Calculation of the nuclear contribution (g_n)

For a homonuclear diatomic molecule the value of the nuclear contribution is given by the expression[32–34]

$$g_n = \frac{\mu_n}{\mu_B}\frac{Z^*_{eff}}{\mathcal{M}_n}, \tag{13}$$

where $\mathcal{M}_n$ is the mass of the atom forming the molecule. Here μ_B and μ_n are the Bohr and nuclear magnetons, and Z^*_{eff} is the effective nuclear charge produced by the atomic core screened by the internal "nonvalence" atomic shell. The value of Z^*_{eff} is obviously not known *a priori*. Its calculation requires knowledge of the electronic wave functions of

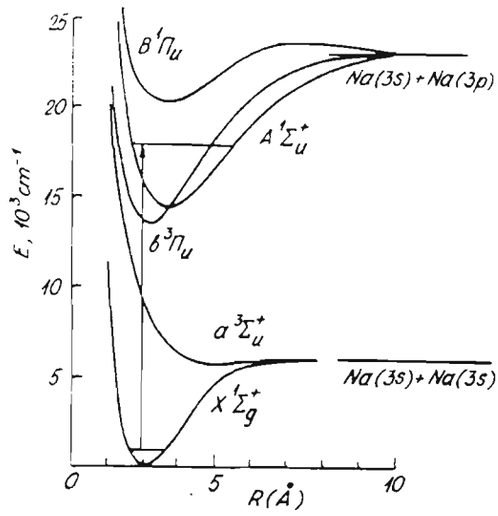

FIG. 6. Potential curves for the electronic states of Na_2 molecule considered in this work.

the molecule. Nevertheless, using a number of simplified model notions on the electronic structure of the given molecule, the value of Z^*_{eff} may be tentatively estimated. Thus, assuming that the electronic structure of alkali metal dimers is hydrogenlike, i.e., assuming that in the formation of the dimer only one external valence electron takes part from each atom, and assuming further that the structure of the internal shells of the atoms does not undergo any change in the transition from isolated atoms to a molecule, one may conclude that the value of Z^*_{eff} for them must be close to unity. In that case the value of the nuclear contribution for the Na_2 molecule must equal 2.4×10^{-5} (in Bohr magnetons).

The viability of the given model of accounting for the nuclear contribution is supported by the fair coincidence between calculated and measured rotational magnetic moment values for the electronic ground states of alkali metal dimers.[34] It ought to be stressed that the nuclear contribution is always positive and does not depend on vibrational and rotational quantum numbers. It appears also to change little from one electronic state to another.

B. Effect of $^1\Sigma$–$^3\Pi$ interaction on the Landè factors of the $A\,^1\Sigma_u^+$ and $b\,^3\Pi_u$ states

Let us first consider in a general way the effect of $^1\Sigma$–$^3\Pi$ perturbation on the Landè factors of interacting states of a diatomic molecule. After that we shall analyze in detail the peculiarities of its manifestation in the case of concrete rovibronic levels of $A\,^1\Sigma_u^+$ and $b\,^3\Pi_u$ states of the Na_2 molecule.

We shall represent the total wave function Ψ_t of the states under consideration in the form of a linear combination of nonperturbed wave functions corresponding to a "pure" Hund's case a

$$\Psi_t = S_\Sigma|^1\Sigma\rangle + S_{\Pi_0}|^3\Pi_0\rangle + S_{\Pi_1}|^3\Pi_1\rangle + S_{\Pi_2}|^3\Pi_2\rangle, \quad (14)$$

and the nonzero interaction matrix elements between $^1\Sigma$ and $^3\Pi_0$, $^3\Pi_1$ components of the $^3\Pi$ state, after Kovács[35] in the form

$$H_{\Sigma\Pi_0} \equiv \xi \approx \xi_{\text{el}}\langle v_\Sigma|v_{\Pi_0}\rangle, \quad (15a)$$

$$H_{\Sigma\Pi_1} = \gamma_{\text{el}}\langle v_\Sigma|v_{\Pi_1}\rangle[J(J+1)]^{1/2}, \quad (15b)$$

where v_Σ, v_Π are vibrational quantum numbers and J denotes the rotational quantum number that must be equal for both interacting states. The strongest $^1\Sigma$–$^3\Pi$ interaction is due to the spin–orbit interaction operator $\Sigma_k a_k l_k s_k$, where the summation is over all valence electrons. This interaction connects the $^1\Sigma$ and the $^3\Pi_0$ components and does not depend on J in explicit form, but does depend on the overlap integral between the vibrational wave functions $|v_\Sigma\rangle$ and $|v_{\Pi_0}\rangle$ of the interacting states. The nonzero matrix element of interaction between the $^1\Sigma$ and $^3\Pi_1$ component appears by virtue of the operator terms $-[1/(2\mu R^2)]\times(J^-L^+ + J^+L^-)$, where μ is the reduced mass, and R the internuclear distance (in atomic units). It is assumed here that the pure Hund's case a is disturbed, and the quantum number S of the spin vector S is no longer a good one.[36] The value of the matrix element $H_{\Sigma\Pi_1}$ for the molecules following pure Hund's case a must obviously be smaller than $H_{\Sigma\Pi_0}$. This appears to hold for such light molecules as Li_2 and Na_2.

An expression for the g factors of the states under discussion can be obtained from averaging the Zeeman operator $\hat{H}_Z = \mu_B\hat{B}(\hat{L}+2\hat{S})$,[37] where $\hat{B}$ is the magnetic field operator, over the total wave functions Ψ_t, cf. Eq. (14). Then, using the expressions for the matrix elements of operator $\hat{H}_Z$ acting on the basic wave functions, and corresponding to Hund's case a we find, in first-order perturbation theory[32]

$$\begin{aligned} g^t_\omega = &-[J(J+1)]^{-1}\{(S^2_{\Pi_1}+4S^2_{\Pi_0}) \\ &+2\sqrt{2}S_{\Pi_1}\left[S_{\Pi_0}\sqrt{J(J+1)}+S_{\Pi_2}\sqrt{J(J+1)-2}\right] \\ &+2S_\Sigma S_{\Pi_1}\sqrt{J(J+1)}\eta_{\text{el}}\langle v_\Sigma|v_{\Pi_1}\rangle\}, \end{aligned} \quad (16a)$$

where

$$\eta_{\text{el}} = \langle^3\Pi_1|l^+ + 2s^+|^1\Sigma\rangle. \quad (16b)$$

Expression (16) is valid for describing Landè factors for the $^1\Sigma$ state, as well as for each component of the $^3\Pi_t$ state. Thus in absence of $^1\Sigma$–$^3\Pi$ interaction ($S_\Sigma = 0$), formula (16) gets transformed into the well known expression for the g factor of the nonperturbed $^3\Pi$ state.[32] The characteristic dependence of Landè factors of each component of the nonperturbed $b\,^3\Pi_u$ state of Na_2 on the rotational quantum number J is represented in Fig. 7. It ought to be noted that the values of the $g^{^3\Pi_t}_\omega$ factors are practically independent of the vibrational quantum number v.

The value of the electronic matrix element η_{el}, similar to γ_{el} from Eq. (15b), must theoretically tend towards zero in the case of closeness of the electronic states under consideration to pure Hund's case a or b. One may, accordingly, easily neglect the last terms in Eq. (16a) for such light molecules as Li_2 and Na_2. With this in mind, we obtain a simple expression for the Landè factor of the perturbed $^1\Sigma$ state

$$g^{^1\Sigma}_\omega \approx -2\sqrt{2}S_{\Pi_1}(S_{\Pi_0}-S_{\Pi_2})/J. \quad (17)$$

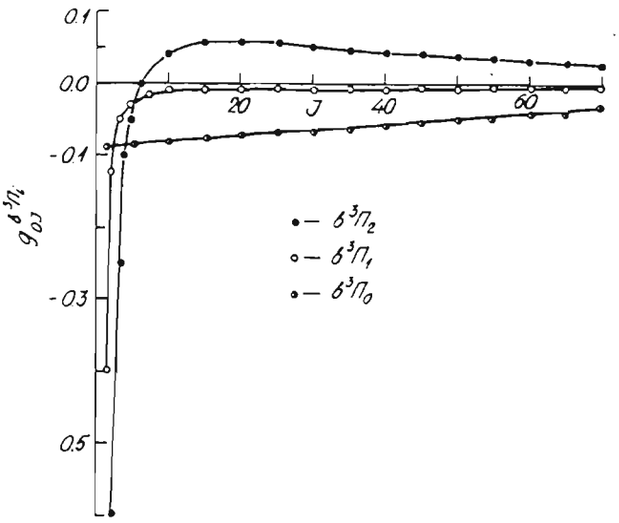

FIG. 7. The Lande factors' variation with the rotational quantum number J for the $^3\Pi_i$ components of nonperturbed Na_2 ($b\,^3\Pi_u$) triplet state with $v = 0$.

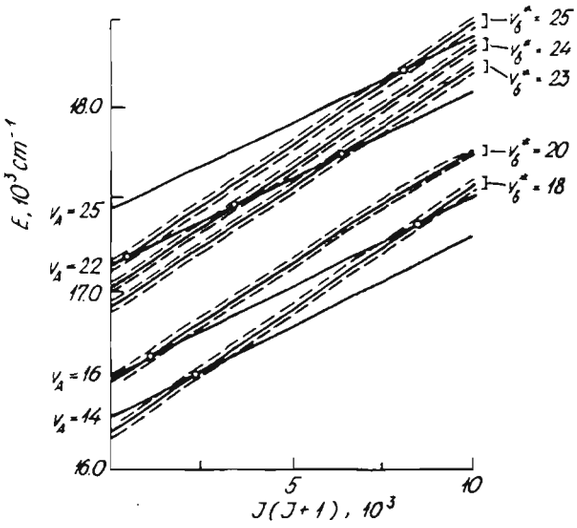

FIG. 8. Intersection of rovibronic levels $Na_2(A\,^1\Sigma_u^+, v_A, J)$ and $Na_2(b\,^3\Pi_u, v^*, J)$ for vibration states involved in this work. The values of triplet splitting for $b\,^3\Pi_u$ state (dashed lines) are strongly exaggerated.

We wish to draw attention to the following peculiarity of $^1\Sigma$–$^3\Pi$ interaction effect on the magnetic properties of the $^1\Sigma$ state. As mentioned above, for pure Hund's case a, nonzero matrix elements exist only between the $^1\Sigma$ state and the $^3\Pi_0$ component, which is itself diamagnetic, like the $^1\Sigma$ state ($\Omega = 0$). It follows that this component cannot contribute towards the magnetic moments of the $^1\Sigma$ state. The magnetism of the latter is, in this case, determined by indirect interaction with the paramagnetic $^3\Pi_1$ and $^3\Pi_2$ components through $^3\Pi_0$. This effect is analogous to well known phenomenon of accidental predissociation.[38] It is interesting to note that the degree of interaction of the $^3\Pi_1$ and $^3\Pi_2$ components with the $^1\Sigma$ state increases with increasing rotational quantum number J, cf. Eq. (16a). On the other hand, the rotational magnetic moment of a molecule is well known to decrease with increasing rotation.[10,32,38] The resulting magnetic moment is thus determined by the competition between these two processes.

We now consider specific results for the Na_2 molecule. As may be seen from Fig. 6, the potential curves of the $A\,^1\Sigma_u^+$ and $b\,^3\Pi_u$ states of Na_2 intersect and are strongly displaced with respect to each other. It follows that interaction between them is of distinctly local nature. Accordingly, the Landè factors of these states ought to depend strongly not only on rotational quantum numbers (J), but also on vibrational ones (v) in these regions. All vibrational levels of the $A\,^1\Sigma_u^+$ state are known to be perturbed by at least one, more frequently by two, and sometimes, within the observed J range, even by three levels of the $b\,^3\Pi_u$ state.[4,7,8] In each of these regions there are three resonances corresponding to maximum interaction with components $^3\Pi_2$, $^3\Pi_1$, and $^3\Pi_0$, respectively, as shown in Fig. 8. In order to study the peculiarities of the behavior of the g factors of perturbed $A\,^1\Sigma_u^+$ and all components of $b\,^3\Pi_i$ states ($i = 0,1,2$), as well as for analysis of their dependence on the absolute value of J and on the sign of the overlap integral $\langle v_A | v_b \rangle$, cf. Eq. (15a), a number of vibrational levels of the $A\,^1\Sigma_u^+$ state were selected, having various ranges of J values, cf. Fig. 9. The g-factor values for these levels were calculated according to formula (16a), assuming $\eta_{el} = 0$, cf. Eq. (16b). To this purpose, at first the full wave functions were found through numerical diagonalization of the 4×4 Hamilton matrix, cf. Eq. (14). The matrix elements were given in the form proposed in Ref. 7. The vibrational wave functions of the interacting states used in the calculations of $\langle v_A | v_b \rangle$, cf. Eq. (15a) were found from a numerical solution of the radial Schrödinger equation with RKR potentials for the $A\,^1\Sigma_u^+$ and $b\,^3\Pi_u$ states over deperturbed molecular states, according to Ref. 3 and 7, respectively. The electronic matrix element ξ_{el} was assumed to be independent of the internuclear distance.

It was found that in the vicinity of the points of intersection, i.e., in the vicinity of resonances, as shown in Fig. 8, the values and signs of mixing coefficients, i.e., of the Landè factors as well, are strongly dependent on the accuracy of the employed matrix elements of the Hamiltonian matrix, and are determined by the accuracy of the vibrational and rotational molecular constants for the $A\,^1\Sigma_u^+$ and $b\,^3\Pi_u$ states. However, the reliability of the deperturbed molecular constants for both states, as given in the literature, is regrettably small, the constants of centrifugal distortion D_v, H_v, etc., being particularly poorly known (in percent). This, in its turn, dramatically affects the accuracy of the calculated g factors at large J values. We therefore used effective sets of molecular constants and matrix elements in the Hamiltonian matrix for more accurate calculation of full wave functions of these levels. These sets are valid only within a limited range of values of v_A, v_b, and J.[4,7,8] The results of calculations of the rovibronic levels of the $A\,^1\Sigma_u^+$ state, for which the Landè factors have been measured in the present work (cf. Sec. II) are given in Table I in form of mixing coeffi-

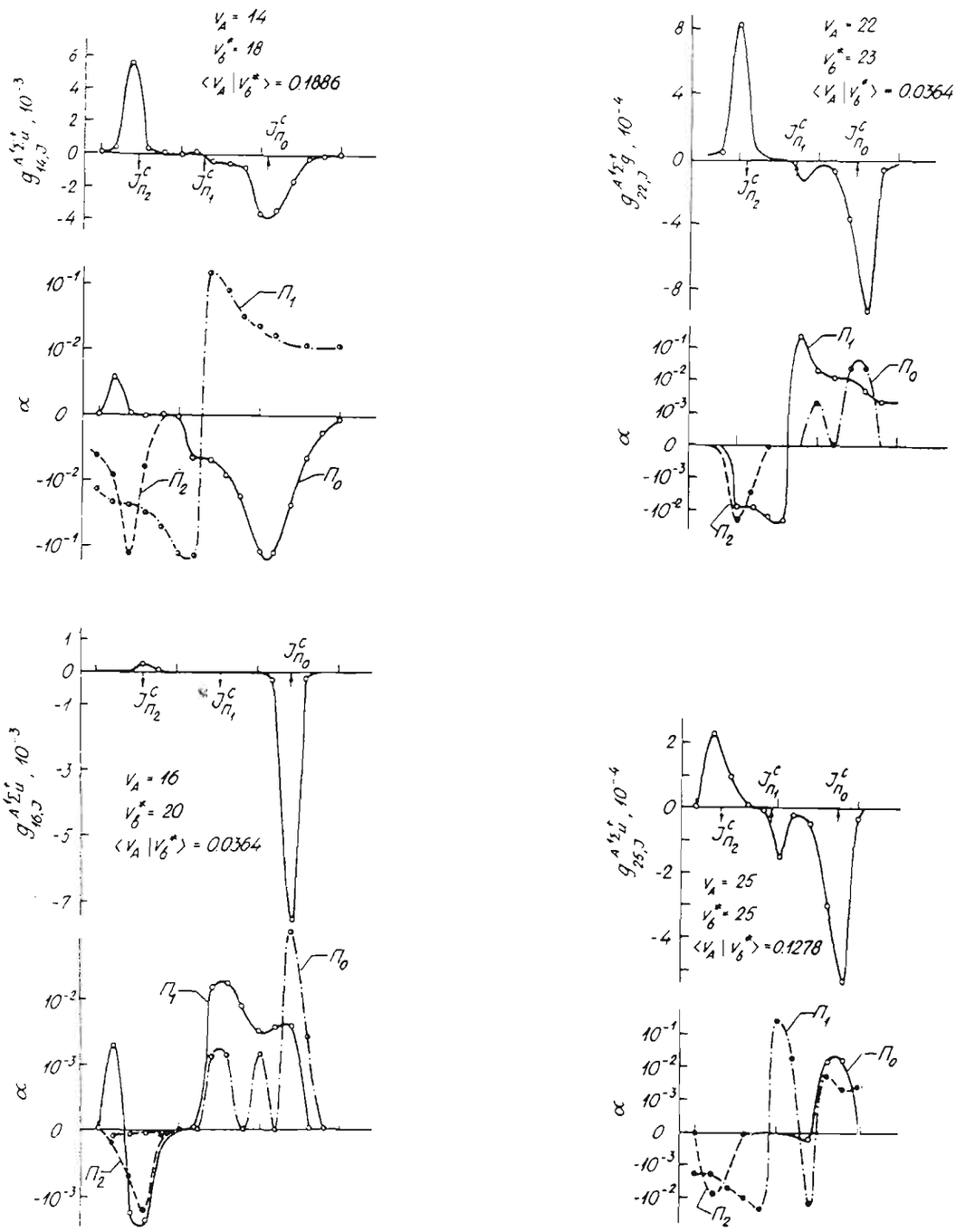

FIG. 9. J dependence of $g_{\omega J}^{A\,^1\Sigma_u^-}$ factors for $A\,^1\Sigma_u^-$ state, as well as of coefficients $\alpha = (g - g^*)/g$ for the components of $b\,^3\Pi_i$ state. Mutual $b\,^3\Pi_u$–$A\,^1\Sigma_u^+$ perturbation is considered according to Eq. (4). Ranges of J are 45–60 for $v_A = 14$, 25–40 for $v_A = 16$, 80–90 for $v_A = 22$, and 85–95 for $v_A = 25$.

cients and g factors. It may be seen from the presented data that level $v_A = 16$, $J = 17$ may be considered as nonperturbed with respect to other levels, i.e., its magnetism is not determined by $A\,^1\Sigma_u^+$–$b\,^3\Pi_u$ interaction.

On the whole, the following conclusions can be drawn from the results of our calculations of Landè factor dependences and of mixing factors, as dependent on quantum number J values, and presented in Fig. 9:

(i) As expected, the g factors $g_{\omega J}^{A\,^1\Sigma_u^+}$ of the $A\,^1\Sigma_u^+$ state change relatively considerably more than the g factors of the $b\,^3\Pi_u$ state. Maximum changes of the values of $g_{\omega J}^{A\,^1\Sigma_u^+}$ are observed in the vicinity of intersection with the $^3\Pi_2$ component (positive sign of the g factor), and with the $^3\Pi_0$ component (negative sign of the g factor). Absence of or very insignificant resonance in the vicinity of intersection with the $^3\Pi_1$

component may be due to opposite signs of mixing coefficients for S_{Π_0} and S_{Π_2}, cf. Eq. (17).

(ii) The absolute value of $g_{vJ}^{A\,^1\Sigma_u^+}$ near the resonances for the given vibrational level v decreases monotonically with increasing rotational quantum number J, assuming values from 10^{-1}–10^{-2} for low J values, down to 10^{-3}–10^{-4} for high ones. This is due to the fact that follows from Eq. (17): the mixing coefficient values in resonance vicinity depend only weakly on absolute J value and are mainly determined by the distance between deperturbed rovibronic levels of $A\,^1\Sigma_u^+$ and $b\,^3\Pi_i$ states near the resonances.

(iii) The nature of the J dependence of g factors of perturbed $b\,^3\Pi_i$ states in the vicinity of resonances is affected by circumstances: first, the distance between nonperturbed rovibronic levels of the $A\,^1\Sigma_u^+$ and $b\,^3\Pi_u$ states, and second, the steepness of the J dependence of nonperturbed components of the $b\,^3\Pi_u$ state, cf. Fig. 7. [For sake of convenience relative additions to the nonperturbed g factors in form of $\alpha = (g^* - g)/g$ are presented in Fig. 9.] It is for both these reasons, as may be seen from Fig. 9, that the relative addition to the g factor of $b\,^3\Pi_i$ state is most drastically dependent on J.

C. Effect of $^1\Sigma$–$^1\Pi$ interaction of the $A\,^1\Sigma_u^+$ and $B\,^1\Pi_u$ state Landè factors. Connection between Landè factors and Λ-doubling constants

The singlet $^1\Pi$ and $^1\Sigma$ states of diatomic molecules of similar parity ($u \leftrightarrow u$ and $g \leftrightarrow g$) interact owing to nonzero matrix elements of operator $[-1/(2\mu R^2)] \times (J^- L^- + J^- L^-)$. In energy characteristics this leads to Λ doubling of the $^1\Pi$ state, which manifests itself experimentally in the splitting of the $^1\Pi$ state levels with different parity ($+ \leftrightarrow +$ or $- \leftrightarrow -$). The Λ-doubling constant (q) is determined by the dependence[38]

$$q_{vJ} = 2 \sum_{v^*} \langle v_J^* | L^-(R)/R^2 | v_J \rangle^2 / \Delta T_{v^* vJ}, \tag{18a}$$

where

$$L^-(R) = \langle {}^1\Pi | L^- | {}^1\Sigma \rangle, \tag{18b}$$

$$\Delta T_{v^* vJ} = E_{vJ} - E_{v^* J}. \tag{18c}$$

In the case of the $^1\Sigma$ state this interaction leads to a change in the value of the experimentally found rotational constant $B_v^{\text{eff}} = B_v^{\text{true}} + q_v$. An experimental determination of the divergence of the effective rotational constant B_v^{eff} from the value B_v^{true} is difficult in the case of regular perturbations, by virtue of the smallness of q_v and its smooth dependence on the vibrational quantum number. Here B_v^{true} must be considered as the so-called "deperturbed" value of the rotational constant.[38]

The given interaction is also known to lead to a change in the Landè factors of the states under discussion[32]

$$g_{vJ} = -2 \sum_{v^*} \langle v_J^* | L^-(R)/R^2 | v_J \rangle \times \langle v_J^* | L^-(R) | v_J \rangle / \Delta T_{v^* vJ}. \tag{19}$$

As may be seen, using expressions (18a) and (19) for calculating g and q factors it is necessary to perform the summing (integrating) over all vibrational states of both the discrete and the continuous spectrum. The difficulty here is due to the necessity of executing a numerical solution of the radial Schrödinger equation for a large (in the general case, an infinite) number of levels of the discrete spectrum (v_J^*) and the continuous spectrum (ϵ_J), in order to satisfy the well known sum rule

$$\sum_{v^*} \langle v_J | v_J^* \rangle^2 + \int_{\epsilon_J} \langle v_J | \epsilon_J \rangle^2 \, d\epsilon_J = 1. \tag{20}$$

This problem becomes particularly acute in the case where the potential curves of the interacting electronic states are strongly displaced with respect to each other. Then condition (20) is approximately satisfied only in case of a very large number of terms in the summation and integration process in Eqs. (18a) and (19). We have used simple expressions for estimating effects of distant electronic states on q and the g factor without performing the summation and the integration over the nonbounded rovibronic levels of the perturbing state (cf. the Appendix). These expressions prove to be extremely time and labor saving in calculations.

Since there is one cause leading both to Λ doubling of rotational levels as well as to change in Landè factors, there must obviously exist a connection between the constants characterizing both effects. If such a connection is found, it becomes possible to estimate the effect of remote electronic states by means of experimentally accessible magnitudes. Hence, in order to assess such an effect in the case of interacting $A\,^1\Sigma_u^+$ and $B\,^1\Pi_u$ states of Na_2, let us start by finding in a general form the connection between q and the g factors of the interacting singlet states.

If we assume that for $^1\Pi$ and $^1\Sigma$ states $L^-(R) \approx |L^-| = \text{const}$ and $\Delta T_{v^* vJ} \approx \Delta T_e = \text{const}$, Eqs. (18a) and (19) can be written in following form:

$$q_{v^*}^{\,^1\Pi} \approx 2 |L^-|^2 (B_{v^*}^{\,^1\Pi})^2 / \Delta T_e, \tag{21a}$$

$$g_v^{\,^1\Sigma} \approx -2 |L^-|^2 B_v^{\,^1\Sigma} / \Delta T_e. \tag{21b}$$

Then, using Eqs. (21), we can easily find the connection between Λ-doubling constant of the $^1\Pi$ state and Landè factor of the $^1\Sigma$ state

$$g_{vJ}^{\,^1\Sigma} \approx -q_{v^* J}^{\,^1\Pi} B_v^{\,^1\Sigma} / (B_{v^*}^{\,^1\Pi})^2. \tag{22}$$

The interaction between the $A\,^1\Sigma_u^+$ and $B\,^1\Pi_u$ states of Na_2 is known to have been experimentally established in the course of studying the Λ doubling of the rotational levels of the $B\,^1\Pi_u$ state.[39] In order to estimate the effect of this interaction on the Landè factors of the $A\,^1\Sigma_u^+$ state, we employed expressions (18a) and (19), as well as approximate relations (A9) and (A10). Before we did this, however, we checked the feasibility of Eqs. (A6) and (A7) for the states where relation (20) is valid, i.e., $0 \leqslant v \leqslant 10$ and $0 \leqslant v^* \leqslant 10$. In order to simplify the calculations we assumed that $|L^-| = 1$. Calculation results for q and g factors obtained with the aid of formula (18a), Eqs. (19), (A9), and (A10) were compared for above-mentioned v values, as well as for those used in the experiment. In all cases the relative difference of the results given by Eqs. (18a), (19), (A9), and (A10) does not exceed

$\sim 2 \times 10^{-4}$, which lies far below experimental error range.

In order to construct the potential curve for the $B\,^1\Pi_u$ state we used data according to Refs. 39–41. Subsequently, formula (A9) was employed under the assumption $L^-(R) = \text{const}$ for calculating the values of factors q_{v^*J} for the levels of the $B\,^1\Pi_u$ state, viz. for $0 \leqslant v^* \leqslant 30$ and $0 \leqslant J \leqslant 100$. A comparison between experimental values of Λ-doubling constants, $q^{\text{exp}}_{v^*J}$ as presented in Ref. 39, and theoretical $q^{\text{th}}_{v^*J}$ ones shows that the magnitude $|L^-|$ can be considered as constant for all levels under study with 5% accuracy: $|L^-| = 1.42 \pm 0.05$. This demonstrates, on the one hand, the validity of the assumption $L^-(R) = \text{const}$ for the states under consideration, and confirms, on the other hand, with respect to these states, the hypothesis of pure Van Vleck precession:[42] $\langle {}^1\Pi | L^- | {}^1\Sigma \rangle = \sqrt{l(l+1)} = \sqrt{2}$. After that, using $|L^-|$, as obtained by means of formulas (A9) and (A10) the values of the q factors for the $B\,^1\Pi_u$ state were evaluated, as well as the g factor of the $A\,^1\Sigma_u^-$ state. The dependences of the values obtained for the vibrational (v) and rotational (J) quantum numbers are presented in Fig. 10.

Thus the interaction between the $A\,^1\Sigma_u^-$ and $B\,^1\Pi_u$ states leads to the production of a negative magnetic moment of the order of 7.5×10^{-5} in the $A\,^1\Sigma_u^-$ state, which only slightly depends on v and J.

D. Effect of indirect $A\,^1\Sigma_u^+$–$b\,^3\Pi_u$–$a\,^3\Sigma_u^+$ interaction on the Landè factors of the $A\,^1\Sigma_u^+$ state

As may be seen from Fig. 6, the next nearest to $A\,^1\Sigma_u^-$ paramagnetic state after $b\,^3\Pi_u$ and $B\,^1\Pi_u$ is the weakly bonded $a\,^3\Sigma_u^+$ state.[43,44] Interaction with the latter can also contribute towards the rotational magnetic moment of the $A\,^1\Sigma_u^-$ state. The peculiarity of this interaction consists in the circumstance that it is of indirect nature, since any non-zero matrix elements between the $^1\Sigma_u^-$ and the $^3\Sigma_u^-$ state do not exist, subject to pure Hund's case a.[35] This interaction therefore takes place through the $b\,^3\Pi_0$ component of the $b\,^3\Pi_u$ state. Another important feature of this A–b–a interactions is due to the repulsive nature of the potential curve of the $a\,^3\Sigma_u^-$ state in the relevant region of internuclear distances (Fig. 6). It may be of interest to note that in the case of the Li_2 molecule the potential curves of the $a\,^3\Sigma_u^-$ and $b\,^3\Pi_u$ states intersect,[45] and the interaction produces an effect of indirect predissociation.[46] Such an effect may take place also in the case of Na_2, but only for very high vibrational quantum numbers of the $A\,^1\Sigma_u^+$ state.[43] In the case of the rovibronic levels of the $A\,^1\Sigma_u^-$ state under consideration interaction between the $b\,^3\Pi_0^-$ and $a\,^3\Sigma_1^-$ levels is small and is of regular nature owing to the remoteness of the $a\,^3\Sigma_u^+$ state $[\Delta T_e = T_e(b\,^3\Pi_u) - T_e(a\,^3\Sigma_u^-) \approx 7000\ \text{cm}^{-1}]$. Nevertheless, by virtue of locality of $A\,^1\Sigma_u^+$–$b\,^3\Pi_0$ interaction, the total effect of $a\,^3\Sigma_u^-$ on the magnetism of the $A\,^1\Sigma_u^-$ state is also of local nature. Using the expression for the matrix elements of $^3\Pi_0^-$–$^3\Sigma_1^-$ interaction,[35] viz.,

$$H_{\Pi_0\Sigma_1} = \langle v_b | \beta(R)/R^2 | v_a^* \rangle \sqrt{J(J-1)}, \tag{23a}$$

where

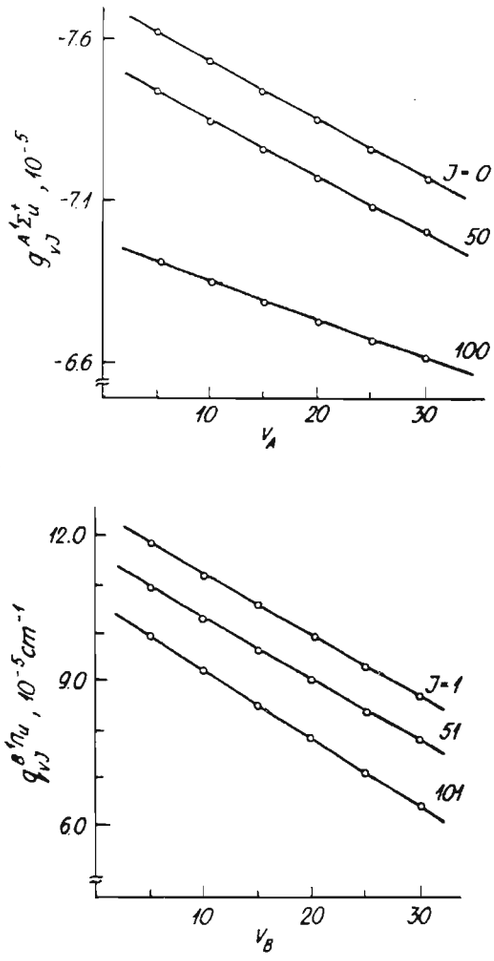

FIG. 10. v dependence of g'_{vJ} for $A\,^1\Sigma_u^-$ and q_{vJ} factors for $B\,^1\Pi_u$ states of Na_2 as calculated according to Eqs. (A9) and (A10) for various J.

$$\beta(R) = \langle {}^3\Sigma_1^- | L^- | {}^3\Pi_0 \rangle, \tag{23b}$$

we obtain in first-order perturbation theory an expression for the contribution of the $a\,^3\Sigma_u^+$ state to the g factor of the $A\,^1\Sigma_u^+$ state

$$g_{vJ}^{A\,^1\Sigma} = 2S_{\Pi_0} \sum_{v_a^*}^{\infty} [\langle v_b | \beta(R)/R^2 | v_a^* \rangle \times \langle v_a^* | \beta(R) | v_b \rangle]/(E_{v_aJ} - E_{v_a^*J}). \tag{24}$$

It ought to be stressed that, owing to the almost repulsive nature of the $a\,^3\Sigma_u^-$ state, it is necessary to perform the integration over the non-bonded states of the continuous spectrum [cf. Eq. (A1)].

Expression (24) can be easily simplified on assuming that Eq. (A2) is valid in the case of the states under discussion. Then we can use the approximate dependence (A10), thus obtaining

$$g_{vJ}^{A\,^1\Sigma} \approx 2S_{\Pi_0} \langle v_b | \beta^2(R)/[R^2 \Delta U(R)] | v_b \rangle, \tag{25a}$$

where (cf. Fig. 11)

$$\Delta U(R) = U_a(R) - U_A(R). \tag{25b}$$

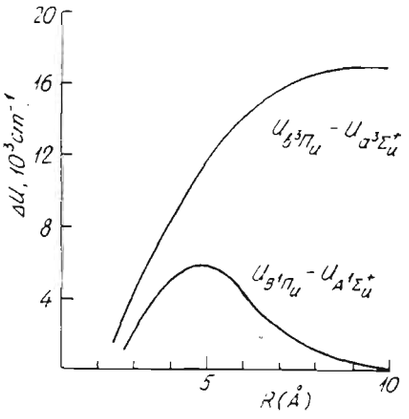

FIG. 11. The difference potential $\Delta U(R)$ between $B\,^1\Pi_u$–$A\,^1\Sigma_u^-$ and $b\,^3\Pi_u$–$a\,^3\Sigma_u^-$ states of Na_2.

Assuming further that the $b\,^3\Pi_u$ and $a\,^3\Sigma_u^-$ states, as well as the $A\,^1\Sigma_u^-$ and the $B\,^1\Pi_u$ states follow the Van Vleck "pure precession" hypothesis,[42] the magnitude $\beta(R)$ can be estimated as $\beta(R) \approx \text{const} = 2$. We then obtain a rough assessment of the contribution of the $a\,^3\Sigma_u^-$ state

$$g_{\omega J}^{A\,^1\Sigma} \simeq 4 S_{\Pi_0} B_v^{b\,^3\Pi_u} / \Delta T_e. \tag{26}$$

The contribution of the $a\,^3\Sigma_u^-$ state into the g factor of the $A\,^1\Sigma_u^-$ state as evaluated according to Eq. (26) does not exceed 0.01–0.1 of the contribution from the $b\,^3\Pi_u$ state. From our point of view it is small enough to neglect this effect for the vibrational levels under consideration. However, the influence of the $a\,^3\Sigma_u^-$ state may increase dramatically in the vicinity of intersection of the curves of the $b\,^3\Pi_u$ and $a\,^3\Sigma_u^+$ states when $[\Delta U(R)]^{-1} \to \infty$. In this situation expression (24) clearly ceases to apply, and the $b\,^3\Pi_u$–$a\,^3\Sigma_u^+$ perturbation changes from regular to local, such as in the case of $A\,^1\Sigma^+$–$b\,^3\Pi_u$ mixing.

IV. DISCUSSION

The resulting g-factor values, as obtained for Na_2 ($A\,^1\Sigma_u^-$) from measurements ($g_{v'J'}^{\exp}$) and from calculations ($g_{v'J'}^{\text{th}}$) presented in Table I are, in principle, not in contradiction to each other. The best coincidence, for $v' = 16$, $J' = 17$, might be due to the circumstance that, in this case, the contribution from $A\,^1\Sigma_u^+$–$b\,^3\Pi_u$ interaction is negligibly small. On the other hand, inaccuracy in the calculation of this interaction can affect most strongly the relative error in $g_{v'J'}^{\text{th}}$ (tot) in a situation when the g-factor value (or, rather, its electronic part $g_{v'J'}^{e}$) is the difference of two partial contributions of interactions with the states $b\,^3\Pi_u$ and $B\,^1\Pi_u$, these contributions being comparable in value, but opposite in sign. This may be the cause of the deviation from the experimental results for levels with $v' = 14$, and $v' = 25$.

We performed an analysis, in order to elucidate the accuracy of calculations of the contribution of the $b\,^3\Pi_u$–$A\,^1\Sigma_u^-$ interaction to the Landè factor value of the $A\,^1\Sigma_u^-$ state. We found this contribution to be highly sensitive to the accuracy of the unperturbed molecular constants used. This was most striking at high J values. Thus, for example, a change in the constant of centrifugal distortion D_{v^*}, for $v^* = 25$ of the $b\,^3\Pi_u$ level by 20% (which lies far below the experimental error in its determination) causes a change in Landè factor values of the $v' = 25$ level of the $A\,^1\Sigma_g^+$ state in the resonance region ($85 < J < 95$) by several orders of magnitude. It may be expected that systematic high precision measurements of g factors of the $A\,^1\Sigma_u^+$ state for each J value within the probable resonance range might permit, by solving the reverse problem, readjust the position of the rotational number of the points of intersection (cf. Figs. 8 and 9), and thus obtain more accurate values of the molecular constants.

Owing to the circumstance that the discussed electronic states of Na_2 are, in our opinion, subject to pure Hund's case a, the interference term in Eq. (16a), which corresponds to direct interaction, turns out to be negligibly small. It is known, however, that with increasing nuclear charge in the molecular series K_2, Rb_2, and Cs_2 (Ref. 47), an increase in relativistic effects takes place. In particular, the value of spin–orbit interaction becomes larger,[13] and it is not excluded that the interference term in Eq. (16a) may play some role in the formation of the Landè factors of the state, particularly for the levels with high J values.

Moreover, with increase in spin splitting of the triplet one may apparently neglect the effect of $A\,^1\Sigma_u^+$ interaction with the components of $b\,^3\Pi_0$ and $b\,^3\Pi_2$ on the g factors of the $A\,^1\Sigma_u^-$ state. It will be the direct interaction between $A\,^1\Sigma_u^-$ and the $b\,^3\Pi_1^-$ component of $b\,^3\Pi_u$, which will play the main part in the formation of the nonzero magnetic moment of the A state. Expression (16a) will then assume the form

$$g_{\omega J}^{A\,^1\Sigma_u^-} = \frac{2 S_\Sigma S_{\Pi_1} \eta_{\text{el}} \langle v_\Sigma | v_{\Pi_1}^* \rangle}{\sqrt{J(J+1)}} + \frac{S_{\Pi_1}^2}{J(J+1)}, \tag{27a}$$

where

$$\eta_{\text{el}} = \langle {}^1\Sigma^+ | J_a^+ | {}^3\Pi_1^- \rangle. \tag{27b}$$

The present example of $A\,^1\Sigma_u^+$–$B\,^1\Pi_u$ interaction permits one to draw an interesting conclusion on how it is possible to study experimentally the characteristics of a distant electronic state. As may be seen, the effect of distant electronic states on the position of rovibronic levels of the $^1\Sigma$ state are practically impossible to observe experimentally by virtue of the insignificance of q_v with respect to the deperturbed B_v^{true} values. At the same time this effect can be easily assessed experimentally from the change in Landè factor value, since this change is very considerable against the zero value g factor of the unperturbed $A\,^1\Sigma_u^-$ state. In opposition to this, it appears to be experimentally simpler to notice and measure the Λ-doubling effect in the $^1\Pi$ state, since the change in Landè factor value can be experimentally noticed only at very large J values, when the intrinsic magnetism of the $^1\Pi$ state $g_J = -1/[J(J+1)]$ is negligible. The connection between q and the g factors, as employed in the present work, makes it possible to establish an unequivocal connection between the results of physical experiments which are alien to each other. This circumstance acts in addition to the

previously established[48] connection between g factors and constants of hyperfine (spin–orbital) interaction. Thus results of magnetism studies may in certain cases be used for the determination of structural parameters of molecules more accurately than possible by direct measurements.

Study of the effect of the above-mentioned interactions magnetic properties appears to be of interest also from the point of view of studies of the peculiarities of their manifestations in states belonging to various cases of Hund coupling in the $Li_2 \rightarrow Cs_2$ sequence. Thus, for example, in the case of the Li_2 molecule the peculiarity of the effect of the interactions under discussion is connected with the circumstance that for such a light molecule the value of spin–orbital interaction is lower by an order of magnitude than in the case of Na_2, leading to a Hund's case b.[47] Apparently, this leads both to considerable weakening of $A\,^1\Sigma_u^+$–$b\,^3\Pi_u$ interaction effect on the magnetic properties of the $A\,^1\Sigma_u^+$ state and narrowing of the resonance signal's (in $g_{vJ}^{A\,^1\Sigma_u^+}$) dependence on J. Recently the magnetism in Li_2 ($A\,^1\Sigma_u^+$) was studied in Ref. 49 using the Faraday rotation method. On the other hand, with diminishing reduced mass value of the molecule an increase of the contribution of nuclear rotation takes place, cf. Eq. 13), as well as of the electronic contribution on the part of the distant $B\,^1\Pi_u$ state, cf. Eq. (3). Another peculiarity in the behavior of Li_2 is connected with the fact that, owing to mutual intersection of the potential curves of $b\,^3\Pi_u$ and $^3\Sigma_u^+$, there is a noticeable increase in the effect of the $^3\Sigma_u^+$ state (in comparison with Na_2), this effect necessarily being of pronounced local nature. As a further consequence of this intersection there must be a diminution in the lifetime of the perturbed levels of the $A\,^1\Sigma_u^+$ state, caused by accidental predissociation.[46]

I. CONCLUSION

The approach used in the present work for studying perturbations, based on Landè factor measurements of perturbed diamagnetic ($\Omega = 0$) states, appears to us to be a highly competitive method permitting detailed investigation not only of local, but also of weak regular perturbations, the analysis of which may be inaccessible by traditional high-resolution spectroscopic methods.

APPENDIX

In the assessment of the effect of distant electronic states on the characteristics under discussion [cf., e.g., expressions (18a) and (19)] of the given rovibronic state it is necessary to calculate the following form[38,50]

$$F = \sum_{v^*} \frac{\langle v_J|f(R)|v_J^*\rangle\langle v_J^*|\mu(R)|v_J\rangle}{E_{vJ} - E_{v^*J}} + \int \frac{\langle v_J|f(R)|\epsilon_J\rangle\langle\epsilon_J|\mu(R)|v_J\rangle d\epsilon_J}{E_{vJ} - \epsilon_J}, \qquad \text{(A1)}$$

where summation and integration is performed over all rovibronic states of the discrete and continuous spectrum, $f(R)$ and $\mu(R)$ being known continuous functions of the internuclear distance.

In the case then the perturbing electronic state is far off the perturbed one, we propose a simple form for estimating the expressions of (A1) type

$$F \approx \langle v_J|f(R)\mu(R)/\Delta U(R)|v_J\rangle, \qquad \text{(A2)}$$

where $\Delta U(R)$ is a potential difference of the states under consideration. Let us consider the conditions when the approximation (A2) is valid. For this purpose let us use the expansion of $\Delta U(R)$ into a Taylor series in the vicinity of the point R_c

$$\Delta U(R) = \Delta U(R_c) + \Delta U'(R_c)\Delta R + \Delta U''(R_c)(\Delta R)^2/2 + \cdots, \qquad \text{(A3)}$$

where $\Delta R = R - R_c$, and $R_c = \langle v_J|R\,|v_J^*\rangle/\langle v_J|v_J^*\rangle$ is so-called R centroid.[51] Then neglecting the higher powers in Eq. (A3) one can obtain

$$\frac{f(R)}{\Delta U(R)} \approx \frac{f(R)}{\Delta U(R_c)}\left[1 - y_1\Delta R + (y_1^2 - y_2)(\Delta R)^2\right], \qquad \text{(A4)}$$

where $y_1 = \Delta U'(R_c)/\Delta U(R_c)$, $y_2 = \Delta U''(R_c)/[2\Delta U(R_c)]$. Taking into account that[52]

$$E_{vJ} - E_{v^*J} = \langle v_J|\Delta U(R)|v_J^*\rangle/\langle v_J|v_J^*\rangle \approx \Delta U(R_c)(1 + y_2 Y_2 + \cdots), \qquad \text{(A5)}$$

where $Y_2 = \langle v_J|(\Delta R)^2|v_J^*\rangle/\langle v_J|v_J^*\rangle$, and assuming that $f(R) \approx f(R_c) + f'(R_c)\Delta R$ is weakly dependent on R after integrating the both parts of Eq. (A4) we can obtain

$$\langle v_J|f(R)/\Delta U(R)|v_J^*\rangle \approx \frac{\langle v_J|f(R)|v_J^* - y_1 f'(R_c)X_2 + f(R_c)[X_2(y_1^2 - y_2) - Y_2 y_2]}{E_{vJ} - E_{v^*J}}, \qquad \text{(A6)}$$

where $X_2 = \langle v_J|(\Delta R)^2|v_J^*\rangle$. Then multiplying both parts of Eq. (A6) with $\langle v_J^*|\mu(R)|v_J\rangle$ and using the sum rule (20) it is possible to get the approximation (A2) and also to estimate its relative error ξ_F as

$$\xi_F \approx \sum_{v^*} \{[(f_1 - y_1)y_1 - y_2]X_2 - y_2 Y_2\}, \qquad \text{(A7)}$$

where $f_1 = f'(R_c)/f(R_c)$. It is clear that $\xi_F = 0$ in the R-centroid approximation. In real case the ξ_F value is the smaller, the larger is the distance $\Delta U(R)$ between the interacting electronic states, and the closer to each other are the shapes of their potential curves, i.e., the smaller the difference between their vibrational and rotational constants. The $\Delta U = U_{1_\Pi} - U_{1_\Sigma}$ and $\Delta U = U_{b^3\Pi} - U_{a^3\Sigma}$ values, as dependent on internuclear distance R are represented in Fig. 11 for the electronic states discussed in this paper. Additionally, the ξ_F is smaller for the low vibrational levels and for the states with small values of the parameter $\gamma = B_e/\omega_e$.[53] It may be of interest to know that the obtained expression

(A2) is similar to the approximation for lifetime estimation[54]

$$\tau_{vJ}^{-1} \approx \langle v_J | [\Delta U(R)]^3 \mu^2(R) | v_J \rangle. \quad \text{(A8)}$$

Thus substituting $f(R) = L^-(R)/R^2$, $\mu(R) = L^+(R)$ into Eq. (A2), we obtain the following expressions for the q and g factors:

$$q_{v^*J} \approx 2\langle v_J^* | [L^-(R)]^2/[R^4 \Delta U(R)] | v_J^* \rangle, \quad \text{(A9)}$$

$$g_{vJ} \approx -2\langle v_J | [L^+(R)]^2/[R^2 \Delta U(R)] | v_J \rangle. \quad \text{(A10)}$$

[1] R. S. Mulliken, Rev. Mod. Phys. **4**, 15 (1932).
[2] T. Carrol, Phys. Rev. **52**, 822 (1937).
[3] M. E. Kaminsky, J. Chem. Phys. **66**, 4951 (1977).
[4] J. B. Atkinson, J. Becker, and W. Demtröder, Chem. Phys. Lett. **87**, 92 (1982).
[5] F. Engelke, H. Hage, and C. D. Caldwell, Chem. Phys. **64**, 221 (1982).
[6] K. Shimizu and F. Shimizu, J. Chem. Phys. **78**, 1126 (1983).
[7] C. Effantin, O. Babaky, K. Hussein, J. d'Incan, and R. F. Barrow, J. Phys. B **18**, 4077 (1985); O. Babaky and K. Hussein, Z. Naturforsch. Teil A **45**, 795 (1990).
[8] H. Kato, M. Otani, and M. Baba, J. Chem. Phys. **89**, 653 (1988).
[9] O. C. Mullins, C. R. Makon, and T. F. Gollagher, Chem. Phys. Lett. **126**, 501 (1986).
[10] G. Gouedard and J. C. Lehmann, Faraday Discuss. Chem. Soc. **71**, 143 (1981).
[11] R. S. Ferber, O. A. Shmit, and M. Ya. Tamanis, Chem. Phys. Lett. **92**, 393 (1982).
[12] R. S. Ferber, A. I. Okunevich, O. A. Shmit, and M. Ya. Tamanis, Chem. Phys. Lett. **90**, 476 (1982).
[13] A. V. Stolyarov, E. A. Pazyuk, L. A. Kuznetsova, Ya. A. Harya, and R. S. Ferber, Chem. Phys. Lett. **166**, 290 (1990).
[14] K. K. Verma, T. H. Vu, and W. C. Stwalley, J. Mol. Spectrosc. **85**, 131 (1981).
[15] I. P. Klincare, A. V. Stolyarov, M. Ya. Tamanis, and R. S. Ferber, in *Opticheskaya Orientatsia Atomov i Molekul*. Part 2, edited by G. V. Klementyev (Leningrad, RTP LIYaF, 1990), pp. 16–21.
[16] G. Baumgartner, H. Kornmeier, and W. Preuss, Chem. Phys. Lett. **107**, 13 (1984).
[17] F. W. Dalby, J. Vigue, and J. C. Lehmann, Can. J. Phys. **53**, 140 (1975).
[18] M. P. Auzin'sh, M. Ya. Tamanis, and R. S. Ferber, Opt. Spektrosk. **63**, 989 (1987) [Opt. Spectrosc. (USSR) **63**, 582 (1987)].
[19] I. P. Klincare, A. V. Stolyarov, M. Ya. Tamanis, and R. S. Ferber, Opt. Spektrosk. **66**, 1018 (1989).
[20] A. Omont, Prog. Quantum Electron. **5**, 69 (1977).
[21] M. I. Dyakonov, Zh. Eksp. Teor. Fiz. **47**, 2213 (1964) [Sov. Phys. JETP **20**, 1484 (1965)].
[22] K. Blum, *Density Matrix Theory and Applications* (Plenum, New York, 1981).
[23] M. P. Auzin'sh and R. S. Ferber, Phys. Rev. A **43**, 2374 (1991).
[24] P. P. Feofilov, *The Physical Basis of Polarized Emission* (Consultants Buerau Ent., New York, 1961); R. Zare, *Angular Momentum* (Wiley-Interscience, New York, 1988).
[25] W. Hanle, Z. Phys. **30**, 93 (1924).
[26] M. P. Auzin'sh and R. S. Ferber, Zh. Tehn. Fiz. **55**, 1591 (1985) [Sov. Phys. Tech. Phys. **30**, 630 (1985)].
[27] A. N. Nesmeyanov, *The Vapor Pressure of the Chemical Elements* (Akad. Nauk SSSR, Moscow, 1961).
[28] R. N. Drullinger and R. N. Zare, J. Chem. Phys. **51**, 5532 (1969).
[29] R. S. Ferber, O. A. Shmit, and M. Ya. Tamanis, Chem. Phys. Lett. **61**, 441 (1979).
[30] W. Demtröder, *Laser Spectroscopy* (Springer, Berlin, 1982).
[31] N. F. Ramsey, *Molecular Beams* (Oxford University, London, 1955).
[32] M. Mizuchima, *The Theory of Rotating Diatomic Molecules* (Wiley, New York, 1975).
[33] L. Veseth, J. Mol. Spectrosc. **63**, 180 (1976).
[34] R. A. Brooks, C. H. Anderson, and N. F. Ramsay, Phys. Rev. A **136**, 62 (1964).
[35] I. Kovács, *Rotational Structure in the Spectra of Diatomic Molecules* (Higler, London, 1969).
[36] J. T. Hougen, *The Calculations of Rotational Energy Levels and Rotational Line Intensities in Diatomic Molecule*, NBS Monograph, 115 (Natl. Bur. Stand., Washington, D.C., 1970).
[37] L. D. Landau and E. M. Lifshitz, *Quantum Mechanics—Nonrelastivic Theory* (Pergamon, London, 1958).
[38] H. Lefebvre-Brion and R. W. Field, *Perturbations in the Spectra of Diatomic Molecules* (Academic, New York, 1986).
[39] P. Kusch and M. M. Hessel, J. Chem. Phys. **68**, 2591 (1978).
[40] G. K. Chawla, H. Vedder, and R. W. Field, J. Chem. Phys. **86**, 3082 (1987).
[41] E. Tiemann, Z. Phys. D. **5**, 77 (1987).
[42] J. H. Van Vleck, Phys. Rev. **33**, 467 (1929).
[43] D. D. Konowalow, M. E. Rosenkrantz, and M. L. Olson, J. Chem. Phys. **72**, 2612 (1980).
[44] Li Li, S. F. Rice, and R. W. Field, J. Chem. Phys. **82**, 1178 (1985).
[45] J. L. Fish and D. D. Konowalow, Chem. Phys. **84**, 463 (1984).
[46] T. User and A. Dalgarno, Chem. Phys. **51**, 271 (1980).
[47] A. J. Ross, P. Crozet, C. Effantin, J. d'Incan, and R. F. Barrow, J. Phys. B **20**, 6225 (1987).
[48] C. H. Townes and A. L. Schawlow, *Microwave Spectroscopy* (McGraw-Hill, New York, 1955).
[49] W. H. Jeng, X. Xie, L. P. Gold, and R. A. Bernheim, J. Chem. Phys. **93**, 2957 (1990); *ibid.* **94**, 928 (1991).
[50] R. N. Zare, A. L. Schmeltekoph, W. J. Harrop, and D. L. Albritton, J. Mol. Spectrosc. **46**, 37 (1973).
[51] P. A. Fraser, Can. J. Phys. **32**, 515 (1954).
[52] C. Noda and R. F. Zare, J. Mol. Spectrosc. **95**, 254 (1982).
[53] N. E. Kuz'menko and A. V. Stolyarov, J.Q.S.R.T. **35**, 415 (1986).
[54] J. Tellinghuisen and P. S. Julienne, J. Chem. Phys. **81**, 5779 (1984).

Observation of $A\ ^1\Sigma_u^+ \sim b\ ^3\Pi_u$ interaction in g factors of weakly coupled Na_2 $A\ ^1\Sigma_u^+$ state levels

A. V. Stolyarov,[a] I. P. Klincare, M. Ya. Tamanis, and R. S. Ferber
Department of Physics and Mathematics, University of Latvia, Riga, Latvia, 226098

(Received 17 June 1992; accepted 28 September 1992)

The $b\ ^3\Pi_u$–$A\ ^1\Sigma_u^+$ interaction in Na_2 as manifested by $A\ ^1\Sigma_u^+$ state Lande factors was investigated. Landé factors g_A were measured from the dispersion shape Hanle signal in fluorescence excited by 647.1 and 676.4 nm Kr^+-laser lines. The partial contribution g_{Ab} due to weak $A \sim b$ interaction was extracted from measured g factors for v_A, J levels with v_A between 8 and 29. The electronic part of the spin–orbit (SO) interaction matrix element $H_{so}^e = 5.86 \pm 0.20\ cm^{-1}$ was determined by deperturbation fitting of g_{Ab} values. Possible error sources in $A\ ^1\Sigma_u^+$ state g-factor treatment due to imperfection in the physical model employed, inaccuracy of existing set of $b\ ^3\Pi_u$ state molecular constants and nonlinear magnetic field effects were analyzed.

I. INTRODUCTION

Detailed spectroscopic investigation of diatomic molecules with the aim of determining accurate molecular constants often results in a deperturbation problem. The deperturbation procedure strives to obtain the set of "pure" molecular constants, that describe a molecular state undisturbed by interaction with any other state.[1] From another point of view, the deperturbation is used to get information about the perturbing state, which may be unobservable by direct spectroscopic measurements. Increasing accuracy in level shift and lifetime studies allows the detection of weaker perturbations. It is clear however, that the most perturbation sensitive parameters would be those possessing a near zero value in perturbation free conditions. This is obviously not the case for level shifts and lifetimes changes. It is possible to approach the desirable situation by performing either intensity measurements of forbidden transitions or studies of magnetic properties of a diamagnetic state. For example, in Ref. 2 both the anomalous relative intensities in the perpendicular $B0_u^+ \rightarrow X1_g$ transition as well as $B0_u^+$ state Landé factors $g^{\omega J}$ were registered in the Te_2 molecule. As shown in Ref. 3, both features can be described simultaneously as a result of $B0_u^+ \sim A1_u$ interaction with the near by $A1_u$ state. A nice demonstration of the especially high sensitivity of g values to local perturbations is given in Ref. 4 for the $B0_u^+$ state in the $^{80}Se_2$ molecule.

To compare the sensitivity of the above mentioned methods, one has to remember that the level shift value is of the order of $\sim H_{ij}^2/\Delta E_{ij}$, changes in lifetime $\sim (H_{ij}/\Delta E_{ij})^2$, while diamagnetic state g-factor value is $\sim H_{ij}/\Delta E_{ij}$ assuming a zero perturbation free g value. H_{ij} denotes the interaction matrix element, ΔE_{ij} the energy difference between the two deperturbed interacting levels. Hence, Landé factor measurements appear to be most useful for the purpose of observing perturbations which are weak due to the smallness of the interaction matrix element ($H_{ij} < 0.1\ cm^{-1}$).

It is of interest to apply magnetic measurements to such a known and extensively studied test system as the $b\ ^3\Pi_u \sim A\ ^1\Sigma_u^+$ complex of a Na_2 molecule.[5–15] In our previous work[14] Landé factors were determined for four rovibronic v,J levels belonging to the Na_2 $A\ ^1\Sigma_u^+$ state and excited by a 632.8 nm He–Ne laser line. The analysis of the basic causes of appearance of a nonzero g-factor value in the diamagnetic $A\ ^1\Sigma_u^+$ state of Na_2 as performed in Ref. 14 has shown that there are three main sources of magnetism, namely, singlet–triplet interaction with a crossing $b\ ^3\Pi_u$ term, rotationally induced interaction with a distant $B\ ^1\Pi_u$ term, and finally, the rotation of atomic nuclei shielded by inner electronic shell. The last two phenomena are of regular behavior while the first one is typically examplified by a local perturbation producing pronounced resonant shape dependence on vibrational (v) and rotational (J) quantum numbers. The $A\ ^1\Sigma_u^+$ state $g^{\omega J}$ factor for a given v,J level exhibits an increase of up to 1–2 orders of magnitude when conditions of energy resonance with Ω components of $b\ ^3\Pi_u$ state are met. Thus the $g^{\omega J}$ factors are able to supply a lot of high precision information about molecular structure, including interaction constants. However, such resonances can be studied successfully by high resolution spectroscopic detection of level shifts[6,7,9,12,13] or by performing sufficiently accurate lifetime measurements.[10,11] At the same time for v,J values beyond the region of resonance the size of the $A \sim b$ interaction in Na_2, as can be seen from calculation and the experimental results of Ref. 14, is too small to be registered in level shifts or lifetime changes. It is just these cases that are treated in the present work. We calculate g-factor values using a definite set of deperturbed molecular constants (a direct problem), and also determine the spin–orbit interaction parameters using experimentally measured g values (an inverse problem) for weakly coupled $A \sim b$ levels.

It is rather obvious that the precision of a description of g factors is from one point of view connected with the inadequacy of the applied physical model, while from an-

[a] Permanent address: Department of Chemistry, Moscow M. Lomonosov State University, Moscow W-234, 119899, Russia.

 0021-9606/93/020826-10$6.00

other with insufficient accuracy of the existing set of deperturbed constants. Moreover, the very small Landé factors are known[15] to be extremely sensitive to the structural molecular parameters. That is why special attention is payed here to the procedure for choosing the most reliable set of molecular constants and evaluating the effect of its errors on calculated g factors.

The organization of the paper is as follows. In Sec. II we present a brief description of the experimental method and the results of Na_2 $A\,^1\Sigma_u^+$ state g-factor measurements using zero field crossing signal (Hanle effect) in laser induced fluorescence (LIF) excited by Kr^+-laser lines. The main part of the paper, Sec. III, details the theoretical description and the possibility to obtain information about $A\sim b$ interaction parameters from measured g_A^{wJ} values. After presentation of a basic approach (Sec. III A) and the method of extracting a partial contribution g_{Ab} to the total g_A factor caused by $A\sim b$ interaction (Sec. III B), we, in Sec. III C, analyze in detail the procedure for choosing the molecular constants and the effect of errors originated both from imperfections in the physical model employed and the uncertainty in $b\,^3\Pi_u$ state molecular constants as available from literature. In Sec. III D calculated g_{Ab}^{wJ} factors and their variations are presented and compared with the experimentally measured values. The possibility of applying some of the measured g_A^{exp} factors to determine the value of the electronic part (H_{so}^e) of the spin–orbit $A\sim b$ interaction is demonstrated (Sec. III E). The methodologically important question of possible external magnetic field influence on g-factor values is examined in Sec. IV.

II. EXPERIMENT

The method of measurement and data processing for the experimental determination of Na_2 $A\,^1\Sigma_u^+$ state g factors is the same as described in more detail in Ref. 14. We employed here the same modification of a dispersion shape Hanle signal in $A\,^1\Sigma_u^+\rightarrow X\,^1\Sigma_g^+$ LIF under circular polarized excitation allowing us to determine very small values of the product $g\tau\cong 10^{-12}$ s. We managed to observe the very beginning part of the magnetic field ($\mathscr{B}\leqslant 1T$) dependence of the degree of circularity $\mathscr{C}=(I_r-I_l)/(I_r+I_l)$ by detecting the fluorescence intensities circularly polarized along the right (I_r) or left (I_l) circle, cf. Fig. 1(a). Fluorescence was observed at right angles both to field $\mathscr{B}$ and exciting laser beam directions. The circularly polarized irradiation lines 647.1 and 676.4 nm of a 100 mW cw Kr^+ laser were used to excite the sodium vapor in a glass cell at a temperature of 600–630 K. Using 647.1 nm excitation we found the seven LIF progressions mentioned in Ref. 16 and originating from the Na_2 $A\,^1\Sigma_u^+$ state v,J levels listed in Table I. We also identified three new LIF progressions using 676.4 nm excitation. This pumps $X\rightarrow A$ transitions with following v,J numbers: $(1,42)\rightarrow(3,43)$, $(2,106)\rightarrow(8,107)$, and $(10,30)\rightarrow(15,29)$.

An example of the experimentally measured $\mathscr{C}(\mathscr{B})$ dependence is given in Fig. 1(b). As previously,[14] the $\mathscr{C}(\mathscr{B})$ values obtained were approximated with straight lines assuming $\mathscr{C}=(10/13)\alpha g_A^{exp}\mu_0/\hbar\Gamma+\delta$, where adjusting parameters α and δ are introduced to account for inaccuracies in calibration of the I_r and I_l channels. The spontaneous lifetime value was taken from Ref. 17 as equal to $\tau=12.4$ ns, and a small correction of about 3% accounting for collisions was introduced. The g_A^{exp} factors obtained are listed in Table I together with estimated error values. For 676.4 nm excitation a g-factor value for $v=8$, $J=107$ only is given. The results for two other levels are not presented because of great errors due to weak fluorescence intensity.

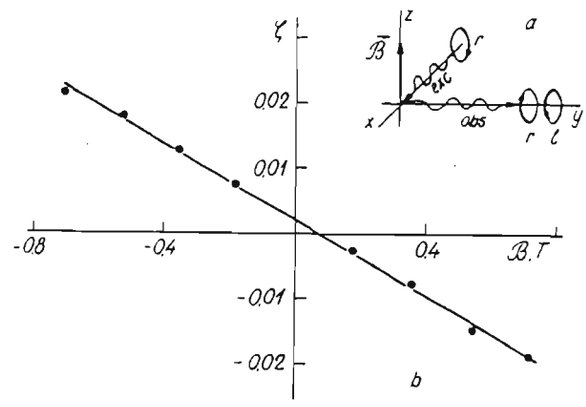

FIG. 1. Experimental geometry (a), and magnetic field dependence of the degree of circularity $\mathscr{C}$ (b), measured for LIF transition $X\,^1\Sigma_g^+$, $v=4$, $J=34\rightarrow A\,^1\Sigma_u^+$, $v=13$, $J=35\rightarrow X\,^1\Sigma_g^+$, $v=2$, $J=34$.

III. CALCULATION OF $A\,^1\Sigma_u^+$ STATE g FACTORS AND DETERMINATION OF $A\,^1\Sigma_u^+\sim b\,^3\Pi_u$ INTERACTION PARAMETERS

A. Expressions for g factors

It is convenient to use the following form of expressions for g factors arising due to $A\,^1\Sigma_u^+\sim b\,^3\Pi_u$ interaction:

$$g_A^{wJ}=\{g_b^n+S_A^2(g_A^n-g_b^n)\}+\{g_{ba}^{wJ}(1+2S_{\Pi_0}S_{\Pi_1})+S_A^2(g_{Ab}^{wJ}-g_{ba}^{wJ})\}+g_{AB}^{wJ}, \quad (1)$$

where in addition to the similar expression given in Ref. 14 regular $A\,^1\Sigma_u^+\sim B\,^1\Pi_u$ and $b\,^3\Pi_u\sim a\,^3\Sigma_u^+$ interactions are taken into account. Here g_{Ab}^{wJ} is the contribution caused by direct $A\sim b$ interaction[18]

$$g_{Ab}^{wJ}=-\{g_l(S_{\Pi_1}^2+2S_{\Pi_2}^2)+g_s(2S_{\Pi_2}^2)\}/X-\{2(g_s+g_{ba}^{wJ})S_{\Pi_2}(S_{\Pi_2}+S_{\Pi_1})\}/\sqrt{2X}, \quad (2)$$

where $X=J(J+1)$, $g_l=1$, and $g_s=2.0023$ are orbital and spin electronic g factors, S_A, S_{Π_i} are the mixing coefficients of the levels of the $A\sim b$ complex as obtained by diagonalization of a 4×4 Hamiltonian matrix of the H_0+V_{so} operator.[9] The nonzero elements of this matrix are represented by the following simplified expressions:

TABLE I. The exciting line λ_{exc}, excited v_A, J levels, calculated (g_{Ab}^{vJ}, $g_A^n+g_{AB}^{vJ}$ and $g_A^n+g_{AB}^{vJ}+g_{Ab}^{vJ}$) and experimentally measured (g_A^{exp}) g-factor values as well as calculated energy shifts δE and lifetime changes $\delta\tau$ for Na_2 $A\,^1\Sigma_u^+$ state. Values in parentheses after g_{Ab}^{vJ} are variations in the last digits.

λ_{exc} nm	v_A	J	g_{Ab}^{vJ}	$g_A^n+g_{AB}^{vJ}$	$g_A^n+g_{AB}^{vJ}+g_{Ab}^{vJ}$	g_A^{exp}	δE cm^{-1}	$\delta\tau$ ns
				(in 10^{-5} Bohr magnetons)				
676.4	8	107	−6.6(42)	−5.1	−11.7	−10.8±1.6	0.01	0.06
647.1	10	59	−0.9(2)	−5.1	−6.0	−7.6±1.5	0.03	0.01
	12	41	−0.6(1)	−5.2	−5.8	−5.1±1.0	0.01	0.01
	13	35	0.0(2)	−5.2	−5.2	−4.7±0.7	0.00	0.00
	13	83	−0.2(5)	−4.8	−5.0	−5.6±0.6	0.05	0.04
632.8	14	45	+9.4(8)	−5.1	+4.3	+3.1[a]	0.05	0.04
	16	17	0.0(1)	−5.2	−5.2	−5.3[a]	0.00	0.00
647.1	20	33	+1.5(8)	−5.1	−3.7	−4.8±1.5	0.01	0.01
	20	98	−0.4(45)	−4.5	−4.9	−9.2±1.8	0.00	0.00
632.8	22	86	−9.6(36)	−4.6	−14.2	−13.6[a]	0.01	0.06
	25	87	+6.1(41)	−4.6	+1.5	+2.4[a]	0.01	0.06
647.1	29	50	−2.9(16)	−4.9	−7.8	−7.7±0.8	0.03	0.02

[a]As measured in Ref. 14.

$$H_{AA}=T_A+B_AX-D_AX^2+H_AX^3,$$

$$H_{00}=T_b-A_b+B_b(X+1)-D_b(X^2+4X+1)+H_b(X+1)\times(X^2+8X+1),$$

$$H_{11}=T_b+B_b(X+1)-D_b(X^2+6X-3)+H_b(X^3+15X^2-5X-5),$$

$$H_{22}=T_b+A_b+B_b(X-3)-D_b(X^2-4X+5)+H_b(X^3-3X^2+5X-7), \quad (3)$$

$$H_{01}=H_{10}=-\sqrt{2X}[B_b-2D_b(X+1)+H_b(3X^2+10X-1)],$$

$$H_{12}=H_{21}=-\sqrt{2(X-2)}[B_b-2D_b(X+1)+H_b(3X^2-2X+3)],$$

$$H_{A0}=H_{0A}=\xi_{Ab},$$

where A, 0, 1, and 2 denote $A\,^1\Sigma_u^+$, $b\,^3\Pi_{0u}$, $b\,^3\Pi_{1u}$, and $b\,^3\Pi_{2u}$, respectively, T is the vibronic energy, B rotational constant, D and H centrifugal distortion constants, A_b the $b\,^3\Pi_u$ spin–orbit constant, and ξ_{Ab} the spin–orbit interaction parameter. The spin–spin constant and Λ-type doubling in the $b\,^3\Pi_u$ state are neglected here. g_{AB}^{vJ} in Eq. (1) and g_{ba}^{vJ} in Eq. (2) are partial contributions to the $A\,^1\Sigma_u^+$ and $b\,^3\Pi_u$ state g factors caused by interactions with $B\,^1\Pi_u$ and $a\,^3\Sigma_u^+$ states, respectively, while terms with g_A^n and g_b^n in Eq. (1) describe the "nuclear" contribution appearing due to the rotation of the shielded nuclei in the Na_2 molecule.[19]

The present study deals only with $A\,^1\Sigma_u^+$ state levels weakly coupled to the $b\,^3\Pi_u$ state, i.e., $S_A\approx 1$, $S_{\Pi_i}\ll 1$, in which case Eq. (1) is simplified,

$$g_A^{vJ}=g_A^n+g_{AB}^{vJ}+g_{Ab}^{vJ}, \quad (4)$$

thus allowing us to consider additive contributions of the three sources of $A\,^1\Sigma_u^+$ state magnetism.

B. Estimation of g_{AB}^{vJ}, g_{ba}^{vJ} and g_A^n factors

g_{AB}^{vJ} and g_{ba}^{vJ} values were calculated for experimentally studied $A\,^1\Sigma_u^+$ and $b\,^3\Pi_u$ state levels according to expressions (19) and (A10) in Ref. 14. Calculations were based on internuclear potentials[14,20–22] $U_i(R)$ and matrix elements of the electronic-rotation interaction[14,23] $L_{ij}^+(R)$. The following expression was used:

$$g_{ij}^{vJ}=2g_l\sum_{v_j}\langle v_i^J|L_{ij}^+(R)|v_j^J\rangle\langle v_j^J|L_{ij}^+(R)\times[\hbar^2/2mR^2]|v_i^J\rangle/(E_{v_iJ}-E_{v_jJ})$$

$$\cong 2g_l\langle v_i^J|[L_{ij}^+(R)]^2[\hbar^2/2mR^2\Delta U_{ij}(R)]|v_i^J\rangle, \quad (5)$$

where m is the reduced mass of a molecule and $\Delta U_{ij}(R)=U_i(R)-U_j(R)$ are the difference potentials. Indices i and j denote $A\,^1\Sigma_u^+$ or $b\,^3\Pi_u$ and $B\,^1\Pi_u$ or $a\,^3\Sigma_u^+$ states, respectively. As expected, g_{AB}^{vJ} and g_{ba}^{vJ} are weakly dependent on vibrational and rotational quantum numbers. Their approximate values are $g_{AB}^{vJ}\approx -7.0\times10^{-5}$ and $g_{ba}^{vJ}\approx +1.4\times10^{-4}$ (in Bohr magnetons). It can be seen from Eq. (2) that $g_{ba}^{vJ}\ll g_s$, thus allowing us to neglect the $a\,^3\Sigma_u^+$ state contribution to the total magnetic moment of the $A\,^1\Sigma_u^+$ state. The nuclear g_A^n factor of the $A\,^1\Sigma_u^+$ state was assumed to be independent of v and J, and a g_A^n value of $+2.4\times10^{-5}$ (in Bohr magnetons) was estimated according to Ref. 19. The summary $g_A^n+g_{AB}^{vJ}$ values are given in Table I for the $A\,^1\Sigma_u^+$ levels under investigation.

C. Molecular constants and error analysis in g_{Ab}^{vJ} calculations

1. Dunham constants and RKR potential for $b\,^3\Pi_u$ state

As may be easily seen from Eq. (3), the computation of g_{Ab}^{vJ} values starts with the search of deperturbed sets of the Dunham constants for the interacting $A\,^1\Sigma_u^+$ and $b\,^3\Pi_u$ state levels. Molecular constants and RKR potentials for the $A\,^1\Sigma_u^+$ state have been known with sufficiently high precision for 15 years.[24] Since the main source of information about the $b\,^3\Pi_u$ state is from analysis of local pertur-

TABLE II. Molecular constants in cm^{-1} for $b(1)\,^3\Pi_u$ state of Na_2 compiled in this work and corresponding constants from Refs. 7 and 9. (Values in parentheses are standard deviations in the last digits.)

	This work	From Refs. 7 and 9
T_e	13 524.29(39)	13 523.19(137)
A_e	7.09(1)	7.08(6)
α_A	−0.016 2(4)	−0.015 6(35)
ω_e	153.62(7)	153.84(31)
$\omega_e x_e$	0.440 7(36)	0.453 8(223)
$10^3\omega_e y_e$	−0.901 4(58)	−0.652(451)
B_e	0.151 87(4)	0.151 13(40)
$10^3\alpha_e$	0.626 6(41)	0.560(54)
$10^5\gamma_e$	−0.184(11)	−0.32(16)
$10^7 D_e$	5.00(27)	5.12(184)
$10^8\beta_e$	0.193(144)	0.118(62)
$10^{10}H_e$	0.10(4)	0.139(52)

bations between the $A\,^1\Sigma_u^+$ and $b\,^3\Pi_u$ states, the molecular constants describing the last are known with considerably lower precision and only for a limited v interval ($6 \leqslant v \leqslant 25$).[9] We investigate here $A\,^1\Sigma_u^+$ state levels having v values up to $v=29$, the last being perturbed by the $b\,^3\Pi_u$ state level with $v=30$. We have critically examined the available originally reported[6,7,9,12] data which lead to the values of T_b, B_b, A_b, D_b, and H_b for various $b\,^3\Pi_u$ state levels, and then by means of linear least-squares fitting procedure obtained a new set of molecular constants valid up to $v=34$ (Table II), which was further used to compute the RKR potential (Table III).

2. Overlap integrals $\langle v_A^J | v_b^J \rangle$ and spin–orbit interaction matrix elements ξ_{Ab}

Using the RKR potential for the $b\,^3\Pi_u$ state from Table III and that for $A\,^1\Sigma_u^+$ state from Ref. 20 we performed the renormalized Numerov[25] computation of a radial Schrödinger equation, thus obtaining the two state zero order vibrational wave functions, used further to compute spin–orbit interaction matrix element $\xi_{Ab} = \langle v_A^J | H_{so} | v_b^J \rangle$ values. The vibration–rotation interaction effect on the quantities $\langle v_A^J | v_b^J \rangle$ (sometimes called the Franck–Condon factors, or FCFs) was accounted for by solving the Schrödinger equation with an effective internuclear potential $U_{RKR}(R,J=0)+J(J+1)\hbar^2/(2mR^2)$. As expected,[26] this interaction affects mostly the overlap integrals of small absolute values (see Table IV).

When performing ξ_{Ab} computations of this kind, it is common to assume that the electronic part of spin–orbit interaction H_{so}^e is not dependent on internuclear distance R_x^{Ab}, leading to $\xi_{Ab} = H_{so}^e(R_x^{Ab})\langle v_A^J | v_b^J \rangle$, where $R_x^{Ab} \cong 3.75$ Å is the crossing point for potential curves of the $A\,^1\Sigma_u^+$ and $b\,^3\Pi_u$ states. It holds well because effective electronic coupling elements defined as $\langle v_A^J | H_{so}^e(R) | v_b^J \rangle / \langle v_A^J | v_b^J \rangle$ vary only slightly around $H_{so}^e(R_x^{Ab})$, except for cases with very small FCF's. However, for some levels studied here FCF values appear to be very small (Table IV), and the factorization $\xi_{Ab} = H_{so}^e(R_x^{Ab})\langle v_A^J | v_b^J \rangle$ may not be justified. Owing to this, we tried to employ as R-centroid approximation[27] in order to obtain the semiempirical dependence $H_{so}^e(R_c)$,

TABLE III. Vibrational energies, rotational constants, and turning points of the $b(1)\,^3\Pi_u$ state of Na_2 up to $v=34$. (Values in parentheses are standard deviations in the last digits.)

v	$G(v)$ cm^{-1}	R_{min} Å	R_{max} Å	$B(v)$ cm^{-1}
0	76.70(1)	2.9743(46)	3.2510(45)	0.151 56(41)
1	229.44(2)	2.8830(45)	3.3633(45)	0.150 93(44)
2	381.28(4)	2.8229(45)	3.4446(45)	0.150 30(44)
3	532.23(6)	2.7756(46)	3.5130(46)	0.149 66(45)
4	682.28(8)	2.7359(46)	3.5742(46)	0.149 02(45)
5	831.43(10)	2.7013(47)	3.6303(46)	0.148 37(46)
6	979.67(12)	2.6704(47)	3.6830(47)	0.147 72(47)
7	1126.98(14)	2.6424(48)	3.7328(47)	0.147 07(49)
8	1273.38(16)	2.6167(49)	3.7806(48)	0.146 42(51)
9	1418.85(19)	2.5929(50)	3.8266(49)	0.145 76(52)
10	1563.38(21)	2.5707(51)	3.8711(50)	0.145 09(55)
11	1706.98(24)	2.5498(52)	3.9145(51)	0.144 43(57)
12	1849.64(26)	2.5302(54)	3.9568(53)	0.143 75(60)
13	1991.34(29)	2.5116(55)	3.9983(54)	0.143 08(63)
14	2132.09(32)	2.4940(57)	4.0390(56)	0.142 40(66)
15	2271.89(34)	2.4771(59)	4.0790(57)	0.141 72(69)
16	2410.71(37)	2.4611(61)	4.1185(59)	0.141 03(72)
17	2548.57(40)	2.4457(63)	4.1575(61)	0.140 34(76)
18	2685.45(43)	2.4309(65)	4.1961(64)	0.139 65(80)
19	2891.34(46)	2.4167(68)	4.2343(66)	0.138 96(84)
20	2956.26(49)	2.4030(71)	4.2721(68)	0.138 26(88)
21	3090.18(51)	2.3898(73)	4.3097(71)	0.137 55(92)
22	3223.10(54)	2.3770(76)	4.3471(74)	0.136 84(97)
23	3355.01(57)	2.3647(79)	4.3842(77)	0.136 13(101)
24	3485.92(60)	2.3528(82)	4.4212(80)	0.135 42(112)
25	3615.82(62)	2.3412(86)	4.4580(83)	0.134 70(115)
26	3744.70(65)	2.3299(89)	4.4948(86)	0.133 98(121)
27	3872.55(68)	2.3190(93)	4.5314(90)	0.133 25(127)
28	3999.37(70)	2.3084(97)	4.5680(93)	0.132 52(132)
29	4125.16(73)	2.2980(100)	4.6045(97)	0.131 79(138)
30	4249.90(75)	2.2880(105)	4.6410(106)	0.131 05(143)
31	4373.60(78)	2.2782(112)	4.6775(111)	0.130 31(147)
32	4496.25(80)	2.2686(117)	4.7140(116)	0.129 56(154)
33	4617.84(82)	2.2592(121)	4.7506(119)	0.128 82(161)
34	4738.37(84)	2.2501(125)	4.7872(123)	0.128 06(166)

where $R_c = \langle v_A^J | R | v_b^J \rangle / \langle v_A^J | v_b^J \rangle$ is the so-called R centroid.[28] For this purpose experimental ξ_{Ab}^{exp} values were used as reported previously[6,7,9,12,13] from level shifts and[10] from lifetime measurements. In both cases $A\,^1\Sigma_u^+$ state levels close to energy resonance with $b\,^3\Pi_u$ state levels were investigated. ξ_{Ab}^{exp} values were transformed into $H_{so}^e(R_c)$, see Table V, by means of $\langle v_A^J | v_b^J \rangle$ and R_c values as computed in this work. The linear approximation of $H_{so}^e(R_c)$ was performed, leading to

$$H_{so}^e(R_c) = H_{so}^e(R_X^{Ab}) + H_{so}^{e'}(R_X^{Ab})(R_c - R_X^{Ab}). \quad (6)$$

Linear least-square fitting of Eq. (6) gives the following parameters: $H_{so}^e(R_X^{Ab}) = 5.98(0.01)$ cm^{-1} and $H_{so}^{e'}(R_X^{Ab}) = -9.3(0.7)$ $cm^{-1}/Å$. Unfortunately, Eq. (6) appears to be valid only within a narrow R_c range, $(3.72 \leqslant R_c \leqslant 3.78)$ Å. This is quite understandable, as only levels with large FCF's were involved in the $H_{so}^e(R_c)$ computation (see Table V). Hence, extrapolation of Eq. (6) beyond the mentioned R_c region can lead to considerable errors in calculated ξ_{Ab} values when the vibrational overlap is small. Hence, the average quantity $H_{so}^e = 5.97 \pm 0.15$ cm^{-1} was used here for ξ_{Ab}. In order to obtain the $H_{so}^e(R)$ depen-

TABLE IV. The calculated overlap integrals $\langle v_A^J | v_b^J \rangle$, energy differences $\Delta E_{Ab}^0 = E_A^0 - E_b^0$, mixing coefficients S_A, S_{Π_i}, R centroids, and matrix elements of spin–orbit interactions ξ_{Ab} for investigated levels of $A \sim b$ complex. (The quantities in parentheses below the $\langle v_A^J | v_b^J \rangle$ values correspond to variation of overlap integrals due to systematic errors in molecular constants of $b(1)\,^3\Pi_u$ state; the number $(-n)$ in the S_{Π_i} value denotes 10^{-n}).

v_A	v_b	J	$\langle v_A^J \| v_b^J \rangle$, 10^{-3}	ΔE_{Ab}^0, cm^{-1}	S_A	S_{Π_0}	S_{Π_1}	S_{Π_2}	R_c Å	ξ_{Ab}, cm^{-1}
8	11	107	−204 ± 4 (−186)	+27.8	0.997	5.50(−3)	−5.54(−2)	−4.99(−2)	3.7539	−1.31
10	15	59	−194 ± 5 (−199)	−51.6	1.000	2.73(−2)	6.44(−3)	1.29(−3)	3.7669	−1.15
12	17	41	−127 ± 6 (−120)	−43.7	1.000	2.12(−2)	4.05(−3)	6.56(−4)	3.7839	−0.75
13	18	35	−15 ± 15 (−6)	−55.7	1.000	1.60(−3)	2.02(−4)	2.25(−5)	3.9655	−0.09
13	16	83	131 ± 7 (106)	+6.5	0.997	5.92(−2)	−2.23(−4)	−5.91(−2)	3.7601	0.77
14	18	45	186 ± 6 (182)	+21.6	0.942	4.65(−2)	−2.50(−2)	1.45(−2)	3.7184	1.10
16	20	17	23 ± 12 (20)	+27.9	1.000	3.64(−3)	−4.56(−4)	7.20(−5)	3.8548	0.14
20	23	33	51 ± 15 (62)	+16.5	1.000	1.64(−2)	−8.44(−3)	5.26(−3)	3.7020	0.30
20	21	98	15 ± 30 (−38)	−39.2	1.000	−1.45(−2)	−8.12(−3)	−3.22(−3)	3.9629	0.09
22	23	86	−141 ± 7 (−156)	−14.3	0.958	−8.11(−3)	−5.63(−2)	−4.32(−2)	3.7458	−0.83
25	25	87	134 ± 8 (150)	+18.6	0.998	5.70(−3)	4.08(−2)	−5.31(−2)	3.7325	0.79
29	30	50	147 ± 8 (146)	−31.6	1.000	−3.90(−2)	−1.21(−2)	−2.95(−3)	3.7633	0.87

dence valid within a sufficiently large R region, it is necessary to know ξ_{Ab} values corresponding to small FCF's (when the R-centroid approximation becomes incorrect[29]). This can be achieved in principle using g-factor measurements, see Sec. I.

During computation of the matrix elements ξ_{Ab}, we also made an attempt to take into account the distortion of $b\,^3\Pi_{0u}$ state wave functions caused both by the R dependence of the spin–orbit $A \sim b$ interaction constant, as well as by the electronic-rotation interaction with $b\,^3\Pi_{1u}$ state v_b^J levels, $v_b^J \neq v_b^J$. Then using a Van Vleck transformation, it is easy to obtain corresponding second order corrections to matrix elements $\langle v_A^J | H_{so}^e | v_b^J \rangle$,

$$\xi_{Ab}^{(2)} = \sum_{v_b \neq v_b} \frac{[(E_{v_A J} + E_{v_b J})/2 - E_{v_b J}] \langle v_A^J | H_{so}^e | v_b^J \rangle \langle v_b^J | A_b(R) - B(R)\sqrt{2X} | v_b^J \rangle}{(E_{v_A J} - E_{v_b J})(E_{v_b J} - E_{v_b J})}. \tag{7}$$

The off-diagonal matrix elements $\langle v_b^J | A_b(R) - B(R)\sqrt{2X} | v_b^J \rangle$ appearing here due to interaction between the $b\,^3\Pi_0$ and $b\,^3\Pi_{1u}$ components with different v_b^J and v_b^J can be evaluated by considering the following expansions of the $A_b(R)$ and $B(R)$ functions:

$$A_b(R) = A_e + A_b'(R_e)(R - R_e)/R_e + \cdots, \tag{8}$$

$$B(R) = B_e - 2B_e(R - R_e)/R_e + \cdots, \tag{9}$$

where $R_e = 3.101$ Å is the equilibrium distance of the $b\,^3\Pi_u$ state potential. Introducing the harmonic oscillator eigenfunctions, the matrix elements $\langle v_b^J | A_b(R) - B(R)\sqrt{2X} | v_b^J \rangle$ can be estimated as $[A_b'(R_e) - 2B_e\sqrt{2X}]\sqrt{B_e/\omega_e}$, where ω_e is the b state vibrational frequency. Then, Eq. (7) is approximated as

$$\xi_{Ab}^{(2)} \approx \sum_{v_b \neq v_b \pm 1} \frac{[(E_{v_A J} + E_{v_b J})/2 - E_{v_b J}] \langle v_A^J | H_{so} | v_b^J \rangle [A_b'(R_e) - 2B_e\sqrt{2X}]\sqrt{B_e/\omega_e}}{(E_{v_A J} - E_{v_b J})(E_{v_b J} - E_{v_b J})}. \tag{10}$$

TABLE V. The absolute values of experimental spin–orbit interaction matrix elements ξ_{Ab}^{exp}, calculated overlap integrals $\langle v_A^J | v_b^J \rangle$, R centroids, and electronic parts of the spin–orbit interaction $H_{so}^e(R_c)$.

v_A	v_b	J	ξ_{Ab}^{exp}, cm^{-1}	$\langle v_A^J \vert v_b^J \rangle$	R_c Å	$H_{so}^e(R_c)$ cm^{-1}	Ref.
0	6	80	2.50	0.427	3.751	5.86	9
0	7	50	2.26	0.379	3.752	5.96	
1	7	75	1.39	0.236	3.757	5.89	
1	8	40	2.05	0.343	3.754	5.98	
2	8	69	0.5	0.081	3.732	6.30	
2	9	28	0.65	0.112	3.767	5.85	
3	9	63	1.58	0.265	3.750	5.96	
4	10	55	1.43	0.241	3.755	5.93	
5	11	48	0.42	0.075	3.778	5.59	
6	12	39	0.69	0.111	3.736	6.22	
7	12	67	1.15	0.190	3.758	6.05	
7	13	25	1.33	0.221	3.748	6.02	
9	14	53	0.58	0.103	3.732	5.63	
10	15	45	1.17	0.196	3.747	5.97	
8	14	8	1.34	0.211	3.759	6.35	7
8	14	8	1.272±0.001	0.211	3.759	6.04	13
3	10	10	0.81±0.05	0.133	3.742	6.09	10
7	13	25	1.33±0.05	0.221	3.748	6.02	
8	14	8	1.34±0.05	0.211	3.759	6.35	
12	17	22	0.694±0.02	0.122	3.766	5.69	6
17	21	16	0.501±0.02	0.078	3.723	6.45	
22	25	10	0.977±0.015	0.163	3.751	6.01	
26	28	50	0.8942±0.0018	0.154	3.782	5.81	12
34	34	36	0.5334±0.0075	0.092	3.773	5.79	
8	11	107	−1.12±0.10	0.204	3.7539	5.51	This work
14	18	45	1.04±0.05	0.186	3.7184	5.59	
22	23	86	−0.82±0.06	0.141	3.7458	5.80	
25	25	87	0.83±0.06	0.134	3.7325	6.17	
29	30	50	0.92±0.08	0.147	3.7633	6.23	

Parameters in Eq. (8) as obtained in a semiempirical way from the existing experimental v dependence[6,7,8,12] of A_b are as follows (in cm^{-1}): $A_e=7.05(0.01)$, $A_b'(R_e)=-2.6(0.6)$. In particular, A_b values for various v levels were taken both from high precision line position measurements in LIF spectra of strongly forbidden $b\,^3\Pi_{0u}\rightarrow X\,^1\Sigma_g^+$ and $b\,^3\Pi_{1u}\rightarrow X\,^1\Sigma_g^+$ transitions,[8] as well as from a deperturbation analysis of strongly perturbed a-state levels observed in Doppler-free $X\,^1\Sigma_g^+\rightarrow A\,^1\Sigma_u^+$ excitation spectra.[6,7,12] Following from Eq. (10), the correction $\xi_{Ab}^{(2)}$ may play a considerable role only for large J and small $\langle v_A^J | v_b^J \rangle$ values under conditions when FCF's for the neighboring terms of the v_b^J progression are not small. Nevertheless, even for such levels the $\xi_{Ab}^{(2)}$ does not exceed 0.03 cm^{-1}.

3. The influence of direct $A\,^1\Sigma_u^+\sim b\,^3\Pi_{1u}$ interaction

In the above performed treatment of $A\sim b$ perturbation, the nonzero value of interaction matrix element between $A\,^1\Sigma_u^+$ and the $b\,^3\Pi_{1u}$ component of b state was neglected. The matrix element appears as a result of nonvalidity of "pure" Hund's case (a) coupling, and this matrix element can be evaluated as follows:

$$H_{A1}=H_{1A}=\langle v_A^J | \mathbf{d}[F(F+1)-I(I+1)-X]/\sqrt{X} + \eta\sqrt{2X} | v_b^J \rangle, \quad (11)$$

where $\mathbf{d}$ and η define the reduced matrix elements of a nuclear spin–electron spin and electronic-rotation coupling, respectively. The $\mathbf{d}$ value is of the order of 10^{-4} as measured experimentally in Ref. 30. The parameter η value is unknown, but it can be roughly estimated in a following way. Spin–orbit interaction mixes the $b\,^3\Pi_{1u}$ component of the b state with the $B\,^1\Pi_u$ state. Consequently, the perturbed wave function $|b\,^3\Pi_{1u}\rangle_p$ can be described in the form $|b\,^3\Pi_{1u}\rangle_p=|b\,^3\Pi_{1u}\rangle+\gamma|B\,^1\Pi_u\rangle$, and γ can be estimated according to perturbation theory as $\gamma=\langle b\,^3\Pi_{1u}|H_{so}|B\,^1\Pi_u\rangle/(E_b-E_B)$. Since $\langle b\,^3\Pi_{1u}|H_{so}|B\,^1\Pi_u\rangle\cong A_b$, γ can be estimated as $A_b/(T_b-T_B)\cong -10^{-3}$. This gives the value of $\eta=\langle A\,^1\Sigma_u^+|L^+(R)/R^2|b\,^3\Pi_{1u}\rangle_p\cong\gamma\langle A\,^1\Sigma_u^+|L^+(R)/R^2|B\,^1\Pi_u\rangle\cong 2B_b\gamma\cong -2\times10^{-4}$ cm^{-1}, $L^+(R)\cong\sqrt{2}$ being the electronic-rotation interaction matrix element between the A and B states. As is clear, the breakdown of the pure Hund's case (a) description leads also to the appearance of an additional contribution to the g_{Ab} factor in Eq. (2), namely, $-2cS_AS_{\Pi_1}\langle v_A^J | v_b^J \rangle/\sqrt{2X}$, where

$c=\langle A\,^1\Sigma_u^+|L^+(R)|b\,^3\Pi_{1u}\rangle_p$ can be estimated in a similar way as $c\cong 2\gamma\cong -2\times 10^{-3}$.

Due to the smallness of c,d, and η values as estimated above one can safely neglect the influence of a direct $A\,^1\Sigma_u^+\sim b\,^3\Pi_{1u}$ interaction within the J values for the levels under study.

4. The effect of molecular constant errors on rovibronic level energies, RKR potentials and $\langle v_A^J|v_b^J\rangle$ values

As was mentioned previously, the $b\,^3\Pi_u$ state molecular constants are known with considerably less precision than that for $A\,^1\Sigma_u^+$ state, thus only the effect of $b\,^3\Pi_u$ state constant errors will be considered.

First, let us discuss the influence of imperfection in vibration–rotation molecular constants on the calculation accuracy of RKR potential turning points and overlap integrals $\langle v_A^J|v_b^J\rangle$. Assuming the errors are small, the "true" potential can be treated as a sum of first order RKR potential $U^0_{\mathrm{RKR}}(\alpha_i,R)$ as calculated using a given molecular constant set and a small additional term $\delta U(\alpha,R)=\Sigma_{\alpha_i}(\partial U^0/\partial\alpha_i)\delta\alpha_i$. Note that here the parameters α_i are describing the potential and are treated as molecular constant functions. Then, using first order perturbation theory we obtain relative changes in overlap integrals as $\Sigma_{v_b\neq v_b}\langle v_b^J|\delta U|v_b^J\rangle\langle v_b^J|v_A^J\rangle/[(E_{v_bJ}-E_{v_bJ})\langle v_A^J|v_b^J\rangle]$. Therefore, the most pronounced relative changes are expected for small $\langle v_A^J|v_b^J\rangle$ values, especially if neighboring terms $\langle v_b^J|v_A^J\rangle$ in v^J progression are large.

Computation of the $\delta U(\alpha_i,R)$ functions using a numerical RKR potential is by no means a simple task.[31] That is why in order to calculate variations in the turning points and $\langle v_A^J|v_b^J\rangle$ values we use Monte Carlo sampling method, according to which the input parameters $(\omega_e,\omega_e x_e,\ldots,B_e,\alpha_e,\ldots,)$ were subjected to random variations within one (normal or systematic) standard deviation of their obtained values (see Table II).

Variations in turning points and $\langle v_A^J|v_b^J\rangle$ values caused by systematic errors (estimated as the differences between molecular constants obtained in this work and in Ref. 9, see Table II) exceed normal deviations considerably. Owing to this, we present here only the results of systematic error simulations (see Tables III and IV). As expected, the variations are more pronounced for small $\langle v_A^J|v_b^J\rangle$ values, see Table IV. Note also, that the differences between turning points of RKR potentials as computed with our set of molecular constants and that given in Ref. 32 are within systematic variations.

Let us now consider the effect of molecular constant errors on the accuracy of calculated deperturbed $b\,^3\Pi_u$ state rovibronic term values E^0_{vJ}. From Monte Carlo simulations (see Table III), the effect of E^0_{vJ} due to vibrational constant errors does not exceed 0.8 cm^{-1}, while average B_b error value is about 6.6×10^{-4} cm^{-1}. Error values for D_b and H_b estimated as the differences between the values obtained here and reported previously[7,9] (see Table II) are about $\cong 1\times 10^{-7}$ and 4×10^{-12} cm^{-1}, respectively. It is evident that the absolute values of E^0_{vJ} errors are increasing with J. Thus for $J=50$ the error contribution into B_b, D_b, and H_b is, respectively, 1.6, 0.6, and 0.05 cm^{-1}, whereas that for $J=100$ gets to 6.6, 10, and 4 cm^{-1}. Hence, inaccuracies in E^0_{vJ} values in the case of large J are caused mainly by imperfection of the centrifugal distortion constants. The same conclusion is confirmed by comparison of the differences between E^0_{vJ} as calculated using a given set of molecular constants and that obtained as a solution of radial Schrödinger equation. The differences are about 0.1 cm^{-1} for small J, about 1 cm^{-1} for $J=50$, and come to 10 cm^{-1} for $J=100$. Similar considerations will be used in the next section to calculate g^{vJ}_{Ab} values (a direct problem) and to obtain spin–orbit interaction parameters ξ_{Ab} from experimentally measured A state Landé factors (an inverse problem), as well as to estimate the accuracy of these procedures.

D. Calculated g^{vJ}_{Ab} values and their variations. Comparison with experimental results

The matrix elements given by Eq. (3) were calculated using ξ_{Ab} values from Table IV, the vibration–rotation constant set derived in the present work (Table II), and $A\,^1\Sigma_u^+$ state molecular constants from Ref. 24. The numerical diagonalization of the 4×4 matrix gave the mixing coefficients S_A, S_{Π_i}. Then g^{vJ}_{Ab} values were computed according to Eq. (2) for the $A\,^1\Sigma_u^+$ state levels studied in this work, as well as those measured previously in Ref. 14. The results are given in Table I. It must be mentioned that some differences between the results in Table I compared to the quantities calculated for identical v,J levels in Ref. 14 is due to the choice of parameters as discussed in Sec. III C. Additionally, considering the evaluation of systematic errors in $\langle v_A^J|v_b^J\rangle$, H^e_{so}, and in $b\,^3\Pi_u$ state molecular constants by means of Monte Carlo simulation analysis we obtain g^{vJ}_{Ab} variations (Table I). As can be seen from the table, calculated $g^n_A+g^{vJ}_{AB}+g^{vJ}_{Ab}$ values are in agreement with experimentally measured $g^{\exp}_A$ within experimental error, when errors due to imperfection of the treatment are accounted for one exception is $g^{\exp}_A$ as measured for the level with $v_A=20$, $J=98$, being of more negative value than the calculated one.

It is well known that the strength of a perturbation is determined both by the interaction matrix element value and the energy difference between deperturbed levels. As can be seen from Table IV, the spin–orbit interaction matrix element ξ_{Ab} comes to a considerable absolute value for the levels with $v_A=8$, 10, 12, 13($J=83$), 14, 22, 25, and 29, while energy differences ΔE^0_{Ab} are relatively small for 8, 13($J=83$), 14, 20($J=33$), 22, and 25. Hence, the perturbation is expected to be of a considerable value for $v_A=8$, 13($J=83$), 14, 22, and 25. This is more or less in agreement with computed g^{vJ}_{Ab} values, see Table I. It is of interest to mention that the levels with $v_A=8$, 13($J=83$), 22, and 25 are situated within the $b\,^3\Pi_u$ state triplet complex, thus being very sensitive to the accuracy of the b state molecular constants. Good agreement between the measured and calculated g factors for these levels proves the accuracy of the chosen set of molecular constants and the reliability of the theoretical approach. It ought to be noted that the level

$13(J=83)$ demonstrates a special situation, its interaction with the $^3\Pi_{0u}$ and $^3\Pi_{2u}$ components being opposite in sign are practically compensating each other ($S_{\Pi_0}+S_{\Pi_2}\cong -1.0\times 10^{-4}$). Due to this peculiarity the $v_A=13$, $J=83$ level is almost insensitive to the changes in spin–orbit interaction constant ξ_{Ab}.

As follows from g_{Ab} values in Table I, $v_A(J)$ levels 12(41) and 16(17) practically do not interact with the $b\,^3\Pi_u$ state, that is why the coincidence of measured and calculated g factors confirms reliability of calculated $g_A^J+g_{AB}^{\omega J}$ values. For comparison, we also calculated the level shifts δE and lifetime increasing values $\delta\tau$ appearing due to $A\sim b$ interaction for the $A\,^1\Sigma_u^+$ state levels under study. The results as presented in Table I are showing that for all levels employed in the present work the upper limit of these quantities is $\delta E\cong 0.05$ cm^{-1} and $\delta\tau\cong 0.06$ ns, respectively, thus being practically unmeasurable.

E. $\xi_{Ab}^{\exp}$ and H_{so}^e determination from experimentally measured g factors

We made an attempt to employ the experimental $g_A^{\exp}$ values of the $v_A(J)$ levels undergoing not too small $A\sim b$ interaction, namely, 8(107), 14(45), 22(86), 25(87), 29(50), in order to carry out some kind of "inverse" treatment. The aim was to achieve the best coincidence of measured $g_A^{\exp}$ and calculated $g_A^J+g_{AB}^{\omega J}+g_{Ab}^{\omega J}$ quantities by means of variation of spin–orbit interaction parameter ξ_{Ab}. The results of this fitting procedure are presented in Table V. As can be seen, $\xi_{Ab}^{\exp}$ values obtained in this work are in a good agreement with ξ values obtained earlier by means of level shift and radiative lifetime measurements. However, the R_c region range for $\xi_{Ab}^{\exp}$ in our studies is not broad enough to get the $H_{so}^e(R)$ dependence in a semiempirical way. At the same time, the $\xi_{Ab}^{\exp}$ values obtained here lead to an averaged value of the electronic part of spin–orbit interaction equal to $H_{so}^e=5.86\pm 0.20$ cm^{-1}, which is in excellent agreement with the value of 5.97 cm^{-1} as obtained by averaging all data reported in literature and listed in Table V.

IV. THE EXTERNAL MAGNETIC FIELD EFFECT ON THE g_{Ab} AND g_{AB} FACTORS

In the last section we discussed the reliability in our situation of the simplest assumption that the g_i factor is the only coefficient necessary to describe the linear Zeeman effect of a rovibronic level in form $E_i=\langle i|H^{mg}|i\rangle=-\mu_0\langle i|g_l\mathbf{L}+g_s\mathbf{S}|i\rangle\mathscr{B}=\mu_0 g_i M\mathscr{B}$, g_i being independent of the external magnetic field strength $\mathscr{B}$ and J-projection quantum number M. Here i labels a discrete v,J level, while $\mu_0=4.669\times 10^{-5}$ cm^{-1}/Gauss is the Bohr magneton. Let us first consider the effect of magnetic field on $A\sim b$ interaction and $g_{Ab}^{\omega J}$ factor values. For this purpose we have to analyze the 4×4 Hamilton matrix for the $A\sim b$ complex, see Eq. (3). As the Zeeman part H^{mg} of a Hamiltonian is able to mix only the states with $\Omega'-\Omega''=\Delta\Omega=0,\pm 1$ (except for $\Omega'=\Omega''=0$), the nonzero matrix elements of H^{mg} operator in a matrix of $A\sim b$ complex[18] will be

$$
\begin{aligned}
H_{11}^{mg}&=Sg_l/X,\\
H_{22}^{mg}&=2S(g_l+g_s)/X,\\
H_{01}^{mg}&=H_{10}^{mg}=Sg_s/\sqrt{2X},\\
H_{12}^{mg}&=H_{21}^{mg}=Sg_s\sqrt{(X-2)}/\sqrt{2X},\\
H_{02}^{mg}&=H_{20}^{mg}=-Sg_{ba}\sqrt{(X-2)}/\sqrt{X},
\end{aligned}
\tag{12}
$$

where $S=-\mu_0 M\mathscr{B}$. It is easy to understand from Eq. (12) that since H_{11} and $H_{22}\propto X^{-1}$ the additive Zeeman energy corrections to corresponding matrix elements of Eq. (3) are small compared to the energy of a deperturbed level. At the same time, the off-diagonal ($\Delta\Omega=\pm 1$) matrix elements are proportional to $X^{-1/2}$, thus being comparable with corresponding terms in Eq. (3) assuming sufficiently strong field $\mathscr{B}$ and large J values. Moreover, the dependence of such an effect on the sign of M must cause the interference phenomena between intramolecular (electronic-rotation) and external (magnetic) interactions. Performing a numerical diagonalization of a matrix equal to the sum of matrices given by Eqs. (3) and (12), it is easy to compute the mixing coefficients S_A, S_{Π_i} and $g_{Ab}^{\omega J}$ factors for $A\sim b$ complex, cf. Eq. (2), including the external magnetic field effect. In particular, we calculated the M dependence of $g_{Ab}^{\omega J}$ factors for magnetic fields up to 1 T for considerably interacting $A\sim b$ levels used for the $\xi_{Ab}^{\exp}$ determination (Sec. IV D, Table V). The results, presented in Fig. 2, allow for a conclusion that the external magnetic field is able both to increase or to diminish the $g_{Ab}^{\omega J}$ values (dependent on the sign of M), and the function $g_{Ab}^{\omega J}(M)$ does not possess $\pm M$ symmetry.

Some peculiarity in the magnetic field effect on $g_{Ab}^{\omega J}$ values is connected with the fact that Zeeman operator obeys not only a $\Delta J=0$ selection rule, but also $\Delta J=\pm 1$ one. Therefore, in the case of $A\sim B$ interaction there exist nonzero H^{mg} operator matrix elements not only between $|A\,^1\Sigma_u^+,J\rangle$ and $|B\,^1\Pi_u^+,J\rangle$, but also between $|A\,^1\Sigma_u^+,J\rangle$

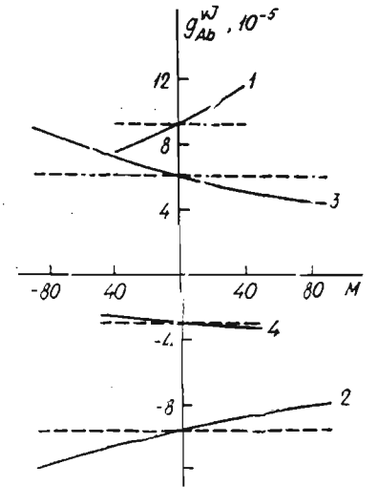

FIG. 2. Landé factor $g_{Ab}^{\omega J}$ value dependence on magnetic quantum number M calculated for magnetic field $\mathscr{B}=1$ T (dashes denote $\mathscr{B}=0$). $v_A(J)$ values are (1) 14(45), (2) 22(86), (3) 25(87), (4) 29(50).

and $|B\,^1\Pi_u^-, J\pm1\rangle$ state levels, e.g., magnetic field gives some admixture of the negative $B\,^1\Pi_u$ state component. Consequently, the energy expression contains terms corresponding to a quadratic Zeeman effect $E_i=\langle i|H^{mg}|i\rangle+\Sigma_j\langle i|H^{mg}|j\rangle^2/(E_i-E_j)$. Note, that the two interacting A and B states are sufficiently far apart in energy, thus allowing to consider with satisfactory accuracy that $E_{v_AJ}-E_{v_BJ\pm1}\cong E_{v_AJ}-E_{v_BJ}$ and the quadratic term can therefore be comparable with a linear one. Accordingly, using an explicit form for diagonal and off-diagonal H^{mg} operator matrix elements, see Ref. 18, it is easy to obtain an expression for the A state Zeeman energy due to $A\sim B$ interaction in a following form:

$$E_i=2\mu_0 g_\mu M\mathscr{B}\sum_{v_B}\langle v_A^J|L^+(R)|v_B^J\rangle\langle v_A^J|L^+(R)[\hbar^2/(2mR^2)+\mu_0 g_\mu M\mathscr{B}/(2X)]|v_b^J\rangle/(E_{v_AJ}-E_{v_BJ})$$
$$+\mu_0^2 g_l^2\mathscr{B}^2\sum_{v_B}\{\langle v_A^J|L^+(R)|v_B^{J+1}\rangle^2(J+1)(J+2)T(J+1,M)/(E_{v_AJ}-E_{v_BJ+1})$$
$$+\langle v_A^J|L^+(R)|v_B^{J-1}\rangle^2 J(J-1)T(J,M)/(E_{v_AJ}-E_{v_BJ-1})\}, \qquad (13)$$

where $T(J,M)=(J^2-M^2)/[2J^2(4J^2-1)]$. Similar to the case of the $A\sim b$ interaction, the first term in Eq. (13) contains an interference factor dependent on the sign and value of M. Besides, Eq. (13) shows that, in contradiction to the case of the $A\sim b$ interaction, the second (negative) term being a function of M^2 may play a considerable role, especially for small M values. For the purpose of approximate calculations, Eq. (13) can be simplified using the approximation procedure as developed in our previous paper,[14] leading to

$$E_i=2\mu_0 g_\mu M\mathscr{B}\langle v_A^J|L^+(R)^2[\hbar^2/(2mR^2)$$
$$+\mu_0 g_\mu M\mathscr{B}/(2X)]/\Delta U_{AB}(R)|v_A^J\rangle$$
$$+\mu_0^2 g_l^2\mathscr{B}^2\langle v_A^J|L^+(R)^2/\Delta U_{AB}(R)|v_A^J\rangle[(J+1)$$
$$\times(J+2)T(J+1,M)+J(J-1)T(J,M)]. \qquad (14)$$

Based on Eq. (14), we carried out as an example the calculation of M dependence of μ_{v_AJ}/μ_0 values for $v_A=16$, $J=17$, μ_{v_AJ} being the magnetic moment determined as $E_i=-\mu_A^{wJ}\mathscr{B}$. This specific level was chosen because its g factor is practically inaffected by the $A\sim b$ interaction, and its J value is the smallest of all involved in our studies (see Table I). The results are presented in Fig. 3 for a maximal field value of 1 T available in our measurements.

It is rather obvious that the external magnetic field effect on the observed signal, as discussed in this section, depends on a number of parameters, including J and $g\times\tau$ values, the geometry of the arrangement for Hanle effect measurements (direction of observation and excitation, field direction, the type of molecular transition and light polarization), etc. The estimations were made for the case of our measurements (Fig. 1), showing that relative changes in $\mathscr{C}$ values due to nonlinear magnetic field effects does not exceed 5% for field value of $\mathscr{B}=1$ T.

V. CONCLUDING REMARKS

The local $A\sim b$ interaction in Na_2 molecule is showing itself in A state g_A^{wJ} factors as an admixture g_{Ab}^{wJ} on the background of regular contribution being of the order of $g_A^n+g_{AB}^{wJ}\cong-5\times10^{-5}$. From this point of view, $A\,^1\Sigma_u^+$ state levels can be devided into three groups accounting for the effectivity of manifestation of $A\sim b$ interaction in g factors: (i) *strongly coupled levels*, where $A\sim b$ interaction is strong both due to a large interaction matrix element value ξ_{Ab} as well as the smallness of zero order energy level differences ΔE_{Ab}^0 (energetic resonance). Here interaction is pronounced noticeably in g_A^{wJ} factors (showing the growth of absolute values up to 1–2 orders of magnitude as compared to the regular "background" value, cf. Ref. 14), in level

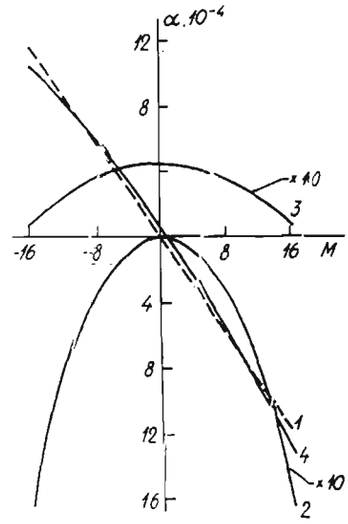

FIG. 3. M dependence of $\alpha=\mu_{v_AJ}(M,\mathscr{B})/\mu_0$ as calculated at $\mathscr{B}=1$ T according to Eqs. (13) and (14) for Na_2 $A\,^1\Sigma_u^+$ state level $v_A(J)=16(17)$. (1) Linear term. (2) The term caused by interference factor ($\Delta J=0$). (3) The term caused by quadratic ($\Delta J=\pm1$) effect. (4) The summary term. Curves 2 and 3 are ten times exaggerated.

frequency shifts (up to 1 cm^{-1}), as well as in lifetime changes (the increase up to 20 ns). (ii) *Weakly coupled levels*, where $A \sim b$ interaction is weak because of the large ΔE^0_{Ab} and (or) small ξ_{Ab} values, but nevertheless it is possible to gain information from magnetic measurements. Landé factor measurements are most favorable to study perturbations being weak due to small overlap integrals $\langle v^J_A | v^J_b \rangle$, because it is just the case when g-factor values are most sensitive to the accuracy of Dunham constants and spin-orbit electronic interaction values H^e_{so}. (iii) *Practically noncoupled levels*, where $A \sim b$ interaction is so weak due to small ξ_{Ab} and large ΔE^0_{Ab}, that $g^{wJ}_{Ab} \ll g^J_A + g^{wJ}_{AB}$, therefore g^{wJ}_A-factor measurements are practically noninformative from the point of $A \sim b$ interaction investigation.

In the present paper we focused our attention just on the second case (ii). It must be taken into account, however, that deperturbation makes sense only if its results are outside the error range, caused by the inaccuracy of the empirical molecular constants. Besides, note that for very small Landé factor values a great number of subtle perturbation effects must be taken into account. In particular, the weak regular perturbations caused by interactions with distant paramagnetic states ($A \sim B$, and possibly, the other ones), as well as magnetic field effects on measured g values must be considered with great accuracy.

ACKNOWLEDGMENTS

The authors are indebted to E. Tarasevich for assistance in measurements, to Dr. M. P. Auzin'sh for his help in evaluating of the nonlinear effect of the magnetic field, and to Dr. Yelena Pazyuk for useful discussions. Support from Latvian Science Council (Grant No. 90.467) is gratefully acknowledged.

[1] H. Lefebvre-Brion and R. W. Field, *Perturbations in the Spectra of Diatomic Molecules* (Academic, New York, 1986).
[2] I. P. Klincare, A. V. Stolyarov, M. Ya. Tamanis, Ya. A. Harya, and R. S. Ferber, Opt.i Spectrosk. **66**, 1018 (1989) [Opt. Spectrosc. (U.S.S.R.) **66**, 595 (1989)].
[3] A. V. Stolyarov, E. A. Pazyuk, L. A. Kuznetsova, Ya. A. Harya, and R. S. Ferber, Chem. Phys. Lett. **166**, 290 (1990).
[4] G. Gouedard and J. C. Lehmann, Faraday Discuss. Chem. Soc. **71**, 143 (1981).
[5] T. Carrol, Phys. Rev. **52**, 822 (1937).
[6] J. B. Atkinson, J. Berker, and W. Demtröder, Chem. Phys. Lett. **87**, 92 (1982).
[7] F. Engelke, H. Hage, and C. D. Caldwell, Chem. Phys. **64**, 221 (1982).
[8] K. Shimizu and F. Shimizu, J. Chem. Phys. **78**, 1126 (1983).
[9] C. Effantin, O. Babaky, K. Hussein, J. d'Incan, and R. F. Barrow, J. Phys. B **18**, 4077 (1985).
[10] O. C. Mullins, C. R. Mahon, and T. F. Gallagher, Chem. Phys. Lett. **126**, 501 (1986).
[11] B. E. Miller and P. A. Schulz, American Institute of Physics Conference Proceeding No. 146 (AIP, New York, 1986), p. 464.
[12] M. Li, C. Wang, Y. Wang and L. Li, J. Mol. Spectrosc. **123**, 161 (1987).
[13] H. Kato, M. Otani, and M. Baba, J. Chem. Phys. **89**, 653 (1988), J. Chem. Phys. **91**, 5124 (1989).
[14] A. V. Stolyarov, I. P. Klincare, M. Ya. Tamanis, M. P. Auzin'sh, and R. S. Ferber, J. Chem. Phys. **96**, 3510 (1992).
[15] R. W. Field (private communication).
[16] O. Babaky and K. Hussein, Can. J. Phys. **67**, 912 (1989).
[17] G. Baumgartner, H. Kornmeir, and W. Preuss, Chem. Phys. Lett. **107**, 13 (1984).
[18] M. Mizuchima, *The Theory of Rotating Diatomic Molecules* (Wiley, New York, 1975).
[19] R. A. Brooks, C. H. Anderson, and N. F. Ramsey, Phys. Rev. A **136**, 62 (1964).
[20] M. E. Kaminsky, J. Chem. Phys. **73**, 3520 (1980).
[21] P. Kusch and M. M. Hessel, J. Chem. Phys. **68**, 2591 (1977).
[22] D. D. Konowalow, M. E. Rozenkrantz, and M. L. Olson, J. Chem. Phys. **72**, 2612 (1980).
[23] D. D. Konowalow, M. E. Rozenkrantz, and D. S. Hochhauser, J. Mol. Spectrosc. **99**, 321 (1983).
[24] M. E. Kaminsky, J. Chem. Phys. **66**, 4951 (1977).
[25] B. R. Johnson, J. Chem. Phys. **67**, 4086 (1977).
[26] A. V. Stolyarov and N. E. Kuz'menko, Spectrosc. Lett. **19**, 1113 (1986).
[27] C. Noda and R. F. Zare, J. Mol. Spectrosc. **95**, 254 (1982).
[28] P. A. Fraser, Canad. J. Phys. **32**, 515 (1954).
[29] A. V. Stolyarov, N. E. Kuz'menko, Ya. A. Harya, and R. S. Ferber, J. Mol. Spectrosc. **137**, 251 (1989).
[30] J. B. Atkinson, J. Berker, and W. Demtröder, Chem. Phys. Lett. **87**, 128 (1982).
[31] J. Tellingshuisen, J. Mol. Spectrosc. **141**, 258 (1990).
[32] O. Babaky and K. Hussein, Z. Naturforsch. Teil A **45**, 795 (1990).

Alignment-orientation conversion by quadratic Zeeman effect: Analysis and observation for Te_2

I. P. Klincare, M. Ya. Tamanis, A. V. Stolyarov,[a] M. P. Auzinsh, and R. S. Ferber
Department of Physics, University of Latvia, Riga LV-1586, Latvia

(Received 27 April 1993; accepted 8 July 1993)

This paper reports the observation of the molecular fluorescence circularity under irradiation with linear polarized light. The phenomenon arises as a result of partial transformation from alignment of the ensemble of molecular angular momenta into orientation due to quadratic correction to Zeeman effect. Circularity rate up to 0.05 at magnetic field 0.4 T was registered in $B\,^3\Sigma_u^-(1_u^-) \rightarrow X\,^3\Sigma_g^-(1_g^-)$ fluorescence of $^{130}Te_2$ molecules at angle $\pi/4$ with respect to $\hat{\mathbf{E}}$ vector of linear polarized exciting light. Quadratic magnetic energy terms are associated with magnetic field induced $\Delta J=\pm 1$ e/f mixing between $1_u^- \sim 1_u^+$ and $1_u^- \sim 0_u^+$ states. Circularity data fitting shows that the electronic part of Landé factor caused by $1_u^- \sim 0_u^+$ interaction is equal to $G_\pm \cong g_l\langle 0_u|\mathbf{J}_{a\pm}|1_u\rangle + (g_s-g_l)\langle 0_u|\mathbf{S}_\pm|1_u\rangle \cong 2.72$.

I. INTRODUCTION

In the preceding paper[1] a theoretical consideration was presented allowing to predict the appearance of orientation of angular momenta under excitation by broadband linear polarized light through the action of external perturbation causing asymmetric splitting between coherent $M,M\pm 1$ magnetic sublevels when the corresponding magnetic splitting frequencies $\omega_{MM\pm 1} \neq \omega_{-M\mp 1-M}$. In this situation one is inclined to speak about anisotropic destruction of coherence, and the external field may play the same role as anisotropic collisions, which, as was first forecast in Refs. 2 and 3, are able to produce partial transformation from alignment to orientation. Significant interest in such a phenomenon of alignment-orientation conversion is connected with changing the symmetry type of angular momenta distribution, namely, with breaking the symmetry in respect to the reflection in the plane perpendicular to the axis of alignment. Nevertheless, as far as we know, there exist up to now only a few direct experimental observations, cf. Refs. 4–7, demonstrating the above mentioned effect of alignment-orientation transformation, which have been performed on atoms under anisotropic collisions. As is, in principle, clear,[1] any kind of external field action may cause the effect, if necessary asymmetric magnetic sublevel splitting is produced. In Ref. 8 it was proposed to achieve effective J-selective angular momenta orientation of aligned linear molecules moving in a beam with a fixed velocity by means of quadratic Stark effect.

An interesting possibility appears to be the use of the quadratic correction to the Zeeman effect in diatomic molecules. In particular, we direct now our attention on external magnetic field $\mathscr{B}$ induced interaction between the levels with $\Delta J=\pm 1$, leading to quadratic Zeeman energy dependence on field strength. We have chosen the Te_2 molecule as a convenient object for analysis and experimental observation of the effect. Indeed, sufficiently enough data are known about the energetic and radiative properties of low-lying excited electronic states of Te_2, among them the closely positioned $B0_u^+$ and $1_u^\pm$ states (cf. Refs. 9–13 and works cited therein). A number of data about g factors of these states have been obtained previously by measuring Hanle effect in laser induced fluorescence[14–16] supposing that only a linear Zeeman effect is taking place. In fact, as recently established by deperturbation analysis in Ref. 13, the $1_u^\pm$ state mentioned above is, most likely, predominantly a $\Omega=1$ component of the $B\,^3\Sigma_u^-$ state, and not of the $A^3\Pi_u$ state, as previously supposed,[9,10] hence the notation $B\,^3\Sigma_u^-(1_u)$ will be used herein for this state. It is worth mentioning that the 1_u^- component can be considered, with fair approximation, as unperturbed by heterogeneous electron–rotation $\Delta J=0$ interaction with 0_u^+ state. For this reason the 1_u^- component of Te_2 molecule was chosen here in order to demonstrate the appearance of alignment-orientation transformation induced by quadratic Zeeman effect.

II. ZEEMAN ENERGY CALCULATION

The Zeeman operator $\mathscr{H}_{\text{mag}}$ for Hund's (c) coupling case can be written in the following form:[17]

$$\mathscr{H}_{\text{mag}} = -\mu_B \mathscr{B}[g_l \mathbf{J}_{az} + (g_s - g_l)\mathbf{S}]. \tag{1}$$

We suppose here that the space-fixed z axis of quantization is directed along the external magnetic field $\mathscr{B}$, $g_l=1$ is the orbital electronic g factor, $g_s \cong 2.0023$ is the spin electronic g factor, $\mathbf{J}_a=\mathbf{L}+\mathbf{S}$ is an overall electronic orbital and electronic spin angular momentum of the molecule, μ_B is the Bohr magneton.

In contrast to intramolecular perturbations the Zeeman operator has nonzero off-diagonal ($\Delta J=\pm 1$) matrix elements,[18,19] hence, a magnetic field is able to induce interaction between levels with different J in $0_u^+ \sim 1_u^\pm$ complex of $B\,^3\Sigma_u^-$ state. As follows from the rigorously valid selection rule, total parity $\oplus$ or $\ominus$ is conserved, cf. Fig. 1. In terms of e/f labeling,[18] this means that allowed interactions with $\Delta J=\pm 1$ are $1_u^- \sim 1_u^+$ and $1_u^- \sim 0_u^+$, thus leading to magnetic field induced $e \sim f$ mixing. At the same time, the 1_u^- state can be considered as nonperturbed by

[a]Present address: Department of Chemistry, Moscow M. Lomonosov State University, Moscow W-234, 119899, Russia.

 0021-9606/93/99(8)/5748/6/$6.00

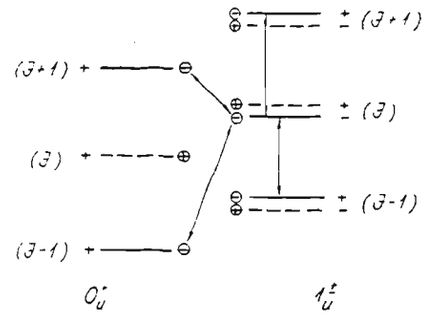

FIG. 1. Magnetic field induced mixing between 1_u^- and 1_u^-, 0_u^+ state levels with $\Delta J=\pm 1$. For an even isotopic $^{130}Te_2$ molecule J possesses an even integer value and the levels shown with dashed lines are not realised due to symmetry considerations. $\oplus,\ominus$ is the total parity, whilst $+,-$ is the electronic parity corresponding to e,f states, respectively.

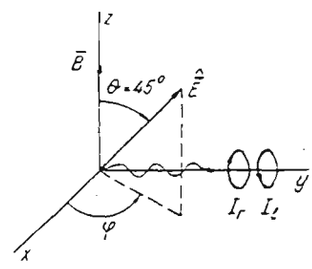

FIG. 2. Excitation and observation geometry.

both intramolecular electron rotation $1_u^-\sim 0_u^+$ as well as by diagonal over $J(\Delta J=0)$ magnetic $1_u^-\sim 1_u^+$, $1_u^-\sim 0_u^+$ interactions; it is the 1_u^- state which is of interest to study in order to analyze the role of quadratic Zeeman effect. Indeed, neglecting diamagnetic terms[19,20] the quadratic over $\mathscr{B}$ contribution ΔE_M to magnetic energy can be written for 1_u^- state as

$$\Delta E_M(1_u^-,v_1,J)=\frac{\langle 1_u^-(J)|\mathscr{H}_{\rm mag}|1_u^+(J\pm1)\rangle^2}{E^{v_1J}_{1_u^-}-E^{v_1J\pm1}_{1_u^+}}+\frac{\langle 1_u^-(J)|\mathscr{H}_{\rm mag}|0_u^+(J\pm1)\rangle^2}{E^{v_1J}_{1_u^-}-E^{v_0J\pm1}_{0_u^+}}. \quad (2)$$

Here v_0 and v_1 denote the vibrational levels of 0_u^+ and 1_u^-, 1_u^+ states, respectively.

We further neglect the heterogeneous $0_u^+\sim 1_u^+$ interaction effect on rovibronic level energies of 0_u^+ and 1_u^+ states and their wave functions. Then, assuming that the electronic part of the Zeeman operator $\mathscr{H}_{\rm mag}$ is independent of internuclear distance, the total magnetic energy of a certain rovibronic level (v_1,J) takes the form

$$E_M(1_u^-,v_1,J)=\frac{G_z}{J(J+1)}M\mu_B\mathscr{B}+G_z^2A(M,J)\mu_B^2\mathscr{B}^2+G_\pm^2B(M,J)\mu_B^2\mathscr{B}^2, \quad (3)$$

where the first term corresponds to linear Zeeman effect. G_z is the electronic part of the molecular g factor in the $\Omega=1$ state, which is equal to[17,18]

$$G_z=[g_l\Omega+(g_s-g_l)\langle\Omega|S_z|\Omega\rangle]\Omega. \quad (4)$$

The second term of Eq. (3), in agreement with Eq. (2), is emerging due to $1_u^+\sim 1_u^-$, $\Delta J=\pm 1$ interaction. The "geometric" factor $A(M,J)$ in Eq. (3) can be found by application of direct cosine matrix elements[18,21] α_{11}

$$A(M,J)=\frac{\alpha_{11}^2(M,J;M,J+1)}{E^{v_1J}_{1_u^-}-E^{v_1J+1}_{1_u^+}}+\frac{\alpha_{11}^2(M,J;M,J-1)}{E^{v_1J}_{1_u^-}-E^{v_1J-1}_{1_u^+}},$$

$$\alpha_{11}^2(M,J;M,J+1)=J(J+2)f(J,M),$$

$$\alpha_{11}^2(M,J;M,J-1)=(J^2-1)h(J,M),$$

$$f(J,M)=\frac{1}{(J+1)^2}\left[\frac{(J+1)^2-M^2}{4(J+1)^2-1}\right],$$

$$h(J,M)=\frac{1}{J^2}\left(\frac{J^2-M^2}{4J^2-1}\right). \quad (5)$$

We are neglecting here the interaction between different vibronic 1_u^- state levels, supposing that the overlap integrals $\langle v_1^J|v_1^{J\pm1}\rangle\cong 0$ for $v_1\neq v_1$, where v_Ω, $v_{\Omega'}$ are different 1_u^- state vibrational quantum numbers. Then, neglecting the centrifugal distortion terms in expressions for energies entering Eq. (5), we get

$$A(M,J)\cong\frac{1}{2B_v}\left[\frac{\alpha_{11}^2(M,J;M,J-1)}{J}-\frac{\alpha_{11}^2(M,J;M,J+1)}{J+1}\right]. \quad (6)$$

The second quadratic term in Eq. (3) describes the magnetic field induced $1_u^-\sim 0_u^+$, $\Delta J=\pm 1$ interaction, and $G_\pm$ is the component of the electronic part of the g factor caused by heterogeneous $(\Omega'-\Omega=\Delta\Omega=1)$ interaction[17,18]

$$G_\pm=g_l\langle\Omega|J_{a\pm}|\Omega'\rangle+(g_s-g_l)\langle\Omega|S_\pm|\Omega'\rangle. \quad (7)$$

The geometric factor $B(M,J)$ then appears as

$$B(M,J)=\alpha_{10}^2(M,J;M,J+1)S_1+\alpha_{10}^2(M,J;M,J-1)S_2,$$

$$\alpha_{10}^2(M,J;M,J+1)=\frac{J(J+1)}{2}f(J,M),$$

$$\alpha_{10}^2(M,J;M,J-1)=\frac{J(J+1)}{2}h(J,M), \quad (8)$$

where

$$S_1=\sum_{v_0}\frac{\langle v_1^J|v_0^{J+1}\rangle^2}{E^{v_1J}_{1_u^-}-E^{v_0J+1}_{0_u^+}},\quad S_2=\sum_{v_0}\frac{\langle v_1^J|v_0^{J-1}\rangle^2}{E^{v_1J}_{1_u^-}-E^{v_0J-1}_{0_u^+}}. \quad (9)$$

The direction cosine matrix elements[21] α_{11} and α_{10} in Eqs. (6) and (8) are arising in the transformation from the molecule-fixed coordinate system to a space-fixed one. The overlap integrals and energy differences entering into Eq. (9) can be calculated for given v, J values using molecular constant set.[9,10]

Thus the problem of getting Zeeman energy $E_M(1_u^-, v, J)$ values accounted for quadratic terms due to magnetic field induced interaction, cf. Eq. (3), is reduced to a minimum number of adjustable parameters, namely, G_z and $G_\pm$.

III. CALCULATION OF FLUORESCENCE CIRCULARITY

The general requirements imposed on the Zeeman sublevel splitting matrix $\omega_{MM'}=(E_M-E_{M'})/\hbar$ which are necessary to observe the occurrence of circularity under linear polarized excitation were examined in Ref. 1. According to this, the nonzero even rank X coefficient ω_0^X value has to appear in $\omega_{MM'}$ expansion over irreducible tensor operators of the rotation group. This is equivalent to the condition

$$\omega_{MM+1}\neq\omega_{-M-1-M}, \tag{10}$$

which is fulfilled for the case described by Eq. (3) together with Eqs. (6) and (8) due to the M^2 dependence of α_{11}, α_{10}. By substitution the analytical expressions for the α_{11} and α_{10} values into Eqs. (6), (8) and then into Eq. (3), we get the explicit form for E_M

$$E_M(1_u^-, v_1, J)=\frac{G_z M\mu_B\mathscr{B}}{J(J+1)}+\frac{G_z^2\mu_B^2\mathscr{B}^2}{2B_v}\left[\frac{(J^2-1)(J^2-M^2)}{J^3(4J^2-1)}-\frac{J(J+2)[(J+1)^2-M^2]}{(J+1)^3[4(J+1)^2-1]}\right]$$
$$+\frac{G_\pm^2\mu_B^2\mathscr{B}^2}{2}\left[\frac{J[(J+1)^2-M^2]}{(J+1)[4(J+1)^2-1]}S_1+\frac{(J+1)(J^2-M^2)}{J(4J^2-1)}S_2\right]. \tag{11}$$

This leads to

$$\omega_{MM+1}=\omega_L[-1-(a_J+b_J)\omega_L(2M+1)],$$
$$\omega_{-M-1-M}=\omega_L[-1+(a_J+b_J)\omega_L(2M+1)], \tag{12}$$

where

$$\omega_L=\frac{G_z}{J(J+1)}\mu_B\frac{\mathscr{B}}{\hbar}, \tag{13}$$

and a_J and b_J are M-independent factors arising from $A(M,J)$ and $B(M,J)$, respectively. As is evident from Eqs. (11)–(13), condition (10) holds and hence the appearance of circularity I_r-I_l is expected, I_r,I_l being fluorescence intensities in the cycle $J''\rightarrow J'\rightarrow J_1''$ possessing right-handed and left-handed circular polarization, respectively. Let us discuss the geometry of excitation and observation, cf. Fig. 2. The $\hat{E}$-vector of linear polarized excitation is directed at spherical angles θ,φ, whilst the direction of observation is chosen along y axis. Expressions for I_r-I_l and I_r+I_l at arbitrary θ,φ are given in Ref. 1. The optimal θ value equal to $\pi/4$, will be supposed in further treatment, and we obtain

$$I_r-I_l\propto\sum_M\frac{\Gamma_p(\Gamma\sin\varphi+\omega_{MM+1}\cos\varphi)}{\Gamma^2+\omega_{MM+1}^2}$$
$$\times(C^{J'M}_{J''M+11-1}C^{J'M+1}_{J''M+110}-C^{J'M}_{J''M10}C^{J'M+1}_{J''M11})$$
$$\times(C^{J'M}_{J_1'M10}C^{J'M+1}_{J_1'M11}+C^{J'M}_{J_1'M+11-1}C^{J'M+1}_{J_1'M+110}). \tag{14}$$

where $C^{\gamma}_{\alpha a b\beta}$ are Clebsch–Gordan coefficients, Γ is the excited state relaxation rate and Γ_p is the pumping (excitation) rate.

Figure 3 demonstrates the results of numeric calculation of the expected value of circularity rate $\mathscr{C}=(I_r-I_l)/(I_r+I_l)$ as dependent on a dimensionless parameter $\omega_L/\Gamma\propto\mathscr{B}$, cf. Eq. (13). The I_r+I_l value has been calculated according to Eq. (15) from Ref. 1. Fig. 3(a) demonstrates the case when $\varphi=\pi/2$ which is fulfilled when the exciting beam is perpendicular to the direction of observation, cf. Fig. 2. Figure 3(b) refer to the geometry when $\varphi=0$, which can be achieved when fluorescence is observed along the exciting beam direction. Parameters involved in the calculation refer to the $B\,^3\Sigma_u^-(1_u^-)$ state of $^{130}Te_2$ with $v_1=2(J=96)$, as studied in Refs. 13, 14, and 16. The $J-1\rightarrow J\rightarrow J+1$ cycle was considered. We used here $G_z=-1.86$ and $\Gamma=\tau^{-1}=8.55\times10^6\ s^{-1}$ obtained from Hanle effect and lifetime measurements. Deperturbed molecular constants were taken from Refs. 13 and 22.

Curves 1 in Figs. 3(a) and 3(b) correspond to the situation when we suppose $G_\pm=0$ in Eqs. (3) and (11) leading to $b_J=0$ in Eq. (12). Thus we are neglecting the magnetic field induced $1_u^-\sim0_u^+$ interaction. This assumption means that the G_z is the only parameter describing the magnetic energy, and the quadratic term arises due to $1_u^-\sim1_u^+$, $\Delta J=\pm1$ interaction. As may be seen, curve 1 in Fig. 3(a) is of dispersion type, being an odd ω_L/Γ function with a maximum at $\omega_L/\Gamma\sim1.5$, and the appearing circularity does not exceed 0.1. The orientation signal $\mathscr{C}(\omega_L/\Gamma)$ in Fig. 3(b), cf. curve 1, is an even ω_L/Γ function and shows a more subtle form changing its sign in the vicinity of $\omega_L/\Gamma=1$. The fact that curves in Fig. 3(a) are odd by reversing the magnetic field whilst those in Fig. 3(b) are even has a simple geometric interpretation. The orientation is always created perpendicular to the plane defined by the light $\hat{E}$ vector and the direction of perturbation causing alignment-orientation conversion.[1,8] In the case of Figs. 3(a) and 3(b) the created orientation is perpendicular to the $\hat{E}$, $\mathscr{B}$ plane. The appeared orientation starts to precess in the magnetic field $\mathscr{B}$. For the geometry of Fig. 3(a) the orientation is created perpendicular to the direction of observation. Hence, the fluorescence circularity depends strictly on the direction of precession (defined by the sign

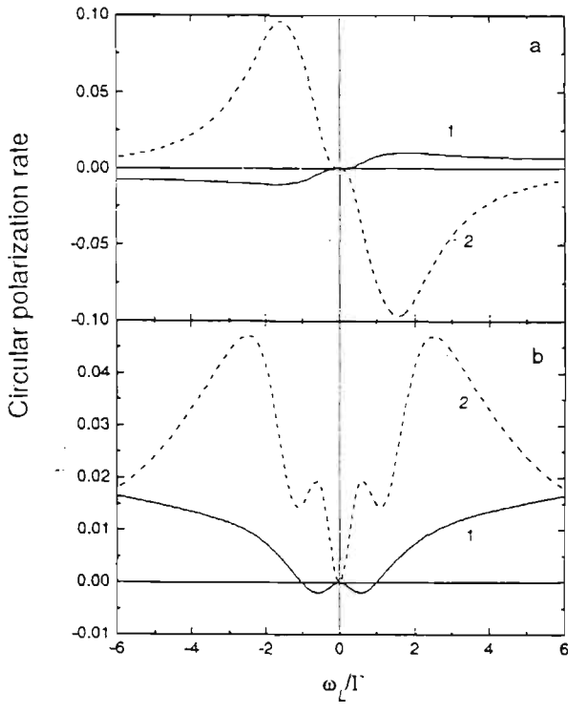

FIG. 3. Calculated circularity rate $\mathscr{C}$ as dependent on parameter ω_L/Γ, which is proportional to magnetic field strength $\mathscr{B}$. (a) For E vector directed at $\theta=\pi/4$, $\varphi=\pi/2$ (cf. Fig. 2), (b) $\theta=\pi/4$, $\varphi=0$. Curves 1 correspond to $G_\pm=0$. Curves 2 correspond to $G_\pm=2.9$.

of magnetic field) and can be described by the odd type $\mathscr{C}(\mathscr{B})$ function. In the case of geometry of Fig. 3(b) the orientation is created in the direction of observation. It means that the observed fluorescence circularity is independent on the direction of precession of orientation and can be described by the even type $\mathscr{C}(\mathscr{B})$ function.

Let us now include magnetic field induced $1_u^- \sim 0_u^+$ mixing which follows the selection rule $\Delta J=\pm 1$. Using molecular constant sets[13] for 1_u and 0_u^+ states we get for $v_1=2(J=96)$ the following values for the sums entering Eq. (11): $S_1=-0.019$ 1/cm^{-1}, $S_2=-0.029$ 1/cm^{-1}. If the G_z value is known, $G_\pm$ remains the only adjustable parameter. Curves 2 in Fig. 3(a) and 3(b) demonstrate the total circularity signal which appears owing to both $1_u^- \sim 1_u^+$ and $1_u^- \sim 0_u^+$ Zeeman mixing. The concrete $G_\pm=2.9$ value was used as established in Ref. 13 by "global" deperturbation analysis from simultaneous processing of magnetic and radiative data. As is seen, the circularity caused owing to $1_u^- \sim 0_u^+$ interaction dominates in this case. Circularity signals, as shown by curves 1 and 2 for the more simple dependence in Fig. 3(a), are of opposite sign due to the opposite sign of a_J and b_J in Eq. (12). Figure 4 demonstrates high sensitivity of the appeared orientation signal to $G_\pm$ changes. Hence, it is promising to use the alignment-orientation conversion effect in order to determine $G_\pm$ values and thus to pass to the matrix element of the heterogeneous electronic interaction.

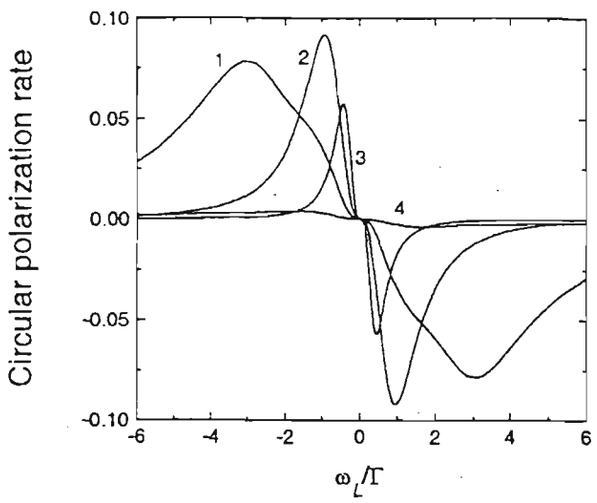

FIG. 4. The same dependence as shown by curve 2 in Fig. 3(a) for different $G_\pm$ values: (1) $G_\pm=8$, (2) $G_\pm=4$, (3) $G_\pm=2$, (4) $G_\pm=1$.

IV. EXPERIMENTAL RESULTS AND DISCUSSION

Molecular fluorescence from $^{130}Te_2$ vapor was induced by a linear polarized line 514.5 nm from an Ar^+ laser operating in a multimode regime. The tellurium isotope was held in a fused silica cell at a temperature $T=650$ K and connected with a vacuum system through a dry valve. The R-type molecular transition $(X1_g^-, v''=4, J''=95) \rightarrow (B1_u^-, v'=2, J'=96)$ was excited.[9]

The degree of circularity was measured at the geometry shown in Fig. 2 when $\theta=\pi/4$, $\varphi=\pi/2$. The external magnetic field was varied between $\mathscr{B}=-0.4$ and $+0.4$ T. The results for a fluorescence transition $(B1_u^-, v'=2, J'=96) \rightarrow (X1_g^-, v''=8, J''=97)$ are presented in Fig. 5. showing the appearance of circularity up to $\mathscr{C}=0.05$. The solid line was calculated in the same way as the curve 1 in Fig. 3(a) using $G_\pm$ as the only nonlinear fitting parameter, and the value $G_\pm=2.72$ yielding by fitting is in excellent agreement with the results obtained in a

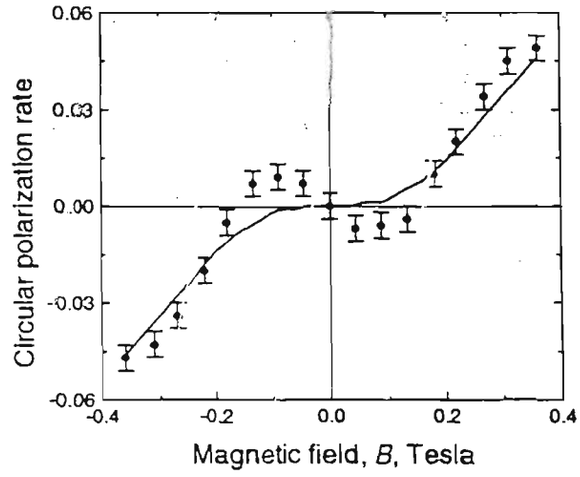

FIG. 5. Measured circularity signal for $v_1=2(J=96)$ level of $B\,^3\Sigma_u^-(1_u^-)$ state in $^{130}Te_2$. Full line is obtained by fitting according to Eq. (17).

different way in Ref. 13. As it may be seen from Fig. 5, the general behavior of the calculated dependence reflects, to a major extent, the main behavior of the measured circularity values. It seems, however, that one can notice some distinction which is beyond the statistical error limit. The discrepancy in the small $\mathscr{B}$ region can not be explained by accounting for the simultaneous 1_u^-, 0_u^+, and 1_u^+ interaction, which gives an additional contribution to the quadratic Zeeman term in Eqs. (3) and (11) and is able to change only slightly the $G_\pm$ value yielded by fitting, without changing the shape of the signal at a small magnetic field. The higher order magnetic terms not involved in our description are also unable to produce the structure. Thus, up to now we can only suppose that the discrepancy may be due to either some systematic experimental errors, or else, because the broad excitation line approximation is not valid with sufficient precision.

It is interesting to compare the information available from magnetic field induced alignment-orientation conversion with that yielded by conventional Landé factor measurements supposing the linear Zeeman effect conditions. Landé factors $g_{B0_u^+}$ of a diamagnetic ($\Omega=0$) $B0_u^+$ state of $^{130}Te_2$ were obtained in Ref. 15. The $g_{B0_u^+}$ values are determined by electron-rotation $0_u^+ \sim 1_u^+$ interaction with $\Delta J=0$. The $g_{B0_u^+}$ data interpretation needs, however, the notion of the electronic matrix element $\eta=\langle\Omega|J_{a\pm}|\Omega'\rangle$ for heterogeneous electron-rotation state mixing $|\Omega'-\Omega|=1$ of the coupled 0_u^+ and 1_u^+ states. For weakly coupled levels we get[13,15,22]

$$g_{B0_u^+}=2G_\pm\eta\sum_{v_1'}\frac{\langle v_0|B(R)|v_1'\rangle\langle v_0|v_1'\rangle}{E_{0_u^+}^{v_0J}-E_{1_u^+}^{v_1'J}}. \tag{15}$$

Hence, the $g_{B0_u^+}$ factor data yield only the product $G_\pm\eta$ and does not allow to determine $G_\pm$ in a direct way. The η value for $0_u^+\sim 1_u^+$ mixing in Te_2 was determined[13] from energetic and radiative data as $\eta\cong 1.43$. This leads, for instance, to $G_\pm\cong 2.9$ for the $B0_u^+$ state level $v_0=0(J=179)$. This result is in a good agreement with the $G_\pm$ values obtained in a direct and independent way in the present work. Such an agreement confirms once more that the $G_\pm$ value is very close to 2η, and thus we have an additional reason for the conclusion[13] that the $Te_2(1_u)$ state studied here is in main a $^3\Sigma_1$ component of the $B\,^3\Sigma_u^-$ state. Indeed, as follows from Eqs. (7) and (15), $G_\pm$ and η are not independent, and $G_\pm-\eta=\langle\Omega|S_\pm|\Omega'\rangle$. Passing to Hund's case (a) basis set, we get $G_\pm\cong g_s\langle^3\Sigma_0|S_\pm|^3\Sigma_1\rangle=2\eta$. If the 1_u state is a $^3\Pi_1$ component of the $A\,^3\Pi_u$ state according to the point of view of the authors of Refs. 9 and 10, it should be $G_\pm\cong g_l\langle^3\Sigma_0|L_\pm|^3\Pi_1\rangle=\eta$.

It is worth mentioning that the alignment-orientation conversion induced by nonlinear Zeeman mixing gives the possibility to study the weak intramolecular interaction effects via magnetic characteristics of not only diamagnetic but paramagnetic states as well. For instance, the 1_u^- state of Te_2 studied here was always treated as unperturbed by $1_u\sim 0_u^+$ interaction and its magnetic properties were described by the G_z value only.[13,14,16]

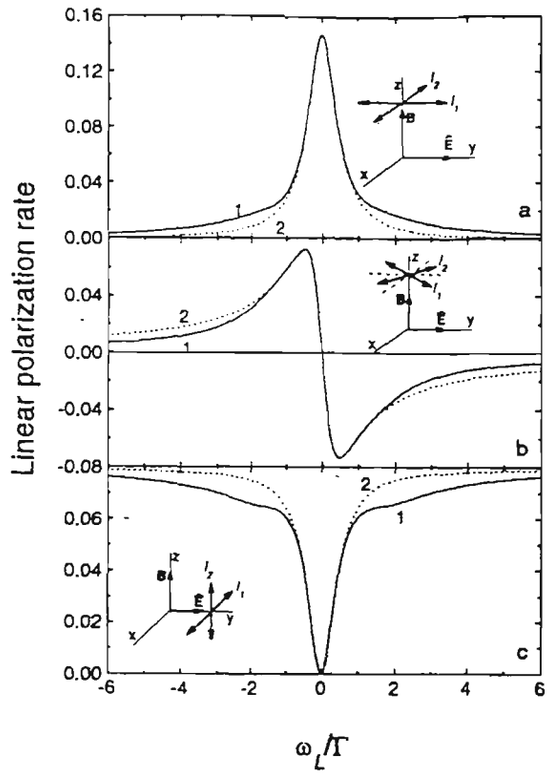

FIG. 6. Calculated linear polarization rate $\mathscr{P}=(I_1-I_2)/(I_1+I_2)$ as dependent on ω_L/Γ for various observation-excitation schemes. Curve 1—with accounting on quadratic Zeeman term in Eq. (11), curve 2—the ordinary Hanle effect signal.

Let us now follow the influence of quadratic Zeeman effect terms in Eqs. (3) and (11) on the Hanle effect signal measured in linear polarization of laser induced fluorescence. The results of calculations of linear polarization rate $(I_1-I_2)/(I_1+I_2)$ of fluorescence as dependent on magnetic field strength $\mathscr{B}$ are presented in Fig. 6 for three different excitation-observation schemes for the same molecular transitions and parameters as in Fig. 5. As one may see, the dependencies accounting for nonlinear Zeeman term (curves 1) do not differ much from the signal caused by linear Zeeman effect (curves 2). The "traditional" Hanle signal of Lorenz shape, cf. Fig. 6(a), was the one used in the experiments[14,16] in order to determine G_z for $v_1=2(J=96)$ of the $B\,^3\Sigma_u^-(1_u^-)$ state in $^{130}Te_2$. The uncertainty caused in this case by using the Lorenzian dependence does not considerably exceed the experimental error value. The most favorable is the situation in the case of dispersion shape signal, cf. Fig. 6(b), when one can determine G_z value from the positions of signal maxima without any influence of the quadratic Zeeman term. By contrast, the geometry presented in Fig. 6(c) leads to the largest changes due to the quadratic effect. Nevertheless, this geometry is very convenient technically and, besides, has its advantages allowing to measure both circularity rate and linear polarization rate in one and the same experimental scheme when the exciting light beam is directed orthogonally to both magnetic field and observation directions. One needs only to turn E vector of exciting beam to obtain

$\theta=\pi/4$ (cf. Fig. 2) and to remove the $\lambda/4$ plate. Thus at least at certain parameters of the studied molecular state it is possible to determine G_z from the linear polarization rate signal and $G_\pm$ by measuring the circularity appeared at linear polarized excitation as a result of magnetic e/f mixing.

V. CONCLUDING REMARKS

We demonstrated and analyzed the transformation of alignment of molecular angular momenta into their orientation under the influence of nonlinear Zeeman effect. This effect of breaking the reflection symmetry manifests itself in the occurrence of fluorescence circularity under linear polarized excitation. Owing to the presence of a linear term of Zeeman energy the dispersion shape magnetic field dependence of the circularity signal can be observed if fluorescence is viewed in the plane containing the exciting light E vector and the magnetic field vector $\mathscr{B}$, the signal being zero in the case of pure quadratic external perturbation as in the case of Stark effect.[1] Sufficiently effective alignment-orientation conversion was registered in a 1_u^- component of $B\,^3\Sigma_u^-$ state of Te_2 caused predominantly by magnetic field induced $1_u^-\sim 0_u^+$ mixing with $\Delta J=\pm 1$. It is important to mention that since the linear Zeeman effect is not able to cause orientation, the registration of circularity at linear polarized excitation makes it possible to separate this effect from the own 1_u-state paramagnetism. Hence, the measurement of magnetic properties can be used to study intramolecular interaction not only in diamagnetic ($\Lambda=0$ or $\Omega=0$) states which appeared to be an extremely sensitive test of weak perturbations[3,15,18,23,24] but can be applied also to paramagnetic states. In doing so, it is possible by combining the circularity measurement with the traditional (linear) Hanle effect measurement to determine both matrix elements G_z and $G_\pm$ of the electronic Landé factor, in one and the same experiment. Generally speaking, the emergence of circularity may serve as a test of any kind of external perturbation causing asymmetric magnetic sublevel splitting, including hyperfine structure effects. Finally, since the quite noticeable degree of orientation can be maintained, alignment-orientation conversion may be considered as an additional possibility to achieve orientation of a molecular ensemble.

ACKNOWLEDGMENTS

The authors are indebted to E. Tarasevich for assistance in measurements. Support from the Science Council of Latvia (Grant No. 90.467) is gratefully acknowledged.

[1] M. P. Auzinsh and R. S. Ferber, J. Chem. Phys. **99**, 5742 (1993).
[2] V. N. Rebane, Opt. Spectrosk. **24**, 309 (1968).
[3] M. Lombardi, Compt. Rend. B **265**, 191 (1967).
[4] E. Chamoun, M. Lombardi, M. Carré, and M. L. Gaillard, J. Phys. (Paris) **38**, 591 (1977).
[5] T. Manabe, T. Yabuzaki, and T. Ogawa, Phys. Rev. Lett. **46**, 637 (1981).
[6] N. G. Lukomsky, V. A. Polishchuk, and M. P. Chaika, Opt. Spektrosk. **58**, 474 (1985); **59**, 1008 (1985).
[7] M. Elbel, M. Simson, and Th. Strauss, Ann. Phys. Leipzig **47**, 467 (1990).
[8] M. P. Auzinsh and R. S. Ferber, Phys. Rev. Lett. **69**, 3463 (1992).
[9] J. Verges, C. Effantin, O. Babaky, J. d'Incan, S. J. Prosser and R. F. Barrow, Phys. Scr. **25**, 338 (1982).
[10] J. Verges, J. d'Incan, C. Effantin, D. J. Greenwood, and R. F. Barrow, J. Phys. B **12**, 4301 (1979).
[11] R. S. Ferber, O. A. Shmit, and M. Ya. Tamanis, Chem. Phys. Lett. **92**, 393 (1982).
[12] R. S. Ferber, Ya. A. Harya, and A. V. Stolyarov, J. Quant. Spectrosc. Radiat Transf. **47**, 143 (1992).
[13] E. A. Pazyuk, A. V. Stolyarov, M. Ya. Tamanis, and R. S. Ferber, J. Chem. Phys. (in press).
[14] I. P. Klintsare, M. Ya. Tamanis, and R. S. Ferber, Opt. Spektrosk. **67**, 1222 (1989) [Opt. Spectrosc. (USSR) **67**, 720 (1989)].
[15] I. P. Klintsare, A. V. Stolyarov, M. Ya. Tamanis, R. S. Ferber, and Ya. A. Kharya, Opt. Spektrosk. **66**, 1018 (1989) [Opt. Spectrosc. (USSR) **66**, 595 (1989)].
[16] I. P. Klincare and M. Ya. Tamanis, Chem. Phys. Lett. **180**, 63 (1991).
[17] L. Veseth, J. Mol. Spectrosc. **63**, 180 (1976).
[18] H. Lefebvre-Brion and R. F. Field, *Perturbations in the Spectra of Diatomic Molecules* (Academic, New York, 1986).
[19] M. Mizushima, *The Theory of Rotating Diatomic Molecules* (Wiley, New York, 1975).
[20] J. H. Van Vleck, Phys. Rev. **31**, 587 (1928).
[21] J. T. Hougen, *The Calculations of Rotational Energy Levels and Rotation Line Intensities in Diatomic Molecules*, NBS Monograph, 115 (Nat. Bur. Stand., Washington, D.C., 1970).
[22] A. V. Stolyarov, E. A. Pazyuk, L. E. Kuznetsova, Ya. A. Harya, and R. S. Ferber, Chem. Phys. Lett. **166**, 290 (1990).
[23] A. V. Stolyarov, I. P. Klincare, M. Ya. Tamanis, M. P. Auzin'sh, and R. S. Ferber, J. Chem. Phys. **96**, 3510 (1992).
[24] A. V. Stolyarov, I. P. Klincare, M. Ya. Tamanis, and R. S. Ferber, J. Chem. Phys. **98**, 826 (1993).

Global deperturbation analysis from energetic, magnetic, and radiative measurements: Application to Te_2

E. A. Pazyuk,[a] A. V. Stolyarov,[a] M. Ya. Tamanis, and R. S. Ferber
Department of Physics, University of Latvia, Riga, Latvia, LV-1586

(Received 8 February 1993; accepted 12 July 1993)

In the framework of a unified physical model, employed as a basis Hund's case "c," a quantitative description has been worked out for experimental data of term values, g factors, and lifetimes of excited $B0_u^+$ and $A1_u$ states, as well as for relative intensities in $B0_u^+-X0_g^+$, $A1_u-X1_g$, and $B0_u^+-X1_g$ transitions. The model includes a minimum number of adjustable fitting parameters: deperturbed molecular constants for both states, intramolecular interaction matrix element (η), two electronic matrix elements of magnetic interactions ($G_z, G_\pm$), as well as two parallel ($R_{e\parallel}^{B0_u^+-X0_g^+}, R_{e\parallel}^{A1_u-X1_g}$) and two perpendicular ($R_{e\perp}^{B0_u^+-X1_g}, R_{e\perp}^{A1_u-X0_g^+}$) electronic transition moments. The $B0_u^+$ state g factors and the intensity distribution over P, R, Q branches in $B0_u^+-X1_g$ transition was found to be most sensitive to weak heterogeneous ($\Delta\Omega=\pm1$) perturbations, and a simple analytic connection between those characteristics has been proposed. The Ω-doubling constant for $A1_u$ state levels was evaluated. By transforming the responsible electronic matrix elements to Hund's case "a" basis, the $A1_u$ state has been found to be basically a $^3\Sigma_1$ component of the $B\,^3\Sigma_u^-$ state, with a small admixture ($<14\%$) of a $^3\Pi_1$ component of the $A\,^3\Pi_u$ state, and a change in term notation from $A1_u$ to $B1_u$ is proposed.

I. INTRODUCTION

As is often the case in practical spectroscopy, the main difficulty in a correct analysis of structural and dynamical properties in the excited states of diatomic molecules is due to the presence of various perturbations. At the same time, if the nature of a perturbation can be understood, one gets a unique source of information unobtainable in any other way.[1,2] Perturbations can be more or less pronounced in all experimentally observed molecular characteristics, such as *energetic* (term values, level shifts), *radiative* (lifetimes and relative intensities), *magnetic* (Landé factors), etc. All of them can be, at least hypothetically, considered as useful in order to solve the inversed spectroscopic problem, namely the deperturbation treatment. Each of the mentioned characteristics possesses both advantages and disadvantages caused, on the one hand, by different value and accuracy of existing experimental material and, on the other hand, by different sensitivity towards the type and power of the intramolecular perturbation,[2–5] the latter being particularly important in the case of weak perturbations. This can be easily understood, if one remembers that level shifts and lifetime changes are proportional to the squared interaction matrix element H_{ij}^2, while g factors of diamagnetic states as well as intensities of forbidden transitions are proportional to H_{ij}. Besides, essentially different phenomenological models were historically developed to describe various characteristics, thus hindering their joint usage in performing a *global deperturbation analysis* (GDA). This situation seems somewhat unnatural, since the common origin of the aforementioned effects is intuitively rather obvious. Therefore, the need has arisen to create a unified view at a differently manifested perturbation. The Te_2 molecule is a convenient test object for demonstrating the GDA for a heavy dimer, free of hyperfine structure (HFS) for an even isotope and possessing a Hund's case "c" coupling scheme. Indeed, during the last 20 years different Te_2 molecule characteristics were measured for the same conditions in tellurium vapor, in many cases for the same rovibronic levels. The present paper presents an attempt to interpret the comprehensive combination of existing experimental data of term values, g factors, lifetimes for some rovibronic levels of $B0_u^+$ and $A1_u$ states, as well as the relative intensities of $B0_u^+-X0_g^+$, $A1_u-X1_g$, and $B0_u^+-X1_g$ transitions, in the framework of the unified physical model with minimum number of adjustable fitting parameters.

It may be easy noticed that involving of any new physical characteristic into the GDA fitting process requires including additional adjustable parameters into the adopted model. These parameters are from the theoretical point of view equivalent to matrix elements of electronic wave functions of correspondent quantum operators describing the physical quantity. In particular, for energy characteristics it is the zero order Hamiltonian $\mathcal{H}_0$ as well as the intramolecular interaction operator V_p; for magnetic interactions the Zeeman operator $\mathcal{H}_{mag} = -\mu_B\mathcal{B}(g_l\mathbf{L}+g_S\mathbf{S})$; and for radiative characteristics the electric dipole transition moments $\mathbf{d}=\Sigma_i e_i\mathbf{r}_i$. The number of such parameters can be sufficiently large[6] when the most common Hund's case "c" basis is used. Nevertheless, this number may be considerably diminished by expanding the general case "c" matrix elements over a case "a" basis set.[7] In spite of the fact that Hund's case "a"

[a]Present address: Department of Chemistry, Moscow M. Lomonosov State University, Moscow W-234, 119899, Russia.

approximation seems to be too limited (especially for heavy molecules possessing considerable spin–orbit interaction), a change to an "a" basis allows to ascertain the connection between differing matrix elements and, in some cases, as, for example, in the case when pure precession approximation[8] is employed, also to estimate the absolute value of the matrix element. Moreover, by passing over to Hund's case "a" approximation, it becomes possible to evaluate the contribution of different electronic states to the "a" matrix element, or in other words, to compute mixing coefficients. This, in turn, allows unambiguous electronic assignment of the interacting states.

The principal difference is to be pointed out between the magnetic and radiative characteristics. Indeed, computation of the latter needs detailed knowledge of the electronic wave functions in any basis set of Hund's case "a," "b," or "c" functions. This is why the corresponding matrix elements are used as adjustable parameters in most of semiempirical models.[9] On the other hand, angular momenta L and S matrix elements used for g factor computation can be calculated in the framework of Hund's case "a" basis set. Besides, certain relations exist between magnetic and intramolecular matrix elements, because most of intramolecular interactions are dependent on the same operators.[10,11] A description of this relation results in better understanding of the origin of an intramolecular interaction. In order to demonstrate this possibility we have performed, in the present work, an empiric fitting procedure of magnetic matrix elements in Hund's case "a" basis. This leads to a somewhat unexpected conclusion that, in opposition to the previous assumption,[12] the $A1_u$ state is mainly (in $\sim$86%) a $^3\Sigma_1$ component of the $B\,^3\Sigma_u^-$ state, and in $\leqslant$14% a $^3\Pi_1$ component of the $A\,^3\Pi_u$ state. This conclusion is supported by processing of absolute strengths of the $A1_u$–$X1_g$ and $A1_u$–$X0_g^+$ transitions and of their dependence on internuclear distance.

The organization of the present paper is as follows. The existing experimental information about the Te_2 molecule used for the deperturbation analysis is summarized in Sec. II. The theoretical model describing energetic, radiative, and magnetic characteristics is detailed in Sec. III. The results of a least-squares fit procedure are presented in Sec. IV. The connection between considered characteristics and the values of related electronic parameters is discussed in Sec. V. The origin of the 1_u state studied here is discussed in Sec. VI.

II. EXISTING EXPERIMENTAL DATA

Details of spectroscopic techniques and energetic, magnetic, and radiative measurements which led to the development of the deperturbation model for coupled $B0_u^+$ and $A1_u$ states of $^{130}Te_2$, cf. Fig. 1, have been described previously.[12–27] A few of the main experimental features are summarized here. The range of vibrational levels included in the present consideration will be as follows: $0\leqslant v_{B0}\leqslant 10$ for $B0_u^+$ state and $0\leqslant v_{A1}\leqslant 12$ for $A1_u$ state.

Energetic data such as the energy of the vibronic term T_v, the value of the effective rotational constant B_v, etc. for $B0_u^+$ state levels with $v_{B0}\geqslant 5$ have been obtained in Ref.

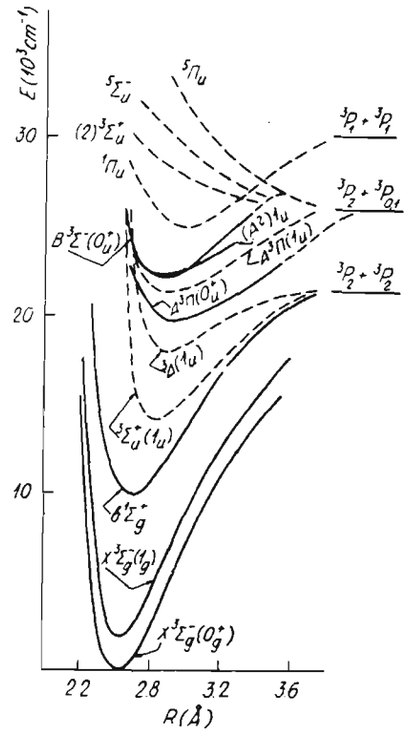

FIG. 1. Potential energy curves for the lowest electronic states of the Te molecule. Solid lines denote spectroscopically investigated states.

13 from high-resolution absorption and emission spectra o the $B0_u^+$–$X0_g^+$ transition. For $B0_u^+$ state levels with v_B <5, as well as for $A1_u$ state levels these characteristic: were taken from Refs. 12 and 14–17, where the laser induced fluorescence (LIF) spectra, excited by fixed Ar^- and Kr^+ laser lines, were analyzed. Data given for th tellurium isotope $^{128}Te_2$ were transformed and included i our analysis, too. For levels $v_{B0}=v_{A1}=0$, which had beer indicated in Refs. 12, 14, and 16, as strongly perturbed, w reestimated the values of the rovibronic terms T_{vJ} by ap plying highly precise molecular constants of the groun $X0_g^+$, $X1_g$ states and the known laser frequency causin the particular $v''J''\rightarrow v'J'$ transition.[12]

Lifetimes τ_{sp} of $B0_u^+$ and $A1_u$ state $v'J'$ levels hav been taken from Refs. 20 and 22–24. Values of τ_{sp} for $B0_u^+$ levels with $v_{B0}=0$, 8, and 9, as obtained in Ref. 25, ar close to those used here, but were not taken into accoun because they were measured without selection over rota tional levels. Lifetimes were measured directly by register ing LIF decay kinetics applying a time-correlated single photon-counting technique. Exciting Ar^+ or He–Cd laser light pulses had 80–120 ns widths and $\approx$40 ns front The shape of the exciting pulses was taken into accoun when decay signals were processed by least square metho The negligible effect of the exciting light intensity on values was confirmed. Errors caused by collisions at give concentrations were accounted for by means of small cor rections with given quenching cross sections.[22,27] Statistic errors were evaluated to be 5–10% for $\tau_{sp}\approx 100$ ns an 20–30% for $\tau_{sp}\approx 10$ ns.

Lande factors of $B0_u^+$ and $A1_u$ state $v'J'$ levels have een measured by us earlier using the Hanle effect ıethod.[19,20,22,26] Absolute values of the $g\tau$ product were btained from Lorentz shaped signals, and measured τ val-es were used to extract g factors. The signs of g were etermined from dispersion-shaped Hanle signals. Errors f the Lande factors reflected mainly lifetime uncertainties ıd were evaluated as 15–20%.

Relative intensities in LIF progressions, as well as in-ınsity ratios of the P, R, and Q components were also ɔnsidered. These data have been given in Refs. 18 and 21 ɔr $B0_u^+-X0_g^+$ transitions starting from levels $v_{B0}=0(J$ =107), $v_{B0}=2(J=197)$, and $v_{B0}=5(J=103)$, and in ef. 21 for $A1_u^-X1_g^-$ transitions from $v_{A1}=2(J=96)$ as ell as for $B0_u^+-X1_g$ transitions from $v_{B0}=0(J=107)$ nd $v_{B0}=5(J=103)$ levels. Intensity distribution for $0_u^+-X1_g$ transitions from $v_{B0}=1(J=243)$, $v_{B0}=3(J$ =251), and $v_{B0}=5(J=137)$ has been given in Ref. 12. nly the ratios of the P, R, and Q component intensities ave been taken from Ref. 12 because, as pointed out by ıe authors themselves, it was difficult to make a quanti-ıtive comparison of the intensities in different spectral ɛgions. On the other hand, in Refs. 18 and 21 special ıeans were used to remove various systematic errors by erforming a careful calibration of the spectral sensitivity f the registering system. Thus, an accuracy up to 3% for ɪrong lines and up to 20% for extremely weak lines was nsured. It ought to be mentioned that in Ref. 21 the ranching coefficients of $B0_u^+-X0_g^+$ and $B0_u^+-X1_g$ transi-ons from $v_{B0}=0(J=107)$ and $v_{B0}=5(J=103)$ were lso determined.

I. DEPERTURBATION MODEL

.. Energy properties

The electronic states of the Te_2 molecule are known to e characterized by large spin–orbit splitting.[12] It is there-ɔre quite natural to describe them using Hund case "c" asis set functions. Hence, the most reasonable choice of ıe unperturbed Hamiltonian seems to be $\mathscr{H}_0=\mathscr{H}_e+\mathscr{H}_v$ $-B(R)\mathbf{J}^2$, where $\mathscr{H}_e$ represents the electronic part in-luding not only Coulomb but also all types of relativistic ıteractions (spin–orbit, spin-other orbit, spin–spin), $\mathscr{H}_v$ enotes the vibrational part, and $B(R)=1/(2mR^2)$ is the entrifugal term, m being the reduced molecular mass.

Further, we suppose that the eigenvalues of $\mathscr{H}_0$ could e found from the radial Schrödinger equation

$$\frac{d^2|v_\Omega\rangle}{2md R^2}+[E_\Omega^0(R)+B(R)J(J+1)]\,|v_\Omega\rangle=E_{vJ}^0|v_\Omega\rangle, \tag{1}$$

ith a certain effective internuclear potential $E_\Omega^0(R)$ for ach electronic state (or, more precisely, for the state with definite Ω value).[28] The E_{vJ}^0 dependence on v and J can e represented in form of a Dunham expansion,[29] while the otential $E_\Omega^0(R)$ for a given E_{vJ}^0 can be found by solving n inverse spectroscopic problem using, for instance, the KR procedure.[30] In this assumption the perturbation op-rator has the form

$$\mathbf{V}_p=-2B(R)\mathbf{J}\mathbf{J}_a+B(R)\mathbf{J}_a^2, \tag{2}$$

where $\mathbf{J}_a=\mathbf{L}+\mathbf{S}$. Let us be reminded that the first term in Eq. (2) is responsible for the heterogeneous ($\Delta\Omega=\pm1$) interaction, while the second term describes the homogeneous ($\Delta\Omega=0$) interaction. Then, if the symmetrized basis

$$|\Psi_p\rangle=\sum_i c_i|J\Omega\rangle\,|v_i\rangle+\sum_j c_j|J\Omega^*\rangle\,|v_j^*\rangle \tag{3}$$

is used, the matrix elements of the Hamiltonian matrix describing electron-rotation interaction between the two electronic states with $\Omega=0$ and $\Omega^*=1$, take the form

$$H_{ii}=\sum_{kl}Y_{kl}^\Omega(v+1/2)^k[J(J+1)-2\Omega^2]^l, \tag{4}$$

$$H_{ij}=-P_{ij}[2J(J+1)]^{1/2}, \tag{5}$$

where Y_{kl}^Ω are Dunham coefficients, P_{ij} $=\langle v_i|B(R)\eta|v_j^*\rangle$, where $\eta=\langle\Omega|J_{a\pm}|\Omega^*\rangle$ is the electronic matrix element of electron-rotation interaction. We shall hereafter suppose that the matrix element η is independent on the internuclear distance. Besides, for the situation when the interacting levels are close to energetic resonance we shall often use the simplest two-level interaction scheme, leading to $P_{ij}\equiv P$ in Eq. (5). In this case, for $A1_u$ and $B0_u^+$ state mixing, the eigenfunction $|\Psi_p\rangle$ is equal to

$$|\Psi_p\rangle=c_{B0}|J\Omega=0\rangle\,|v_{B0}\rangle+c_{A1}|J\Omega^*=1\rangle\,|v_{A1}\rangle, \tag{6}$$

where c_{B0} and c_{A1} are the corresponding mixing coefficients. Since in the two-level scheme the Hamiltonian matrix has 2×2 dimension, the analytical solution is also available, in order to find the eigenvalues and eigenfunctions (to be more exactly, the mixing coefficients):[31]

$$E_{B0,A1}=\tfrac{1}{2}\{H_{BB}+H_{AA}\pm[(H_{BB}-H_{AA})^2+4H_{BA}^2]^{1/2}\}, \tag{7}$$

$$c_{A1}=\pm\left[\frac{H_{AB}}{2|H_{BA}|}\left(1\mp\frac{H_{BB}-H_{AA}}{[(H_{BB}-H_{AA})^2+4H_{BA}^2]}\right)\right]^{1/2}, \tag{8}$$

$$c_{B0}=(1-c_{A1}^2)^{1/2}.$$

In the case when the interacting levels are well apart from the energy resonance, the heterogeneous perturbation manifests itself in the variation $\delta B_{v_{B0}}$ of $B0_u^+$ state effective rotational constant B_v^{eff}

$$\delta B_{v_{B0}}=\sum_{v_{A1}}2\langle v_{B0}|B(R)\eta|v_{A1}\rangle^2/(E_{v_{B0}}^0-E_{v_{A1}}^0), \tag{9}$$

as well as in the Ω-doubling effect of the $A1_u$ state. The latter effect is characterized by the q factor

$$q_{v_{A1}}=-\sum_{v_{B0}}2\langle v_{A1}|B(R)\eta|v_{B0}\rangle^2/(E_{v_{B0}}^0-E_{v_{A1}}^0). \tag{10}$$

Note that the 1_u^- component of the $A1_u$ state remains un-

perturbed in the proposed model according to the selection rules for homonuclear molecules. Thus, to describe term values, at least one interaction parameter η must be known, along with the two sets of Dunham coefficients. The number of Dunham coefficients is dependent on v and J ranges used in the fitting procedure.

B. Magnetic properties

Neglecting the nuclear spin (being zero for even isotopes ^{130}Te and ^{128}Te) and the rotational g factor caused by rotation of the shielded nuclei (being of the order of 10^{-6} bohr magneton[32]), the Zeeman operator $\mathscr{H}_{mag}$ can be represented in the form:[33] $\mathscr{H}_{mag}=-\mu_B\mathscr{B}[g_l\mathbf{J}_{az}+(g_s-g_l)\mathbf{S}_z]$, where $g_l=1$ and $g_s=2.0023$ are the orbital and spin electronic g factors, respectively, and the space-fixed z axis is directed along the magnetic field $\mathscr{B}$. Then, using the symmetrized "c" basis set functions, see Eq. (3) and neglecting second order magnetic effects, the resulting general expressions for the electronic parts of the molecular g factor of Ω and Ω^* states are

$$G_z=[g_l\Omega+(g_s-g_l)\langle\Omega|\mathbf{S}_z|\Omega\rangle]\Omega, \tag{11}$$

$$G_\pm=g_l\langle\Omega|J_{a\pm}|\Omega^*\rangle+(g_s-g_l)\langle\Omega|\mathbf{S}_\pm|\Omega^*\rangle, \tag{12}$$

while the total g factor of a given rovibronic level, accounted for vibrational and rotational movement, is equal to[11,33]

$$g_{1^-}^{vJ}=-\langle v|G_z|v^*\rangle/J(J+1), \tag{13}$$

$$g_{0,1^+}^{vJ}=-2\frac{\Sigma_{ij}c_ic_j\langle v_i|G_\pm|v_j^*\rangle}{[2J(J+1)]^{1/2}}-\frac{\Sigma_jc_j^2\langle v_j|G_z|v_j^*\rangle}{J(J+1)}. \tag{14}$$

Note that Eq. (13) defines g factors of noninteracting 1_u^- component of the $A1_u$ state, while Eq. (14) allows to find g factors of the coupled $B0_u^+$ and $A1_u^+$ states. In further treatment we shall neglect the dependence of matrix elements G_z and $G_\pm$ on the internuclear distance. Besides, Eq. (14) can be simplified if the two-level model is employed, cf. Eqs. (6) and (8). Then Eq. (14) takes the form

$$g_{B0,A1^+}^{vJ}=\frac{-2G_\pm c_{B0}c_{A1}\langle v_{B0}|v_{A1}\rangle}{[2J(J+1)]^{1/2}}-\frac{c_{A1}^2G_z}{J(J+1)}. \tag{15}$$

If, by contrast, the interaction is weak (the levels are far from resonance), the approximate expressions for $B0_u^+$ and $A1_u^+$ state g factors can be written in the form

$$g_{B0}^{vJ}=2G_\pm\eta\sum_{v_{A1}}\frac{\langle v_{B0}|B(R)|v_{A1}^*\rangle\langle v_{B0}|v_{A1}^*\rangle}{E_{v_{B0}}^0-E_{v_{A1}}^0}, \tag{16}$$

$$g_{A1^+}^{vJ}=-2G_\pm\eta\sum_{v_{B0}}\frac{\langle v_{A1}|B(R)|v_{B0}^*\rangle\langle v_{A1}|v_{B0}^*\rangle}{E_{v_{B0}}^0-E_{v_{A1}}^0}-\frac{G_z}{J(J+1)}. \tag{17}$$

Hence, two additional adjustable parameters G_z and $G_\pm$ are needed to describe the $B0_u^+$ and $A1_u$ state g factors as compared to the energetic characteristics.

C. Radiative properties

To describe the lifetimes of $B0_u^+$ and $A1_u$ state levels as well as intensity distribution in LIF progressions of the parallel ($\|$) transition ($\Delta\Omega=0$, such as $B0_u^+-X0_g^+$, $A1_u-X1_g$) or of the perpendicular ($\perp$) transition ($\Delta\Omega=\pm1$, such as $B0_u^+-X1_g$), we shall, similarly to Eq. (3), account not only for the $B0_u^+\sim A1_u$ interaction, but for the $X0_g^+\sim X1_g$ interaction as well. Then it is possible to present the matrix elements of the rovibronic transition in the form

$$\begin{aligned}\langle n|\hat{\mathbf{d}}|m\rangle=&\sum_{v_{B0}}c_{B0}\sum_{v_{X0}}c_{X0}\mu_\|^{B0-X0}\alpha(J_{B0},J_{X0},\Delta\Omega=0)\\&+\sum_{v_{B0}}c_{B0}\sum_{v_{X1}}c_{X1}\mu_\perp^{B0-X1}\alpha(J_{B0},J_{X1},\Delta\Omega=1)\\&+\sum_{v_{A1}}c_{A1}\sum_{v_{X0}}c_{X0}\mu_\perp^{A1-X0}\alpha(J_{A1},J_{X0},\Delta\Omega=1)\\&+\sum_{v_{A1}}c_{A1}\sum_{v_{X1}}c_{X1}\mu_\|^{A1-X1}\alpha(J_{A1},J_{X1},\Delta\Omega=0),\end{aligned} \tag{18}$$

where

$$\mu^{n-m}=\langle v_n|R_e^{n-m}(R)|v_m\rangle\cong R_e^{n-m}(R_c^{n-m})\langle v_n|v_m\rangle$$

is the matrix element of an electronic vibrational transition in the molecule-fixed coordinate system; $R_e^{n-m}(R)$ is the matrix element of the electron transition dipole moment as dependent on internuclear distance; n stands for $B0_u^+$ or $A1_u$, and m for $X0_g$ or $X1_g$;

$$R_c^{n-m}=\langle v_n|R|v_m\rangle/\langle v_n|v_m\rangle\equiv R_{v_nv_m}^{n-m}$$

is the R centroid;[34] $\langle v_n|v_m\rangle$ is the overlap integral of FCF type; and α, the direction cosine matrix element.[1,2] Note that in the context of a heterogeneous perturbation model the $A1_u^-\sim X1_g^-$ transition is considered to be unperturbed.

1. Relative intensities

Using the explicit form of α, see Refs. 1 and 2, we obtain from Eq. (18) expressions for the intensities of R, P, and Q branches of a spontaneous $n\to m$ transition, namely,

$$I^P = N_J \nu_P^3 (J+1)\Bigg(\sum_{v_{B0}} c_{B0} \sum_{v_{X0}} c_{X0}\mu_{\parallel}^{B0-X0} + \sum_{v_{B0}} c_{B0} \sum_{v_{X1}} c_{X1}\mu_{\perp}^{B0-X1}[J/(J+1)]^{1/2}$$

$$+ \sum_{v_{A1}} c_{A1} \sum_{v_{X1}} c_{X1}\mu_{\parallel}^{A1-X1}[J(J+2)]^{1/2}/(J+1) - \sum_{v_{A1}} c_{A1} \sum_{v_{X0}} c_{X0}\mu_{\perp}^{A1-X0}[(J+2)/(J+1)]^{1/2}\Bigg)^2, \tag{19}$$

$$I^R = N_J \nu_R^3 J\Bigg(\sum_{v_{B0}} c_{B0} \sum_{v_{X0}} c_{X0}\mu_{\parallel}^{B0-X0} - \sum_{v_{B0}} c_{B0} \sum_{v_{X1}} c_{X1}\mu_{\perp}^{B0-X1}[(J+1)/J]^{1/2}$$

$$+ \sum_{v_{A1}} c_{A1} \sum_{v_{X1}} c_{X1}\mu_{\parallel}^{A1-X1}(J^2-1)^{1/2}/J + \sum_{v_{A1}} c_{A1} \sum_{v_{X0}} c_{X0}\mu_{\perp}^{A1-X0}[(J-1)/J]^{1/2}\Bigg)^2, \tag{20}$$

$$I^Q = N_J \nu_Q^3 (2J+1)\Bigg(\sum_{v_{B0}} c_{B0} \sum_{v_{X1}} c_{X1}\mu_{\perp}^{B0-X1} + \sum_{v_{A1}} c_{A1} \sum_{v_{X1}} c_{X1}\mu_{\parallel}^{A1-X1}[J(J+1)]^{-1/2} + \sum_{v_{A1}} c_{A1} \sum_{v_{X0}} c_{X0}\mu_{\perp}^{A1-X0}\Bigg)^2, \tag{21}$$

where ν is the transition frequency, $J \equiv J_n$, and the factor N_J is dependent only on the molecular concentration of the v_n, J_n level and on the normalization rule of rotational wave functions.

To simplify further treatment let us introduce new variables:

$$i^P = [I^P/N_J \nu_P^3 (J+1)]^{1/2},$$

$$i^R = (I^R/N_J \nu_R^3 J)^{1/2},$$

$$i^Q = [I^Q/N_J \nu_Q^3 (2J+1)]^{1/2}.$$

Then, assuming $J \gg 1$ (the error incurred by such an assumption that is less then 1% for the rovibronic levels under consideration), we get from Eqs. (19)–(21) the following expressions for i^P and i^R:

$$\frac{i^P - i^R}{2} = \sum_{v_{B0}} c_{B0} \sum_{v_{X1}} c_{X1}\mu_{\perp}^{B0-X1} - \sum_{v_{A1}} c_{A1} \sum_{v_{X0}} c_{X0}\mu_{\perp}^{A1-X0}, \tag{22}$$

$$\frac{i^P + i^R}{2} = \sum_{v_{B0}} c_{B0} \sum_{v_{X0}} c_{X0}\mu_{\parallel}^{B0-X0} + \sum_{v_{A1}} c_{A1} \sum_{v_{X1}} c_{X1}\mu_{\parallel}^{A1-X1}. \tag{23}$$

The $X0_g \sim X1_g$ interaction is sufficiently small as compared to $B0_u^+ \sim A1_u$ interaction leading to $c_{X0} \approx 1 \gg c_{X1} \approx 0$ for the transition to the $X0_g^+$ state and $c_{X1} \approx 1 \gg c_{X0}$ for the transition to the $X1_g$ state. Moreover, since $\mu_{\parallel}^{B0-X0} \sim \mu_{\parallel}^{A1-X1}$ as well as $\mu_{\perp}^{B0-X1} \sim \mu_{\perp}^{A1-X0}$, while $\mu_{\parallel}$ exceeds $\mu_{\perp}$ by more than an order of magnitude, Eqs. (22) and (23) can be further simplified. For this purpose it is convenient to introduce a dimensionless parameter χ which characterizes the manifestation of nonadiabacity in intensity distribution:

$$\chi_{\perp}^{PR} = \frac{\Sigma_{v_{A1}} c_{A1}\mu_{\parallel}^{A1-X1}}{\Sigma_{v_{B0}} c_{B0}\mu_{\perp}^{B0-X1}} \cong \frac{i_{\perp}^P + i_{\perp}^R}{i_{\perp}^P - i_{\perp}^R} \cong \frac{1+(I_{\perp}^P/I_{\perp}^R)^{1/2}}{1-(I_{\perp}^P/I_{\perp}^R)^{1/2}}, \tag{24}$$

$$\chi_{\parallel}^{PR} = \frac{\Sigma_{v_{A1}} c_{A1}\mu_{\perp}^{A1-X0}}{\Sigma_{v_{B0}} c_{B0}\mu_{\parallel}^{B0-X0}} \cong \frac{i_{\parallel}^P - i_{\parallel}^R}{i_{\parallel}^P + i_{\parallel}^R} \cong \frac{1-(I_{\parallel}^P/I_{\parallel}^R)^{1/2}}{1+(I_{\parallel}^P/I_{\parallel}^R)^{1/2}}, \tag{25}$$

$$\chi_{\perp}^{PQR} = \frac{\Sigma_{v_{A1}} c_{A1}\mu_{\parallel}^{A1-X1}}{\Sigma_{v_{B0}} c_{B0}\mu_{\perp}^{B0-X1}} \cong \frac{i_{\perp}^P + i_{\perp}^R}{2i_{\perp}^Q} \cong (I_{\perp}^P/2I_{\perp}^Q)^{1/2} + (I_{\perp}^R/2I_{\perp}^Q)^{1/2}. \tag{26}$$

Besides, if both parallel and perpendicular intensities starting from the same upper level are measured simultaneously, it is possible to arrive at the following relationships:

$$\frac{i_{\perp}^P - i_{\perp}^R}{i_{\parallel}^P + i_{\parallel}^R} \cong \frac{\mu_{\perp}^{B0-X1}}{\mu_{\parallel}^{B0-X0}}, \tag{27}$$

$$\frac{2i_{\perp}^Q}{i_{\parallel}^P + i_{\parallel}^R} \cong \frac{\mu_{\perp}^{B0-X1}}{\mu_{\parallel}^{B0-X0}}, \tag{28}$$

$$\frac{i_{\perp}^P + i_{\perp}^R}{i_{\parallel}^P + i_{\parallel}^R} \cong \frac{\Sigma_{v_{A1}} c_{A1}\mu_{\parallel}^{A1-X1}}{\Sigma_{v_{B0}} c_{B0}\mu_{\parallel}^{B0-X0}}. \tag{29}$$

It is quite clear from the aforementioned expressions that intensity distribution in the LIF spectrum depends not only on the extent of state mixing, but also on the relative probability of the parallel and perpendicular transitions. The perturbation impact is more pronounced for weak perpendicular transitions, thus giving the possibility of determining the ratio $\mu_{\perp}/\mu_{\parallel}$, if the mixing coefficients are known, and vice versa. At the same time, if state mixing is not that large, the parallel transitions can be considered as unperturbed one. Besides, as follows from the analysis of Eq. (28), the $I_{\perp}^Q(v_{X1})$ distribution of the $B0_u^- \sim X1_g$ tran-

sition can also be treated as an unperturbed. Hence, the intensity distribution in LIF progressions of such transitions follows the usual Franck–Condon distribution, thus allowing to determine the relative semiempirical dependence of the electronic transition strength on internuclear distance in a standard way, using, e.g., the R-centroid approximation.[9] This leads to the ratio

$$\frac{R_e^{n-m}(R_{v_n l}^{n-m})}{R_e^{n-m}(R_{v_n v_m}^{n-m})}=\left[\left(\frac{\langle v_n|v_m\rangle}{\langle v_n|l\rangle}\right)^2\left(\frac{\nu_{v_n v_m}^{n-m}}{\nu_{v_n l}^{n-m}}\right)^3\frac{I_{v_n l}^{n-m}}{I_{v_n v_m}^{n-m}}\right]^{1/2}, \quad (30)$$

where $l=v_m=0,1,2,...$, and $R_e^{n-m}(R_{v_n v_m}^{n-m})$ = const. for a given l-progression.

2. Lifetimes

As is known, the lifetime of a rovibronic level is equal to the inverted sum of the probabilities of spontaneous transitions to all lower lying levels (of course, if we neglect all radiationless processes). Then, in accordance with the aforementioned model [cf. Eq. (1)] and including for transitions not only to $X0_g^+$ and $X1_g$, but also to the $b\,^1\Sigma_g^+$ state (see Fig. 1), it is easy to obtain an approximate lifetime expression for the rovibronic level v_n, J_n of the $B0_u^+\sim A1_u$ complex, namely,

$$\tau_{v_n J_n}^{-1}\cong c_{B0}^2\Big(\sum_k(2-\delta_{0,\Omega_k})\nu_{B0-k}^3\mu_{B0-k}^2\alpha^2(J_n,J_k,\Omega_{B0}=0,\Omega_k)\Big)+c_{A1}^2\Big(\sum_l(2-\delta_{1,\Omega_l})\nu_{A1-l}^3\mu_{A1-l}^2\alpha^2\times(J_n,J_l,\Omega_A=1,\Omega_l)\Big), \quad (31)$$

where the indices k and l denote summation over rovibronic levels of the $X0_g^+$, $X1_g$, $b\,^1\Sigma_g$, and $X0_g^+$, $X1_g$ states, respectively. Obviously the number of the summands in the sums over k, l in Eq. (31) depends on how fast the corresponding FCF sums approach unity. The strong relative shift of the potential curves of the interacting states (cf. Fig. 1) leads to a long summation procedure, therefore we used the well approved expression[35,36]

$$\tau_{v_n J_n}^{-1}\cong c_{B0}^2\Big(\sum_k(2-\delta_{0,\Omega_k})\langle v_{B0}|[U^{B0-k}(R)]\times[R_e^{B0-k}(R)]^2|v_{B0}\rangle\Big)+c_{A1}^2\Big(\sum_l(2-\delta_{1,\Omega_l})\times\langle v_{A1}|[\Delta U^{A1-l}(R)]^3[R_e^{A1-l}(R)]^2|v_{A1}\rangle\Big), \quad (32)$$

where $\Delta U^{n-m}(R)=U^n(R)-U^m(R)$ is the difference potential between the electronic states.

It is quite clear that in accordance with the above assumptions concerning the relative strength of the parallel and perpendicular transitions, the lifetimes appear to be not very sensitive to the existence of perturbations. Indeed, as the perpendicular transitions are considerably weaker than the parallel ones, the first are giving a notably smaller contribution to the sums over k and l. Hence, the lifetime value is determined mainly by the parallel transition

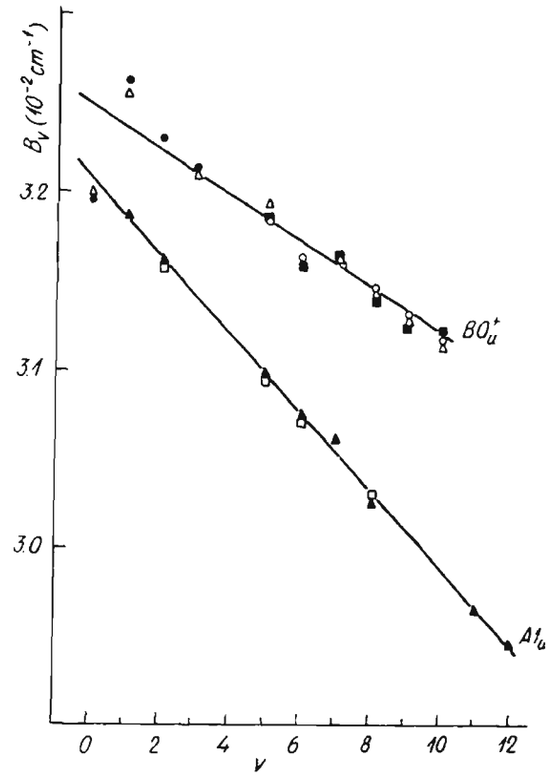

FIG. 2. Effective rotational constant B_v values obtained for $^{130}Te_2$ in different works. For the $B0_u^+$ state see Refs. 14, 12 and 13 (in Ref. 13 for $^{128}Te_2$). For the $A1_u$ state see Refs. 12 and 16. Straight lines represent the analytic approximations of the v dependencies of deperturbed B_v values according to Table I.

strengths. Besides, as the frequencies and strengths of the both parallel transitions $B0_u^+$–$X0_g^+$ and $A1_u$–$X1_g$ are close to each other, we get an estimate $\tau^{-1}\cong(c_{B0}^2+c_{A1}^2)\nu^3\mu_\parallel^2=\nu^3\mu_\parallel^2$, that is, the τ values are independent of the degree of $B0_u^+\sim A1_u$ mixing.

We thus see that the four electron dipole moment transition functions, viz., $R_{e\perp}^{B0-X1}(R)$, $R_{e\parallel}^{B0-X0}(R)$, $R_{e\perp}^{A1-X0}(R)$, and $R_{e\parallel}^{A1-X1}(R)$ are needed to describe $B0_u^+$ and $A1_u$ state lifetimes, together with intensity distributions in $B0_u^+$–$X0_g^+$, $A1_u$–$X1_g$, $B0_u^+$–$X1_g$, and $A1_u$–$X0_g^+$ transitions.

IV. EXPERIMENTAL DATA PROCESSING

Owing to the local nature of the $B0_u^+\sim A1_u$ state coupling in the Te_2 molecule, it seems reasonable to obtain the first approximation of the deperturbed characteristics [such as Dunham coefficients, G_v values, transition dipole moment functions $R_{e\parallel}(R)$ and $R_{e\perp}(R)$] from the levels which are weakly perturbed or, better, unperturbed as are, e.g., $A1_u^-$ state levels.

A. Term values

The first approximation for the deperturbed Dunham constants of $B0_u^+$ and $A1_u$ states has been determined by linear least squares fit (LSF) of the experimental values of their rotational constants B_v and vibronic terms T_v, ex-

TABLE I. Deperturbed molecular constants (in cm^{-1}) for $B0_u^+$ and $A1_u$ state of $^{130}Te_2$.

	$B0_u^+$ state			$A1_u$ state		
	Present work	Ref. 19	Ref. 13	Present work	Ref. 19	Ref. 17
T_e	22 202.83	22 203.5	22 207.4	22 216.72	22 209.2	22 221.9
ω_e	163.70	163.5	162.3	152.20	155.9	150.5
$\omega_e x_e$	0.587	0.563	0.45	2.038	2.57	1.98
$10^3\omega_e y_e$	−6.86	−42.0	−11.09	30.64	53.0	
$10^3 B_e$	32.55	32.58	32.53	32.18	32.16	32.20
$10^4\alpha_e$	1.28	1.35	1.25	2.21	2.17	2.75

cluding data for strongly perturbed levels $v_{B0}=0$ and 1. Figure 2 demonstrates a substantial dispersion of the B_v values for the majority of vibrational levels of $A1_u$ and $B0_u^+$ states analyzed in different experiments. This points towards the presence of weak local heterogeneous perturbations of the studied levels, since considerably different J ranges were used in the corresponding rotational analysis. Besides, the rotational analysis of data of LIF involves difficulties due to limited ranges and high values of J. This, in turn, requires inclusion of strongly correlated centrifugal distortion constants D_v and H_v.

Then, for deperturbation analysis of the strongly perturbed rovibronic level $v_{B0}=v_{A1}=0$, we used the two-level approximation described in Sec. III A, cf. Eq. (6). We estimated the trial values for $B_{v=0}$ and $T_{v=0}$ from the previous linear fits (that is, without accounting for the level $v_{B0}=0$ and 1), while for P is from the "pure precession" hypothesis.[8] The centrifugal distortion constants $D_{v=0}$ and $H_{v=0}$ were evaluated according to the perturbed Morse-oscillator model[37] using the estimated trial values of Y_{01} and Y_{11}. The deperturbed $T_{v=0}$ and $B_{v=0}$ values for both states were obtained by the weighted nonlinear LSF (Ref. 38) of the experimental energies $E^{ex}_{B0,A1}$ using Eq. (7). These values were then approximated by Dunham series for $l=0$ [see Eq. (4)], together with analogous data for the other vibrational levels. The resulting molecular constants for $B0_u^+$ and $A1_u$ states are presented in Table I. Visual demonstration of v, J ranges of energetic resonances between deperturbed $B0_u^+$ and $A1_u$ state levels are presented in Fig. 3. The data from Table I were used in order to construct[39] the RKR potentials for both electronic states (cf. Tables II and III) and to solve the radial Schrödinger equation [see Eq. (1)] by the renormalized Numerov method.[40–42] Furthermore, the Franck–Condon type overlap integrals between vibrational wave functions of corresponding levels of $B0_u^+$ and $A1_u$ states were obtained using the Simpson rule. The mixing coefficients c^{ex}_{B0} and c^{ex}_{A1} were determined (see Table IV) by means of a deperturbation procedure [cf. Eq. (8)] of the terms with $v_{B0}=0$, $J=107$ and 179, for which radiative and magnetic data are also available. In the same way the matrix element P of intramolecular electron-vibration interaction [see Eq. (5)] was evaluated as $P^{ex}=0.0448\ cm^{-1}$. It is of interest to compare this value with an analogous parameter $H_{12}=0.035\,66\ cm^{-1}$ which has been obtained[12] from the deperturbation analysis of the levels $v_{A1}=12$ and $v_{B0}=10$. Note that H_{12} must differ from P by the factor of $\sqrt{2}$ since the unsymmetrized basis was used in Ref. 12. Taking this into account and calculating the integrals $\langle v_{B0}|B(R)|v_{A1}\rangle$ we get the matrix element of "pure" electronic interaction, namely $\eta^{el}=P^{ex}/\langle v_{B0}|B(R)|v_{A1}\rangle$, see Table V.

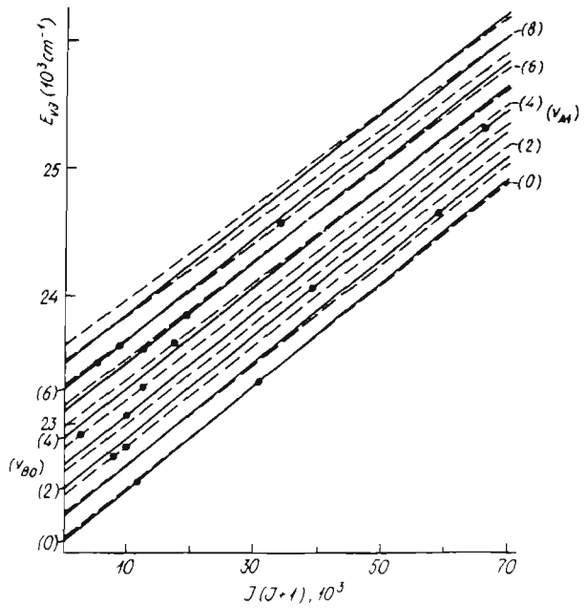

FIG. 3. Deperturbed term values of $B0_u^+$ (solid lines) and $A1_u$ (dashed lines) states of $^{130}Te_2$ as dependent on vibrational (v) and rotational (J) quantum numbers. The circles denote rovibronic levels for which radiative and/or magnetic data are available.

TABLE II. Rydberg–Klein–Rees (RKR) potential for the $B0_u^+$ state.

v	E_v (cm^{-1})	R_{min} (Å)	R_{max} (Å)
0	81.71	2.769 75	2.882 54
1	244.21	2.733 01	2.928 98
2	405.48	2.708 97	2.962 78
3	565.47	2.690 13	2.991 44
4	724.14	2.674 30	3.017 14
5	881.45	2.660 50	3.040 88
6	1037.36	2.648 17	3.063 22
7	1191.83	2.636 97	3.084 50
8	1344.81	2.626 64	3.104 97
9	1496.27	2.617 04	3.124 79
10	1646.16	2.608 04	3.144 10

TABLE III. Rydberg–Klein–Rees (RKR) potential for the $A1_u$ state.

v	E_v (cm^{-1})	R_{min} (Å)	R_{max} (Å)
0	75.42	2.785 13	2.902 44
1	223.64	2.748 79	2.954 38
2	368.07	2.725 33	2.993 66
3	508.88	2.707 08	3.027 94
4	646.25	2.691 83	3.059 43
5	780.38	2.678 60	3.089 09
6	911.44	2.666 86	3.117 46
7	1039.61	2.656 28	3.144 87
8	1165.09	2.646 66	3.171 51
9	1288.06	2.637 84	3.197 53
10	1408.69	2.629 72	3.223 02
11	1527.18	2.622 24	3.248 03
12	1643.71	2.615 34	3.272 62

B. *g* factors

We shall start *g* factor data processing with the four levels belonging to the $A1_u^-$ component (see Table VI), which can be considered as unperturbed in the frame of our model. Using the approximation given by Eq. (13) and the weighted LSF procedure, we obtain $G_z^{ex} = 1.86(9)$.

We shall begin the $B0_u^+$ state *g* factor data analysis with the two $v_{B0}=0$ levels, with $J=107$ and $J=179$, possessing *g* values for more than an order of magnitude larger than the other levels, see Table VI. The two-level model was applied in this case, cf. Eq. (15). We calculated the correspondent integrals $\langle v_{B0}|v_{A1}\rangle$, thus obtaining the electronic parameter $G_\pm^{ex}$ given in Table IV. In doing so we used the experimental mixing coefficient values c_{B0}^{ex} and c_{A1}^{ex} obtained in Sec. IV A, cf. Table IV. It is easy to see from the comparison between $G_\pm^{ex}$ and η^{cn} values, cf. Tables IV and V, that, as $G_\pm - \eta = 1.5(4)$, we get $G_\pm \cong 2\eta$.

Other $B0_u^+$ state *g* factors were treated by means of the nonresonant approach, cf. Eq. (16). In the process of calculating corresponding integrals $\langle v_{B0}|B(R)|v_{A1}\rangle$ and $\langle v_{B0}|v_{A1}\rangle$ and of energy differences between the unperturbed levels $E^0_{v_{B0}}$ and $E^0_{v_{A1}}$, we found the product $G_\pm\eta$ for each level. Assuming $G_\pm = 2\eta$, we get η^{mag} values presented in Table VI. The average value $\eta^{mag}_{av}=1.37$ is close enough to the η^{cn} values obtained from energy measurements, cf. Table V.

In order to demonstrate the possibility of extrapolation of the electronic parameters obtained, namely G_z, $G_\pm$, and η^{mag}_{av}, we calculated by means of Eq. (17) the experimentally studied *g* factors not only for $B0_u^+$ and $A1_u^-$, but for the $A1_u^+$ state as well. Since the levels of the $A1_u^+$ component are mixed with $B0_u^+$ state levels, the $A1_u^+$ state *g* factor values are determined not only and not so much by the own paramagnetism, as mainly by the interaction with the $B0_u^+$ state, up to changing sign, as in the case of $v_{A1}=5(J=131)$. The results of *g* factor calculations for all investigated $B0_u^+$ and $A1_u$ state levels are presented in Table VI (see column a), demonstrating good agreement with the experimentally measured quantities. The exception of the $v_{A1}=8(J=181)$ level is probably connected with uncertainties in lifetime measurements due to relatively short τ values ($\tau \cong 14$ ns). Finally, we found it useful to exploit the calculated *g* factors in order to evaluate lifetime values from the $g\tau$ products measured, see the column b in Table VI.

TABLE IV. Mixing coefficients c_{A1}^{ex}, c_{B0}^{ex} obtained from term values using Eq. (8), as well as magnetic parameters of electronic interaction $G_\pm$. The experimental values $G_\pm^{ex}$ are obtained using Eq. (15), while $G_\pm^{est}$ are estimated according to Eq. (38).

v_n J_n	C_{B0}^{ex}	C_{A1}^{ex}	$G_\pm^{ex}$	$G_\pm^{est}$
0 107	0.776	0.603	3.0(4)	2.65
0 179	0.601	0.799	2.9(4)	

TABLE V. Matrix element values of vibrational interaction ($\langle v_{B0}|B(R)|v_{A1}\rangle$), electron-vibration interaction (P^{ex}) and electronic interaction (η^{cn}).

v_{B0}	v_{A1}	$\langle v_{B0}\|B(R)\|v_{A1}\rangle$ (cm^{-1})	P^{ex} (cm^{-1})	η^{cn}
0	0	0.0312	0.0448(25)	1.44(8)
10	12	0.0174	0.0252(1)	1.45(2)

C. Intensities and lifetimes

1. Unperturbed progressions

We shall begin the data processing of radiative characteristics with obtaining relative electronic transition dipole moments $R_e(R_c)$, as dependent on internuclear distance, assuming that the combining levels are unperturbed and using the *R*-centroid approximation.[43] For this purpose we shall employ the results[18,21] on intensity distribution over *R* and *P* branches of v_m-progressions in "strong" parallel $B0_u^+$–$X0_g^+$ and $A1_u^-$–$X1_g^-$ LIF transitions, as well as on unperturbed *Q* branches in a perpendicular $B0_u^+$–$X1_g$ transition, cf. Eq. (28). We exploited progressions starting from $v_{A1}=2(J=96)$ for a $A1_u^-$–$X1_g^-$ system and from $v_{B0}=0(J=107)$, $v_{B0}=2(J=197)$, $v_{B0}=5(J=103)$ for a $B0_u^+$–$X0_g^+$ system. Data processing was performed according to Eq. (30). Since we used here a new set of $B0_u^+$ and $A1_u$ state molecular constants, as against Refs. 17 and 19, the $R_e(R_c)$ dependencies were calculated (as compared to that in Ref. 21) for some progressions studied in the present work. Let us mention that the lower state ($X0_g^+$ and $X1_g$) vibrational wave functions involved in FCF and R_e calculations were found from numeric solution of Eq. (1) with RKR potentials constructed by means of molecular constants from Ref. 12.

The dependencies obtained for $B0_u^+$–$X0_g^+$, $A1_u$–$X1_g$, and $B0_u^+$–$X1_g$ systems were normalized with the experimental lifetimes, see Eq. (32) and Table VI. For $A1_u$–$X1_g$ system the lifetime of $v_{A1}=2(J=96)$ level was used, while that of $v_{B0}=5(J=103)$ was used for the $B0_u^+$–$X0_g^+$ system. These lifetimes were supposed to be 'purely' spontaneous. Note that the normalization of a $B0_u^+$–$X0_g^+$ transition was carried out accounting for $B0_u^+$ and $A1_u$ state mixing, as well as for experimentally measured[21] branching coefficients of radiation transitions to $b^1\Sigma_g^+$ and $X1_g$ states.

TABLE VI. g factors (g), electronic interaction matrix elements (η^{mag}), and experimental ($g\tau$) values and lifetimes (τ).

State	v_n	J_n	g (10^{-4}) (bohr mag.) ex	g (10^{-4}) (bohr mag.) a	$\eta^{mag}_{v_n J_n}$	$g\tau$ (10^{-10}) (s^{-1})	τ (ns) ex	τ (ns) b	τ (ns) c
$B0_u^+$	0	107	−200(25)	−183	1.50(20)	12.8	64(5)	70	71
	0	179	−115(5)	−109	1.45(20)	8.6	75(4)	79	82
	1	243	+36(4)	+37	1.36(15)	2.1	59(5)	57	58
	2	197	+16(3)	+21	1.20(22)	1.2	75(12)	57	55
	3	99	+15(2)	+16	1.31(17)	1.0	68(5)	62	56
	3	251	−30(3)	−25	1.50(15)	1.6	54(5)	65	59
	5	103	−23(3)	−25	1.30(17)	1.3	57(3)	52	56
	5	137	−36(4)	−40	1.30(14)	1.6	45(6)	38	57
	7	95	+30(4)	+29	1.42(19)	1.7	55(5)	58	58
$A1_u^-$	2	86	−2.7(2)	−2.5		0.29	107(7)	115	109
	2	96	−2.0(2)	−2.0		0.23	117(11)	117	110
	4	52	−6.4(5)	−6.7		0.31	49(4)	46	112
	8	70	−3.3(7)	−3.7		0.033	10(2)	9	121
$A1_u^+$	4	111	−3.8(3)	−4.9		0.25	66(5)	51	115
	5	131	+15.0(20)	+11.2		0.68	45(6)	60	120
	8	181	−2.7(4)	−5.6		0.038	14(2)	7	133

[a]Estimated from η^{mag}_{av} and G^{ex}_{τ} by Eqs. (15)–(17).
[b]Calculated using experimental $g\tau$ and estimated g values.
[c]Estimated from radiative measurements by Eq. (32).

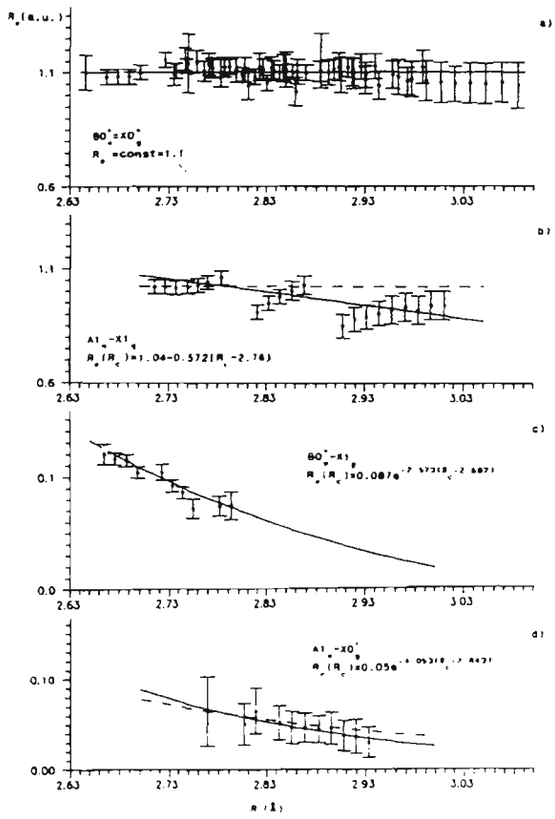

FIG. 4. Experimental values of electronic transition matrix element (R_e) as dependent on R centroid (R_c). (a) For $B0_u^+$–$X0_g^+$; (b) for $A1_u$–$X1_g$; (c) for $B0_u^+$–$X1_g$; (d) for $A1_u$–$X0_g^+$ transition. Solid lines denote the approximating functions presented. Dashed lines are calculated according to (a) Eq. (40) and (d) Eq. (41).

Resulting normalized $R_e(R_c)$ values are given in Figs. 4(a)–4(c), respectively, along with their approximations by smooth functions. As the dependence $R_{e\perp}^{B0-X1}(R_c)$ falls off steeply, we used the exponential approximation to provide monotonous approach of $R_e(R_c)$ to zero values.[44] The dependencies obtained are further used to calculate the mixing coefficients c_{A1}, c_{B0}, and thus to get η^{rad}, cf. Table VII.

2. Perturbed progressions

Let us now pass to the $R_e(R_c)$ treatment with regard to perturbations. First, the analysis of Eq. (25), with accounting for Eq. (18), leads to a somewhat surprising conclusion: when the mixing coefficients c_{A1}, c_{B0} are known, one can get the dependence $R_{e\perp}^{A1-X0}(R_c)$ of a perpendicular $A1_u$–$X0_g^+$ transition using the intensity ratio of P and R branches of a parallel $B0_u^+$–$X0_g^+$ transition. It is obvious, however, that this opportunity can be realized only for the levels possessing strong $A1_u \sim B0_u^+$ interaction, because otherwise the difference $i_{\parallel}^P - i_{\parallel}^R$ approaches zero, thus making it impossible to get information from Eq. (25). Fortunately, the level $v_{B0}=0(J=107)$ appeared suitable for this procedure. Therefore, using experimental data[18] on I_P/I_R and mixing coefficients c_{B0}^{ex}, c_{A1}^{ex} obtained from the energetic measurements (see Table IV and Sec. IV A), we determined the dependence $R_{e\perp}^{A1-X0}(R_c)$, see Fig. 4(d). The values obtained were approximated by an exponential function similarly to the case of $R_{e\perp}^{B0-X1}(R_c)$. It is interesting that both the absolute values and the run of the curves obtained for $A1_u$–$X0_g^+$ and $B0_u^+$–$X1_g$ transitions are similar to each other.

Next, we shall show that it is possible to get information about the $R_{e\perp}^{B0-X1}(R_c)$ dependence in a different way, employing the doublet component intensity difference of strongly perturbed P and R branches which belong to the

TABLE VII. Experimentally obtained (χ_1^{ex}) and calculated (χ_1^{cal}) nonadiabacity parameter χ values for v_m progression of the $B0_u^+-X1_g$ transition with fixed v_n, J_n. The electronic interaction matrix elements $\eta^{rad}_{v_n,J_n}$ as obtained from χ_1^{ex} are also represented.

$B0_u^+$	$X1_g$	χ_1^{ex}		χ_1^{cal}	
v_n, J_n	v_m	χ_1^{PR}	χ_1^{PRQ}	$\chi(\eta_{av}^{rad})$	Eq. (34)
0 107	4	−7.1		−6.3	−7.5
	5	−8.0		−6.8	−8.2
	6	−7.7		−7.4	−8.9
	7	−7.8		−8.0	−9.6
	8	−8.8		−8.7	−10.5
	9	−9.9		−9.4	−11.3
	10	−10.3		−10.4	−12.5
	11	−11.1		−11.4	−13.7
	12	−12.9		−12.4	−14.9
	13	−12.9		−13.6	−16.4
	14	−14.8		−15.0	−18.0
	15	−15.6		−16.6	−19.9
	16	−16.2		−18.3	−22.0
	17	−18.0		−20.3	−24.4
	18	−22.0		−22.7	−27.3
	19	−25.2		−25.3	−30.4
	20	−25.3		−28.5	−34.3
	21	−35.2		−32.3	−38.7
	$\eta^{rad}_{v_n,J_n}=1.45(5)$				
1 243	9	2.6	2.3	4.4	3.7
	10	3.4	3.1	5.3	4.5
	11	5.3	4.6	6.7	5.6
	18	3.2	3.4	4.6	3.9
	19	4.9	4.5	5.9	5.0
	$\eta^{rad}_{v_n,J_n}=1.23(25)$				
3 251	11	−4.2	−4.5	−4.4	−4.0
	12	−4.9	−6.0	−5.5	−5.0
	16	−4.7	−4.8	−4.5	−4.1
	17	−5.7	−5.7	−5.7	−5.2
	18	−6.5	−5.9	−6.6	−6.0
	$\eta^{rad}_{v_n,J_n}=1.40(11)$				
5 103	2	−2.0	−1.5	−1.4	−1.0
	3	−1.8	−1.6	−1.5	−1.1
	4	−2.0	−1.8	−1.6	−1.2
	5	−2.8	−2.1	−2.1	−1.6
	8	−1.7	−1.5	−1.4	−1.4
	9	−2.2	−1.9	−2.0	−1.5
	10	−3.5	−3.3	−3.4	−2.5
	13	−2.1	−1.9	−2.0	−1.5
	14	−3.8		−3.1	−2.3
	$\eta^{rad}_{v_n,J_n}=1.58(21)$				
5 137	19	−8.1	−6.5	−8.7	−7.0
	21	−2.9	−3.2	−2.6	−2.1
	22	−3.8	−4.4	−4.2	−3.4
	23	−4.6	−5.1	−5.3	−4.3
	$\eta^{rad}_{v_n,J_n}=1.39(15)$				

same vibronic transition starting from $v_{B0}=5(J=103)$ and $v_{B0}=0(J=107)$. We determined, according to Eq. (27), the ratio $R_{e\|}^{B0-X0}(R_c)/R_{e\perp}^{B0-X1}(R_c)$ as dependent on R_c of a $B0_u^+-X1_g$ transition, cf. Fig. 5(a). For comparison, the analogous dependence obtained from unperturbed functions [cf. Figs. 4(a) and 4(c)] is presented in the same Fig. 5(a) (solid line). As can be seen, the agreement is sufficiently good. Note that the values of

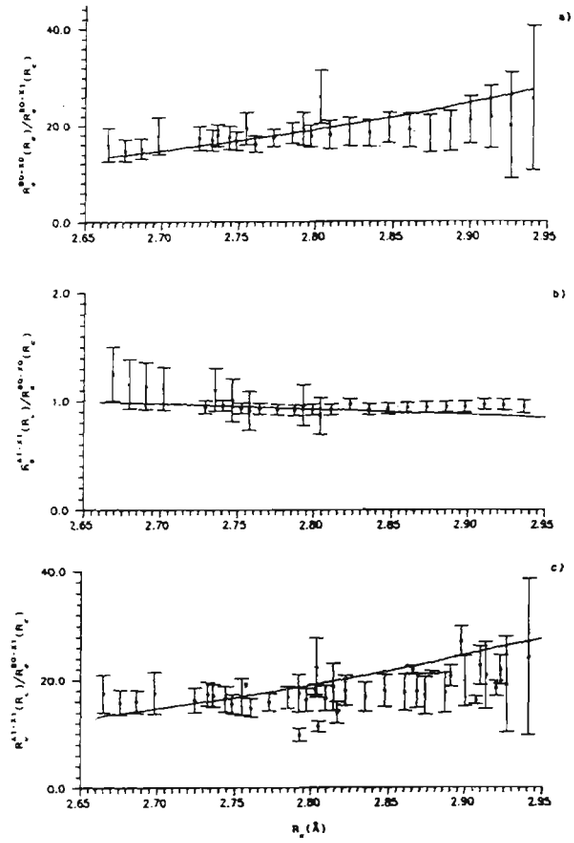

FIG. 5. Experimental ratios of electronic transition matrix elements obtained from intensity ratios of P and R branches. (a) For $(B0_u^+-X0_g^+)/(B0_u^+-X1_g)$; (b) for $(A1_u-X1_g)/(B0_u^+-X0_g^+)$; (c) for $(A1_u-X1_g)/(B0_u^+-X1_g)$ as dependent on R centroid (R_c) of a $B0_u^+-X1_g$, $A1_u-X1_g$ and $B0_u^+-X1_g$ transition, respectively. Solid lines denote the analogous dependencies obtained from unperturbed functions presented in Fig. 4.

$B0_u^+\sim A1_u$ mixing coefficients c_{A1} and c_{B0} are not needed in getting $R_{e\perp}^{B0-X1}(R_c)$.

It must be stressed that the absolute values of parallel and perpendicular transitions considered above correspond perfectly to the assumption made in Sec. III A, namely that $\mu_{\|}^{B0-X0}\cong\mu_{\|}^{A1-X1}\gg\mu_{\perp}^{B0-X1}\cong\mu_{\perp}^{A1-X0}$. As can be seen from Eqs. (24), (26), and (29), the measured intensities of P and R branches of the $B0_u^+-X1_g$ transition can be used: (i) in order to get the ratio of mixing coefficients c_{A1}/c_{B0} or (ii) in order to get the ratios $R_{e\|}^{A1-X1}(R_c)/R_{e\perp}^{B0-X1}(R_c)$ and $R_{e\|}^{A1-X1}(R_c)/R_{e\|}^{B0-X0}(R_c)$.

Let us first discuss the second possibility (ii). By means of the quantity η_{av}^{en} (see Table VIII), we computed

TABLE VIII. Averaged over v_n and J_n electronic interaction matrix elements η obtained from energetic (η_{av}^{en}), magnetic (η_{av}^{mag}), and radiative (η_{av}^{rad}) measurements, as well as η^{ext} values calculated according to Eq. (37).

η_{av}^{en}	η_{av}^{mag}	η_{av}^{rad}	η^{ext}
1.44(8)	1.37(15)	1.42(13)	1.32

the mixing coefficients between corresponding A and B state levels in a two-level approach, cf. Eq. (8). Then we calculated the overlap integrals $\langle v_{B0}|v_{X0}\rangle$, $\langle v_{B0}|v_{X1}\rangle$, and $\langle v_{A1}|v_{X1}\rangle$. Using the known intensities of P and R branches in $B0_u^+-X1_g$ and $B0_u^+-X0_g^+$ transitions starting from $v_{B0}=5(J=103)$ and $v_{B0}=0(J=107)$, we calculated the ratio $R_{e\|}^{A1-X1}(R_c)/R_{e\|}^{B0-X0}(R_c)$ according to Refs. 18 and 36, see Fig. 5(b). The results are in good conformance with a smooth dependence [cf. solid line in Fig. 5(b)], calculated from $R_{e\|}^{A1-X1}(R_c)$ and $R_{e\|}^{B0-X0}(R_c)$ obtained earlier [see Figs. 4(a) and 4(b)]. Let us now turn to the intensity relations of P, R, and Q lines belonging to the same vibronic transition. Basing on Eqs. (24) and (26), we processed these data in $B0_u^+-X1_g$ LIF progressions from $v_{B0}=0(J=107)$, $v_{B0}=1(J=243)$, $v_{B0}=3(J=251)$, $v_{B0}=5(J=103)$, and $v_{B0}=5(J=137)$, thus obtaining $R_{e\|}^{A1-X1}(R_c)/R_{e\perp}^{B0-X1}(R_c)$ as dependent on R-centroid values of the $B0_u^+-X1_g$ transition, cf. Fig. 5(c). The points in Fig. 5(c) are in good agreement with the solid line, which shows the analogous function $R_{e\|}^{A1-X1}(R_c)/R_{e\perp}^{B0-X1}(R_c)$, as calculated from the unperturbed progressions (see solid lines in Figs. 4(b) and 4(c). It is significant that the ratio $R_{e\|}^{A1-X1}(R_c)/R_{e\perp}^{B0-X1}(R_c)$ as district from $R_{e\|}^{A1-X1}(R_c)/R_{e\|}^{B0-X0}(R_c)$ can be determined without simultaneous measuring the $B0_u^+-X0_g^+$ transition intensities as follows from the comparison of Eqs. (24) and (29). Besides, as intensity relations between $I_\perp^P$, $I_\perp^R$, and $I_\perp^Q$ are analyzed independently for different v_m-progression terms, it is almost unnecessary to account for spectral sensitivity corrections of the detector.

Evidently, the above presented matter confirms that the chosen model is self-consistent in describing the radiative characteristics (lifetimes and intensity distributions), both of parallel and perpendicular transitions.

Now let us demonstrate the feasibility of the first approach (i). As follows from Eqs. (24) and (26), in order to obtain the mixing coefficient ratio c_{A1}/c_{B0} it is necessary to know $\mu_\|/\mu_\perp$ and $\chi_\perp$. The latter was taken from the experimental data of $B0_u^+-X1_g$ intensities presented in Refs. 12 and 21 (cf. $\chi_\perp^{ex}$ in Table VII), while $\mu_\|/\mu_\perp$ were determined according to Eq. (18) using the dependencies $R_{e\|}^{A1-X1}(R_c)$ and $R_{e\perp}^{B0-X1}(R_c)$ obtained from the unperturbed transitions (cf. Figs. 4(b) and 4(c), solid lines). c_{A1}/c_{B0} values thus obtained for the fixed v_m were then substituted into Eqs. (8) and (5) in order to get $\eta_{v_nJ_n}^{rad}(v_m)$. The v_m-averaged $\eta_{v_nJ_n}^{rad}$ values are given in Table VII for v_n, J_n levels studied here. After averaging them over v_n, J_n, we get η_{av}^{rad} (see Table VIII), further involved in an inverted procedure, namely in the calculation of smoothed (averaged) values of the nonadiabacity parameter $\chi_\perp^{cal}$, cf. Table VII. Let us point out that η_{av}^{rad} values are in good agreement with the corresponding values of η_{av}^{en} and η_{av}^{mag}, as obtained from energetic and magnetic measurements, cf. Table VIII.

We would like to pay attention to the manifestation of the heterogeneous interaction in the intensities of a weak perpendicular transition. As can be seen from Eqs. (24)–(26), the maximum intensity changes in P or R branches are expected for the transitions having χ value close to unity, or, in other words, when $c_{A1}\mu_\|^{A1-X1}/c_{B0}\mu_\perp^{B0-X1}\cong 1$. Hence, if $\mu_\| \gg \mu_\perp$, the smaller the interaction (or, otherwise, the smaller c_{A1}/c_{B0}), the more I^P/I^R differs from unity. Nevertheless this, at first glance, paradoxical conclusion agrees quite favorably with the experimental results. Thus, while for the level of strongest interaction, namely $v_{B0}=0(J=107)$, the relative difference between I^P and I^R is about 40%, for the level possessing the smallest perturbation, namely $v_{B0}=5(J=103)$, the intensities differ already by a factor of 10, see Table VII and also Ref. 21. Hence, the magnitude

$$K=R_{e\|}^{A1-X1}(R_c)\langle v_{A1}|v_{X1}\rangle/[R_{e\perp}^{B0-X1}(R_c)\times\langle v_{B0}|v_{X1}\rangle]$$

can be considered as a special kind of interaction amplification factor, K therewith exhibiting sharp dependence not only on v_{A1}, but on v_{X1} as well. Thus we are able to vary K by choosing the convenient band in LIF spectrum, in order to meet the condition of closeness χ to unity. This distinction of relative intensities from other characteristics seems to us to be of principal importance.

Summing up, basing ourselves on dipole moment functions and mixing coefficients obtained here, we found it useful to calculate the lifetimes of the levels considered in present work (see column c in Table VI) by means of Eq. (32). As expected, the lifetimes appeared less sensitive to the extent of $A\sim B$ mixing. Thus, even for strongly interacting levels $v_{A1}=v_{B0}=0$ the $B0_u^+$ state lifetimes are increasing only by 15–20% as compared with the unperturbed levels. Let us also mention that while the experimental $B0_u^+$ state lifetimes are in more or less satisfactory agreement with the calculated values, the measured lifetimes τ_{vJ} for both 1_u^+ and 1_u^- components of the $A1_u$ state are diminishing with the growth of v, as opposed to the calculated values (cf. column c in Table VI). This indicates the weak predissociation of the $A1_u$ state levels probably caused by weak homogeneous ($\Delta\Omega=0$) interaction with an unknown unbound 1_u state. It must be mentioned that the analogous predissociation was observed[45] for the $B1_u$ component of the $B\,^3\Sigma_u^-$ state of Se_2, where the levels with $v_{B1}>6$ were not observed at all, owing to strong homogeneous predissociation, in contrast to the $B0_u^+$ component.

V. RELATION BETWEEN ENERGETIC, RADIATIVE, AND MAGNETIC CHARACTERISTICS

Let us examine to what extent the parameters of electronic interaction obtained in Sec. IV from energetic, magnetic and radiative measurements are mutually compatible. For this purpose it is useful to follow the connection between the mentioned characteristics. In our recent paper[5] the approximate relation has been derived between the g factor and the Λ-doubling constant values, applying Hund's case "a" basis for singlet states. The analogous

relation between the g factors and the Ω-doubling constants (q) for the $A1_u$ state can be obtained by comparing Eqs. (10) and (17), namely,

$$g^{vJ}_{A1_u^+} - g^{vJ}_{A1_u^-} \cong \frac{q^v_{A1_u} G_\pm}{B^v_{A1}\eta} \cong \frac{(B^v_{A1_u^+} - B^v_{A1_u^-})2G_\pm}{(B^v_{A1_u^+} + B^v_{A1_u^-})\eta}. \quad (33)$$

Therefore, knowing the experimental g factor values of the $Te_2(A1_u^+)$ component and using expression (13) for the g factors of the $A1_u^-$ component we are able to evaluate the Ω-doubling constant $q^v_{A1_u}$. For the levels $v_{A1}=4$ and $v_{A1}=8$ (cf. Table VI) we get $q^v_{A1_u} = -3.7\times10^{-6}$ cm^{-1} and -3.3×10^{-6} cm^{-1}, respectively. In Ref. 12 experimental values of rotational constants $B(1^+)=0.030\,238\,6(18)$ cm^{-1} and $B(1^-)=0.030\,237\,5(15)$ cm^{-1} were determined for $v=8$ leading to $q^{v=8}_{A1_u} = B(1^+) - B(1^-) \approx (1.1 \pm 2.3)\times10^{-6}$ cm^{-1} which is not in contradiction with the negative q value given above especially if one takes into account that they are obtained for different J regions.

It is notable that the $q^v_{A1_u}$ factor for Te_2 has not been measured experimentally till now, because its value is beyond the accuracy limit for direct energetic measurements.[12] Hence, it can only be obtained from the absorption spectrum of the perpendicular transition $X0_g^+ - A1_u$, which is rather weak [cf. Fig. 4(d)] and has not been observed. More experimental data are available for the $B1_u$ component of the $B\,^3\Sigma_u^-$ state of the Se_2 molecule where the rotational constant B_e values have been measured[45,46] separately for the $B1_u^+$ and $B1_u^-$ component, yielding $B_e(B1_u^+) - B_e(B1_u^-) \cong 3.3\times10^{-4}$ cm^{-1}. Using the averaged $B1_u$ state rotational constant value 0.0708 cm^{-1} and Eq. (33), we get the averaged one over v values for the difference: $g(B1_u^+) - g(B1_u^-) = 9.4\times10^{-3}$. Since we have $g(B1_u^-) < g(B1_u^+)$ for high J ($J>100$) values [cf. Eqs. (13) and (14)], it is easy to evaluate $g(B1_u^+) \cong 9.4\times10^{-3}$, it being in good agreement with the experimental $g(B1_u^+)$ value $8.0\pm0.8\times10^{-3}$ for the Se_2 molecule.[47]

From the comparison of Eqs. (16) and (24) one can easily obtain the approximate relation between the g factors of a diamagnetic ($B0_u^+$) state, and the nonadiabacity parameter χ_1^{PR} of a perpendicular $B0_u^+ - X1_g$ transition:

$$\frac{1+(I_1^P/I_1^R)^{1/2}}{1-(I_1^P/I_1^R)^{1/2}} \cong \chi_1^{PR} \cong g^{vJ}_{B0}[2J(J+1)]^{1/2} \times \left(\frac{R_{e\parallel}^{A1-X1}(R_c)}{2G_\pm R_{e^\perp}^{B0-X1}(R_c)} \times \frac{\langle v_{A1}|v_{X1}\rangle}{\langle v_{B0}|v_{A1}\rangle\langle v_{B0}|v_{X1}\rangle} \right). \quad (34)$$

Since the sign of the quantity in the large parentheses is not dependent on vibrational quantum numbers, the g factor sign correlates with the sign of χ_1^{PR} which, in turn, is uniquely determined by the sign of the intensity difference $I^P - I^R$. In other words, if the g factor is negative, I_1^P exceeds I_1^R, and vice versa. This interesting qualitative conclusion is supported by experimental observations. Indeed, the g factor sign is positive for the $v_{B0}=1$ ($J=243$) level, (cf. Table VI), and for the LIF progression from this level only we have $\chi_1^{ex}>0$ (cf. Table VII), and accordingly $I_1^P < I_1^R$, in agreement with the results in Ref. 12. Moreover, Eq. (34) makes it possible to describe the intensity distribution using experimental g values in the case when $R_{e\parallel}$, $R_{e^\perp}$, and $G_\pm$ are known. To confirm this, we evaluated by means of Eq. (34) the nonadiabacity parameter χ_1^{PR} values (see Table VII), which are in good agreement with the data obtained from the intensities.

Thus, the values of rovibronic terms, g factors, lifetimes, and relative intensities for interacting levels of $B0_u^+$ and $A1_u^+$ states are connected with each other through Franck–Condon type overlap integrals. At the same time, the electronic parameter values corresponding to the discussed characteristics (η, G_z, $G_\pm$, $R_{e\parallel}$, and $R_{e^\perp}$) were considered by us, until now, as independent adjustable fitting parameters. It is intuitively clear, however, that at least some of them, such as, e.g., η and $G_\pm$, are not independent, since $G_\pm - \eta = \langle\Omega|S_\pm|\Omega^*\rangle$, as follows directly from Eqs. (5) and (12). To determine the detailed relationships of the considered parameters it is obviously necessary to have more information about the electronic structure of the interacting states.

It is important that the absolute values of the treated parameters are dependent on the type of the corresponding electronic state, thus allowing to use the parameters in order to establish the origin of this state. It will be of greatest interest for us to clarify the problem of the genesis of the $A1_u$ state: Is it the $^3\Pi_1$ component of the $A\,^3\Pi_u$ state or the $^3\Sigma_1$ component of the $B\,^3\Sigma_u^-$ state (cf. Fig. 1)? For this purpose it is convenient to pass from the Hund's case "c" basis set to the "a" basis. By analogy with the electronic structure of other VI A group dimers,[48] namely O_2, S_2, and Se_2, it seems reasonable to suppose that the discussed $\Omega=0$ and $\Omega^*=1$ states may be presented as a mixture of the corresponding components of $^3\Sigma_u^-$ and $^3\Pi_u$ states, connected by the spin–orbit interaction:

$$|\Omega=0\rangle = c_{\Sigma_0}|^3\Sigma_0\rangle + c_{\Pi_0}|^3\Pi_0\rangle, \quad (35)$$

$$|\Omega^*=1\rangle = c_{\Sigma_1}|^3\Sigma_1\rangle + c_{\Pi_{\parallel}}|^3\Pi_1\rangle. \quad (36)$$

It is easy to obtain approximate expressions, transformed into this basis, for corresponding intramolecular and magnetic electronic matrix elements;[11,32]

$$\eta \cong c_{\Sigma_0}c_{\Sigma_1}\langle^3\Sigma_0|S_\pm|^3\Sigma_{\parallel}\rangle + c_{\Sigma_0}c_{\Pi_{\parallel}}\langle^3\Sigma_0|L_\pm|^3\Pi_1\rangle + c_{\Sigma_1}c_{\Pi_0}\langle^3\Sigma_1|L_\pm|^3\Pi_0\rangle, \quad (37)$$

$$G_\pm \cong g_s c_{\Sigma_0}c_{\Sigma_1}\langle^3\Sigma_0|S_\pm|^3\Sigma_1\rangle + g_l c_{\Sigma_0}c_{\Pi_1}\langle^3\Sigma_0|L_\pm|^3\Pi_1\rangle + g_l c_{\Sigma_1}c_{\Pi_0}\langle^3\Sigma_1|L_\pm|^3\Pi_0\rangle, \quad (38)$$

$$G_z \cong g_l + (g_s - g_l)c_{\Sigma_1}^2. \quad (39)$$

As can be seen from expression (39), if the $\Omega^*=1$ state is predominantly a $^3\Pi_1$ components, than $G_z \to 1$ (as c_{Σ_1}

$\rightarrow 0$). At the same time, if $\Omega^*=1$ state is largely a $^3\Sigma_1$ component, then $G_z \rightarrow 2$ (as $c_{\Sigma_1} \rightarrow 1$). Further, when Eq. (37) is compared with the Eq. (38), it is apparent that $G_\pm - \eta \cong c_{\Sigma_0} c_{\Sigma_1} \langle {}^3\Sigma_0 | S_\pm | {}^3\Sigma_1 \rangle$. Now assuming the $\Omega=0(B0_u^+)$ state to be predominantly a $^3\Sigma_0$ component (that is, $c_{\Sigma_0} \cong 1$), it is easy to make the following conclusions. If the $\Omega^*=1$ state is predominantly a $^3\Pi_1$ component, then the $G_\pm$ value tends to η, while if the $\Omega^*=1$ state is chiefly a $^3\Sigma_1$ component, then $G_\pm$ tends to 2η. Hence, assuming the 'pure precession' hypothesis[8] we get $\eta=1.41$, $G_\pm=1.41$, and $G_z=1$ for a pure $\Omega^*=1(^3\Pi_1)$ state and $\eta=1.41$, $G_\pm=2.82$, and $G_z=2$ for a pure $\Omega^*=1(^3\Sigma_1)$ state. It is obvious that the latter set of parameters is the closest to the experimental magnitudes, thus testifying of the $^3\Sigma_1$ origin of the $\Omega^*=1$ state. It is of interest that the intramolecular interaction parameter η is weakly dependent on the origin of the $\Omega^*=1$ state, as distinct from the magnetic parameters $G_\pm$ and G_z. As also follows from Eq. (39), g factor measurements for the nonperturbed $A1_u^-$ component allows to evaluate c_{Σ_1}, thus yielding a partial contribution of the $^3\Sigma_1$ component to the $A1_u$ state. Indeed, insertion of the experimental value $G_z^{ex} = 1.86$ discussed in Sec. IV B into Eq. (39) leads to $(c_{\Sigma_1})^2=0.86$. Knowing $(c_{\Sigma_1})^2$ and neglecting the interaction with the $^3\Pi_1$ component, we easily get the assessments $\eta^{est}=1.32$ and $G_\pm^{est}=2.65$ which are close enough to the experimental values of these quantities, see Tables IV, V, and VIII.

The electronic transition matrix elements are not all independent in the model employed. Thus, the electron dipole moment functions for $A1_u$–$X1_g$ and $A1_u$–$X0_g^+$ transitions can be represented approximately as

$$R_{e\|}^{A1-X1}(R_c) \cong c_{\Sigma_1} R_{e\|}^{B0-X0}(R_c), \tag{40}$$

$$R_{e\perp}^{A1-X0}(R_c) \cong c_{\Sigma_1} R_{e\perp}^{B0-X1}(R_c). \tag{41}$$

Knowing the mixing coefficient, c_{Σ_1} as well as the semiempirical functions $R_{e\|}^{B0-X0}(R_c)$ and $R_{e\perp}^{B0-X1}(R_c)$, we have used Eqs. (40) and (41) in order to calculate the dependencies $R_{e\|}^{A1-X1}(R_c)$ and $R_{e\perp}^{A1-X0}(R_c)$, as presented in Figs. 4(b) and 4(d), respectively (cf. the dashed lines). Taking into account the rather crude nature of such an approximation, one must agree that both the absolute values and general run of the obtained dependencies show a reasonable fit to the experimental data. Let us mention that if the Ω^* state should be in main a $^3\Pi_1$ component of the $A\,^3\Pi_u$ state, the function $R_{e\|}^{A1-X1}(R_c)$ ought to be similar to the corresponding function of the $A0_u^+$–$X0_g^+$ transition, that is to be ca. three times smaller in its strength and to decrease steeply with growing internuclear distance, see Ref. 18.

Thus, the good coincidence between η, $G_\pm$, $R_{e\perp}^{A1-X0}(R_c)$, and $R_{e\|}^{A1-X1}(R_c)$ as obtained from energetic, magnetic, and radiative measurements, together with their good agreement with theoretical estimations [Tables IV and VIII; Figs. 4(b) and 4(d)] can be considered as an unambiguous test of the consistency of various observations and of validity of the aforementioned suggested model of $^3\Sigma_u$ and $^3\Pi_u$ state interaction. Finally, we conclude, that the 1_u state studied here is predominantly (>86%) a $^3\Sigma_1$ component of the $B\,^3\Sigma_u^-$ state and only slightly (<14%) a $^3\Pi_1$ component of the $A\,^3\Pi_u$ state.

VI. DISCUSSION: THE ORIGIN OF THE $A1_u$ STATE

The last conclusion of Sec. V about the 1_u state basically belonging to the $B\,^3\Sigma_u^+$ state comes into conflict with the presently accepted notion in most publications (except experimental studies[15,27] and *ab initio* calculations[49]). We shall therefore discuss this aspect in greater detail. Previously,[12] on the basis of energy characteristics, the 1_u state was assigned to a $^3\Pi_{1u}$ component of the $A\,^3\Pi_u$ state, and not to a $^3\Sigma_{1u}$ component of the $B\,^3\Sigma_u^-$ state. The following arguments have been or could have been used to confirm this assignment. The experimental distance $\Delta T_e \cong 13\ cm^{-1}$ between the $B0_u^+$ and 1_u states is too small for spin–orbit splitting ($\lambda_{S.O.}$) of such a heavy molecule as the tellurium dimer. Thus, the experimental value of $2\lambda_{S.O.}$ for the lighter molecule Se_2 is as much as $\cong 78\ cm^{-1}$.[50] The empiric extrapolation of $2\lambda_{S.O.}$ in the progression of VI A group dimers O_2, S_2, Se_2, and Te_2, based on spin–orbit splitting of corresponding ^3P atoms leads to an estimated value of the order of $2\lambda_{S.O.} \cong 150$–$200\ cm^{-1}$ for $Te_2(B\,^3\Sigma_u^-)$. Besides, similar behavior of 1_u and $A0_u^+$ state potential curves is observed, cf. Fig. 1, as well as closeness of the discussed 1_u state term value $T_e(1_u)$ to that of $T_e(A0_u^+)+A_{S.O.}$, where $A_{S.O.} \cong 2177\ cm^{-1}$ is the evaluated value of the $A\,^3\Pi_u$ state spin–orbit splitting constant.[2]

Nevertheless, this obvious contradiction between the assignments based, on the one hand, on magnetic and radiative treatment and, on the other hand, on energetic measurements, may be eliminated if we take into account the following evidences. By analogy with O_2 and Se_2 molecules, we may suppose that the $B\,^3\Sigma_u^-$ state in Te_2 exhibits spin–orbit mixing not only with $^3\Pi_u$ but with $^1\Pi_u$, $(2)^3\Sigma_u^+$, $^5\Sigma_u^-$, and $^5\Pi_u$ states as well.[46,51] These states, as shown by calculations for O_2, are unbounded and are responsible for the predissociation of the $B\,^3\Sigma_u^-$ state.[51] The authors of *ab initio* calculations of electronic terms of Se_2 and Te_2 (Refs. 48 and 49) point out the presence of a strong spin–orbit interaction between isoconfigurated $^3\Pi_u$ and $^1\Pi_u$ states, growing with internuclear distance. Consequently, as can be expected from the proximity of energies between the $B\,^3\Sigma_u^-$ state and the aforementioned states, most of them (except of $^1\Pi_u$) are dissociating to the $^3P_2 + {}^3P_{0,1}$ limit, cf. Fig. 1. Even relatively small, for such heavy molecule as Te_2, spin–orbit interaction ($\sim 1000\ cm^{-1}$) is able to cause a noticeable shift ($\sim 200\ cm^{-1}$) and potential curve deformation (towards more weakly bounded) of the $B\,^3\Sigma_u^-$ state. Due to selection rules $\Delta\Omega=0$, $0_u^- \not\leftrightarrow 0_u^+$, the spin–orbit interaction does not take place between $^1\Pi_u$, $^3\Sigma_u^+$, and $^5\Sigma_u^-$ states and the $^3\Sigma_0^-(0_u^+)$ component; the discussed interaction has to have an effect chiefly upon the position and shape of the $^3\Sigma_1(1_u)$ component. Indeed, an estimate of $A1_u$ state dissociation energy, based on molecular constants given in Table I is about $2840\ cm^{-1}$, thus showing that this state dissociates towards the $^3P_2 + {}^3P_{0,1}$ limit. Then the $^3\Pi_1$

component of the $A\,^1\Pi_u$ state lies probably slightly ($\cong 500$ cm^{-1}) below the $B0_u^+$ state, and appears to be shallow. This $^3\Pi_1(1_u)$ state is not identified in spectroscopic measurements, possibly due to its strong shift with respect to the ground state, see Fig. 1. At the same time it is, most likely, just this state which is responsible for the heterogeneous perturbations of the $B0_u^+$ state levels $v_{B0}=18$ and 19,[12,23] as well as of $v_{B0}=2(J\cong 202)$.[52] Note also that as the observed $A1_u$ state predissociation begins below the $^3P_2 + {}^3P_{0,1}$ limit, none of the previous listed states is responsible for this predissociation. This means that the state causing predissociation has to approach the $^3P_2 + {}^3P_2$ limit and to possess 1_u type symmetry, see Sec. IV C, as is, for example, the corresponding component of a bound $^3\Sigma^+(1_u)$ or/and $^3\Delta(1_u)$ state,[48,51] cf. Fig. 1. The predissociation of $A1_u$ state levels is of c^- or c^0 type[53] emerging through the repulsive part of a corresponding bound state. This mechanism is confirmed by the weakness of the predissociation and by its unsensitivity to the rotational quantum number J (cf. column c in Table VI) as distinct from the strong c^+ type predissociation of the $B0_u^+$ ($v_{B0}>18$) levels caused, most probably, by the repulsive potential of the $^5\Pi_u(0)$ state.

The above considerations, at our glance, provide enough reason to indicate the state 1_u treated here as $B1_u$ instead of $A1_u$, thus underlining its belonging to $B\,^3\Sigma_u^-$. However, in order to avoid misunderstanding, the indication ($A1_u$), presently accepted in bibliographic sources, has been used throughout the text.

VII. CONCLUSIONS

The present GDA concept demonstrates the possibility of describing all existing data obtained from energetic, magnetic, and radiative measurements in a unified model with a minimum number of adjustable fitting parameters and possessing definite physical meaning. A comparative analysis of the characteristics listed earlier reveals that the g factors of a diamagnetic state, as well as the relative intensities of a perpendicular (i.e., $B0_u^+ - X1_g$) transition, are much more sensitive to weak local perturbations than level shifts and lifetime changes, thus allowing to investigate weak nonresonant interactions beyond the reach of the energetic measurements. Moreover, the radiative and especially the magnetic characteristics "remember" the longest of their "electronic origin," as compared to the internuclear potential and molecular constants. Consequently, the measurements of absolute values and signs of g factors, as well as those of electron transition probabilities may help to perform an unambiguous electronic assignment of interacting states, which is difficult to achieve basing only on energetic characteristics, in particular, for the states possessing large spin–orbit splitting, as in Hund's case "c". Additionally, as shown in our just accomplished studies,[54] the alignment-orientation conversion phenomenon allows to extract the effect of magnetic field induced $1_u \sim 0_u^+$ ($\Delta J = \pm 1$) interaction yielding directly the parameter $G_\pm$ and thus giving the possibility to determine separately η and $G_\pm$ from magnetic measurements only.

ACKNOWLEDGMENTS

The authors are indebted to Dr. Ilze Klincare for helpful discussions. Support from the Latvian Science Council (Grant No. 90.467) is gratefully acknowledged.

[1] J. T. Hougen, The Calculations of Rotational Energy Levels and Rotational Line Intensities in Diatomic Molecules, Natl. Bur. Stand. (U.S.) Monograph No. 115 (U.S. G.P.O., Washington, D.C., 1970).
[2] H. Lefebvre-Brion and R. W. Field, *Perturbations in the Spectra of Diatomic Molecules* (Academic, New York, 1986).
[3] J. Vigue, Ann. Phys. Fr. 3, 155 (1983).
[4] G. Gouedard and J. C. Lehmann, Faraday Discuss. Chem. Soc. 71, 143 (1981).
[5] A. V. Stolyarov, I. P. Klincare, M. Ya. Tamanis, M. P. Auzin'sh, and R. S. Ferber, J. Chem. Phys. 96, 3510 (1992).
[6] L. Veseth, J. Mol. Spectrosc. 59, 51 (1976).
[7] H. Christensen and L. Veseth, J. Mol. Spectrosc. 72, 438 (1978).
[8] J. H. Van Vleck, Phys. Rev. 33, 467 (1929).
[9] A. V. Stolyarov, N. E. Kuz'menko, Ya. A. Harya, and R. S. Ferber, J. Mol. Spectrosc. 137, 251 (1989).
[10] R. N. Zare, A. L. Schmeltekoph, W. J. Harrop, and D. L. Albritton, J. Mol. Spectrosc. 46, 37 (1973).
[11] M. Mizuchima, *The Theory of Rotating Diatomic Molecules* (Wiley, New York, 1975).
[12] J. Verges, C. Effantin, O. Babaky, J. d'Incan, S. J. Prosser, and R. F. Barrow, Phys. Scr. 25, 338 (1982).
[13] R. F. Barrow and R. P. duParcq, Proc. R. Soc. London Ser. A 327, 279 (1972).
[14] K. K. Yee and R. F. Barrow, J. Chem. Soc. Faraday. Trans. 68, 1397 (1972).
[15] T. J. Stone and R. F. Barrow, Can. J. Phys. 53, 1976 (1975).
[16] J. Verges, J. d'Incan, C. Effantin, D. J. Greenwood, and R. F. Barrow, J. Phys. B 12, L301 (1979).
[17] C. Effantin, J. d'Incan, J. Verges, M. T. Macpherson, and R. F. Barrow, Chem. Phys. Lett. 70, 560 (1980).
[18] Ya. A. Harya, R. S. Ferber, N. E. Kuz'menko, O. A. Shmit, and A. V. Stolyarov, J. Mol. Spectrosc. 125, 1 (1987).
[19] A. V. Stolyarov, E. A. Pazyuk, L. A. Kuznetsova, Ya. A. Harya, and R. S. Ferber, Chem. Phys. Lett. 166, 290 (1990).
[20] I. P. Klincare and M. Ya. Tamanis, Chem. Phys. Lett. 180, 63 (1991).
[21] R. S. Ferber, Ya. A. Harya, and A. V. Stolyarov, J. Quant. Spectrosc. Radiat. Trans. 47, 143 (1992).
[22] R. S. Ferber, O. A. Shmit, and M. Ya. Tamanis, Chem. Phys. Lett. 92, 393 (1982).
[23] M. A. Auzin'sh, M. Ya. Tamanis, and Ya. A. Harya, *The XX-th All-Union Spectroscopy Congress*, Kiev, Sept. 1988. Proceedings, Part 1, p. 263 (Naukova Dumka, Kiew, 1988).
[24] M. A. Auzin'sh, M. Ya. Tamanis, and Ya. A. Harya, *Radiational and Collisional Characteristics of Atoms and Molecules. Tellurium*, edited by A. Ubelis (Latvian University, Riga, 1989).
[25] W. G. Thorpe, W. R. Carper, and S. I. Davis, Chem. Phys. Lett. 123, 493 (1986).
[26] I. P. Klintsare, A. V. Stolyarov, M. Ya. Tamanis, R. S. Ferber, and Ya. A. Kharya, Opt. Spectrosc. (USSR) 66, 595 (1989).
[27] I. P. Klintsare, M. Ya. Tamanis, and R. S. Ferber, Opt. Spectrosc. (USSR) 67, 720 (1989).
[28] L. Veseth, J. Phys. B 6, 1473 (1973).
[29] J. L. Dunham, Phys. Rev. 41, 721 (1932).
[30] R. Rydberg, Z. Phys. 73, 376 (1931); O. Klein, *ibid*, 76, 226 (1932); A. L. G. Rees, Proc. Phys. Soc. 59, 998 (1974).
[31] L. P. Landau and E. F. Lifshitz, *Quantum Mechanics* (Pergamon, London, 1965).
[32] R. A. Brooks, C. H. Anderson, and N. F. Ramsay, Phys. Rev. A 136, 62 (1964).
[33] L. Veseth, J. Mol. Spectrosc. 63, 180 (1976).
[34] P. A. Fraser, Can. J. Phys. 32, 515 (1954).
[35] J. Tellinghuisen and P. S. Julienne, J. Chem. Phys. 81, 5779 (1984).
[36] A. V. Stolyarov and V. I. Pupychev, Phys. Rev. (to be published).
[37] J. N. Huffaker, J. Chem. Phys. 64, 3175 (1975).
[38] W. H. Press, B. P. Flannery, S. A. Teukolsky, and W. T. Vetterling, *Numerical Recipes* (Cambridge University, Cambridge, 1986).
[39] H. Telle and U. Telle, J. Mol. Spectrosc. 85, 248 (1981).

[40] B. R. Johnson, J. Chem. Phys. **67**, 4086 (1977).
[41] A. V. Abarenov and A. V. Stolyarov, J. Phys. B **23**, 2419 (1990).
[42] A. V. Stolyarov and A. V. Abarenov, Spectrosc. Lett. **25**, 271 (1992).
[43] C. Noda and R. N. Zare, J. Mol. Spectrosc. **95**, 254 (1982).
[44] V. I. Pupyshev, V. A. Kozlov, and L. A. Kuznetsova, Opt. Spectrosc. USSR (in Russian) **64**, 1228 (1988).
[45] R. F. Barrow, W. F. Chandler, D. A. Meyer, Pros. R. Soc. London Ser. A **260**, 395, (1966).
[46] A. Jenouvrier, Can. J. Phys. **61**, 1531 (1983).
[47] G. Gouedard and J. C. Lehmann, J. Phys. **38**, L85 (1977).
[48] K. Balasubramanian, J. Phys. Chem. **91**, 5166 (1987).
[49] K. Balasubramanian and Ch. Ravimohan, J. Mol. Spectrosc. **126**, 220 (1987).
[50] D. J. Greenwood and R. F. Barrow, J. Phys. B **9**, 2123 (1976).
[51] P. S. Julienne, J. Mol. Spectrosc. **63**, 60 (1976).
[52] A. Topouzkhanian, O. Babaky, J. Verges, R. Willers, and B. Wellegehausen, J. Mol. Spectrosc. **113**, 39 (1985).
[53] R. S. Mulliken, J. Chem. Phys. **33**, 247 (1960).
[54] I. P. Klincare, M. Ya. Tamanis, A. V. Stolyarov, M. P. Auzinsh, and R. S. Ferber, J. Chem. Phys. **99**, 5748 (1993).

Magnetic field induced alignment–orientation conversion: Nonlinear energy shift and predissociation in Te_2 $B1_u$ state

M. Auzinsh, A. V. Stolyarov,[a] M. Tamanis, and R. Ferber
Department of Physics, University of Latvia, Riga, LV-1586, Latvia

(Received 29 December 1995; accepted 28 March 1996)

The paper analyzes magnetic field induced alignment–orientation conversion (AOC) phenomenon caused by simultaneous effect of quadratic terms in Zeeman energy shift and magnetic predissociation (PD), producing asymmetry either in energy splitting $\omega_{MM\pm1}\neq\omega_{-M\mp1-M}$ or in relaxation of coherence $\Gamma_{MM\pm1}\neq\Gamma_{-M\mp1-M}$ between coherently excited M, $M\pm1$ magnetic sublevels. The AOC is registered via the appearance of circular polarization (C) of fluorescence under linearly polarized excitation. The unified perturbation treatment of a molecule in external magnetic field B is presented, accounting for magnetic and intramolecular perturbations via interaction with bonded or continuum states, considering Hund's (c)-case coupling and dividing the intramolecular perturbation operator into homogeneous ($\Delta\Omega=0$) and heterogeneous ($\Delta\Omega=\pm1$) parts. Explicit expressions up to B^2 terms are given for energy shift and PD rate, adapted to 1_u state in conditions relevant to the $B\,^3\Sigma_u^-$ complex of Te_2 molecule. Numeric simulation revealed that nonlinear magnetic energy shift and heterogeneous magnetic PD produce dispersion type fluorescence circularity signals $C(B)$ of different sign. Fitting of experimental data on $B1_u^-$, $v(J)=2(96)$ state of $^{130}Te_2$ molecule allowed to determine the electronic matrix element of paramagnetic Hamiltonian $(\Omega=0|\hat{H}_{pm}|\Omega=1)\equiv G_{\pm}=2.7$, as well as the natural $C_v^{het}=\pm6\ s^{-1/2}$ and the magnetic $\alpha_v^{het}=\mp9\times10^3\ s^{-1/2}T^{-1}$ rate constants of heterogeneous PD, supposing that the $B1_u^-$ state PD takes place through 0_u^- state continuum. As a result, magnetic AOC represents a sensitive method to investigate molecular structure and intramolecular interaction between both bonded and continuum states. Additionally, it has been shown that the magnetic PD effect leads to strong amplification of nonzero field level crossing signals caused by B^2 terms in Zeeman energy shift.
 [S0021-9606(96)01325-6]

I. INTRODUCTION

The anisotropic spatial distribution of angular momenta in the ensemble of atoms or molecules is characterized in terms of alignment and orientation. One speaks of *alignment* when the distribution is symmetrical with respect to the reflection in the plane which is perpendicular to a certain symmetry axis, and of *orientation* if such symmetry is absent, thus bringing into existence a preferable direction along the symmetry axis. For clarity reason one may imagine that alignment behaves like a double-headed arrow (⇔) whereas orientation behaves like a single-headed one (⇒). In particular, excitation with linear polarized light creates alignment only, and $\hat{E}$-vector defines the axis of cylindrical symmetry. It has been interest for a long time, starting from Refs. 1–3, to study the perturbing factors, which are able to break the reflection symmetry and thus to cause alignment–orientation conversion (AOC). The more recent publications, dealing with different versions of AOC in atoms and molecules, can be found as references given in Ref. 4, to which, for completeness sake, we would like to add the works of Refs. 5–12. The case of AOC in diatomic molecules was investigated in Refs. 4, 8–13. It is easy to understand the main reasons for AOC if one remembers that the ensemble density matrix element $f_{MM'}$ which is obtained as a solution of the stationary density matrix equation of motion and which describes the coherence between sublevels with magnetic quantum numbers M and M' in the state with definite angular momentum J value, contains a factor $(\Gamma_{MM'}+i\omega_{MM'})^{-1}$, namely

$$f_{MM'}\propto\frac{1}{\Gamma_{MM'}+i\omega_{MM'}}, \tag{1}$$

where

$$\omega_{MM'}=\frac{E_M-E_{M'}}{\hbar} \tag{2}$$

is the splitting between Zeeman sublevels M,M' with energies $E_M, E_{M'}$, while

$$\Gamma_{MM'}=\frac{\Gamma_M+\Gamma_{M'}}{2} \tag{3}$$

is the rate of relaxation of coherence between M,M' sublevels, Γ_M and $\Gamma_{M'}$ being relaxation rate constants of respective states. It can be seen from the form of Eq. (1) that, generally speaking, at broad spectral line excitation there are two basic reasons for the appearance of AOC in the excited state angular momenta ensemble. Indeed, as it follows from the analysis presented in Ref. 12, one must have such a perturbation which leads to the asymmetry, with respect to the M,M', either in energy splittings

[a]Present address: Department of Chemistry, Moscow State University, 119899, Moscow, Russia.

 0021-9606/96/105(1)/37/13/$10.00

$$\omega_{MM\pm1} \neq \omega_{-M\mp1-M}, \tag{4}$$

or in M-dependent coherence relaxation rate constants

$$\Gamma_{MM\pm1} \neq \Gamma_{-M\mp1-M}. \tag{5}$$

In a number of our previous publications[4,11–13] the AOC effect in diatomic molecules was treated theoretically and demonstrated experimentally in the case when it has been caused by nonlinear, in particular quadratic Zeeman energy E_M dependence on external static magnetic (B) or electric (E) field strength, as well as on magnetic quantum numbers M, thus entailing the condition (4). Sufficiently pronounced AOC signal was registered[11] in $B1_u^-$ component of the Te_2 $B\,^3\Sigma_u^-$ state complex as the appearance of the degree of fluorescence circularity $C(B)$ up to 0.05, under linearly polarized $X1_g^- \rightarrow B1_u^-$ excitation in the presence of static magnetic field up to $B=0.4$ T. The effect has been described as a result of the asymmetric splitting of Zeeman sublevels, see Eq. (4), due to the presence of quadratic Zeeman effect energy shift term. We found it to be a nice example of the magnetic field assisted $\Delta J=\pm1$ mixing of states with different electronic parity, or $e\sim f$ mixing, not only between Ω-doubling components $B1_u^- \sim B1_u^+$ of the electronic $B\,^3\Sigma_u^-$ state, but rather that of the $B1_u^- \sim B0_u^+$ close together situated components interaction. It is important to stress that both interactions are forbidden in the absence of the external magnetic field. Such a heavy diatomic molecule, without hyperfine structure, as Te_2, possessing well enough investigated energy levels and dynamic parameters (molecular constants, intramolecular interaction parameters, lifetimes, Landé factors, etc.), see Refs. 14 and 15 and references therein, can be considered as one of the "test" objects in molecular spectroscopy, along with such diatomics as Na_2, I_2, and others. At the same time, whilst the general behavior of AOC in Te_2 ($B1_u^-$) was well enough described by the treatment developed in Ref. 11, there remained the unexplained additional structure of the experimentally registered signal. To explain such a structure, it needs to be ascertained if there is some influence of another fundamental reason for AOC, namely of the asymmetric over M, $M\pm1$, in the sense of condition (5), relaxation rates $\Gamma_{MM'}$. Indeed, as it was demonstrated in Refs. 8 and 9 on the iodine molecule I_2 in the $B\,^3\Pi_{0_u^+}$ state, fluorescence circularity may appear owing to magnetic field effected M-selective predissociation (PD). The authors of Refs. 8 and 9 have presented the detailed PD theory,[10] accounting for rotational, magnetic, and hyperfine PD, but they neglected the possible influence of Zeeman effect induced energy shifts in signal description. As it becomes clear even from the first glance at the dense electronic term scheme of Te_2 molecule,[15,16] it is highly probable that such AOC mechanism as the magnetic PD effect, causing the fulfillment of condition (5), has to be taken into account, along with quadratic Zeeman effect terms in energy shift, causing the fulfillment of condition (4).

The main purpose of the present article is to develop an extended treatment of AOC by accounting simultaneously both for quadratic terms in Zeeman effect induced energy shift as well as for magnetic field induced PD. The consideration presented supplies more satisfactory interpretation of experimental results of Ref. 11 on Te_2 $B1_u^-$ state and demonstrates the possibility to determine separately the electronic mixing parameters, to distinguish between homogeneous and heterogeneous PD types and to determine the parameters of very weak natural and magnetic PD.

The paper has a following structure. In Sec. II we will remind briefly the analytical expressions for density matrix elements and fluorescence intensity with a definite, in particular circular polarization, dependent on magnetic field affected $\omega_{MM'}$ and $\Gamma_{MM'}$. In Sec. III a general approach is developed to describe a diatomic molecule in external magnetic field, including both magnetic energy shifts and magnetic PD. A quick description of Te_2 excited electronic states, which are involved in the processes under discussion, is given in Sec. IV. In Sec. V we will pass to the simulations of expected signals in conditions typical for the $B\,^3\Sigma_u^-$ state of Te_2 molecule, including fluorescence circularity under linear polarized excitation, as well as to the fitting of experimentally obtained data, ending with a summarizing discussion in Sec. VI.

II. FLUORESCENCE INTENSITY

We will discuss the manifestation of AOC in fluorescence signal as the appearance of circular polarization under linear polarized broad spectral line excitation. The detailed treatment is given elsewhere[4,12] and we will stress hereafter the main points only. Let us assume that the weak linearly polarized cw broad spectral light had prepared excited (J') state density matrix $f_{MM'}$.[12,17] The explicit form of intensity expression I_f for light emitted at a $J' \rightarrow J_1''$ transition is

$$I_f(\hat{E}_f) = \frac{K|(J_1''\|D\|J')|^2}{2J'+1} \sum_{\mu MM' q_1 q_2} f_{MM'}(-1)^{q_1+q_2} \times (E_f^{-q_1})^*(E_f^{-q_2}) C^{J'M}_{J_1''\mu 1 q_1} C^{J'M'}_{J_1''\mu 1 q_2}, \tag{6}$$

where $E_f^{q_i}$, $q_i=0,\pm1$ are cyclic components of unit fluorescence polarization vector $\hat{E}_f$, $C^{J'M}_{J_1''\mu 1 q_1}$ are Clebsch–Gordan coefficients, M, M', and μ are respective excited (J') and ground (J_1'') state magnetic quantum numbers, $(J_1''\|D\|J')$ denotes reduced matrix element for electric dipole transition, K is proportionality factor. The excited state orientation is certified through circularity of fluorescence,

$$C = \frac{I_r - I_l}{I_r + I_l}, \tag{7}$$

$I_{r,l}$ being right-handed and left-handed circularly polarized light intensities. The excited state density matrix elements $f_{MM'}$ are formed in $|J''\mu\rangle \rightarrow |J'M\rangle$ absorption and can be found as stationary solution of the equation of motion[12] as

$$f_{MM'}=\frac{\tilde{\Gamma}_p|(J'\|D\|J'')|^2}{2J'+1}\frac{1}{\Gamma_{MM'}+i\omega_{MM'}}\times\sum_{\mu q_1 q_2}(E^{q_1})^*(E^{q_2})C^{J'M}_{J''\mu 1 q_1}C^{J'M'}_{J''\mu 1 q_2}, \tag{8}$$

where the factor $\tilde{\Gamma}_p|(J'\|D\|J'')|^2/(2J'+1)$ is the dynamic part of absorption probability, E^{q_i} are cyclic components of exciting light vector $\hat{\mathbf{E}}$. Let us assume that the exciting light linear polarization vector $\mathbf{E}(\vartheta,\varphi)$ is directed at angles ϑ,φ with respect to the quantization axis $\mathbf{z}\|\mathbf{B}$, while fluorescence is observed along y axis. These conditions make it possible to find exciting light and fluorescence light vector cyclic components E^{q_i} and $E_f^{q_i}$ by means of Wigner D matrices, thus allowing to write explicitly the expressions for I_r-I_l and I_r+I_l (Refs. 4 and 12) entering Eq. (7). The final expression for the difference I_r-I_l which describes the appearance of orientation can be written as

$$I_r-I_l\propto\Gamma_p\frac{\sin 2\vartheta}{2}\sum_M\frac{\Gamma_{MM+1}\sin\varphi+\omega_{MM+1}\cos\varphi}{\Gamma^2_{MM+1}+\omega^2_{MM+1}}\times(C^{J'M}_{J''M+11-1}C^{J'M+1}_{J''M+110}-C^{J'M}_{J''M10}C^{J'M+1}_{J''M11})\times(C^{J'M}_{J_1''M10}C^{J'M+1}_{J_1''M11}+C^{J'M}_{J_1''M+11-1}C^{J'M+1}_{J_1''M+110}). \tag{9}$$

Expression for I_r+I_l takes the form:

$$I_r+I_l\propto\sum_M\left\{\frac{\Gamma_p}{\Gamma_{MM}}\left\{\frac{\sin^2\vartheta}{2}[(C^{J'M}_{J''M-111})^2+(C^{J'M}_{J''M+11-1})^2]+\cos^2\vartheta(C^{J'M}_{J''M10})^2\right\}\left[\frac{1}{2}(C^{J'M}_{J_1''M-111})^2+(C^{J'M}_{J_1''M10})^2+\frac{1}{2}(C^{J'M}_{J_1''M+11-1})^2\right]+\Gamma_p\frac{\sin^2\vartheta}{2}\frac{\Gamma_{M-1M+1}\cos 2\varphi-\omega_{M-1M+1}\sin 2\varphi}{\Gamma^2_{M-1M+1}+\omega^2_{M-1M+1}}\times C^{J'M-1}_{J''M1-1}C^{J'M+1}_{J''M11}C^{J'M-1}_{J_1''M1-1}C^{J'M+1}_{J_1''M11}\right\}. \tag{10}$$

Consequently, as it follows clearly from Eqs. (9) and (10), in order to analyze the appearance of magnetic field induced orientation, one has to calculate:

(i) the magnetic field induced energy splitting $\omega_{MM'}$ values, which are defined by the magnetic sublevel energy set $E_M(B)$, see Eq. (2);

(ii) the magnetic field affected coherence relaxation constant values $\Gamma_{MM'}$ between M,M' sublevels, which are defined by the magnetic field-dependent relaxation constant set $\Gamma_M(B)$, see Eq. (3).

For this purpose we will further consider the Zeeman effect induced energy shifts to account for (i), as well as the magnetic predissociation to account for (ii).

III. LINEAR AND QUADRATIC TERMS IN ZEEMAN SHIFT AND MAGNETIC PREDISSOCIATION

The Hamiltonian $\hat{\mathbf{H}}$ of a molecule in external stationary homogeneous magnetic field $\mathbf{B}$ can be presented in a simplified form as[18]

$$\hat{\mathbf{H}}=\hat{\mathbf{H}}_0+\hat{\mathbf{V}}+\hat{\mathbf{H}}_{\rm pm}+\hat{\mathbf{H}}_{\rm dm}, \tag{11}$$

where $\hat{\mathbf{H}}_0+\hat{\mathbf{V}}$ is the Hamiltonian of an isolated molecule without external field, $\hat{\mathbf{H}}_0$ is the Hamiltonian zero approximation, $\hat{\mathbf{V}}$ is the perturbation operator of intramolecular interactions,

$$\hat{\mathbf{H}}_{\rm pm}=-\mu_B\mathbf{B}(g_l\mathbf{J}_a+(g_s-g_l)\mathbf{S}) \tag{12}$$

is the so-called paramagnetic term, μ_B is Bohr magneton, g_l and g_s are orbital and spin electronic g factors, respectively ($g_l=-1$ and $g_s=-2$), $\mathbf{J}_a=\mathbf{L}+\mathbf{S}$ is the total electronic angular momentum

$$\hat{\mathbf{H}}_{\rm dm}=K_{\rm dm}\sum_i[\mathbf{B}\times\mathbf{r}_i]^2 \tag{13}$$

is the so-called diamagnetic term, i denoting summation over all electrons, $K_{\rm dm}=e^2/8m_ec^2=\mu_B^2m_e/2\hbar^2\simeq 2.2\times10^{-4}\mu_B^2$ (in atomic units). In Eqs. (11)–(13) we have neglected the nuclear spins and the relativistic effects leading to quantumelectrodynamical correction to g_l and g_s values.

We will further consider that $\hat{\mathbf{V}}$, $\hat{\mathbf{H}}_{\rm pm}$, and $\hat{\mathbf{H}}_{\rm dm}$ are small in comparison with $\hat{\mathbf{H}}_0$, which allows one to use first- and second-order nondegenerative perturbation theory to describe the Zeeman effect induced energy shifts as well as the intramolecular interaction effects. We will use Fermi–Wentzel golden rule do describe natural and magnetic PD.[19] In further consideration we will account for magnetic field and intramolecular perturbation influence on the eigenfunctions, but neglect the level shifts caused by PD. Then, since we are interested mainly in $\omega_{MM'}$ and $\Gamma_{MM'}$ dependencies on magnetic quantum numbers M and magnetic field strength B, and restricting our consideration up to terms containing B^2, we have to pass from Eqs. (11)–(13) to the following expressions for level energy E_M and predissociation rate Γ_M:

$$E_M^{\Phi J}=E_{\rm nat}^{\Phi J}+\langle\Phi_pJM|\hat{\mathbf{H}}_{\rm pm}|\Phi_pJM\rangle+\sum_{\Phi_p'J'}\frac{|\langle\Phi_pJM|\hat{\mathbf{H}}_{\rm pm}|\Phi_p'J'M\rangle|^2}{E_M^{\Phi_pJ}-E_M^{\Phi_p'J'}}+\langle\Phi_pJM|\hat{\mathbf{H}}_{\rm dm}|\Phi_pJM\rangle, \tag{14}$$

$$\Gamma_M^{\Phi J}=\Gamma_{\rm nat}^{\Phi J}+\frac{2\pi}{\hbar}\left[\sum_{\Phi'J'}\left|\langle\Phi JM|\hat{\mathbf{H}}_{\rm pm}|\Phi'J'M\rangle\right|^2+2\sum_{\Phi'}\langle\Phi JM|\hat{\mathbf{V}}|\Phi'JM\rangle\langle\Phi JM|\hat{\mathbf{H}}_{\rm pm}+\hat{\mathbf{H}}_{\rm dm}|\Phi'JM\rangle\right|, \tag{15}$$

where $E_{\rm nat}^{\Phi J}$ and $\Gamma_{\rm nat}^{\Phi J}$ are respective energy shift and predissociation rate values for a certain rovibrational level in ab-

sence of external field, $|\Phi JM\rangle$ are eigenfunctions of the $\hat{\mathbf{H}}_0$ Hamiltonian, while $E_M^{\Phi_p J}$ and $|\Phi_p J' M\rangle$ are eigenvalues and eigenfunctions of the $\hat{\mathbf{H}}_0+\hat{\mathbf{V}}$ Hamiltonian. For the reason which will be clear from the following discussion, the diamagnetic perturbation has been taken into account only to the first order perturbation theory in Eq. (14). Functions $|\Phi_p' J' M\rangle$ or $|\Phi' JM\rangle$ may correspond either to bonded [Eq. (14)] or to continuum [Eq. (15)] states, with which intramolecular interaction is taking place. It is supposed that $|\Phi' JM\rangle$ in Eq. (15) are the energy-normalized continuum wave functions. Summands containing $\hat{\mathbf{H}}_{pm}$ in Eq. (14) are the first- and second-order perturbation terms, respectively, the second-order term being the so-called "high-frequency term" according to Van Vleck.[20] Now we can write the eigenfunctions $|\Phi_p^{(B)} JM\rangle$ which are perturbed by magnetic field

$$|\Phi_p^{(B)} JM\rangle = |\Phi_p JM\rangle + \sum_{\Phi_p' J'} \frac{\langle \Phi_p JM|\hat{\mathbf{H}}_{pm}|\Phi_p' J' M\rangle}{E_M^{\Phi_p J} = E_M^{\Phi_p' J'}} |\Phi_p' J' M\rangle, \tag{16}$$

where the symbol $|\Phi_p JM\rangle$ denotes state wave function in the absence of magnetic field, but with accounting for intramolecular perturbations, namely

$$|\Phi_p JM\rangle = |\Phi JM\rangle + \sum_{\Phi'} \frac{\langle \Phi JM|\hat{\mathbf{V}}|\Phi' JM\rangle}{E_J^{\Phi} - E_J^{\Phi'}} |\Phi' JM\rangle. \tag{17}$$

Matrix elements of the $\hat{\mathbf{H}}_0+\hat{\mathbf{V}}$ operator are independent of magnetic quantum number M, whereas $\hat{\mathbf{H}}_{pm}$ and $\hat{\mathbf{H}}_{dm}$ dependence on M is given by Wigner–Eckart theorem in laboratory coordinates[21,22]

$$\langle J' M'|\hat{f}_0^{(k)}|JM\rangle = (-1)^{J'-M'} \begin{pmatrix} J' & kJ \\ -M' & 0M \end{pmatrix} \times \langle J'\|\hat{f}^{(k)}\|J\rangle, \tag{18}$$

where $\hat{f}_0^{(k)}$ denotes operator spherical tensorial components of rank k and projection $q=0$, $\langle J'\|\hat{f}^{(k)}\|J\rangle$ are reduced matrix elements, $\begin{pmatrix} J' & kJ \\ -M' & 0M \end{pmatrix}$ are $3j$ symbols used here because of their higher symmetry instead of Clebsch–Gordan coefficients. Let us remind that the spherical functions Y_{k0} of rank $k=0,1,2$, being a particular type of the spherical tensor, have the following dependence on the spherical angle ϑ': $Y_{00}=\text{const}$, $Y_{10}\propto\cos\vartheta'$ and $Y_{20}\propto(3\cos^2\vartheta'-1)$. As follows from Eq. (12), $\hat{\mathbf{H}}_{pm}$ is defined as the scalar product of two vectors, thus $\hat{\mathbf{H}}_{pm}$ contains $\cos\vartheta'$ and corresponds to the first rank ($k=1$) tensor. At the same time, $\hat{\mathbf{H}}_{dm}$ contains $\sin^2\vartheta'$, see Eq. (13), and thus corresponds to zero ($k=0$) and second ($k=2$) rank tensors. Hence, the respective selection rules over J are: $\Delta J=0,\pm1$ for $\hat{\mathbf{H}}_{pm}$ and $\Delta J=0,\pm1,\pm2$ for $\hat{\mathbf{H}}_{dm}$. Remember that, for the case of intramolecular interaction, the selection rule over J is $\Delta J=0$ only. Besides, the additional symmetry selection rules for both magnetic and intramolecular interactions are $\oplus\leftrightarrow\ominus$ with respect to the full parity and, additionally, $s\leftrightarrow a$ regarding symmetric/antisymmetric states in the case of a homonuclear diatomic molecule (see Fig. 2). In order such requirements to be obeyed, only the $3j$ symbols with $\Delta J=J'-J=0,\pm1,\pm2$ and with $M'=M$ have to be considered. The explicit expressions for $3j$ symbols are given in Table I. In particular, as follows from the table, the diagonal terms of Hamiltonian $\hat{\mathbf{H}}_{pm}^{(1)}$ are linear over M. The diagonal ($J'=J$) Hamiltonian matrix elements are M independent for $\hat{\mathbf{H}}_{dm}^{(0)}$, while for $\hat{\mathbf{H}}_{dm}^{(2)}$ they contain the factor $[3M^2-J(J+1)]$. The squared nondiagonal Hamiltonian matrix elements ($J-J'=\pm1$) contain the factor $(J+1)^2-M^2$ for $\hat{\mathbf{H}}_{pm}^{(1)}$. These considerations allow one to obtain from Eqs. (14)–(15) the general dependence of E_M and Γ_M on M and B in closed form as

$$E_M = a+bMB+(c+dM^2)B^2, \tag{19}$$

$$\Gamma_M = a'+b'MB+(c'+d'M^2)B^2, \tag{20}$$

where parameters a,b,c,d the and a',b',c',d' are independent of M and B, being dependent on other quantum numbers characterizing isolated molecules in the absence of external field. From Eqs. (19)–(20) one may judge immediately that the conditions described by Eqs. (4)–(5) are fulfilled.

Further, since $\hat{\mathbf{V}}$ and $\hat{\mathbf{H}}_{pm}$ are composed from angular momenta J, L, and S, the evaluation of $a-d$ and $a'-d'$ parameters in Eqs. (19)–(20) will depend on the particular type of the angular momenta coupling. We will consider here the primitive Hund's (c)-case coupling scheme,[19] according to which the full rovibrational Hamiltonian can be split into parts in the following way. The zero-order Hamiltonian $\hat{\mathbf{H}}_0$, see Eq. (11), includes:

(i) *electronic* term $\hat{\mathbf{H}}_{el}^0(R,\mathbf{r}_i)$ which, however, contains all relativistic effects caused by spin–orbit and spin–spin interactions;

(ii) *vibrational* term in form $-(1/2\mu)(\partial^2/\partial R^2)$, where μ is reduced mass of the molecule, R is internuclear distance;

(iii) *rotational* term in form $B(R)\mathbf{J}^2$, with eigenvalues $\hbar^2 B(R)J(J+1)$, where $B(R)=1/(2\mu R^2)$.

In doing so, we will also consider that for the eigenfunctions $|\Psi_\Omega(R,\mathbf{r}_i)\rangle$ of Hamiltonian $\hat{\mathbf{H}}_{el}^0(R,\mathbf{r}_i)$, which are obtained via solving the equation $\hat{\mathbf{H}}_{el}^0(R,\mathbf{r}_i)\Psi_\Omega(R,\mathbf{r}_i) = E_{el}^\Omega(R)\Psi_\Omega(R,\mathbf{r}_i)$, the relations $\langle\Psi_\Omega|\partial\Psi_{\Omega'}/\partial R\rangle \equiv \langle\Psi_\Omega|\partial^2\Psi_{\Omega'}/\partial R^2\rangle \equiv 0$ are fulfilled, Ω denoting J projection on internuclear axis. Such a choice of electronic Hamiltonian corresponds to the so-called diabatic approximation. Thus, in the coupling case under consideration, each Ω component of an (a)-case multiplet is regarded as a separate electronic state with its own potential curve $E^\Omega(R)$, the different curves, however, being allowed to intersect each other. According to the described representation of zero-order Hamiltonian $\hat{\mathbf{H}}_0$, the perturbation operator $\hat{\mathbf{V}}$, which enters Eq. (11), is equal to

TABLE I. $3j$-symbols $\begin{pmatrix} J & k & J' \\ M & l & M' \end{pmatrix} = \begin{pmatrix} J' & k & J \\ -M' & -l & -M \end{pmatrix}$.

$\begin{pmatrix} J0J \\ -M0M \end{pmatrix}$	$(-1)^{J-M}\frac{1}{\sqrt{2J+1}}$
$\begin{pmatrix} J1J \\ -M0M \end{pmatrix}$	$\frac{(1-)^{J-M}M}{\sqrt{J(J+1)(2J+1)}}$
$\begin{pmatrix} J1J \\ -M-11M \end{pmatrix}$	$(1-)^{J-M}\sqrt{\frac{(J-M)(J+M+1)}{(J+1)(2J+1)2J}}$
$\begin{pmatrix} J1J+1 \\ -M0M \end{pmatrix}$	$(-1)^{J-M-1}\sqrt{\frac{(J+1)^2-M^2}{(2J+3)(J+1)(2J+1)}}$
$\begin{pmatrix} J1J+1 \\ -M-11M \end{pmatrix}$	$(-1)^{J-M-1}\sqrt{\frac{(J-M)(J-M+1)}{(2J+3)(2J+2)(2J+1)}}$
$\begin{pmatrix} J2J \\ -M0M \end{pmatrix}$	$\frac{(-1)^{J-M}[3M^2-J(J+1)]}{\sqrt{(2J+3)(J+1)(2J+1)J(2J-1)}}$
$\begin{pmatrix} J2J \\ -M-11M \end{pmatrix}$	$(-1)^{J-M}(2M+1)\sqrt{\frac{6(J+M+1)(J-M)}{(2J+3)(2J+2)(2J+1)2J(2J-1)}}$
$\begin{pmatrix} J2J+1 \\ -M0M \end{pmatrix}$	$(-1)^{J-M+1}M\sqrt{\frac{3[(J+1)^2-M^2]}{(J+2)(2J+3)(J+1)(2J+1)J}}$
$\begin{pmatrix} J2J+1 \\ -M-11M \end{pmatrix}$	$(-1)^{J-M+1}2(J+2M+2)\sqrt{\frac{(J-M+1)(J-M)}{(2J+4)(2J+3)(2J+2)(2J+1)2J}}$
$\begin{pmatrix} J2J+2 \\ -M0M \end{pmatrix}$	$(-1)^{J-M}M\sqrt{\frac{6[(J+2)^2-M^2][(J+1)^2-M^2]}{(2J+5)(2J+4)(2J+3)(2J+2)(2J+1)}}$
$\begin{pmatrix} J2J+2 \\ -M-11M \end{pmatrix}$	$2(-1)^{J-M}\sqrt{\frac{(J+M+2)(J-M+2)(J-M+1)(J-M)}{(2J+5)(2J+4)(2J+3)(2J+2)(2J+1)}}$

$$\hat{V}=\hat{V}_{el}(R,r_i)+B(R)J_a^2-2B(R)JJ_a\equiv\hat{V}_{hom}+\hat{V}_{het}, \quad (21)$$

where $\hat{V}_{el}(R,r_i)$ is the part of full electronic Hamiltonian which is not included into $\hat{H}^0_{el}(R,r_i)$, while the remaining terms appear from the rotational part of Hamiltonian due to the fact that pure rotational momentum N is constructed from J and J_a as $N=J-J_a$. First and second terms in Eq. (21) do not depend on J explicitly and, consequently, the matrix elements of these operators follow selection rule $\Delta\Omega=0$, thus defining the homogeneous interaction $\hat{V}_{hom}$. The third term in Eq. (21) is linearly dependent on J and, hence, obeys the $\Delta\Omega=\pm1$ selection rule. As a result, according to selection rules over Ω, the intramolecular perturbation operator $\hat{V}$ is divided into respective *homogeneous* $\hat{V}_{hom}$ ($\Delta\Omega=0$) and *heterogeneous* $\hat{V}_{het}$ ($\Delta\Omega=\pm1$) parts.

The symmetrized basis eigenfunctions $|\Phi JM\rangle$ corresponding to the coupling case under consideration are:

$$|\Phi JM\rangle=\frac{|\Psi_\Omega\rangle}{\sqrt{2}}|v_J\rangle[|\Omega JM\rangle\pm|-\Omega JM\rangle], \quad (22)$$

and for the special case $\Omega=0$:

$$|\Phi JM\rangle=|\Psi_\Omega\rangle|v_J\rangle|\Omega JM\rangle. \quad (23)$$

The vibrational eigenfunction $|v_J\rangle$ is obtained via solution of the radial Schrödinger equation with corresponding effective internuclear potential $U_J^\Omega(R)$:

$$-\frac{1}{2\mu}\frac{d^2|v_J\rangle}{dR^2}+[U_J^\Omega(R)-E_{vJ}^\Omega]|v_J\rangle=0, \quad (24)$$

where $U_J^\Omega(R)=E_{el}^\Omega(R)+J(J+1)/2\mu R^2$ is an eigenvalue of the $\hat{H}^0_{el}(R,r_i)+B(R)J^2$ operator.

Then, rovibronic matrix elements of homogeneous ($\Delta\Omega=0$) and heterogeneous ($\Delta\Omega=1$) intramolecular interaction, see Eq. (21), which correspond to the chosen basis [see Eq. (22)], can be written as

$$\langle v_J^{\Omega'}|\hat{V}_{hom}^{\Omega\Omega'}(R)|v_J^\Omega\rangle, \quad (25)$$

for $\Omega'=\Omega$, and as

$$-\left\langle v_J^{\Omega'}\left|\frac{\eta_{het}^{\Omega\Omega'}(R)}{2\mu R^2}\right|v_J^\Omega\right\rangle\sqrt{J(J+1)-|\Omega|(|\Omega|\pm1)} \quad (26)$$

for $\Omega'=\Omega\pm1$, where

$$\eta_{het}^{\Omega\Omega'}(R)=\langle\Omega'|\hat{J}_{a\pm}|\Omega\rangle. \quad (27)$$

To obtain $\hat{H}_{pm}$ and $\hat{H}_{dm}$ operators dependence on Ω and J quantum numbers, we apply again Wigner–Eckart theorem, now in molecule fixed frame, in order to evaluate the reduced matrix elements which enter Eq. (18):

$$\langle J'\Omega'||\hat{f}^{(k)}||J\Omega\rangle \sim \begin{pmatrix} J' & kJ \\ -\Omega' & l\Omega \end{pmatrix} \langle \Omega'|\hat{f}_l^{(k)}|\Omega\rangle. \tag{28}$$

Considering $\hat{H}_{pm}^{(1)}$ with $k=1$, $l=\Delta\Omega=0,\pm1$, and $\hat{H}_{dm}^{(2)}$ with $k=2$, $l=\Delta\Omega=0,\pm1,\pm2$, we can get the following expressions for corresponding electronic matrix elements $\langle\Omega'|\hat{f}_l^{(k)}|\Omega\rangle$:

$$\Omega'=\Omega:\ \langle\Omega|\hat{H}_{pm}^{(1)}|\Omega'\rangle = g_l\Omega\delta_{\Omega\Omega'}+(g_s-g_l)\langle\Omega|\hat{S}_z|\Omega'\rangle \equiv G_z(R), \tag{29}$$

$$\Omega'=\Omega\pm1:\ \langle\Omega|\hat{H}_{pm}^{(1)}|\Omega'\rangle = g_l\langle\Omega|\hat{J}_{a\pm}|\Omega'\rangle+(g_s-g_l)\langle\Omega|\hat{S}_{\pm}|\Omega'\rangle \equiv G_{\pm}(R), \tag{30}$$

$$\Omega'=\Omega:\begin{cases}\langle\Omega|\hat{H}_{dm}^{(0)}|\Omega'\rangle=\dfrac{2}{3}\left\langle\Omega\left|\sum_i r_i^2\right|\Omega'\right\rangle\equiv h_{00}(R),\\ \langle\Omega|\hat{H}_{dm}^{(2)}|\Omega'\rangle=\left\langle\Omega\left|\sum_i\left(\dfrac{r_i^2}{3}-z_i^2\right)\right|\Omega'\right\rangle\equiv h_{20}(R),\end{cases} \tag{31}$$

$$\Omega'=\Omega\pm1:\ \langle\Omega|\hat{H}_{dm}^{(2)}|\Omega'\rangle = \left\langle\Omega\left|\sum_i (x_i\pm iy_i)z_i\right|\Omega'\right\rangle \equiv h_{21}(R), \tag{32}$$

$$\Omega'=\Omega\pm2:\ \langle\Omega|\hat{H}_{dm}^{(2)}|\Omega'\rangle = \left\langle\Omega\left|\sum_i (x_i\pm iy_i)^2\right|\Omega'\right\rangle \equiv h_{22}(R), \tag{33}$$

where $r_i=\{x_i,y_i,z_i\}$. Using Eqs. (24)–(30) we arrive at following conclusions, which are important for our further discussion:

(1) Homogeneous intramolecular perturbations ($\Delta\Omega=0$) are independent of J whereas the heterogeneous ones increase with J approximately as $[J(J+1)]^{1/2}$, see Eqs. (25), (26);
(2) Homogeneous ($\Delta\Omega=0$) magnetic interaction, caused by $\hat{H}_{pm}$ operator, decreases with J as $[J(J+1)]^{-1}$, whereas the heterogeneous ones decrease as $[J(J+1)]^{-1/2}$;
(3) Homogeneous mixing, caused by $\hat{H}_{pm}$ operator, appears only due to $\langle\Omega|\hat{S}_z|\Omega'\rangle$ term, which is small at least for small internuclear distances since at pure Hund's (a)-case coupling, when $\hat{S}_z$ is a good quantum number, this mixing is absent at all for $\Omega=\Omega'$ belonging to the different electronic states;
(4) Electronic matrix element $\eta(R)$ of the heterogeneous interaction, see Eq. (27), is a part of electronic matrix element of the paramagnetic term $G_{\pm}(R)$, see Eq. (30).

Proceeding from conclusions (1)–(3), one can expect that, for large J values, the heterogeneous interaction, both intramolecular and magnetic, will be more pronounced than the homogeneous one. To simplify our further treatment, we will assume that:

(i) all electronic matrix elements, corresponding to $\hat{V}$, $\hat{H}_{pm}$, and $\hat{H}_{dm}$ operators, are independent of internuclear distance R;
(ii) vibrational wavefunctions belonging to the same vibronic state are coinciding for adjacent J values, namely
$$|v_i^{J+1}\rangle \cong |v_i^{J}\rangle \cong |v_i^{J-1}\rangle. \tag{34}$$

In particular, the above assumptions (i) and (ii) lead to the following relation: $\langle v_i|\hat{G}_z(R)|v_j\rangle = G_z\delta_{v_iv_j}$, where v_i, v_j belong to the same electronic state.

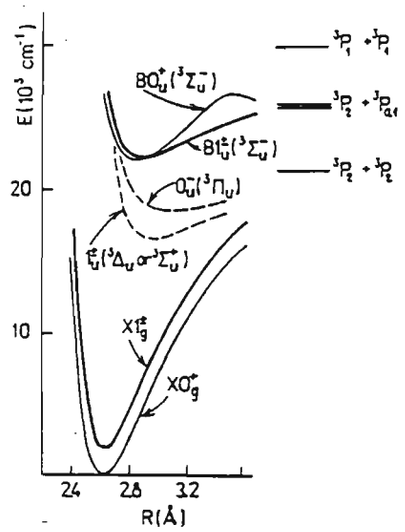

FIG. 1. The pattern of some Te_2 electronic states involved into consideration.

IV. Te_2 TERM PATTERN

Before passing to signal simulation, it is necessary to concentrate briefly onto main features of electronic structure of the molecule under investigation (the even Te_2 isotope will be beard in mind). The detailed inspection of $B\ ^3\Sigma_u^-$ terms of Te_2 molecule is presented in our recent paper,[15] see also references therein. We will further keep ourselves to the term structure as proposed in Ref. 15, that is supposing that the closely located bonded $B0_u^+$ and $B1_u^{\pm}$ states, see Fig. 1, belong basically to the $B\ ^3\Sigma_u^-$ state complex. It is necessary to consider the interaction of $B1_u^+ \sim B0_u^+$ states caused by electron-rotation interaction. The matrix element $h_{het}^{\Omega\Omega'}$ [see Eq. (27)] of such heterogeneous interaction was determined as $\eta\cong1.35$ from unified self-consistent treatment of energetic, magnetic and radiative measurement data.[15]

It is important to mention that $B1_u^{\pm}$ state PD in Te_2 molecule was observed directly as a diminution of spontaneous lifetime with v growing for v_i from 2 up to 8 and J from 52 up to 181, see Table II. Note that all these $B1_u^{\pm}$ state

TABLE II. Experimentally measured (τ_{sp}^{exp}) and theoretically estimated (τ_{sp}^{est}) spontaneous lifetimes of $v(J)$ levels of 1_u^- and 1_u^+ components of $B\,^3\Sigma_u^-$ state of $^{130}Te_2$.

Term	v	J	τ_{sp}^{exp} (ns)	τ_{sp}^{est} (ns)
	2	86	107 (7)	109
	2	96	117(11)	120
1_u^-	4	52	49 (4)	112
	8	70	10 (2)	121
	4	111	66 (5)	115
1_u^+	5	131	45 (6)	120
	8	181	14 (2)	133

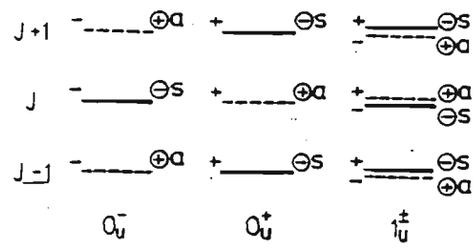

FIG. 2. Symmetry of rovibronic states of Te_2 molecule. The even tellurium isotope and even J value are considered. Dashed lines denote the forbidden states. Symbols +/−, or e/f in different notation, refer to electronic parity, symbols ⊕/⊖ refer to full parity, s/a refer to symmetric/antisymmetric states.

levels are situated below the $^3P_2+^3P_{0,1}$ dissociation limit (ca. 26 000 cm^{-1}), which means that the state responsible for PD must approach $^3P_2+^3P_2$ ground electronic state limit. It has been supposed that PD of the $B\,1_u^{\pm}$ state levels belongs to the so-called c^- classification type after Mulliken,[23] emerging through a repulsive part of bonded 1_u and/or 0_u states, see Fig. 1. This mechanism follows, in particular, from the weakness of PD while speaking of the $v=2$, $J=96$ level of 1_u^- component of the $B\,^3\Sigma_u^-$ state, which can be proved, in particular, by the existing experimental lifetime data given in Table II. The experiments were performed by laser-induced fluorescence method, using $(v''=4,\ J''=95)X1_g^- \rightarrow (v'=2,\ J'=96)B1_u^-$ absorption of 514.5 Ar^+-laser line.[11,15] The estimated[15] value of spontaneous lifetime τ_{sp} is ca. 110–130 ns.

All possible electronic states approaching $^3P_2+^3P_2$ dissociation limit in (c)-Hund's coupling case are: $0_g^+(3),0_u^-(2),1_g(2),1_u(2),2_g(2),2_u,3_g,3_u,4_u$.[24] Hence, due to the $\Delta\Omega=0,\pm1$, $u\leftrightarrow g$ selection rules for intramolecular interaction, only states 2_u^-, $0_u^-(2)$ or $1_u^-(2)$ approaching $^3P_2+^3P_2$ limit may be responsible for natural heterogeneous or homogeneous very weak $B1_u^-$ state PD. It is worth to mention that, as distinct from the well investigated $B\,^3\Sigma_u^-$ complex, no one of the above discussed electronic states, which could be responsible for natural PD of the $B1_u^-$ state, had been observed in spectroscopic measurements, and the reliable information on molecular constants and potential curves does not exist for them. The only existing publication[16] deals with relativistic *ab initio* evaluation of low lying electronic terms of Te_2 molecule. Unfortunately, the paper[16] does not contain spin–orbit and spin–spin splitting parameters of $^3\Sigma_u^+$, $^3\Pi_u$, and $^3\Delta_u$ terms, the Ω components under discussion are most likely originating from. Therefore we were forced to perform crude estimations of relative location of these components by using the semiempirical scheme described in Ref. 19, which is based on the knowledge of leading electronic configuration of $^3\Sigma_u^+$, $^3\Pi_u$, and $^3\Delta_u$ states, as well as on the empirical spin–orbit constants of separated atoms, which the above molecular terms are converging to at $R\rightarrow\infty$. This allowed us to conclude that the electronic states responsible for $B1_u^-$ state PD, which are most preferable from energy consideration, are the 0_u^- component originating from the $^3\Pi_u$ state and the $1_u^{\pm}$ components originating from $^3\Sigma_u^+$ or/and $^3\Delta_u$ states, see Fig. 1. We therefore will restrict ourselves with taking into account in PD treatment $B1_u^-\sim0_u^-$ and $B1_u^-\sim1_u^{\pm}$ interactions only. Since 0_u^- term originates from $^3\Pi_u$, while, $1_u^{\pm}$ term originates from $^3\Sigma_u^+$ or $^3\Delta_u$, we are able to evaluate the order of magnitude of Franck–Condon factors density (FCD) entering expressions for PD rate, see Sec. V.

The symmetry of rovibronic levels of even isotope Te_2 molecule can be understood from Fig. 2, where J is considered to be an even number. Symbols + or −, which correspond to e or f notation respectively, stand for electronic parity, while circled signs ⊕ or ⊖ refer to total parity. Since nuclear spin is zero, all antisymmetric (a) levels disappear.

V. SIGNAL SIMULATION AND DATA PROCESSING

Now we are going to use the theory presented in Secs. II and III in order to simulate fluorescence signals of different polarization, see Eq. (6), including the appearance of fluorescence circularity, see Eq. (9), for the conditions which are relevant to Te_2 molecule $B1_u-\rightarrow X1_g^-$ fluorescence (see Sec. IV) in external magnetic field.

A. Zeeman energy shift, or $\omega_{MM'}$ contribution

Let us first adapt the theory developed in Sec. III to describe the magnetic field dependence of fluorescence polarization and circularity caused by different-order terms in Zeeman effect induced energy shift E_M, see Eq. (14), as appropriate for Te_2 $B1_u^-$ state. Applying Wigner–Eckart theorem, first in laboratory coordinate system, see Eq. (18), and after that in molecular coordinate system, see Eq. (28), accounting for explicit $3j$-symbols formulas (Table I) and implementing vibrational and electronic parts of matrix elements defined by Eqs. (25), (26) and (29)–(33), we arrive at the following energy E_M expressions for the linear paramagnetic term (LPT) and for the high-frequency term (HFT):

$$E_{LPT}(M,B)=\langle\Phi_p JM|\hat{H}_{pml}|\Phi_p JM\rangle=-\frac{\mu_B BMG_z}{J(J+1)}, \qquad (35)$$

$$E_{\mathrm{HFT}}(M,B)=\sum_{\Phi_p'J'}\frac{|\langle\Phi_pJM|\hat{\mathbf{H}}_{\mathrm{pm}}|\Phi_p'J'M\rangle|^2}{E_M^{\Phi J}-E_M^{\Phi' J'}}=\frac{\mu_B^2B^2}{2}\left\{\frac{G_z^2}{B_v}\left[\frac{(J^2-1)T(J,M)(1+\eta G_{\pm}JS_0/G_z)^2}{J^3}\right.\right.$$
$$-\frac{((J+1)^2-1)T(J+1,M)(1-\eta G_{\pm}(J+1)S_0/G_z)^2}{(J+1)^3}\Bigg]+\frac{G_{\pm}^2}{B_v}\left[\frac{JT(J+1,M)}{J+1}\left(S_1-\frac{2G_z\eta S_3}{G_{\pm}(J+1)}\right)\right.$$
$$\left.\left.+\frac{(J+1)T(J,M)}{J}\left(S_2+\frac{2G_z\eta S_4}{G_{\pm}J}\right)\right]\right\}=E_{\mathrm{HFT}}^0+E_{\mathrm{HFT}}^{\mathrm{int}},\tag{36}$$

where $E_{\mathrm{HFT}}^{\mathrm{int}}$ contains the summands proportional to $G_{\pm}G_z$, whereas E_{HFT}^0 coincides with the previous treatment,[11] which was accomplished without accounting for wave function mixing caused by intramolecular perturbation operator η_{het}, see Eq. (26). The $T(J,M)$ and S_i have the following meaning:

$$T(J,M)=\frac{J^2-M^2}{4J^2-1},\tag{37}$$

$$S_0=\sum_{v_0^J}\frac{\langle v_1^J|v_0^J\rangle\langle v_0^J|B(R)|v_1^J\rangle}{E_1^{vJ}-E_0^{vJ}},\tag{38}$$

$$S_1=\sum_{v_0^J}\frac{|\langle v_1^J|v_0^{J+1}\rangle|^2}{E_1^{vJ}-E_0^{vJ+1}},\tag{39}$$

$$S_2=\sum_{v_0^J}\frac{|\langle v_1^J|v_0^{J-1}\rangle|^2}{E_1^{vJ}-E_0^{vJ-1}},\tag{40}$$

$$S_3=\sum_{v_0^J}\frac{\langle v_1^J|v_0^{J-1}\rangle\langle v_0^J|B(R)|v_1^J\rangle}{(E_1^{vJ}-E_0^{vJ-1})(E_0^{vJ}-E_1^{vJ})},\tag{41}$$

$$S_4=\sum_{v_0^J}\frac{\langle v_1^J|v_0^{J+1}\rangle\langle v_0^J|B(R)|v_1^J\rangle}{(E_1^{vJ}-E_0^{vJ+1})(E_0^{vJ}-E_1^{vJ})},\tag{42}$$

and B_v is rotational constant. The diamagnetic term (DMT) takes the form:

$$E_{\mathrm{DMT}}(M^2,B^2)=\langle\Phi_pJM|\hat{\mathbf{H}}_{\mathrm{dm}}|\Phi_pJM\rangle$$
$$=K_{\mathrm{dm}}B^2\left\{h_{00}+\frac{J(J+1)-3M^2}{(2J-1)(2J+3)}\times\left[h_{22}+h_{20}\left(1-\frac{3}{J(J+1)}\right)\right]\right\}.\tag{43}$$

Thus, the closed form of Zeeman energy E_M, given by Eq. (19), in the case of $B1_u^-$ state with fixed v,J,M values can be written as

$$E(B1_u^-,v,J,M)=E_{\mathrm{LPT}}(M,B)+E_{\mathrm{HFT}}(M^2,B^2)+E_{\mathrm{DMT}}(M^2,B^2),\tag{44}$$

where E_{LPT} is linear over M and B, while E_{HFT} and E_{DMT} are quadratic functions of M and B, as defined by the expressions (35)–(43).

In order to determine the $\omega_{MM'}$ values, which govern fluorescence intensities, see Eqs. (9) and (10), let us evaluate the parameters necessary to calculate the energy E_M. The G_z defined by Eq. (29) is the only factor determining the linear LPT term; its numerical value will be taken as $G_z=-1.86$ according to the measurements in Refs. 15 and 25. In signal simulation we will assume $G_{\pm}=2.7=2\eta$ in consistence with the previous data obtained in Refs. 11 and 15. The negative G_z sign for a state with $\Omega=1$ means that we assume that the magnetic moment μ_J possesses the opposite direction with respect to J, the precession angular velocity being equal to $\omega_J=-G_z\mu_BB/[J(J+1)\hbar]$. Rotational constant value $B_{v=2}^{1_u^-}=0.031\,61\ \mathrm{cm}^{-1}$ has been taken from Ref. 14. The S_i values given by Eqs. (38)–(42) were calculated numerically using vibrational wave functions $|v_J\rangle$ obtained by solving Eq. (24) with RKR potentials constructed by means of deperturbed molecular constant sets given in Ref. 15 for $1_u^{\pm}$ and 0_u^+ components of $B\,^3\Sigma_u^-$ state of $^{130}Te_2$. The results (in $1/\mathrm{cm}^{-1}$) for the $v(J)$ level 2(96) of the 1_u^- state have been obtained, accounting for Eq. (34), as: $S_0=-7.2\times10^{-4}$, $S_1=-1.9\times10^{-2}$, $S_2=-2.9\times10^{-2}$, $S_3=-3.14\times10^{-5}$, $S_4=-2.05\times10^{-5}$. It can be seen from S_i values obtained that the main contribution in the first brackets of Eq. (36) is given by the part of interference term proportional to $G_{\pm}G_zS_0$, namely

$$E_{\mathrm{HFT}}^{\mathrm{int}(S_0)}=\frac{2\eta G_{\pm}G_zS_0}{B_v}\left[\frac{J^2-1}{J^2}T(J,M)+\frac{(J^2+1)^2-1}{(J+1)^2}T(J+1,M)\right],\tag{45}$$

which is comparable with the terms in the second brackets of Eq. (36), containing S_1 and S_2.

Let us now try to evaluate the electronic parameters h_{00}, h_{20}, and h_{22} of the DMT, see Eq. (43), which are given by Eqs. (31)–(33). In order to obtain crude evaluation of the order of magnitude of h_{00}, we will assume that the $B\,^3\Sigma_u^-$ complex in Te_2 is of partially Rydberg nature. Then one can estimate the h_{00} value (in a.u.) as $h_{00}=\Sigma_{n=1}^{6}(n^2/2)[5n^2+1-3l(l+1)]$. Taking into account that the atomic configuration of Te atom is $5s^25p^4$, while in the united atom limit Te_2 approaches the ^{104}Ku configuration $6d^27s^2$, we can estimate the upper limit for h_{00} as being somewhere from 10^4 a.u. to 10^5 a.u. Further, we will assume that, for the Te_2 case considered, as well as for the overwhelming majority of diatomic molecules,[26] the h_{20} and h_{22} values do not exceed several a.u. Using these estimations of electronic parameters h_{00}, h_{20}, and h_{22} and comparing expressions for LPT, HFT, and DMT terms given by Eqs. (35)–(43), it is easy to con-

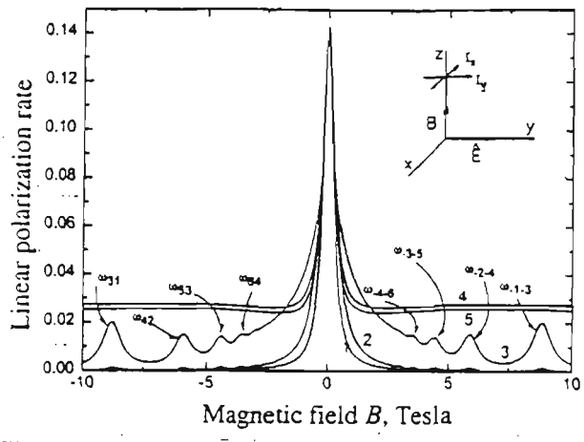

FIG. 3. Calculated magnetic field dependence $P(B)$ of the degree of linear polarization of fluorescence (the geometry is shown in the setting-in). 1—ordinary Lorentz shape Hanle signal in case of linear Zeeman effect term LPT, see Eq. (35); 2—accounting for LPT and for nonlinear Zeeman term HFT, see Eq. (36); 3—accounting for LPT, HFT, homogeneous and heterogeneous magnetic PD; 4—accounting for LPT, heterogeneous and homogeneous magnetic PD; 5—accounting for LPT and heterogeneous magnetic PD. The PD parameters used in calculations are $C_0^{het} = -6\ s^{-1/2}$, $\alpha_0^{het} = 10^4\ s^{-1/2}\ T^{-1}$, $C_0^{hom} = 10^3\ s^{-1/2}$ and $\alpha_0^{hom} = 10^3\ s^{-1/2}\ T^{-2}$.

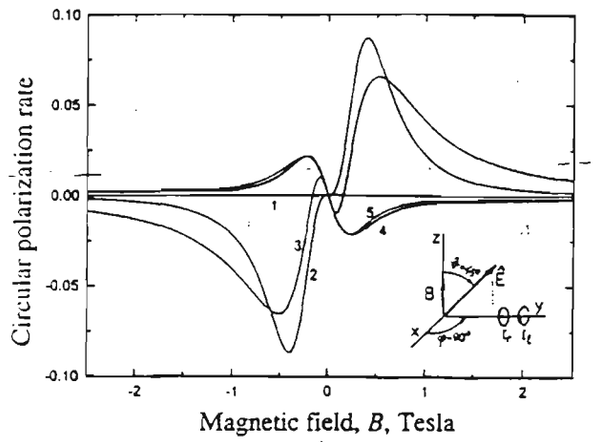

FIG. 4. Calculated magnetic field dependence $C(B)$ of the degree of fluorescence circular polarization, or AOC signal (the geometry is shown in the setting-in). Curves 1–5 are calculated accounting for the same effects as in Fig. 3, respectively.

clude that one can neglect the DMT contribution in the Eq. (44). It is interesting to mention that for low-lying electronic states of diatomic molecules the HFT and DMT values are, as a rule, quite comparable with each other.[26] The latter is caused by the circumstance that, in spite of the fact that diamagnetic constant K_{dm} value in Eq. (13) is approximately 10^4 times smaller than μ_B^2 value in Eq. (12), the large enough energy difference $E_M^{\Phi J} - E_M^{\Phi' J}$ makes the HFT and DMT contributions comparable with each other. As a contrary, in our case of $B\ ^3\Sigma_u^-(Te_2)$ complex we have $E_M^{|\Omega|=1} - E_M^{\Omega=0}$ equal to ca. 13 cm^{-1} only, which leads to $\mu_B^2/(E_M^{|\Omega|=1} - E_M^{\Omega=0}) \gg K_{dm}$ and well explains the smallness of the diamagnetic term DMT with respect to HFT.

Let us start with the simulation of a signal appearing in the experimental geometry, which is traditional for Hanle effect manifestation as decrease of fluorescence linear polarization $P(B)=(I_y-I_x)/(I_y+I_x)$ under external magnetic field effect, see Fig. 3. We assume that $\Gamma_{MM'}$ in Eqs. (9) and (10) possesses a constant value $\Gamma_{MM'} \equiv \Gamma$, being independent of magnetic field, which means the absence of anisotropic collisions (see discussion in Refs. 4 and 12) and of magnetic PD. In particular, the value $\Gamma=8.55\times10^6\ s^{-1}$ was used as determined in Refs. 15 and 27. Curve 1 in the figure corresponds to the "traditional" Hanle signal of Lorentz shape, which appears in the case of linear Zeeman effect containing LPT only, that is when all B^2-dependent terms are neglected in Eq. (44). Accounting for the HFT in the form given by Eq. (36) produces the signal depicted by curve 2 in Fig. 3, which demonstrates the slightly less steepness if compared with curve 1. Additional maxima of very small amplitude can be distinguished on curve 2 in high B region, that is when the fluorescence is already almost completely depolarized by the linear Zeeman effect. These maxima have apparently to be connected with the crossings of magnetic M sublevels with $|M-M'|=2$ caused by nonlinear Zeeman effect.

We will now proceed to the appearance of the degree of circularity $C(B)$, see Eqs. (7), (9), (10), caused by B^2 terms in E_M, when the condition (4) for $\omega_{MM'}$ is fulfilled. The geometry of excitation and observation of fluorescence is shown in Fig. 4 and is consistent with $\vartheta=45°$, $\varphi=90°$ in Eqs. (9) and (10). Curves 1 and 2 in Fig. 4 are calculated for the same $E_M(B)$ dependencies as discussed above in connection with Fig. 3. Curve 1 in Fig. 4 is strictly zero since linear Zeeman effect is not able to cause AOC.[4,12] Curve 2 demonstrates a pronounced AOC phenomenon caused by quadratic Zeeman effect term HFT given by Eq. (36). It is important to stress that such $C(B)$ signal is an odd function of B, having zero derivative at $B=0$. The last feature can be clearly seen from the Fig. 5, curve 2, which is the same curve depicted in

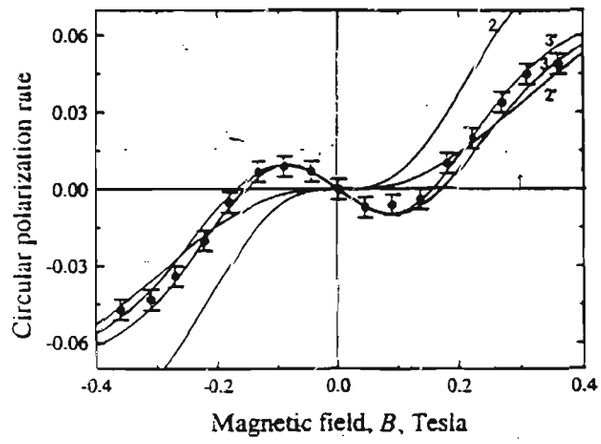

FIG. 5. Fitting of experimentally obtained AOC signal in $C(B)$ at the same geometry as in Fig. 4. Curves 1–3 are the same as in Fig. 4. Curve 2' ignores the interference term E_{HFT}^{int} in quadratic Zeeman effect, see Eq. (36), while curve 3' differs from curve 3 by ignoring homogeneous PD. The parameters obtained by fitting are: $C_0^{het} = -6\ s^{-1/2}$, $\alpha_0^{het} = 9\times10^3\ s^{-1/2}\ T^{-1}$, $G_z = 2.7$.

enlarged scale. Curve 2 in Fig. 5 differs markedly from the signal depicted by curve 2′ in Fig. 5, which was calculated without accounting for $E^{\rm int}_{\rm HFT}$ in Eq. (36), as it had taken place in our previous treatment[11] [unfortunately the sign of G_z in formulas (3), (11) and (13) of Ref. 11 is inconsistent with the definition of G_z following from Eqs. (1) and (4) of Ref. 11]. The major difference between curves 2 and 2′ in Fig. 5 ensures one of the important role of the interference term $E^{\rm int}_{\rm HFT}$ appearing because of $B1^+_u \sim B0^+_u$ wave function mixing by electron–rotation perturbation operator $\hat{\mathbf{V}}$, see Eq. (17). Figure 5 contains also the experimental results (depicted by black circles) taken from Ref. 11. And what is important, the results of the more complete treatment, presented by curve 2, is much farther from describing the experimental points. Moreover, in any choice of fitting parameters (which would lead into contradiction with independently obtained results of Ref. 15), the calculation based on quadratic Zeeman energy shift terms, or on $\omega_{MM'}$ contribution only, are not able to reproduce the additional extrema of experimental $C(B)$ values near $B=\pm 0.1$ T, see Fig. 5.

B. Magnetic PD effect, or $\Gamma_{MM'}$ contribution

Let us now account for $\Gamma_{MM'}$ dependence on magnetic field caused by magnetic field induced PD. We will consider the cases of homogeneous and heterogeneous PD separately, accounting for $1^-_u \sim 1^\mp_u$ and $1^-_u \sim 0^-_u$ interactions respectively, according to the discussion in Sec. IV. Then, adapting again the theory developed in Sec. III, we are able to obtain the explicit formulas for the matrix elements which describe $1^-_u \sim 1^\mp_u$ and $1^-_u \sim 0^-_u$ magnetic PD in Γ_M expression (15). In doing so, for homogeneous PD $1^-_u \sim 1^\mp_u$, one can obtain, by applying Eqs. (18), (29) and Table I, the following expressions for $\hat{\mathbf{H}}_{\rm pm}$ operator matrix elements with $\Omega=\Omega'$:

$$\langle \Omega JM|\hat{\mathbf{H}}_{\rm pm}|\Omega JM\rangle = -\frac{\mu_B {\rm BMG}_z}{J(J+1)}, \tag{46}$$

$$|\langle \Omega JM|\hat{\mathbf{H}}_{\rm pm}|\Omega J-1M\rangle|^2 = \mu_B^2 B^2 G_z^2 \frac{J^2-1}{J^2} T(J,M), \tag{47}$$

where $T(J,M)$ is given by Eq. (37). Analogously, for heterogeneous PD $1^-_u \sim 0^-_u$, the $\hat{\mathbf{H}}_{\rm pm}$ operator matrix elements with $\Omega'=\Omega\pm 1$ can be found, by accounting for Eq. (30), as

$$\langle \Omega JM|\hat{\mathbf{H}}_{\rm pm}|\Omega' JM\rangle = \frac{\mu_B {\rm BMG}_\mp}{\sqrt{J(J+1)}}, \tag{48}$$

whilst the nonzero diamagnetic $\hat{\mathbf{H}}_{\rm dm}$ operator matrix elements can be found, by applying Eqs. (18), (32) and Table I, as

$$\langle \Omega JM|\hat{\mathbf{H}}_{\rm dm}|\Omega' JM\rangle = K_{\rm dm}\frac{B^2 h_{21}}{2}\frac{1}{\sqrt{J(J+1)}}\left[\frac{-J(J+1)+3M^2}{(2J-1)(2J+3)}\right]. \tag{49}$$

Note that for the $1^-_u \sim 0^-_u$ case the interaction matrix elements $\langle \Omega JM|\hat{\mathbf{H}}_{\rm pm}|\Omega' J\pm 1M\rangle$ disappear.

Putting the expressions obtained into Eq. (15) and taking into account the fact that the rovibronic matrix elements of intramolecular interaction can be described by Eqs. (25)–(27), we arrive at final expressions in explicit form:

$$\Gamma^{\rm hom}_M(1^-_u \sim 1^\mp_u) \cong 2\pi|\langle v_J|\epsilon_J\rangle|^2\left[V^2_{\rm hom} - \frac{2\mu_B BMV_{\rm hom}G_z}{J(J+1)} + \frac{\mu_B^2 B^2 G_z^2}{2}\left\{1-\left(\frac{4M^2}{J(J+1)}-\frac{3(4M^2-1)}{(2J-1)(2J+3)}\right)\right\}\right.$$
$$\left. + 2K_{\rm dm}B^2 V_{\rm hom}\left\{h_{00}+\left(h_{22}+h_{20}\left(1-\frac{3}{J(J+1)}\right)\right)\frac{J(J+1)-3M^2}{(2J-1)(2J+3)}\right\}\right] \equiv C_v^2 - \frac{2BMC_v\alpha_v}{J(J+1)} + \frac{B^2\alpha_v^2}{2}\left[1\right.$$
$$\left. -\left(\frac{4M^2}{J(J+1)}-\frac{3(4M^2-1)}{(2J-1)(2J+3)}\right)\right] + 2B^2 C_v\left\{\beta_v^{(0)}+\left[\beta_v^{(1)}+\beta_v^{(2)}\left(1-\frac{3}{J(J+1)}\right)\right]\frac{J(J+1)-3M^2}{(2J-1)(2J+3)}\right\}, \tag{50}$$

$$\Gamma^{\rm het}_M(1^-_u \sim 0^-_u) \cong 2\pi\left[\langle v_J|\epsilon_J\rangle\right|^2\left\{\frac{2\eta^2 J(J+1)}{(2\mu R_c^2)^2}+\frac{2\mu_B BM\eta G_\mp}{2\mu R_c^2}+\frac{\mu_B^2 B^2 M^2 G_\mp^2}{2J(J+1)}-\frac{K_{\rm dm}B^2\eta h_{21}}{2\mu R_c^2}\left(\frac{3M^2-J(J+1)}{(2J-1)(2J+3)}\right)\right\}$$
$$\equiv 2C_v^2 J(J+1)+2C_v\alpha_v BM+\frac{\alpha_v^2 B^2 M^2}{2J(J+1)}-\beta_v^{(3)}C_v B^2\left(\frac{J(J+1)-3M^2}{(2J-1)(2J+3)}\right), \tag{51}$$

where $|\langle v_J|\epsilon_J\rangle|^2$ are the Franck–Condon densities (FCD), R_c is the crossing point of the two potential curves, see Fig. 1, $\beta_v^{(i)}$ are the diamagnetic PD constants, $V_{\rm hom}$ and $\eta \equiv \eta_{\rm het}$ are the electronic parts of the matrix elements of homogeneous and heterogeneous intramolecular interactions, respectively. It is important that all these parameters are independent of M, B, and J in explicit form. We have passed in the second part of Eqs. (50) and (51) to the following traditional notations: C_v is the natural PD constant,

$$C_v^{\rm hom} = \sqrt{2\pi}\langle v_J|\epsilon_J\rangle V_{\rm hom}, \quad C_v^{\rm het} = \sqrt{2\pi}\langle v_J|\epsilon_J\rangle\frac{\eta}{2\mu R_c^2}, \tag{52}$$

whilst α_v is the constant of paramagnetic PD.

$$\alpha_v^{\text{hom}} = \sqrt{2\pi}\langle v_J|\epsilon_J\rangle \mu_B G_z, \quad \alpha_v^{\text{het}} = \sqrt{2\pi}\langle v_J|\epsilon_J\rangle \mu_B G_{\pm}. \tag{53}$$

It can be easy seen that the relations obtained are consistent with the general expression given by Eq. (20). From Eqs. (50) and (51) one can also conclude that for $J \gg 1$ the contribution into Γ_M of the term describing interference between natural and magnetic PD, which is proportional to $C_v \alpha_v$ and linear over BM, is negligible in the case of homogeneous PD when compared to the case of heterogeneous PD. This can be explained by the presence of the factor $1/[J(J+1)]$ in Eq. (50), as distinct from Eq. (51).

Let us now try to estimate the values of C_v, α_v, and $\beta_v^{(i)}$ parameters in Eqs. (50)–(53) for the case of $B1_u^-$ state PD in Te_2. We will start with FCD $|\langle v_J|\epsilon_J\rangle|^2$ evaluation based on Morse shape approximation of 0_u^- and $1_u^{\pm}$ potential curves responsible for the PD. In doing so, we have used vibrational constant ω_e values given in Ref. 16 for $^3\Pi_u$, $^3\Sigma_u^+$, and $^3\Delta_u$ states. The anharmonic constant $\omega_e x_e$ values were estimated from the knowledge of electronic Te_2 terms for these states, as well as from the $^3P_2 + {}^3P_2$ dissociation limit. The equilibrium internuclear distance R_e values for the states under discussion were chosen in the way to provide the condition that intersections of the respective 0_u^- and $1_u^{\pm}$ potential curves with the repulsive branch of the RKR $B1_u^{\pm}$ state potential curve are taking place at reasonable R_c values, namely $2.6\ \text{Å} \leqslant R_c < R_e^{B1_u}$ which correspond to the Mulliken's c^--type PD.[23] The energy-normalized vibrational wave functions $|\epsilon_J\rangle$, belonging to continuum spectrum, were calculated by numeric solving of Eq. (24). As a result, the following FCD estimations were obtained: 10^{-4}–10^{-6} l/cm^{-1} for $B1_u^- \sim 0_u^-$ PD and 10^{-6}–10^{-8} l/cm^{-1} for $B1_u^- \sim 1_u^{\pm}$ PD. The $\hbar^2/2\mu R_c^2$ value is of the order of 0.1 cm^{-1}. Since the natural PD rate of the level can not exceed its reciprocal lifetime τ_{vJ}^{-1}, which is given in Table II, one can easy obtain the following estimations of natural PD rates upper limits: $|C_v^{\text{het}}| \leqslant 60\ \text{s}^{-1/2}$ and $C_v^{\text{hom}} \leqslant 10^3\ \text{s}^{-1/2}$. Let us also suppose that the h_{21} values entering Eq. (50) do not exceed 10^2 a.u., while the values of G_z and $G_{\pm}$ are of the order of one a.u. Then we arrive at the following estimations: $\alpha_v^{\text{hom}} \cong 10^2$–$10^3\ \text{s}^{-1/2}\,\text{T}^{-1}$, $\alpha_v^{\text{het}} \cong 10^3$–$10^4\ \text{s}^{-1/2}\,\text{T}^{-1}$, $\beta_v^{(0)} \leqslant 10^2\ \text{s}^{-1/2}\,\text{T}^{-2}$, $\beta_v^{(1)} \cong \beta_u^{(2)} \leqslant 1\ \text{s}^{-1/2}\,\text{T}^{-2}$, $\beta_v^{(3)} \leqslant 10^{-2}\ \text{s}^{-1/2}\,\text{T}^{-2}$. Thus, if our electronic parameter estimations are correct, we can well neglect the diamagnetic term contribution into Γ_M, see Eqs. (50) and (51), as it had been done in the case of E_M calculations.

Let us pass to PD signals simulations. Figure 6 demonstrates the circularity signals caused exclusively by PD effect, or by $\Gamma_{MM'}$ contribution. Calculations were performed by using the above estimated values of C_v and α_v for either heterogeneous (curve 1) or homogeneous (curve 2) PD. The calculations are made by putting Eq. (50) or Eq. (51), respectively, into expression (3) for $\Gamma_{MM'}$, which enters Eqs. (8)–(10), under assumption that $\omega_{MM'}$ is independent of M, which means that we neglect B^2 terms in Eq. (44) or, equivalently, we neglect $\omega_{MM'}$ contribution into AOC. As it can be seen, the heterogeneous PD produces a pronounced dispersion type circularity signal, whereas the AOC signal produced by homogeneous PD is almost nonobservable.

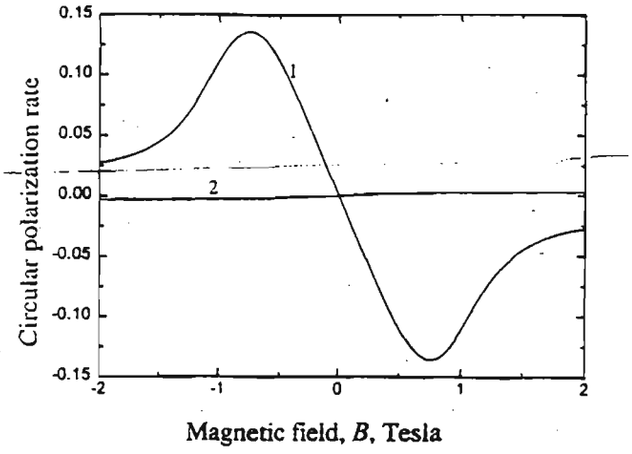

FIG. 6. Comparison of AOC signals in fluorescence circularity $C(B)$ caused by heterogeneous (curve 1) and homogeneous (curve 2) PD, calculated with maximal C_v, α_v values, namely $C_v^{\text{hom}} = |C_v^{\text{het}}|\sqrt{2J(J+1)} \cong 8.2 \times 10^3\ \text{s}^{-1/2}$, $\alpha_v^{\text{hom}} = 10^3\ \text{s}^{-1/2}\,\text{T}^{-1}$, $C_v^{\text{het}} = -60\ \text{s}^{-1/2}$, $\alpha_v^{\text{het}} = 10^4\ \text{s}^{-1/2}\,\text{T}^{-1}$. Geometry and other parameters are the same as in Figs. 4 and 5.

It is interesting to trace the PD manifestation in wide B range Hanle signals $P(B)$, see Fig. 3. Curves 4 and 5 in Fig. 3 demonstrate the distortion of Lorentz's shape Hanle signal, which is caused by magnetic PD only, that is when the B^2 terms are neglected in $\omega_{MM'}$ calculations. It seams that the remaining nonzero degree of polarization at large B values, see curves 4 and 5, is caused by such $\Gamma_{MM'}$ growing with B which does not change much the $\omega_{MM'}/\Gamma_{MM'}$ ratio. The most interesting is the $P(B)$ behavior in the case when all effects are taken into account, see curve 3 in Fig. 3. As it was checked from the E_M pattern calculation, the pronounced signal broadening in B range of (1÷3) T, see curve 3, is caused by numerous overlapping nonzero field crossings of magnetic sublevels $M, M \pm 2$ with $96 > |M| > 6$. Starting from $|B| \geqslant 3$ T, the nonzero field crossings for each particular $|M| \leqslant 6$ value become quite distinguishable, which is understandable for two reasons. First, the absorption–emission cross sections for P-, R-type molecular transitions have maximal values near $M = 0$.[12,21] Second, the level crossing peaks for $|M| \leqslant 6$ are much better separated since they occur at largest $|B|$ for the smallest $|M|$ values, see Eq. (19). Of course, such crossings, produced by the influence of quadratic Zeeman energy terms, can be slightly distinguished also on curve 2, see Fig. 3, possessing, however, much smaller amplitude because of fast coherence destruction. It is thus clear that the nonzero magnetic field level crossing signals are pronounced so well in the case depicted by curve 3 due to the "delay" in $P(B)$ diminution, which occurs because magnetic PD shows the tendency to increase $\Gamma_{MM'}$ with B growing.

The role of $\Gamma_{MM'}$ contribution in wide B range AOC signals is demonstrated by curves 3–5 in Fig. 4, which are calculated using the same parameters as in the case of analogous curves in Fig. 3. The most interesting is the behavior of curve 3, which is calculated accounting for all effects in

$\omega_{MM'}$ and $\Gamma_{MM'}$ and demonstrates the appearance of additional maxima caused by $\Gamma_{MM'}$ contribution, having opposite signs with respect to the maxima caused by B^2 terms in $\omega_{MM'}$. It can be also seen that the nonzero field level crossings do not manifest themselves in the $C(B)$ signal, as distinct from the $P(B)$ dependence. Curves 4 and 5 are calculated neglecting the HFT contribution in $\omega_{MM'}$. Since curve 4, obtained by accounting for both heterogeneous and homogeneous PD, almost coincides with curve 5, in which only heterogeneous PD was taken into account, the role of homogeneous PD is negligible. This result is in consistence with Fig. 6 and its discussion.

Since the PD-induced AOC leads to opposite sign $C(B)$ signal when compared to the quadratic Zeeman effect, see Fig. 4, it looked promising to fit experimental data, given in Fig. 5, by accounting simultaneously for both nonlinear Zeeman effect and magnetic PD. If one neglects the homogeneous PD effect, it is possible to obtain simultaneously three parameters from $C(B)$ data fitting, namely: the electronic matrix element $G_{\pm}$ of paramagnetic Zeeman Hamiltonian defined by Eq. (30), the rate constant α_v^{het} of paramagnetic heterogeneous PD, and the rate constant C_v^{het} of natural heterogeneous PD. The best fitting was obtained at $G_{\pm}=2.7$, $C_v^{\text{het}} = \pm 6\ \text{s}^{-1/2}$ and $\alpha_v^{\text{het}} = \mp 9\times 10^3\ \text{s}^{-1/2}\,\text{T}^{-1}$, see curve 3′ in Fig. 5. It is however impossible to judge about the signs of C_v^{het} and α_v^{het} separately except that their signs have to be opposite. Comparison of curve 3′ with the curve 3, which was calculated by including into calculation the estimated upper limits of homogeneous PD parameters $C_v^{\text{hom}} = 10^3\ \text{s}^{-1/2}$ and $\alpha_v^{\text{hom}} = 10^3\ \text{s}^{-1/2}\,\text{T}^{-1}$, confirms that accounting for $B1_u^- \sim 1_u^{\pm}$ PD practically does not imply the fitting.

VI. DISCUSSION AND CONCLUSIONS

The effect of AOC is an exclusively sensitive tool to investigate the quadratic terms both in Zeeman energy shifts ($\omega_{MM'}$ contribution) and magnetic PD ($\Gamma_{MM'}$ contribution). The above effects produce large enough fluorescence circularity signal $C(B)$ under linear polarized excitation, which disappears completely when the quadratic terms are absent. It should be stressed that the conventional Hanle effect, which is observed via changes of the degree of linear polarization $P(B)$, is almost insensitive to the presence of both quadratic Zeeman energy shift terms and magnetic PD effects in the experimentally applied region of B, as it can be seen from Fig. 7. Indeed, the experimental $P(B)$ data can be equally well described by the simplest Lorentz shape dependence and by the dependence accounting for all abovementioned effects, see curves 1 and 3 in Fig. 7.

Since the influence of $\omega_{MM'}$ and $\Gamma_{MM'}$ produce circularity signals of different sign and shape, see Fig. 4, the $\omega_{MM'}$ and $\Gamma_{MM'}$ contributions can be easy separated, in the processing of $C(B)$ data, at least at certain dynamic parameters of the states under study. The $\omega_{MM'}$ contribution allows, in particular, to determine the electronic matrix element $G_{\pm}$ of magnetic field induced heterogeneous $|\Omega-\Omega'|=1$ interaction which, in its turn, is connected with the electronic matrix element η of electron–rotation Ω, Ω' state mixing, see Eqs.

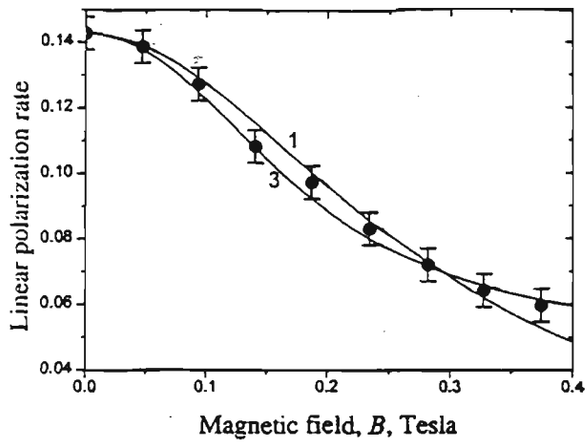

FIG. 7. Fitting of experimentally obtained Hanle signals in degree of linear polarization $P(B)$. Geometry, parameter values and curve numbering are the same as in Fig. 3. 1—Lorentz shape signal; 3—the signal accounting for all effects.

(27) and (30). The $\Gamma_{MM'}$ contribution studies yield new possibilities in investigating PD phenomena. First of all, it is quite surprising that the characteristic additional maxima produced by PD contribution into $C(B)$ signal allow to judge, from the first glance, about the heterogeneous type of PD. And, what is more, it is possible to determine separately, from one fit, both the constant C_v^{het} of natural PD and the constant α_v^{het} of magnetic PD. As it is known from I_2 studies,[8–10] due to the interference term $\alpha_v C_v$ it is possible to determine very weak natural PD rate C_v. Also in the case of $^{130}Te_2$ $B1_u^-$ state we obtained $C_v^{\text{het}} J(J+1) \cong 6.7\times 10^5\ \text{s}^{-1}$, which is only about 8% of the full relaxation rate $\Gamma = 8.55\times 10^6\ \text{s}^{-1}$ for $v=2(96)$ level.

As it can be seen from Eqs. (52) and (53), it is possible to use the PD parameters $C_v^{\text{het}} = \pm 6\ \text{s}^{-1/2}$, $\alpha_v^{\text{het}} = \mp 9\times 10^3\ \text{s}^{-1/2}\,\text{T}^{-1}$, obtained for the $B1_u^-$ state of Te_2, in order to evaluate the ratio of electronic matrix elements $\eta_v^{\text{het}} \equiv \eta$ and $G_{\pm}$:

$$\frac{\alpha_v^{\text{het}}}{C_v^{\text{het}}} \cong \frac{\sqrt{2\pi}\langle v|\epsilon\rangle \mu_B G_{\pm}}{\sqrt{2\pi}\langle v|\epsilon\rangle(\eta/2\mu R_c^2)} = 2\mu R_c^2 \mu_B \frac{G_{\pm}}{\eta}. \tag{54}$$

Using the evaluated $\hbar^2/(2\mu R_c^2) \cong 0.1\ \text{cm}^{-1}$ value and taking $\mu_B = 0.467\ \text{cm}^{-1}\,\text{T}^{-1}$, one obtains, by applying Eqs. (27) and (30), the following $G_{\pm}/\eta$ value:

$$\frac{G_{\pm}}{\eta} = \frac{g_l J_{a\pm} + (g_s - g_l) S_{\pm}}{J_{a\pm}}$$

$$\cong 1 + \frac{S_{\pm}}{J_{a\pm}} \cong \frac{\alpha_v^{\text{het}}}{C_v^{\text{het}} 2\mu R_c^2 \mu_B} \cong -3.2\times 10^2. \tag{55}$$

The fact that $G_{\pm}/\eta$ ratio is so large means that almost complete cancellation of $L_{\pm}$ and $S_{\pm}$ takes place. Indeed, since $\hat{J}_{a\pm} = \hat{L}_{\pm} + \hat{S}_{\pm}$, Eq. (55) yields $L_{\pm} \cong -1.0031 S_{\pm}$. Hence, for $B1_u^-$ state of Te_2 the values of electronic matrix elements $L_{\pm}$ and $S_{\pm}$ almost coincide, being opposite in signs. This

striking point was observed also for the $B\,^3\Pi_{0_u^+}$ state of I_2 molecule,[10] where the ratio $L_{\pm} \cong -1.0435 S_{\pm}$ was obtained.

Let us try to trace how the results of PD studies by magnetic AOC are consistent with other data about dynamic characteristics of $B1_u^-$ state in Te_2 molecule. An interesting possibility to obtain some indirect information about PD based on global deperturbation analysis (GDA) was considered in Ref. 15. In particular, the experimentally measured[28] transition moment dependence on internuclear distance R allowed us to evaluate the "pure" spontaneous lifetime values τ_{sp}^{est} of the level, see the last column of Table II. From comparison of these values with the effective lifetimes τ_{sp}^{exp} of Table II which were directly measured,[27] one can arrive at the following conclusions. First, as it can be seen from the table, τ_{sp}^{exp} exhibits faster decrease with v for the $B1_u^-$ component than for the $B1_u^+$ one, which allows one to suppose the existence of an additional channel for the $B1_u^-$ state decay. Second, the $B1_u$ rovibronic $v(J)$ level energies practically coincide for $v=8(70)$ and 5(131) states, being equal to 1315.66 and 1313.58 cm^{-1}, respectively. Then, if only homogeneous c^--type PD, which is J independent, would take place, one had to expect almost equal PD rates for both levels. However, as it can be seen from Table II, $\tau_{8(70)}^{exp} \ll \tau_{5(131)}^{exp}$. If one supposes that the heterogeneous $B1_u^{\pm}$ state PD takes place via $B1_u^+ \sim 2_u^+$ interaction, then the PD rate for the 5(131) level had to be ca. 131/70 times larger then the one for the 8(70) level, which also disagrees with experimental data. Hence, the only PD mechanism, which is consistent with $\tau_{v(J)}^{exp}$ measurements, is that only the $B1_u^-$ state predissociates heterogeneously, whereas the $B1_u^+$ state does not. And this is possible only if $B1_u^- \sim 0_u^-$ PD takes place, which is in complete consistence with the data obtained from magnetic AOC studies, see Sec. V.

It is worth to mention that only the simplest PD mechanism, namely the direct predissociation, was considered in the present investigation. In the situation of quite dense state pattern, which is the case for Te_2 molecule, one cannot exclude the influence of indirect (or accidental) PD,[19] which takes place via an intermediate state. Due to this fact, as well as because of the restricted amount of experimental data, we do not pretend our analysis of PD mechanisms in $(B1_u^-)Te_2$ to be complete. Nevertheless, the general features of AOC phenomenon, caused by simultaneous effect of magnetic field induced energy shift and changes in PD rate, which were revealed in the present work, will not change with elaboration of PD mechanisms. It is worth to mention that the nonlinear terms both in E_M and in Γ_M magnetic field dependencies occur also under more precise, nonperturbative treatment, which has to be applied at large B values.

ACKNOWLEDGMENTS

The authors are indebted to Professor Jacque Vigue for stimulating exchange with information, to Dr. Elena Pazyuk and Dr. Ilze Klincare for useful discussions, as well as to Olga Nikolayeva for technical assistance. Support from ISF Grant No. LF-7000 and from Joint ISF and Latvian Government Grant LJ 7100 is gratefully acknowledged. Three of us (M.A., M.T., and R.F.) are grateful for the support from Latvian Science Council (Grant No. 93.256), as well as for the support from European Commission in the frame of PECO Human Capital & Mobility (Networks) program, Contract No. ERBCIPDCT940633. One of us (A.V.S.) is grateful for the support from Russian Foundation for Basic Research (Grant No. 93-03-18059).

[1] U. Fano, Phys. Rev. 133, B828 (1964).
[2] V. N. Rebane, Opt. Spectrosc. (USSR) 24, 163 (1968).
[3] M. Lombardi, C. R. Acad. Sci. Ser. B 265 B, 191 (1967).
[4] M. P. Auzinsh, and R. S. Ferber, J. Chem. Phys. 99, 5742 (1993).
[5] X. L. Han, and G. W. Schinn, Phys. Rev. A 43, 266 (1991).
[6] R. C. Hilborn, L. R. Hunter, K. Johnson, S. K. Peck, A. Spencer, and J. Watson, Phys. Rev. A 50, 2467 (1994).
[7] H. Avci, and H.-P. Neitzke, J. Phys. B 22, 495 (1989).
[8] M. Broyer, J. Vigue, and J. C. Lehmann, Chem. Phys. Lett. 22, 313 (1973).
[9] J. Vigue, M. Broyer, and J. C. Lehmann, J. Phys. B 7, L158 (1974).
[10] J. Vigue, M. Broyer, and J. C. Lehmann, J. Phys. 42, 937, 949, 961 (1981).
[11] I. P. Klincare, M. Ya. Tamanis, A. V. Stolyarov, M. P. Auzinsh, and R. S. Ferber, J. Chem. Phys. 99, 5748 (1993).
[12] M. Auzinsh and R. Ferber, *Optical Polarization of Molecules* (Cambridge University, Cambridge, 1995).
[13] M. P. Auzinsh and R. S. Ferber, Phys. Rev. Lett. 69, 3463 (1992).
[14] J. Verges, C. Effantin, O. Babaky, J. d'Incan, S. J. Prosser, and R. F. Barrow, Phys. Scr. 25, 338 (1982).
[15] E. A. Pazyuk, A. V. Stolyarov, M. Ya. Tamanis, and R. F. Ferber, J. Chem. Phys. 99, 7873 (1993).
[16] K. Balasubramanian, and Ch. Ravimohan, J. Mol. Spectrosc. 126, 220 (1987).
[17] C. Cohen-Tannoudji, Ann. Phys. (Paris) 7, 423, 469 (1962).
[18] L. P. Landau and E. M. Lifshitz, *Quantum Mechanics* (Pergamon, London, 1965).
[19] H. Lefebvre-Brion and R. W. Field, *Perturbation in the Spectra of Diatomic Molecules* (Academic, New York, 1986).
[20] J. H. van Vleck, Rev. Mod. Phys. 23, 213 (1951).
[21] R. N. Zare, *Angular Momentum* (Wiley, New York, 1988).
[22] A. R. Edmonds, *Angular Momentum in Quantum Mechanics* (Princeton U.P., Princeton, 1974).
[23] R. S. Mulliken, J. Chem. Phys. 33, 247 (1960).
[24] G. Herzberg, *Molecular Spectra and Molecular Structure. I. Spectra of Diatomic Molecules* (Van Nostrand, Princeton, NJ 1957).
[25] I. P. Klintsare, M. Ya. Tamanis, and R. S. Ferber, Opt. Spectrosc. (USSR) 67, 720 (1989).
[26] M. Mizushima, *Theory of Rotating Diatomic Molecules* (Wiley, New York, 1975).
[27] I. P. Klincare and M. Ya. Tamanis, Chem. Phys. Lett. 180, 63 (1991).
[28] R. S. Ferber, Ya. A. Harya, and A. V. Stolyarov, J. Quant. Spectrosc. Radiat. Transfer 42, 143 (1992).

NaK $D\,^1\Pi$ Electric Dipole Moment Measurement by Stark Level Crossing and e-f Mixing Spectroscopy

M.Tamanis, M.Auzinsh, I.Klincare, O.Nikolayeva, A.V.Stolyarov*
and R.Ferber

Department of Physics, University of Latvia, Riga LV-1586, Latvia

* *Department of Chemistry, Moscow M. Lomonosov State University, Moscow W-234, 119899. Russia*

ABSTRACT

The paper presents the first permanent electric dipole moment d_p measurements for NaK $D\,^1\Pi$ state rovibronic levels. Two different methods were applied to obtain d_p values. Stark effect induced level crossing registered as the changes of fluorescence linear polarization $P(\mathcal{E})$ with external electric field $\mathcal{E}$ yielded from one fit both the electric dipole moment value and the Λ-doubling splitting between e, f substates of an individual rotational state. Another method consisted of obtaining the ratio Δ^J_{ef}/d_p from $\mathcal{E}$-dependence of the forbidden line appearing in fluorescence as a result of e-f Stark mixing, along with direct Δ^J_{ef} measurement by RF - optical double resonance. The respective dipole moment values obtained are 5.9 - 6.4 D for the state $v' = 7$, $J' = 23$, as well as 4.5 - 4.8 D for $v' = 12$, $J' = 7$, the typical errors being ca. 12% - 20%. The d_p value for the latter state reflects d_p diminution expected due to the admixture of the $d^3\Pi$ state caused by intramolecular interaction. Signal simulation and data fitting have been accomplished using direct Hamiltonian diagonalization accounting for Stark interaction within rotational states $J \pm \Delta J$, $\Delta J = 0, 1$ and 2 in the initial, excited and final state.

I. INTRODUCTION

There is interest in determining the permanent electric dipole moment of a molecule since this quantity reflects very sensitively the details of electronic structure. At the same time there is still a lack of information about electric dipole moments for short-lived excited states of diatomic molecules. One of the methods to determine electric dipole moments consists of applying the electric-field-induced analogue to the Hanle effect. The electric-field-caused changes in atomic fluorescence polarization were first revealed by Hanle [1] as early as in 1926, very soon after his discovery of magnetic-field-induced fluorescence depolarization, or the "Hanle effect" [2]. These two phenomena are caused by Stark and Zeeman effects respectively, having their physical origin in removing the degeneracy between coherently excited magnetic sublevels M, being thus called "zero field electric/magnetic field level crossing", see monographs [3–5]. The application of external-field-caused level crossing methods to molecules was proposed by Zare [6]. However, as distinct from widely applied magnetic-field-induced level crossings [3–5], the pure electric-field level crossing signals in resonance fluorescence, first applied to atoms [7,8], for molecules have been observed in relatively few works, see Refs. [9–11]. For the states with closed electronic shells, such as $A\,^1\Sigma$ in BaO [11] and $B\,^3\Pi_{0_u^+}$ in I_2 [10], the monotonic "Stark–Hanle" (Stark analogue of Hanle effect) curves were observed in laser-induced fluorescence (LIF). In these cases it is the second-order Stark effect [12,13] which determines the Stark splitting manifold. This follows directly from the selection rules for the electric-dipole allowed interaction, which connects only the states with different, even or odd, total parity, labelled as + or −, respectively. Hence, the first-order perturbation terms are absent in the non-degenerated perturbation approach for the Stark operator

$$\hat{\mathbf{H}}_{\mathbf{St}} = -\mathbf{d}_{\mathbf{p}}\boldsymbol{\mathcal{E}}. \tag{1}$$

This means that the terms linear over electric field strength $\mathcal{E}$ equal zero for a rovibronic level with fixed rotational quantum number J. The appearance of linear over $\mathcal{E}$ terms is possible only in the case when the states, which are interacting due to $\hat{\mathbf{H}}_{\mathbf{St}}$, are so close in energy that it is impossible to use the non-degenerate perturbation theory. This is the case for quasi-degenerate

electronic states with $\Lambda \neq 0$. In particular, the $^1\Pi$-state possesses two Λ-doublet components of different total parity, + or −, within a rotational state J, see Fig. 1a. The total parity alternates with J, and another type of label, named the e/f symmetry, is often used, which factors out the $(-1)^J$ J-dependence, thus being a rotation–independent label [14,15], see Fig. 1a. The Λ-doublet splitting Δ^J_{ef}, caused by electron-rotation interaction, is regularly given by $\Delta^J_{ef} = q[J(J+1)-\Lambda^2]$, where q is the Λ-doubling constant. This leads, as distinct from the $^1\Sigma$ state, to the "quasi-linear" Stark effect [13] in the $^1\Pi$ state (see Fig. 1b).

A deeper insight into the $^1\Pi$ state Stark effect, including Stark zero-field level crossing, was first given by Klemperer and co-authors [9] and applied to the ($A\,^1\Pi$) CS molecule. Further, in a number of works [16–24], the main attention was paid to the changes in the $^1\Sigma \rightarrow {}^1\Pi \rightarrow {}^1\Sigma$ LIF spectra induced by dc Stark effect mixing of e/f levels. Indeed, due to $\Delta J = 0, \pm 1$ and $+ \leftrightarrow -$ selection rules [14,15], see Fig. 1a, only the (P, R)-doublet emission is allowed at P- or R-type excitation, whereas only Q-singlet emission is allowed at Q-type excitation. If, however, an external electric field is applied, the $+ \leftrightarrow -$, or e/f Stark effect mixing in a $^1\Pi$ state with fixed J gives rise to the appearance of a "forbidden" line. Therefore, one can observe in the LIF progression the whole (P, Q, R)-triplet, instead of either doublets or singlets. The relative intensity of a forbidden line, in the case when Δ^J_{ef} is much larger than the natural width of each Λ-doubling component, is mainly governed by the $|(d_p\mathcal{E})/\Delta^J_{ef}|$ parameter, allowing one to obtain the absolute value of d_p, provided additional information on q values can be obtained.

Concerning electronically excited alkali dimers, there have been, according to our knowledge, two attempts to determine d_p, both for NaK $^1\Pi$ states. Drullinger and co-workers [16] have recorded Stark induced "forbidden" lines in LIF from NaK ($D^1\Pi$), and have also demonstrated the RF - optical double resonance signal on the $v' = 7, J' = 5$ level. However, they present only qualitative information without mentioning any d_p values. Later, Derouard and co-workers [24] made an attempt to determine NaK ($B^1\Pi$) dipole moments by applying Stark e–f mixing. They present dipole moment values for several vibrational states. These are ca. two times smaller than the values obtained from *ab initio* calculations by Stevens, Konowalow and Ratcliff [25]. In this sense, the predicted [25] large permanent electric dipole moment values, reaching 4.5 D

for NaK ($B\,^1\Pi$) and 7.8 D for NaK ($D\,^1\Pi$) have still not been proved experimentally. It seems, however, that there could be some contradictions within the results given in Ref. [24], manifested in the large discrepancy of q values obtained. Thus, there is still a lack of reliable information about excited state dipole moments even for such a "test" alkali dimer as NaK. We also are not aware of such data pertaining to any other alkali dimer. It is important to mention that in Refs. [9,16–24] the description was restricted by the first-order Stark effect, without accounting for Stark mixing of different rotational states, thus the approach used in data processing has to be improved.

The main goals of the present paper are as follows. First, we intend to determine the NaK permanent electric dipole moment values in its $D\,^1\Pi$ state, for which there exists developed spectroscopic information [26–32], including lifetime measurements [33]. We have applied two methods: (i) Stark-induced changes in LIF polarization; (ii) Stark induced "forbidden" line relative intensity ratio measurements in combination with the direct Δ^J_{ef} measurement by RF – optical double resonance method [9,34,35]. Secondly, we developed further the description of $^1\Pi$-state dc Stark effect, allowing one to calculate the $\mathcal{E}$ dependence of fluorescence intensity for any geometry and polarization type. We used different order perturbation theory, as well as the direct numerical diagonalization of the Hamiltonian matrix accounting for the interaction of rotational states with different J, both in the excited $^1\Pi$ state and in the ground $^1\Sigma$ state. At this point we have not considered the influence of hyperfine effects. In the situation under discussion, the Stark energy remains small with respect to the rotational energy, $d_p\mathcal{E} \ll BJ(J+1)$, which means that the main rotational–vibrational pattern is conserved, as distinct from the "pendular states" situation [36], which takes place for extremely strong electric fields, destroying the rotational motion of a molecule.

The paper starts from the theoretical description of the Stark effect manifestation in $^1\Pi \rightarrow {}^1\Sigma$ fluorescence (Section II). After a quick description of the experiment (Section III), the simulation of expected signals in LIF polarization is given (Section IV), followed by the presentation of experimental results (Section V) and discussion (Section VI).

II. THEORETICAL DESCRIPTION

Let us consider the interaction of cw broad band radiation with diatomic molecules causing a $^1\Pi(v', J') \leftarrow {}^1\Sigma(v'', J'')$ rovibronic transition in the presence of an external static electric field. Using the general density matrix approach [5,37-39], one may write the density matrix element $f_{MM'}$ of the excited state as

$$^{kl}f_{MM'} = \frac{\tilde{\Gamma}_p}{\Gamma + i^{kl}\Delta\omega_{MM'}} \sum_{\mu} \langle M' {}^1\Pi k|\hat{\mathbf{E}}^*\hat{\mathbf{D}}|\mu {}^1\Sigma\rangle \langle M' {}^1\Pi l|\hat{\mathbf{E}}^*\hat{\mathbf{D}}|\mu {}^1\Sigma\rangle^*. \tag{2}$$

Here μ are magnetic sublevels of the ground state $^1\Sigma$ with rotational quantum number J'', whilst M, M' are magnetic sublevels of the excited state with rotational quantum number J', belonging to Λ-doublet components k, l. The unit vector $\hat{\mathbf{E}}$ describes the exciting light polarization, $\hat{\mathbf{D}}$ is the transition dipole moment unit vector, $\tilde{\Gamma}_p$ is the reduced absorption rate, Γ is the effective excited state relaxation rate, $^{kl}\Delta\omega_{MM'}$ is the energy splitting between M, M' sublevels, belonging either to the same ($l = k$) or to the different ($l \neq k$) Λ-doublet components, accounting both for Λ-doubling and Stark effect level shifts. The excited state density matrix $^{kl}f_{MM'}$ allows one to calculate the intensity of fluorescence $I_f(\hat{\mathbf{E}}_\mathbf{f})$ with polarization vector $\hat{\mathbf{E}}_\mathbf{f}$, originating from this state in the transition $J' \rightarrow J''_1$, as

$$I_f(\hat{\mathbf{E}}_\mathbf{f}) = I_0 \sum_{MM'\mu} \sum_{kl} \langle M' {}^1\Pi k|\hat{\mathbf{E}}_\mathbf{f}^*\hat{\mathbf{D}}|\mu {}^1\Sigma\rangle \langle M' {}^1\Pi l|\hat{\mathbf{E}}_\mathbf{f}^*\hat{\mathbf{D}}|\mu {}^1\Sigma\rangle^* {}^{kl}f_{MM'}, \tag{3}$$

where I_0 is proportionality coefficient. The structure of Eq. (3) allows one to notice that the terms entering the sums are formed as excited state matrix elements $^{kl}f_{MM'}$ multiplied by the observation matrix elements.

The next step is to represent the molecular wave functions in Eqs. (2), (3) accounting for static external electric field effects. Since the external electric field destroys the spherical symmetry, the rotational quantum number J does not remain a good quantum number any more. At the same time the external electric field does not change the axial symmetry, therefore the projection quantum number M (or μ) is still conserved.

The wave functions included in Eqs. (2) and (3) are obtained in a coupled-basis set as expansions over non-perturbed states with different J'_i ($i = e, f$) and J'' values mixed by the static external electric field. For a $^1\Pi$ excited state we have

$$|M^1\Pi k\rangle = \sum_{J'=1}^{\infty} \sum_{i=e,f} C^k_{\Pi i}(J', M)|J'Mi\rangle, \tag{4}$$

thus obtaining, as it is usually done, a new wave function for each $k = 1, 2$, found as the linear combination of e and f substates, with mixing coefficients $C^k_{\Pi e}(J', M)$ and $C^k_{\Pi f}(J', M)$.

For the ground electronic state $^1\Sigma$, one can represent the wavefunction $|\mu^1\Sigma\rangle$, by accounting for J''-mixing, as

$$|\mu^1\Sigma\rangle = \sum_{J''=0}^{\infty} C_\Sigma(J'', \mu)|J''\mu\rangle. \tag{5}$$

Coefficients $C_{\Pi i}$ and C_Σ have to be found from diagonalization of the Hamiltonian accounting for molecular rotation and the Stark effect (Eq. (1)).

It is easy to see that the respective matrix elements, both in absorption and fluorescence, are proportional to the multiplication of the correspondent mixing coefficients $C^k_{\Pi i}(J', M)$, and $C_\Sigma(J'', \mu)$ or $C_\Sigma(J''_1, \mu)$. For the absorption, one obtains

$$\langle M^1\Pi k|\hat{\mathbf{E}}^*\hat{\mathbf{D}}|\mu^1\Sigma\rangle = \sum_{J'J''i} C^k_{\Pi i}(J', M)C_\Sigma(J'', \mu)\langle J'Mi|\hat{\mathbf{E}}^*\hat{\mathbf{D}}|J''\mu\rangle, \tag{6}$$

and the same for the fluorescence, if one replaces J'' by J''_1 and $\hat{\mathbf{E}}$ by $\hat{\mathbf{E}}_f$. Eq. (6) allows one to apply the Wigner–Eckart theorem [5,39–42]:

$$\langle J'Mi|\hat{\mathbf{E}}^*\hat{\mathbf{D}}|J''\mu\rangle = \sum_q (E^q)^* \frac{1}{\sqrt{2J'+1}} C^{J'M}_{J''\mu 1q}(J', i\|D\|J''), \tag{7}$$

in which, due to the selection rules propagation into the reduced matrix element [41,42], we have

$$(J', e\|D\|J'') = \begin{cases} \sqrt{G(J', J'')}, & J' - J'' = \pm 1 \\ 0, & J' - J'' = 0, \pm 2, \pm 3, \ldots . \end{cases} \tag{8}$$

$$(J', f\|D\|J'') = \begin{cases} \sqrt{G(J', J'')}, & J' - J'' = 0, \\ 0, & J' - J'' = \pm 1, \pm 2, \ldots . \end{cases} \tag{9}$$

The E^q in Eq. (7) are cyclic components of unit vector $\hat{\mathbf{E}}$ describing light polarization [5,43], whilst $G(J', J'')$ in Eqs. (8) and (9) is the Hönl–London factor

$$G(J', J'') = (2J'' + 1)(C^{J'\Lambda'}_{J''\Lambda'' 1\Lambda'-\Lambda''})^2. \tag{10}$$

$C^{c\gamma}_{a\alpha b\beta}$ being Clebsch–Gordan coefficients.

To determine ${}^{kl}\Delta\omega_{MM'}$, one needs Stark energy expressions E^{el}_M. In the first approximation one can obtain first order Stark energies ${}^{(1)}E^{el}_M$ in a simple analytical form (the energy of ${}^1\Pi$ state f-sublevel is considered to be zero):

$$ {}^{(1)}E^{el}_M = \frac{1}{2}\Delta^J_{ef} \pm \sqrt{\frac{(\Delta^J_{ef})^2}{4} + \frac{d_p^2\mathcal{E}^2M^2}{[J(J+1)]^2}}. \qquad (11) $$

It is easy to see that, as $\mathcal{E}$ increases, leading to $d_p\mathcal{E}M/[J(J+1)] \gg \Delta^J_{ef}/2$, Stark energy shifts have linear asymptotic behaviour with respect to $|\mathcal{E}M|$, see Fig. 1b. A second order approximation in the ${}^{kl}\Delta\omega_{MM'}$ calculation takes place if one is accounting for the interaction between J' and adjacent $J' \pm 1$ excited state levels. The Stark-effect-induced energy second-order correction for a ${}^1\Pi$ state can be also written in analytical form, see Ref. [13]. However, with $\mathcal{E}$ increasing, the second-order perturbation treatment becomes incorrect as well, and one has to solve the secular equation system [44] for the relevant Hamiltonian matrix. The analysis of such a treatment, accounting for $J \pm \Delta J$ mixing within a given vibrational state centered at the initial (J''), excited (J') and final (J''_1) rotational state of a $J'' \rightarrow J' \rightarrow J''_1$ transition, will be given in Section IV.

III. EXPERIMENTAL

$^{23}Na^{39}K$ molecules were formed thermally in a glass cell joined to the vacuum system by means of a dry valve. The cylindrical head of the cell was made from a special alkali-resistant glass tube. An electric field was produced by applying a static voltage across a pair of round polished stainless steel parallel Stark plates located inside the cell. Altogether three cells were used, differing in diameter (d) and spacing (l) of the electrodes, namely: (1) $d = 25$ mm, $l = 2.9 \pm 0.1$ mm; (2) $d = 7$ mm, $l = 1.8 \pm 0.1$ mm; (3) $d = 7$ mm, $l = 1.2 \pm 0.1$ mm. The spacing between the electrodes was measured by means of a measuring microscope. The cells were filled with metallic potassium and sodium, via a repeated distillation process, in a weight ratio of approximately 7:3, respectively. The metal-containing reservoir was kept at stabilised temperatures between 270°C and 320°C. The dc voltage was kept below the threshold for electrical breakdown in the cell.

which did not exceed 6 kV/cm at any of the temperatures employed.

The linearly polarized light from a cw Ar^+-laser was used to excite $X^1\Sigma^+ \rightarrow D^1\Pi$ transitions in $^{23}Na^{39}K$ molecules, see Fig. 2. Fluorescence at right angles, both to the laser beam and to the electric field $\mathcal{E}$, originating from the ca. $0.5 - 1.2$ mm diameter laser beam excitation region, was imaged onto the entrance slit of a double monochromator with 5 Å/mm dispersion and resolved by a 1200 lines/mm grating in first diffraction order, providing an overall spectral resolution up to 0.3 Å. We restricted the observation zone to the size of ca. 1.5 mm in height, thus diminishing the possible influence of electric field inhomogenity. The particular $D^1\Pi \rightarrow X^1\Sigma^+$ LIF progressions, originating from the definite $D\,^1\Pi$, v', J' states, were identified from the recorded LIF spectrum by comparison of line positions and relative intensities with the ones calculated by means of spectroscopic constants given by the authors of Ref. [26], for the transitions mentioned by them at excitation by 4765 Å and 4880 Å Ar^+-laser lines. The data from Ref. [45], considering optical depopulation of the ground $^1\Sigma^+$ state of NaK, allowed us to suppose that non-linear optical pumping effects [5,46] are negligible at the range of excitation-relaxation parameters employed. The degree of linear polarization was measured by dividing the entrance slit of the monochromator in height into two parts, placing two orthogonal polarizers in front of them. Light guides conducted fluorescence light from the two respective parts of the exit slit to the two photomultipliers, with subsequent counting of one-photon pulses from the two channels. The unpolarized LIF in the absence of an external electric field, excited by the laser light with $\hat{\mathbf{E}}$-vector set parallel to the observation direction, was used to calibrate the channels before each experiment.

In the case of optical - electric RF double resonance experiments, we used a 1 - 300 MHz (0.2 W, 50 Ω) Wavetek RF oscillator supply, which was connected to the same Stark plates instead of a static electric field source. A fast oscilloscope served as a 50 Ω load and as an RF output drift monitor. The resonance was measured by sweeping the frequency of the RF generator.

IV. SIMULATION OF EXPECTED SIGNALS

We will apply the developed theory to simulate the $^1\Pi$ state Stark signals in the intensity and linear polarization $P(\mathcal{E})$ of $D^1\Pi \rightarrow X^1\Sigma^+$ fluorescence. We use the dynamical parameters close to the ones which can be found in literature, namely, the dipole moment value $d_p = 7$ D (following theoretical prediction in Ref. [25]), the lifetime $\Gamma^{-1} = 20\,\mathrm{ns}$ (as determined in Ref. [33]), the q-factor $q = 1.2 \times 10^{-5}\mathrm{cm}^{-1}$ and the rotational constant B_v values given in Ref. [26]. The absolute values of d_p and q will be assumed hereafter, since their sign does not affect the calculation results.

First, we will present zero-field level-crossing signal simulations for the "traditional" geometry ($\hat{\mathbf{E}} \perp \boldsymbol{\mathcal{E}}$, observation along $\boldsymbol{\mathcal{E}}$). Fig. 3 presents such calculations for the $J' = 23$ level of the $D^1\Pi$ state. In the $\mathcal{E}$ range demonstrated in Fig. 3, the signal is determined by the first-order effect, the difference between the first-order approximation (curve 1) and the second-order one (curve 2) being small, yet still distinguishable. Taking into account the Stark mixing between $J \pm \Delta J$ with $\Delta J > 1$ practically does not change the signal, cf. curves 2 and 3 at the insertion in Fig. 3. The monotonous behaviour of pure quadratic Stark-Hanle effect for a hypothetic $^1\Sigma$ state, supposing the same Γ, d_p and B'_v as for $^1\Pi$ state, is also presented in Fig. 3, see curve 4. A comparison of curves 1 - 3 and curve 4 demonstrates clearly the peculiarity of $^1\Pi$-state Stark effect, the latter possessing a small additional maximum, which appears mainly due to the competition between the M-dependent Stark induced e-f mixing and the destruction of coherence among M-sublevels.

This peculiarity in $P(\mathcal{E})$ is more pronounced at another geometry, when fluorescence is observed "from the end" of $\hat{\mathbf{E}}$-vector, $\hat{\mathbf{E}} \perp \boldsymbol{\mathcal{E}}$ (see Fig. 4). Both first-order ($\Delta J = 0$, curve 1) and second-order ($\Delta J = 1$, curve 2) approximations are insufficient to describe with adequate accuracy the polarization in the coherence destruction region. This can be seen from comparison with curve 3 obtained via Hamiltonian diagonalization accounting for Stark mixing between $J \pm \Delta J$ with $\Delta J = 2$; accounting for $\Delta J > 2$ practically does not affect the result. We will further exploit the geometry shown in Fig. 4, performing ($\Delta J = 2$)-approximation in the calculations of Stark effect signals.

Let us now investigate the sensitivity of the signal presented in Fig. 4 to the variations of

the main parameters of the $^1\Pi$ state, namely to the permanent electric dipole moment d_p, Λ-doubling constant q and relaxation rate Γ values. The results are presented in Figs. 5 and 6. Fig. 5a demonstrates a polarization signal simulation at d_p values taken as 3 D, 5 D and 7 D, when all other parameters remained unchanged. In Fig. 5b, the d_p and q values have been varied simultaneously, whereas their ratio was maintained constant. It can be seen from comparison between Figs. 5a and 5b that the peak amplitude is uniquely determined by the q value, whilst the position of the peak in $\mathcal{E}$-scale and the slope of the growing part are mainly determined by the d_p value. This allows one to determine simultaneously both d_p and q values from one fit, provided that Γ is known. The situation is quite different for the intensity ratios $I_Q/I_{P,R}$ of Stark induced "forbidden" line I_Q to the "parent" line $I_{P,R}$, see Fig. 5c. Indeed, the respective curves in Fig. 5c undergo minor changes at different d_p and q used in calculations presented in Figs. 5a and 5b, if the q/d_p ratio remains unchanged, thus only this ratio can be determined from the fitting. Fig. 6 demonstrates the sensitivity of the signals under discussion with respect to the variation in the relaxation rate Γ. As expected, the changes of polarization signal $P(\mathcal{E})$ with Γ are quite similar to respective $P(\mathcal{E})$ changes with q (cf. Fig. 6a and Fig. 5b). In contrast, the intensity ratios are almost insensitive to Γ variations, especially for the $\boldsymbol{\mathcal{E}} \parallel \hat{\mathbf{E}}_f$ geometry (see curves 1 and 2 in Fig. 6b).

V. MEASUREMENTS AND RESULTS

NaK $D^1\Pi$ state electric dipole moment and Λ-splitting measurements have been carried out by the following methods:

(i) by recording spectrally resolved LIF and measuring the intensity ratio between "forbidden" and allowed ("parent") lines as a function of static voltage;

(ii) by measuring the variation of the degree of linear polarization of the "parent" line with variation in the static voltage;

(iii) by measuring the electric RF – optical double resonance Λ-doublet signal from the "forbidden" line intensity dependence on RF field frequency.

A. Intensity ratios

Fig. 7 demonstrates the effect of static electric field on the spectrally resolved LIF leading to the appearance of forbidden Q line due to e–f mixing. Since the effect is mainly governed by the $\mathcal{E}d_p/\Delta_{ef}^J$ ratio, one needs a larger electric field strength to observe the Q-lines originating from $v' = 7$, $J' = 23$ than from the $v' = 12$, $J' = 7$ state. The (P, Q, R)-triplet component separation for the latter case, being ca. 0.3 Å, is on the edge of the spectral resolution of the monochromator used.

A fitting procedure employing three Gaussians was used to obtain "forbidden"/"parent" line ratio $I_Q/I_{P,R}$. The intensity ratios $I_Q/I_{P,R}$, obtained in different cells (see Section III) and experimental geometries, are shown as insets in Figs. 8 and 9. Least-square data processing yielded q/d_p ratios. The averaged values are $(2.40 \pm 0.25) \times 10^{-6}\mathrm{cm}^{-1}/\mathrm{D}$ for $v' = 7$, $J' = 23$ and $(2.10 \pm 0.20) \times 10^{-6}\mathrm{cm}^{-1}/\mathrm{D}$ for $v' = 12$, $J' = 7$ state. The q/d_p systematic errors are most likely attributable to uncertainties in Stark plate separation. For instance, the curves in Fig. 9b,c demonstrate the $\mathcal{E}$-dependences of I_Q/I_P and I_Q/I_R, which are registered for two different cells and different exciting light vector directions, $\hat{\mathbf{E}} \| \boldsymbol{\mathcal{E}}$ or $\hat{\mathbf{E}} \| \boldsymbol{\mathcal{E}}$, with fluorescence light vector $\hat{\mathbf{E}}_f \| \boldsymbol{\mathcal{E}}$ in both cases. The one-parameter (q/d_p) least-square routine yields the following constant ratios: $q/d_p = 1.9 \times 10^{-6}\mathrm{cm}^{-1}/\mathrm{D}$ for Fig. 9b and $q/d_p = 2.3 \times 10^{-6}\mathrm{cm}^{-1}/\mathrm{D}$ for Fig. 9c, the discrepancy reflecting both statistical and systematic errors.

B. Polarization measurements

Results for the $D^1\Pi$ $(v' = 7,\ J' = 23)$ *state.* Experimentally measured electric field dependencies of the polarization degree are presented in Fig. 8. The results are obtained in two different cells (see Section III), using the most favourable geometry when LIF is viewed from the "end" of exciting light vector $\hat{\mathbf{E}} \perp \boldsymbol{\mathcal{E}}$, as depicted in Fig. 4. The data fitting was realized by accounting for Stark interaction among five rotational states J, $J \pm 1$, $J \pm 2$ for all J'', J' and J_1'' involved in the transition. The best-fit constants q and d_p, obtained from a two-parameter weighted least-square routine, yield the values in question. Cell 1 yields $q = 1.6 \times 10^{-5}\mathrm{cm}^{-1}$ and $d_p = 6.3$ D, whilst cell

2 yields $q = 1.7 \times 10^{-5}\text{cm}^{-1}$ and $d_p = 6.5$ D. Cell 2 allowed us to achieve higher electric field intensities (up to 5.6 kV/cm) owing to the special working of Stark plates surface and edges in order to avoid sparking; the conditions were more favourable also because of lower cell temperatures (ca. 270°C). On the other hand, the results for cell 2 may have a larger systematic error because of smaller plate separation. Evaluation of the possible contribution of both statistical and systematic errors for different cells enabled us to take $d_p = (6.4 \pm 0.8)$D and $q = (1.65 \pm 0.2) \times 10^{-5}\text{cm}^{-1}$ as the averaged permanent electric dipole moment and q-factor values, see Table 1. As it follows from the simulations presented in Figs. 5 and 6, the Λ-doubling constant q obtained from the fit seems to be more subject to the systematic error in absolute polarization values, which can arise, say, from even slight inaccuracies in the calibration of channels and in accounting for background signal, as well as any possible uncertainty in the relaxation constant Γ value.

Results for $D^1\Pi\,(v' = 12,\ J' = 7)$ *state.* Measurements for this state were much more complicated because of the small spectral separation between the triplet components (see Fig. 7b), requiring narrow spectrometer slits to maintain necessary resolution. This leads to considerably larger errors, both statistical and systematic, in polarization measurements (see Fig. 9a). The most favourable conditions were achieved using cell 3 (see Section III). $P(\mathcal{E})$ was registered in P-transitions $(J' = 7) \rightarrow (J_1'' = 8)$ because of better spectral separation. In spite of wide statistical scatter in the results, we have accomplished direct least-square two-parameter fitting, which yielded the values $d_p = 4.5 \pm 0.8$ D and $q = (1.1 \pm 0.2) \times 10^{-5}\text{cm}^{-1}$, see Table 1. The large inaccuracy in the q value accounts for the uncertainty in relaxation rate Γ for this state. We supposed Γ to be $5 \times 10^7\text{s}^{-1}$, that is the same as for the $v' = 7$, $J' = 23$ state [33].

C. Electric RF – optical double resonance

Since the routine based on both d_p and Δ_{ef}^J variation in the fitting of the measured $P(\mathcal{E})$ signal is very sensitive to inaccuracies in absolute $P(\mathcal{E})$ measurements, as well as to Γ values (see Figs. 5 and 6), it seemed important to exploit a method allowing direct Δ_{ef}^J measurement in some independent experiment. For this purpose we have employed the electric RF - optical double resonance method. In order to increase the RF field amplitude $\mathcal{E}_{RF}^{\circ}$, the measurements

were carried out at a Stark-plate separation of 0.85 ± 0.05 mm. The RF field voltage enabled us to produce $\mathcal{E}^{o}_{RF} \lesssim 20$ V/cm. In order to diminish LIF intensity drift during signal accumulation the normalised difference $(I_F - I_{F_o})/I_{F_o}$ was considered to be a result of a single measurement, that is the difference between intensity at current frequency F and at some reference frequency F_o. The signal accumulation time varied from 10 minutes to 1 hour.

Results for $D^1\Pi_u$, $v' = 7$, $J' = 23$ state. Figure 10b (dots) presents experimental data obtained by registering the intensity of a "forbidden" Q-line as dependent on the RF electric field frequency, demonstrating resonance intensity increase, with a maximum near 230 MHz. Although the resonance signal width exceeded the one expected from the natural broadening, probably possessing some structure, we assumed that the signal is reliable enough to determine the e/f separation Δ^J_{ef}, yielding $q = (1.42 \pm 0.07) \times 10^{-5}\text{cm}^{-1}$ as an averaged value. This makes it possible to determine the permanent electric dipole moment d_p in question, using q/d_p values presented in Section VA, as $d_p = 5.9 \pm 0.9$ D.

Results for $D^1\Pi_u$, $v' = 12$, $J' = 7$ state. Fig. 10a presents the experimental data (dots) demonstrating the RF field frequency dependence of the "forbidden" Q-line intensity in $(J'' = 8) \rightarrow (J' = 7) \rightarrow (J''_1 = 7)$ transition. The average of q over a number of experiments is $q = (1.03 \pm 0.08) \times 10^{-5}\text{cm}^{-1}$. Taken together with q/d_p obtained from intensity ratios, see Sec. VA, the dipole moment value is $d_p = (4.8 \pm 0.9)$ D, where the estimated relative error consists of 10% assigned to q/d fitting and 8% assigned to Δ^J_{ef} uncertainty.

VI. DISCUSSION AND CONCLUSIONS

Method. Investigation of permanent electric dipole moments is not an easy matter for short-lived excited molecular states with large rotational numbers ($J \gg 1$). Let us compare the two more or less independent methods exploited in the present work. Both methods are based on analyzing Stark effect induced changes in fluorescence, which are caused predominately by e-f mixing within the same rotational state, which, in turn, is governed mainly by dipole moments (d_p), Λ-splittings (Δ^J_{ef}, or q-factors) and relaxation rates (Γ).

(i) *$\mathcal{E}$-dependence of linear polarization degree $P(\mathcal{E})$.* In the most favourable experimental

geometry $P(\mathcal{E})$ signal is characteristic enough to obtain both q and d_p from the fitting. This demands high accuracy in measuring $P(\mathcal{E})$ and precise knowledge of the relaxation rate Γ.

(ii) *RF - optical double resonance along with $\mathcal{E}$-dependence of intensity ratios* of "forbidden" - to - "parents" lines in LIF triplet exhibit an alternative method. In this case the RF resonance yields directly the Λ-doubling splitting Δ^J_{ef}, whilst the processing of relative intensity data yields Δ^J_{ef}/d_p, the latter procedure being weakly dependent on Γ. Thus, the accuracy of d_p values in question, obtained by this method is only slightly affected by the accuracy of relaxation rate Γ. A crude estimate of Γ gained from the width of the RF–optical double resonance may even work to obtain reliable d_p values without any previous knowledge of molecular lifetime.

The developed theoretical description (Sec. II) and simulations of expected signals (Sec. IV) allowed us to conclude that, even though the main Stark features arise from the 1st order effect, in order to avoid possible inaccuracies in the case when the Stark energy is not too small in comparison with rotational splitting (i.e., in case of not too small $d_p\mathcal{E}/(B'_v J')$), it is necessary, for both methods (i) and (ii), to consider Stark interaction with no less than four neighbouring rotational levels, both in excited and ground (initial and final) states.

Dipole moments and Λ-splittings. The dipole moments determined seem to be reliable, in particular since there is good agreement between the results gained from two independent methods. As for the absolute d_p values, they can be considered as very large when compared to typical dipole moment values which had been measured for diatomic molecules [13,47]. Let us compare the measured d_p values with theoretical quantities given by Stevens, Konowalow and Ratcliff [25]. In order to pass from *ab initio* $d_p^{th}(R)$ dependence presented in Ref. [25] to the predicted d_p values for particular v', J' states, we have used the averaging routine based on either *ab initio* potentials [25], or RKR potentials [26] for the NaK $D^1\Pi$ state. The results differ by no more than 1%, yielding the following predicted $d_p^{th}(v', J')$ values for the states under study: $d_p^{th}(7, 23) = 7.1$ D and $d_p^{th}(12, 7) = 6.5$ D, see Table 1.

As follows from Table 1, the measured d_p value for the $v' = 12$, $J' = 7$ state is smaller than for the $v' = 7$, $J' = 23$, being also markedly smaller than the theoretically predicted value. As is well known [26,31,32], levels belonging to the NaK $D^1\Pi$ state are perturbed, at least to some extent,

by the close lying $d^3\Pi$ state. Basing on Ref. [26], the level $v' = 7$, $J' = 23$ can be considered as almost unperturbed, whereas the level $v' = 12$, $J' = 7$ is shifted to $\Delta E = 0.468\text{cm}^{-1}$ with respect to the deperturbed position. Using the calculated difference of deperturbed $D^1\Pi$ ($v' = 12$) and $d^3\Pi$ ($v' = 13$) terms [31] with $J' = 7$, being $E_{3\Pi} - E_{1\Pi} = 3.87\text{cm}^{-1}$, one can get the estimation for the squared state mixing coefficient $C^2_{3\Pi} = \Delta E/(E_{3\Pi} - E_{1\Pi}) \cong 0.13$. This creates a reduction in pure singlet character of the state to $C^2_{1\Pi} = 1 - C^2_{3\Pi} \cong 0.87$ and allows one to estimate the relative change in the $D^1\Pi$ ($v' = 12$, $J' = 7$) state electric dipole moment, which arises due to singlet–triplet coupling, as $C^2_{1\Pi} + C^2_{3\Pi}(d_p^{3\Pi}/d_p^{1\Pi})$, $d_p^{3\Pi}$ and $d_p^{1\Pi}$ being unperturbed dipole moments. The averaging of the *ab initio* calculations [25] for the $d^3\Pi$, $v' = 13$ state yields $d_p^{3\Pi} \cong -0.7$ D, which is opposite in sign from $d_p^{1\Pi}$. As a result, the experimentally measured d_p value for ($D^1\Pi$, $v' = 12$, $J' = 7$) is expected to be ca. 15% smaller than would be anticipated for the unperturbed state. It is thus not excluded that the difference between d_p values obtained for the two states, see Table 1, reflects the role of perturbations. Indeed, the relative difference between the measured d_p values for $v' = 7$, $J' = 23$ and $v' = 12$, $J' = 7$ is ca. 20% - 25%, which does not contradict the above estimation. Hence, the experimentally measured d_p values do not disprove the *ab initio* calculation in Ref. [25], accounting for the fact that the deperturbed quantities have been calculated.

Regarding the Λ-doubling factor q, it can be noted that its tendency to be smaller for $v' = 12$, $J' = 7$ level, corresponds to what can be expected due to the perturbation, allowing one to estimate a ca. 13% diminution from the following considerations. Although the singlet-triplet $D^1\Pi - d^3\Pi$ interaction does not change the Λ-doubling splitting directly since e and f components of the $D^1\Pi$ state are perturbed by the two Λ-doublet substates of the $d^3\Pi$ state to about the same amount, this singlet-triplet interaction diminishes the singlet character of the perturbed state as $C^2_{1\Pi}$. Hence, the matrix element of electronic–rotational interaction with the remote singlet Σ states, giving rise to Λ-doubling in the $D^1\Pi$ state, has to be $C_{1\Pi}\langle D^1\Pi|L^{\pm}|^1\Sigma\rangle$, since the matrix elements between the states having a different multiplicity vanish. The q value for NaK ($D^1\Pi$) presented in Ref. [26] has been obtained from conventional spectroscopic analysis as $q_v = q_0 - q_1(v+1/2) = 1.16\times10^{-5} - 1.5\times10^{-7}(v+1/2)\text{cm}^{-1}$. The RF - optical double resonance

signal for NaK ($D^1\Pi$, $v' = 7$, $J' = 5$) can be found in Ref. [16], yielding $q = 1.5 \times 10^{-5}\text{cm}^{-1}$. Thus, the q-factor values presented in Table 1 do not disagree much with the previous data. The Λ-doubling constant for $D^1\Pi$ state can be estimated from the well-known relation: $q \approx 4B_e^2/\nu(\Pi,\Sigma)$, where $\nu(\Pi,\Sigma)$ is the difference between the electronic term values $T_\Pi - T_\Sigma$. Then, assuming that $D^1\Pi$ state Λ-doubling arises from the interaction with low-lying $C^1\Sigma$ and $A^1\Sigma$ states, one gets $q \approx 1.2 \times 10^{-5}\text{cm}^{-1}$.

As mentioned above, the experimental data on excited-state electric dipole moments of any alkali diatomic are extremely scanty. The authors of Ref. [24] present d_p values varying from 2.4 to 2.1 D for the NaK $B^1\Pi$ state with v' equaling 1, 5, 10 and 14. The d_p values are smaller than the ones predicted from *ab initio* calculations by Stevens and co-authors [25], which, according to averaging as mentioned above, range from $d_p^{th} = 4.5$ D for $v' = 1$ to $d_p^{th} = 2.8$ D for $v' = 14$. It can be noted however that there are some contradictions in q-factors determined in the measurements [24], presenting, for instance, the absolute values $q = 0.65 \times 10^{-6}\text{cm}^{-1}$ for $v' = 1$ and $q = 1.77 \times 10^{-6}\text{cm}^{-1}$ for $v' = 5$. These quantities disagree with the respective values $q = 2.08 \times 10^{-6}\text{cm}^{-1}$ and $q = 2.36 \times 10^{-6}\text{cm}^{-1}$ obtained for corresponding v' by Baba, Tanaka and Kato [48] using Doppler-free polarization spectroscopy. In order to obtain the same q/d_p ratio as presented in Ref. [24] with q values from Ref. [48] instead of the ones given in Ref. [24], the d_p for $v' = 5$ should be increased from 2.4 D to 3.2 D, the latter being not far from the averaged calculated value $d_p^{th}(v' = 5) = 3.9$ D [25]. The results given in [24] for the $v' = 1$ level of NaK $B^1\Pi$ seem strange since it is hard to imagine so dramatic a change in q (being 3 times smaller than for $v' = 5$), whilst dipole moments remain unchanged, see Table III in Ref. [24].

In conclusion, the measurements constituted in the present work confirm the existence of a large permanent electric dipole moment in the NaK $D^1\Pi$ state. It is of importance to strive to refine the experimental d_p values. Besides increasing the accuracy of measurements and extending the number of vibrational states involved in the investigation, there is reason to believe that further progress is connected with accounting for intramolecular perturbation, the most important of which might involve the simultaneous effects of hyperfine structure and $d^3\Pi \quad D^1\Pi$ interaction.

ACKNOWLEDGMENTS

This work was supported by Long Term Grant LJ7100 (1995) in the frame of the Joint Programme of the Government of Latvia and the International Science Foundation. Four of us (M.T., M.A., I.K. and R.F.) are grateful for the support from Latvian Science Council (Grant 93.256), as well as for the support from the European Commission in the frame of PECO Human Capital & Mobility (Networks) programme, contract ERBCIPDCT940633. One of us (A.V.S.) is grateful for the support from Russian Foundation for Basic Research (Grant 93-03-18059).

It is our pleasant duty to thank Professor Richard N. Zare for fruitful reccomendations. We are also indebted to Dr. Yelena Pazyuk and Professor Pawel Kowalczyk for useful discussions. We are grateful to Vitauts Boreishis for his assistance in experiments, as well as to Dr. Henrik Rudolph and Dr. Henk Dijkerman for granting the RF oscillator.

REFERENCES

[1] W.Hanle, Z. Phys. **5**, 246 (1926)

[2] W.Hanle, Z. Phys. **30**, 93 (1924)

[3] E.B.Alexandrov, M.P.Chaika, and G.I.Khvostenko, *Interference of Atomic States* (Springer-Verlag, New York, 1993)

[4] G.Moruzzi, and F.Strumia, *Hanle Effect and Level-Crossing Spectroscopy* (Plenum Press. New York, London, 1991)

[5] M.Auzinsh, and R.Ferber, *Optical Polarization of Molecules* (Cambridge University Press. 1995)

[6] R.N.Zare, J. Chem. Phys. **45**, 4510 (1966)

[7] A.Khadjavi, A.Lurio, and W.Happer, Phys. Rev. **167**, 128 (1968)

[8] N.D.Bhaskar. and A.Lurio, Phys. Rev. **A10**, 1685 (1974)

[9] S.J.Silvers, T.H.Bergeman, and W.Klemperer, J. Chem. Phys. **52**, 4385 (1970)

[10] F.W.Dalby, M.Broyer. and J.C.Lehmann, Coll. Intern. C.N.R.S. **217**, 227 (1974)

[11] G.Dohnt. A.Hese. A.Renn. and H.S.Schweda, Chem. Phys. **42**, 183 (1979)

[12] C.H.Townes. and A.L.Schawlow, *Microwave Spectroscopy* (McGraw-Hill Publishing Company Ltd., New-York, London, Toronto, 1955)

[13] M.Mizushima, *Theory of Rotating Diatomic Molecules* (J.Wiley and Sons. New York. 1975)

[14] G.Herzberg, *Molecular Spectra and Molecular Structure. I. Spectra of Diatomic Molecules* (D. Van Nostrand Company, Princeton, New Jersey, Toronto, London, New York. 1957)

[15] H.Lefebvre-Brion. and R.W.Field. *Perturbations in the Spectra of Diatomic Molecules* (Academic Press. New York. London. 1986)

[16] R.E.Drullinger. M.M.Hessel. and E.W.Smith. in *Laser Spectroscopy*. edited by S.Haroche *et*

al. (Springer, Berlin, 1975), p. 91

[17] C.A.Moore, G.P.Davis, and R.A.Gottscho, Phys. Rev. Lett. **52**, 538 (1984)

[18] M.L.Mandich, C.E.Gaebe, and R.A.Gottscho, J. Chem. Phys. **83**, 3349 (1985)

[19] R.A.Gottscho, Phys. Rev. A **36**, 2233 (1987)

[20] J.Derouard and N.Sadeghi, Opt. Commun. **57**, 239 (1986)

[21] H.Debontride, J.Derouard, and N.Sadeghi, Ann. Phys. **13**, 97 (1988)

[22] M.H.Alexander, J. Chem. Phys. **83**, 3340 (1985)

[23] J.Derouard and M.H.Alexander, J. Chem. Phys. **85**, 134 (1986)

[24] J.Derouard, H.Debontride, T.D.Nguyen, and N.Sadeghi, J. Chem. Phys. **90**, 5936 (1989)

[25] W.J.Stevens, D.D.Konowalow, and L.B.Ratcliff, J. Chem. Phys. **80**, 1215 (1984)

[26] M.M.Hessel, and S.Giraud-Cotton, NaK *revisited*: The ground $^1\Sigma$ and $D\,^1\Pi$ states. unpublished preprint, (1980).

[27] D.Eisel, D.Zevgolis, and W.Demtröder, J. Chem. Phys. **71**, 2005 (1979)

[28] E.J.Breford, and F.Engelke, Chem. Phys. Lett. **53**, 282 (1978)

[29] E.J.Breford, and F.Engelke, J. Chem. Phys. **71**, 1994 (1979)

[30] H.Katô, and C.Noda, J. Chem. Phys. **73**, 4940 (1980)

[31] P.Kowalczyk, J. Mol. Spectrosc. **136**, 1, (1989)

[32] A.J.Ross, C.Effantin, J.d'Incan, and R.F.Barrow, J. Phys. B **19**, 1449 (1986)

[33] J.Pfaff, M.Stock, and D.Zevgolis, Chem. Phys. Lett. **65**, 310 (1979)

[34] R.W.Field, and T.H.Bergeman, J. Chem. Phys. **54**, 2936 (1971)

[35] T.J.Scholl, R.Cameron, S.D.Rosner, and R.A.Holt, Can. J. Phys. **73**, 101 (1995)

[36] B.Friedrich, and D.R.Herschbach, Nature (London) **353**, 412 (1991)

[37] C.Cohen-Tannoudji, Ann. de Phys. **7**, 423 (1962)

[38] C.Cohen-Tannoudji, Ann. de Phys. **7**, 469 (1962)

[39] K.Blum, *Density Matrix. Theory and Applications* (Plenum Press, New York, London, 1981)

[40] A.R.Edmonds, *Angular Momentum in Quantum Mechanics* (Princeton University Press, Princeton, New Jersey, 1974)

[41] R.N.Zare, *Angular Momentum* (J.Wiley and Sons, New York, 1988)

[42] I.I.Sobelman, *Atomic Spectra and Radiative Transitions* (Springer, Berlin-Heidelberg-New York, 1992)

[43] D.A.Varshalovich, A.N.Moskalev, and V.K.Khersonskii, *Quantum Theory of Angular Momentum* (World Scientific, Singapore, 1988)

[44] I.Røegger, J. Phys. B **4**, 168 (1971)

[45] M.P.Auzinsh, R.S.Ferber, Ya.A.Harya, and I.Ya.Pirags, Chem. Phys. Lett. **124**, 116 (1986)

[46] R.E.Drullinger, and R.N.Zare, J. Chem. Phys. **51**, 5532 (1969)

[47] K.P.Huber, and G.Herzberg, *Molecular Spectra and Molecular Structure. IV. Constants of Diatomic Molecules* (Van Nostrand, New York) (1979)

[48] M.Baba, S.Tanaka, and H.Kato, J. Chem. Phys. **89**, 7049 (1989)

FIGURES

FIG. 1. Selection rules (a) and Stark effect energy shifts (b) for $^1\Sigma$ — $^1\Pi$ transition. Notations for (b) refer to Eqs. (4) and (5).

FIG. 2. Low-lying bonded terms of NaK molecule [25].

FIG. 3. Stark zero-field level-crossing signals calculated in a wide range of electric field $\mathcal{E}$ for degree of linear polarization $P(\mathcal{E}) = (I_y - I_x)/(I_y + I_x)$ in "traditional" Stark–Hanle effect geometry ($\hat{\mathbf{E}} \perp \boldsymbol{\mathcal{E}}$, observation along $\boldsymbol{\mathcal{E}}$) at a transition $(J'' = 22) \rightarrow (J' = 23) \rightarrow (J_1'' = 22)$. 1 — first order. 2 — Hamiltonian diagonalization, $\Delta J' = \Delta J'' = \Delta J_1'' = 1$. 3 — $\Delta J' = \Delta J'' = \Delta J_1'' = 2$. The parameters characteristic for NaK ($D^1\Pi$) state were used for simulation: $\Gamma = 5 \times 10^7 \mathrm{s}^{-1}$ [33]. $B_v' = 0.0643\,\mathrm{cm}^{-1}$ $B_v'' = 0.0945\,\mathrm{cm}^{-1}$, $q = 1.2 \times 10^{-5}\mathrm{cm}^{-1}$ [26], $d_p = 7$ D [25]. Curve 4 (dashed line) refers to pure quadratic Stark effect in a hypothetic $^1\Sigma$ excited state with the same Γ and d_p values.

FIG. 4. Calculated $^1\Pi$ ($J' = 23$) state Stark level crossing signals in degree of linear polarization $P(\mathcal{E}) = (I_z - I_x)/(I_z + I_x)$ of LIF viewed from the "end" of the exciting light vector $\hat{\mathbf{E}}$ as shown in the setting-in. 1 — $\Delta J = 0$ (linear approximation). 2 — $\Delta J = 1$. 3 — $\Delta J = 2$. Curve 4 represents calculated signal for a hypothetic $^1\Sigma$ state. Parameters are the same as in Fig. 3.

FIG. 5. (a) Simulations of Stark level crossing signals in polarization of LIF from $^1\Pi$ ($J' = 23$), assuming the same $q = 1.2 \times 10^{-5}\,\mathrm{cm}^{-1}$ value and different permanent electric dipole moment values: 1 — $d_p = 7$ D, 2 — $d_p = 5$ D, 3 — $d_p = 3$ D. (b) The same signals for different q and d_p values in condition of the constant q/d_p ratio. 1 — $q = 1.2 \times 10^{-5}\,\mathrm{cm}^{-1}$, $d_p = 7$ D. 2 — $q = 0.857 \times 10^{-5}\,\mathrm{cm}^{-1}$, $d_p = 5$ D. 3 — $q = 0.514 \times 10^{-5}\,\mathrm{cm}^{-1}$, $d_p = 3$ D. (c) Correspondent intensity ratios $I_Q/I_{P,R}$ calculated for the same parameters at two orthogonal fluorescence polarization directions. Calculation are performed with fixed relaxation rate $\Gamma = 5 \times 10^7 \mathrm{s}^{-1}$. Geometry and other parameters are the same as in Fig. 4.

FIG. 6. Simulations of Stark level crossing signals in polarization of LIF from $^1\Pi$ ($J' = 23$), and intensity ratio I_Q/I_R, assuming different Γ values. 1 — $\Gamma = 5 \times 10^7 \mathrm{s}^{-1}$. 2 — $\Gamma = 7 \times 10^7 \mathrm{s}^{-1}$. calculations are performed with $q = 1.2 \times 10^{-5}\mathrm{cm}^{-1}$, $d_p = 7$ D. (a) — LIF polarization. (b) — Intensity ratios.

FIG. 7. Effect of electric field on spectrally resolved LIF signal for NaK $D^1\Pi \rightarrow X^1\Sigma^+$ system. (a) transition ($v'' = 1$, $J'' = 22$) $\rightarrow$ ($v' = 7$, $J' = 23$) $\rightarrow$ ($v_1'' = 24$, $J_1'' = 22$ and 24); 4880 Å excitation. (b) transition ($v'' = 0$, $J'' = 8$) $\rightarrow$ ($v' = 12$, $J' = 7$) $\rightarrow$ ($v_1'' = 31$, $J_1'' = 6$ and 8); 4765 Å excitation.

FIG. 8. Linear polarization degree and intensity ratios measured in LIF from NaK ($D^1\Pi$) state with $v' = 7$, $J' = 23$. (a), (c) — electric field dependence of the polarization degree obtained on $R(22)$ component. (b), (d) — electric field dependence of intensity ratios I_Q/I_P or I_Q/I_R. Results are obtained in different cells at geometry depicted in Fig. 4, dots are the measured values, the lines refer to the calculations at fitted parameters.

FIG. 9. Linear polarization degree and intensity ratios measured in LIF from NaK ($D^1\Pi$). $v' = 12$, $J' = 7$. (a) — electric field dependence of polarization degree obtained on $P(8)$ component. (b), (c) — electric field dependence of intensity ratios I_Q/I_P and I_Q/I_R. Data for (a), (b) are obtained at geometry depicted in Fig. 4, whereas for (c) we used $\hat{\mathbf{E}} \| \boldsymbol{\mathcal{E}}$. Dots are the measured values. full lines refer to the calculations with fitted parameters.

FIG. 10. RF-optical double resonance signals. (a) for NaK $D^1\Pi$ $v' = 12$, $J' = 7$ state. (b) for NaK $D^1\Pi$ $v' = 7$, $J' = 23$ state.

TABLES

TABLE I. Experimental values of permanent electric dipole moment d_p and Λ - doubling constant q for NaK ($D^1\Pi$, v', J'). Values d_p^{th} are *ab initio* calculations [25] averaged for particular v'.

v'	J'	q, 10^{-5}cm^{-1}	d_p, Debye	d_p^{th}, Debye
7	23	1.65 ± 0.20^a	6.4 ± 0.8^a	7.1
		1.42 ± 0.07^b	5.9 ± 0.9^c	
12	7	1.10 ± 0.20^a	4.5 ± 0.8^a	6.5
		1.03 ± 0.08^b	4.8 ± 0.9^c	

[a] Values determined from two-parameter fitting of LIF polarization $\mathcal{E}$-dependencies.

[b] Values determined directly from RF - optical double resonance.

[c] Values determined using q/d_p obtained from the $\mathcal{E}$-dependence of $I_Q/I_{P,R}$ and q obtained from RF - optical double resonance.

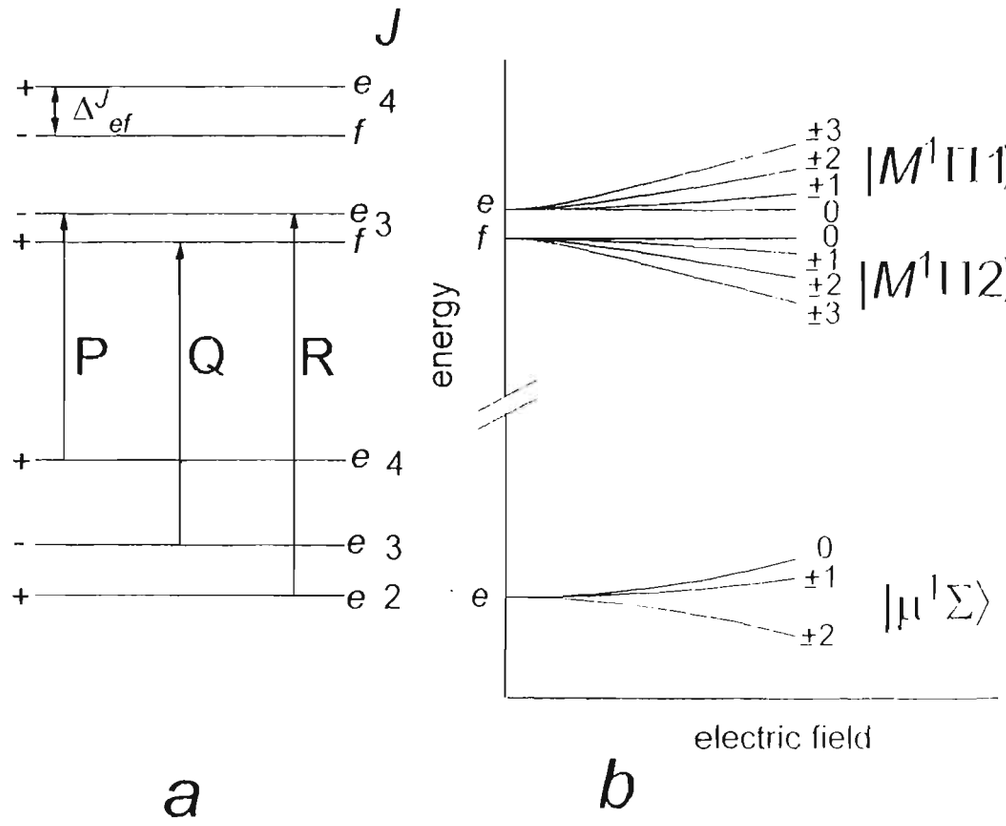
J
+
-
Δ^J_{ef}
e 4
f
e 3
f
P
Q
R
e 4
e 3
e 2
energy
e
f
±3
±2
±1
0
0
±1
±2
±3
$|M^1\Pi 1\rangle$
$|M^1\Pi 2\rangle$
e
0
±1
±2
$|\mu^1\Sigma\rangle$
electric field
a
b

Fig. 1.

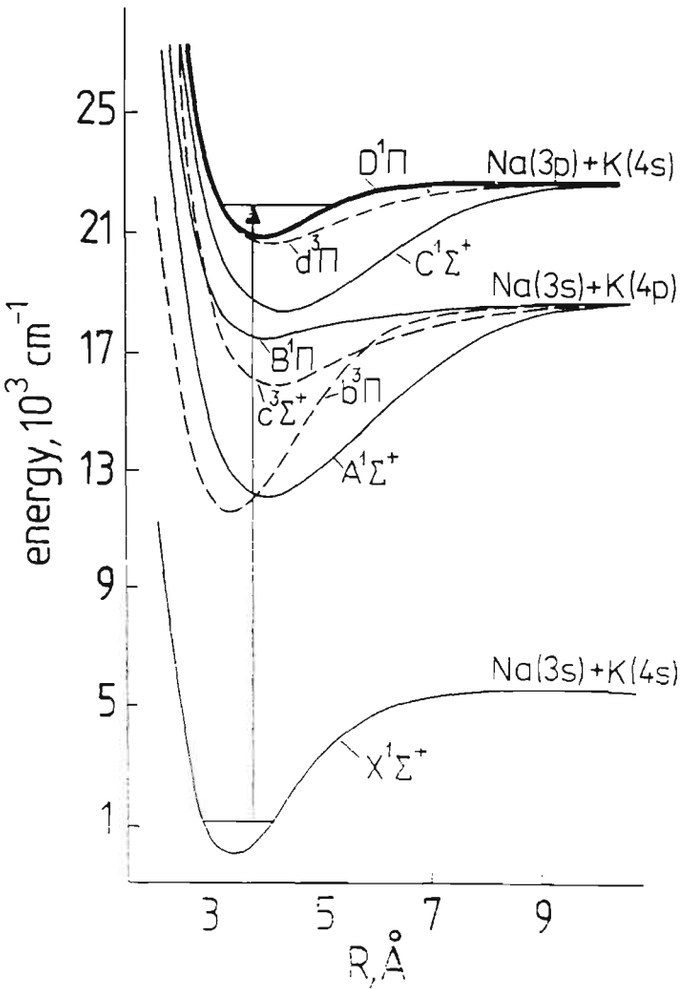
energy, 10^3 cm^{-1}
25
21
17
13
9
5
1
3
5
7
9
R, Å
$D^1\Pi$
Na(3p)+K(4s)
$d^3\Pi$
$C^1\Sigma^+$
Na(3s)+K(4p)
$B^1\Pi$
$c^3\Sigma^+$
$b^3\Pi$
$A^1\Sigma^+$
Na(3s)+K(4s)
$X^1\Sigma^+$

Fig. 2.

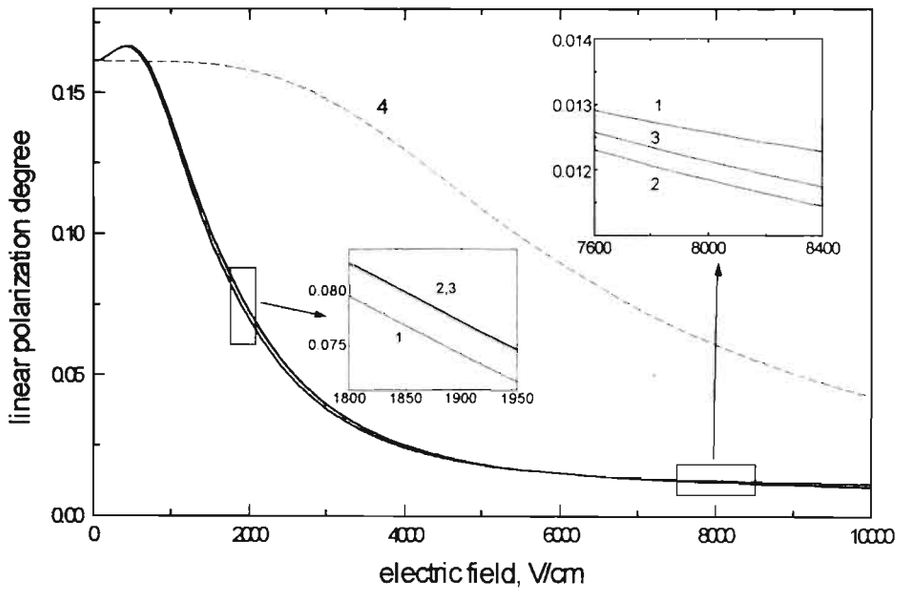
linear polarization degree
electric field, V/cm
0.15
0.10
0.05
0.00
0
2000
4000
6000
8000
10000
4
0.014
0.013
0.012
1
3
2
7600
8000
8400
0.080
0.075
2,3
1
1800
1850
1900
1950

Fig. 3.

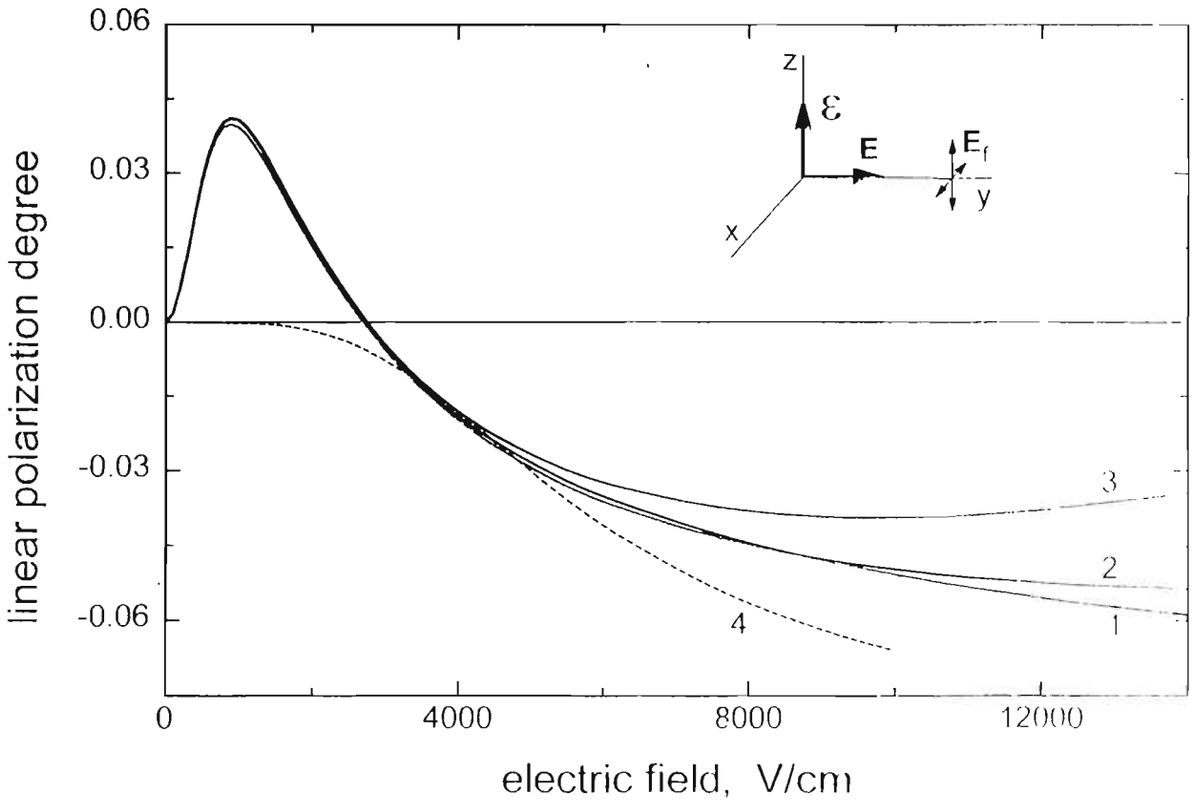
linear polarization degree
electric field, V/cm
0.06
0.03
0.00
-0.03
-0.06
0
4000
8000
12000
z
ε
E
E_f
y
x
3
2
1
4

Fig 4

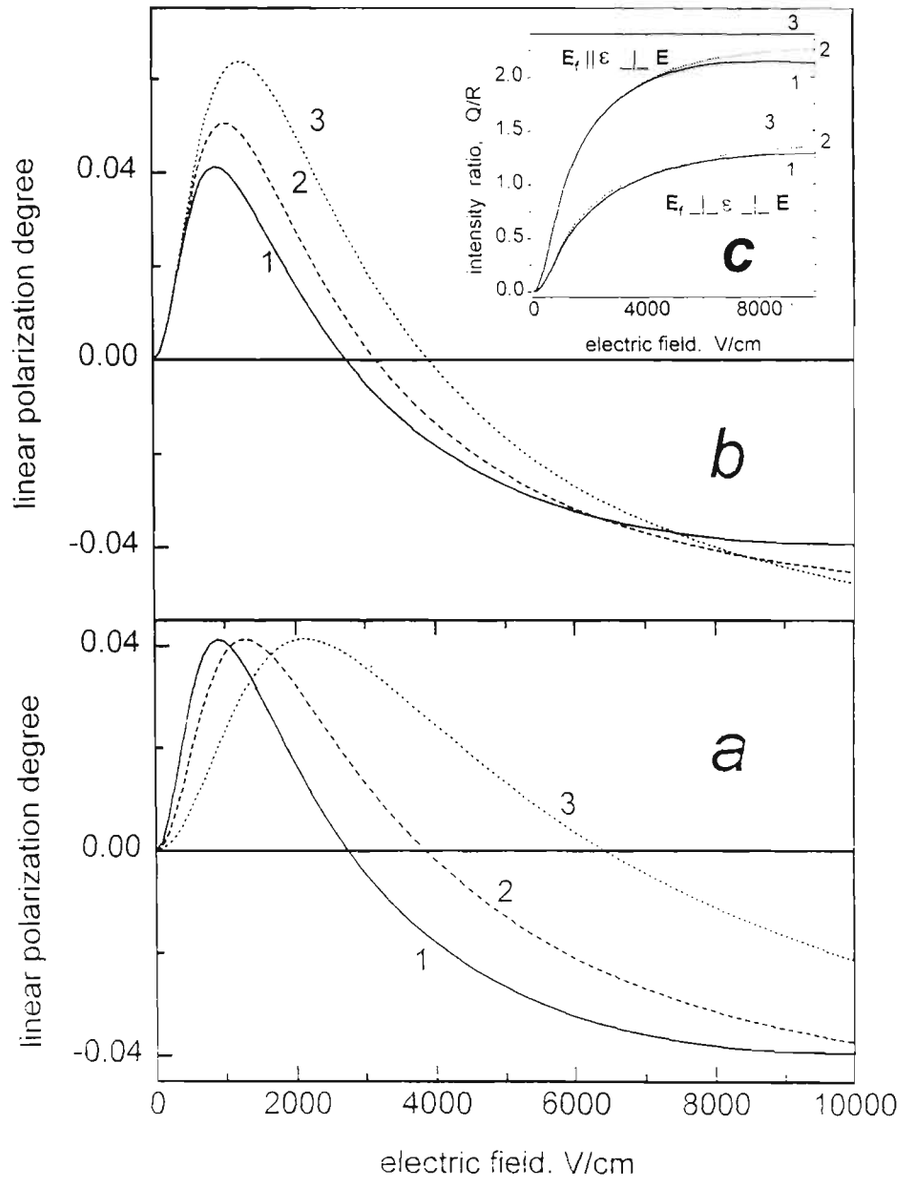
linear polarization degree
0.04
0.00
-0.04
b
1
2
3
intensity ratio, Q/R
2.0
1.5
1.0
0.5
0.0
0
4000
8000
electric field, V/cm
c
a
0
2000
4000
6000
8000
10000
electric field, V/cm

Fig.5.

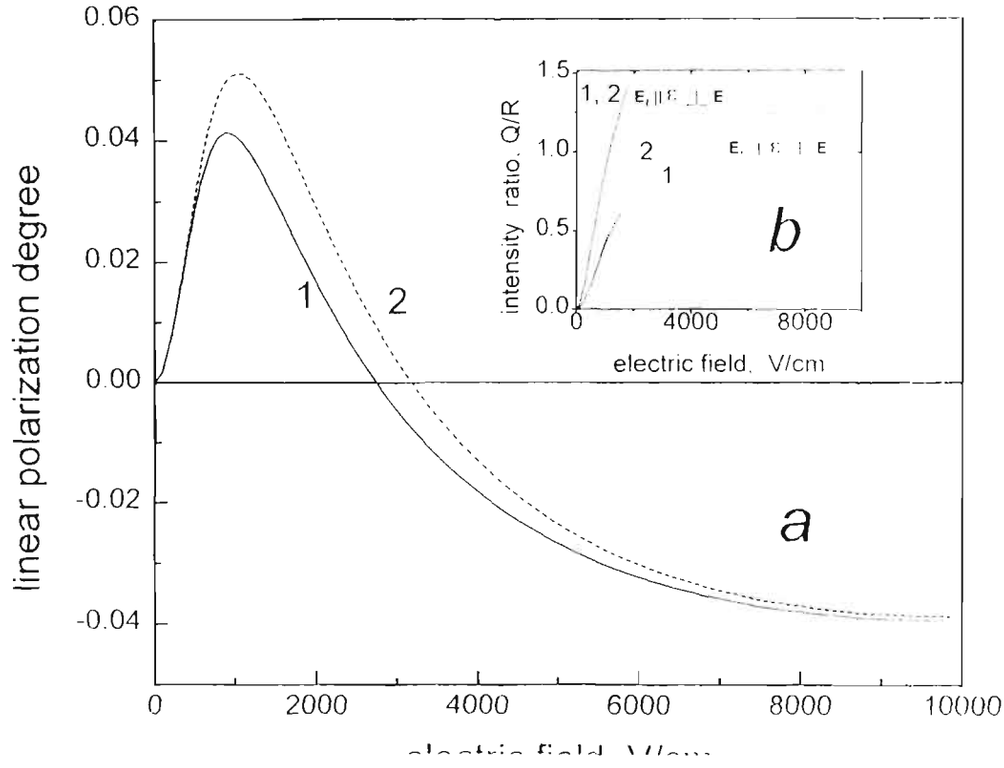
linear polarization degree
0.06
0.04
0.02
0.00
-0.02
-0.04
1
2
intensity ratio, Q/R
1.5
1.0
0.5
0.0
0
4000
8000
electric field, V/cm
b
a
0
2000
4000
6000
8000
10000

Fig.6.

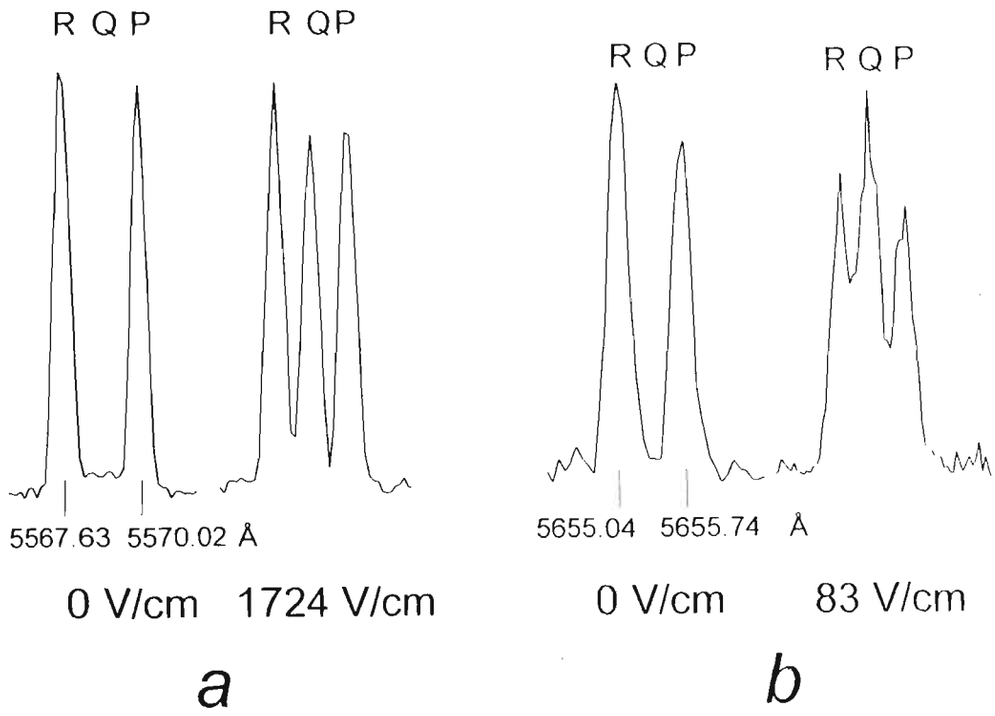
R Q P
R QP
R QP
R Q P
5567.63 5570.02 Å
5655.04 5655.74 Å
0 V/cm 1724 V/cm
0 V/cm 83 V/cm
a
b

Fig.7.

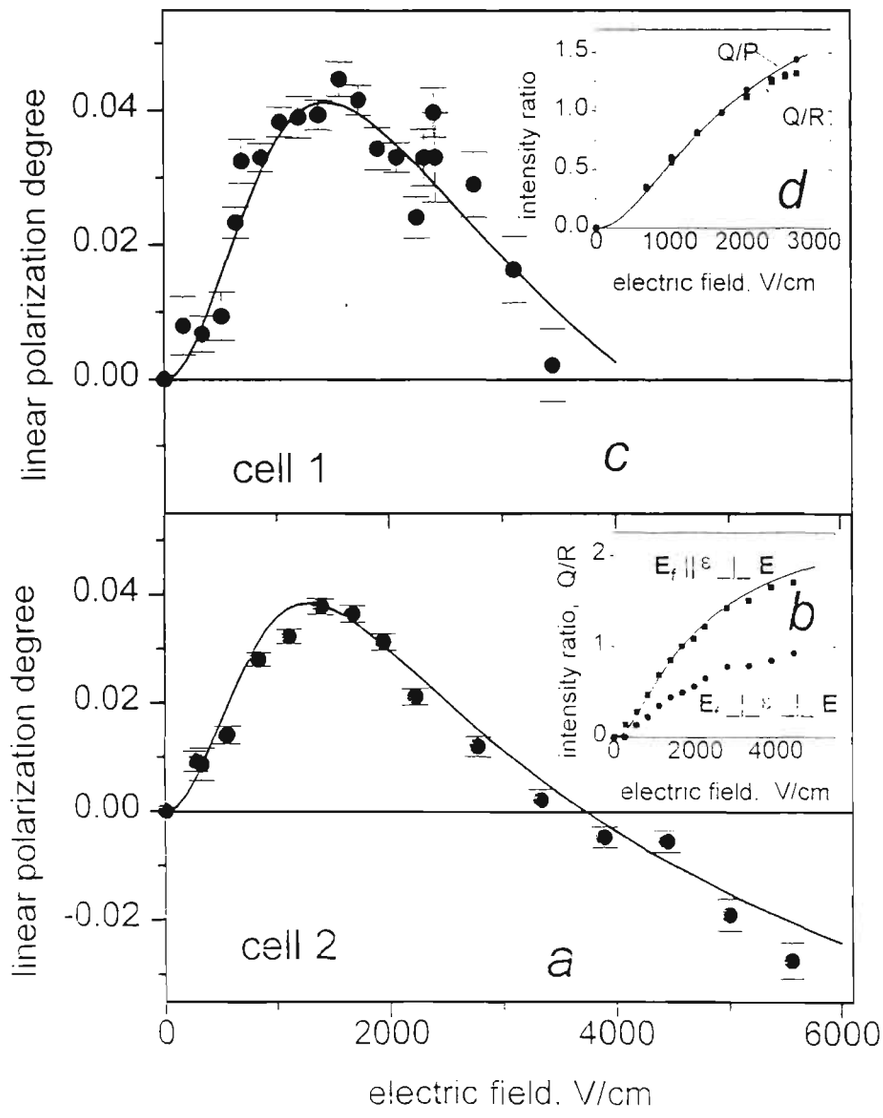
linear polarization degree
0.04
0.02
0.00
-0.02
cell 1
c
cell 2
a
intensity ratio
Q/P
Q/R
d
1.5
1.0
0.5
0.0
0
1000
2000
3000
electric field. V/cm
intensity ratio, Q/R
2
1
0
$E_f \| \varepsilon \perp E$
$E_f \perp \varepsilon \perp E$
b
2000
4000
0
2000
4000
6000
electric field. V/cm

Fig 8

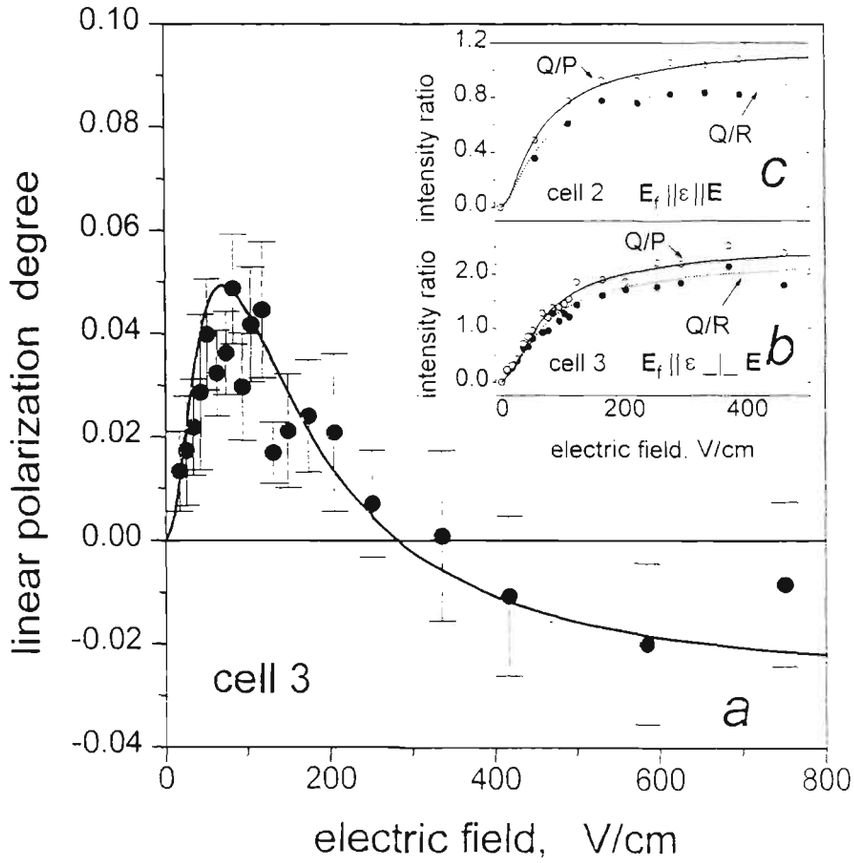
linear polarization degree
0.10
0.08
0.06
0.04
0.02
0.00
-0.02
-0.04
0
200
400
600
800
electric field, V/cm
cell 3
a
intensity ratio
1.2
0.8
0.4
0.0
Q/P
Q/R
cell 2 E_f ||ε||E
c
intensity ratio
2.0
1.0
0.0
Q/P
Q/R
cell 3 E_f ||ε _|_ E
b
0
200
400
electric field. V/cm

Fig.9.

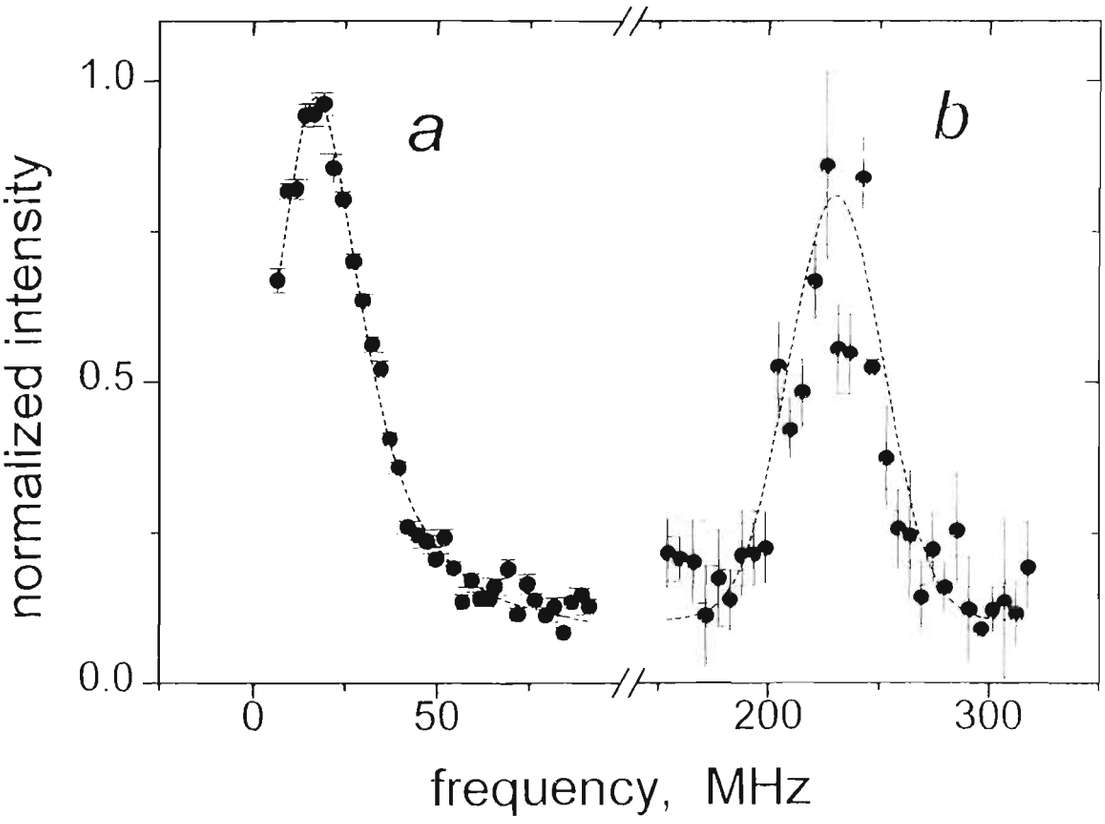
normalized intensity
1.0
0.5
0.0
a
b
0
50
200
300
frequency, MHz

Fig 10.

Electric Dipole Moment and Λ-Doubling Measurement in ($D\,^1\Pi$) NaK

M. Tamanis[1], A.V. Stolyarov[2], M. Auzinsh[1], I.Klincare[1], O.Nikolayeva[1], and R. Ferber[1]

[1] *Department of Physics, University of Latvia, Riga, LV-1586, Latvia*

[2] *Department of Chemistry, Moscow State University, 119899 Moscow, Russia*

We report here [1] the combined application of *dc* Stark induced $e \sim f$ mixing spectroscopy [2,3] and optical - radio frequency (RF) double resonance spectroscopy [4] for individual rotational levels belonging to a short-lived electronically excited rovibronic $v(J)$ state of polar diatomic molecule, allowing to measure the permanent electric dipole moment (d_p) and Λ-doubling splitting energy (Δ^J_{ef}) between Π - state e, f components of opposite symmetry, see Fig. 1. The method was applied to $D\,^1\Pi$ state $^{23}Na^{39}K$ molecules, which were formed thermally (at ca. 300 C°) in an alkali–resistant glass cell. Electric field, both *dc* (up to $\mathcal{E}$ = 6 kV) and RF ($1 \div 300$ MHz, 0.2 W, 50 Ω), was produced by applying voltage across a pair of round stainless steel Stark plates located inside the cell. Linearly polarized *cw* Ar^+ - laser was used to excite $X\,^1\Sigma^+ \rightarrow D\,^1\Pi$ transition with fixed $v(J)$. Fig. 2 demonstrates the effect of *dc* electric field $\mathcal{E}$ on laser–induced fluorescence (LIF), leading to the appearance of forbidden Q-line due to $+ \leftrightarrow -$, or $e \leftrightarrow f$ mixing in $^1\Pi$ state with fixed J. Indeed, as is clear from Fig. 1 and $+ \leftrightarrow -$ selection rule, at $\mathcal{E} = 0$ only (P, R)-doublet emission follows P- or R- type excitation $1(22) \rightarrow 7(23)$ for Fig. 2a and $0(8) \rightarrow 12(7)$ for Fig. 2b. At $\mathcal{E} \neq 0$, the "forbidden" Q-line appears. The relative intensity of a "forbidden"/"parent" line is mainly governed by $\mathcal{E}d_p/\Delta^J_{ef}$ ratio, $\Delta_{ef} = q[J(J+1) - \Lambda^2]$, where q is the Λ-doubling factor.

This allowed us [1] to obtain the q/d_p ratio as $(2.40 \pm 0.25) \times 10^{-6}\mathrm{cm}^{-1}/\mathrm{D}$ for 7(23) state and $(2.10 \pm 0.20) \times 10^{-6}\mathrm{cm}^{-1}/\mathrm{D}$ for 12(7) state. To determine q and d_p separately, we measured Δ^J_{ef} directly by electric RF–optical double resonance. By means of RF frequency sweeping, resonance enhance of "forbidden" line intensity in LIF was detected. The method allows to measure Δ^J_{ef} with resolution below the Doppler limit. Although the resonance signal width exceeded the one expected from natural broadening, with a tendency to exhibit some structure, it allowed to obtained q values for a number of $v(J)$ of ($D\,^1\Pi$) NaK, see Table 1. Using the above q/d_p ratios, we passed to d_p values presented in the table.

$v(J)$	q, $10^{-5}\mathrm{cm}^{-1}$	d_p, Debye	d_p^{th}, Debye
3(23)	1.39 ± 0.06	—	—
4(19)	1.32 ± 0.06	—	—
7(23)	1.42 ± 0.07	5.9 ± 0.9	7.1
	1.65 ± 0.20^P	6.4 ± 0.8^P	
12(7)	1.03 ± 0.08	4.8 ± 0.9	6.5
	1.10 ± 0.20^P	4.5 ± 0.8^P	
14(19)	1.33 ± 0.05	—	—

Table 1. q-factors and dipole moments.

The alternative method was based on *dc* Stark effect induced changes in degree of linear polarization $P(\mathcal{E})$ of P- or R- line in most favourable experimental geometry, when LIF is viewed "from the end" of exciting light **E** - vector [1]. The $P(\mathcal{E})$ dependence was characteristic enough to obtain both q and d_p from the fitting routine, using elaborated theoretical description, accounting for Stark interaction within $J \pm \Delta J$, $\Delta J = 0, 1$ and 2 in initial, excited and final state. The q^P and d_p^P values thus obtained are given in the table.

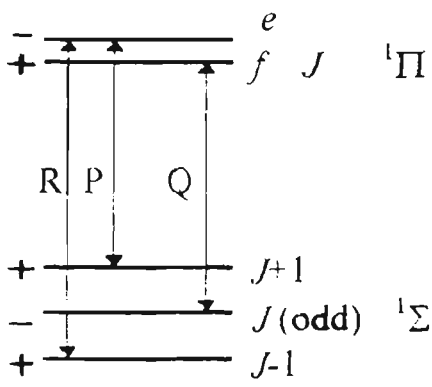

Fig. 1

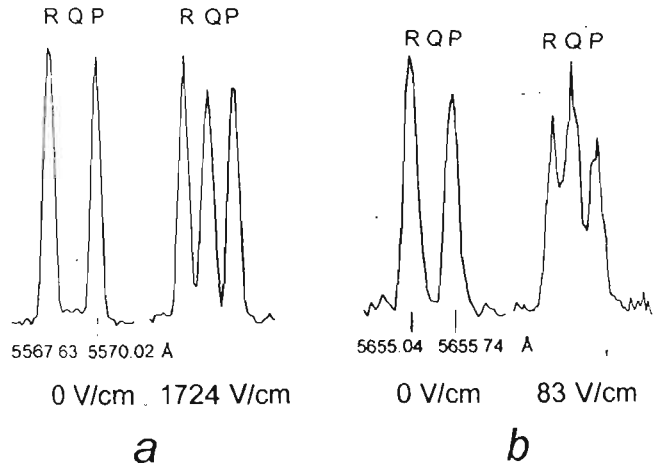

Fig. 2

The d_p value for $D\,^1\Pi$ 7(23) state agrees well enough with the value d_p^{th} obtained from *ab initio* calculations presented in [5], see the table. The smaller q and d_p values for 12(7) state are explained as the influence of local perturbations caused by the close lying $d\,^3\Pi_1$ 13(7) state. Hence, our measurements confirmed the existence of unusually large permanent electric dipole moment in ($D\,^1\Pi$) NaK as predicted in calculations [5]. Till now the only measured value for an electronically excited alkali dimer is given by the authors of [3], presenting d_p varying from 2.1 to 2.4 D for NaK $B\,^1\Pi$ state. The q values presented in Table 1 fall, except for 12(7) state, between $1.16 \times 10^{-5}\mathrm{cm}^{-1}$ estimated for ($D\,^1\Pi$) NaK states with $J \geq 100$ from conventional Doppler limited spectroscopy [6], and $q = 1.45 \times 10^{-5}\mathrm{cm}^{-1}$ as estimated from RF signal given in [2] for 7(5) state. The q values do not disagree much with the estimation $q \approx 4B^2/\nu(\Pi,\Sigma)$, where $\nu(\Pi,\Sigma)$ is the difference between electronic term values $T_\Pi - T_\Sigma$, B is the rotation constant. Assuming that Λ-doubling arises from the interaction with lying below $C\,^1\Sigma$ and $A\,^1\Sigma$ states, we calculated $q^{th} \approx 1.2 \times 10^{-1}\mathrm{cm}^{-1}$.

The work was supported by European Commission PECO Human Capital & Mobility Network, contract ERBCIPDCT940633, and by Latvian Science Council (Grant 93.256). A.V.S. is grateful for support from Russian Basic Research Foundation (Grant 93-B-18059). R.F. is grateful for support from Soros Foundation – Latvia.

[1] M. Tamanis, M. Auzinsh, I. Klincare, O. Nikolayeva, A.V. Stolyarov, and R. Ferber, *submitted to* J. Chem. Phys. (1996)
[2] R.E. Drullinger, M.M. Hessel, and E.W. Smith, in *Laser Spectroscopy*, edited by S. Haroche *et al.* (Springer, Berlin, 1975), p. 91
[3] J. Derouard, H. Debontride, T.D. Nguyen, and N. Sadeghi, J. Chem. Phys. **90**, 5936 (1989)
[4] S.J. Silvers, T.H. Bergeman, and W. Klemperer, J. Chem. Phys. **52**, 4385 (1970)
[5] W.J. Stevens, D.D. Konowalow, and L.B. Ratcliff, J. Chem. Phys. **80**, 1215 (1984)
[6] M.M. Hessel, and S. Giraud-Cotton, NaK *revisited*: The ground $^1\Sigma$ and $D\,^1\Pi$ states, unpublished preprint (1980)